THE JOURNAL
OF
CHEMICAL PHYSICS

VOLUME 18, NUMBER 10 OCTOBER, 1950

Equilibrium at Low Pressure in the Reduction of Barium Oxide by Carbon

CALLAWAY BROWN
General Electric Company, Research Laboratory, Schenectady, New York
(Received January 9, 1950)

An experimental scheme to investigate the reduction equilibrium of barium oxide by carbon is described and analyzed critically. Exploratory results at 950° support the analysis and indicate equilibrium at carbon monoxide pressures below 100μ with barium vapor pressures in the range 0.1 to 0.3μ. The resulting value for the free energy of formation of barium oxide is $-114{,}000$ cal. per mole.

EVEN the most refractory oxides are reduced by carbon at low pressures and at temperatures sufficient to volatilize the reduced metal from the reaction zone. If metal vapor is kept in contact with an oxide-carbon mixture in a closed system, equilibrium should be attained. The reaction,

$$BaO(s)+C(s)=Ba(g)+CO(g),$$

occurs readily in the activation of oxide coated cathodes. Use of a low pressure system to determine the equilibrium constant, $K=p_{CO}\cdot p_{Ba}$, poses substantial difficulties but results reported herewith indicate that it offers a most promising approach to the thermochemistry of barium oxide.

EXPERIMENTAL METHOD

A barium oxide-powdered graphite mixture in a low ash graphite crucible was enclosed in a one-inch quartz tube (Fig. 1). The experimental scheme involves two constant temperature zones: a high temperature zone T_2 for the reaction mixture, and a lower temperature zone T_1 for a reservoir of solid barium. The pressure of barium vapor in contact with the reaction mixture is thereby maintained at a constant value determined by the vapor pressure of barium at T_1. Connection to a McLeod gauge through a capillary tube permits measurement of the carbon monoxide pressure and limits the escape of barium vapor to avoid a pressure gradient between the T_1 and T_2 zones. The capillary tube simulates in effect a closed system with reaction mixture at T_2 and walls at T_1. In principle it can be made as small as desired. The 10-cm long, 2-mm diameter tube used constricts the escape of barium vapor to a value negligible compared with the capacity of the barium reservoir and permits easy evacuation or equalization of the carbon monoxide pressure between the McLeod gauge and the hot zones.

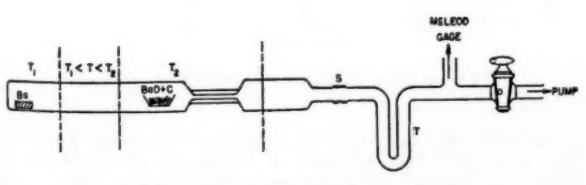

FIG. 1. Apparatus and method.

The pressure of carbon monoxide at equilibrium combined with the known pressure of barium vapor determines the equilibrium constant. Side reactions, such as reaction of barium vapor with the walls, and "gettering" of carbon monoxide by barium outside the T_2 zone, are to be expected. They need not influence the equilibrium pressures provided the equilibria of barium with its vapor at T_1 and of the reduction at T_2 adjust to pressure changes at a rate which is rapid compared with that of non-equilibrium processes. Evidence that this criterion for significant equilibrium results may be realized appears in the results.

The reaction mixture was formed from 200 mg of reagent grade barium carbonate mixed with an excess of powdered graphite. Barium was introduced in the form of nickel clad barium wire, the tube sealed off, evacuated, and heated to 1000° for one hour to convert carbonate to oxide and initiate reduction. The barium was then released from its nickel covering by heating with a high frequency induction coil. The temperature zones were maintained constant within 10° with resistance furnaces, and measured with calibrated chromel-alumel thermocouples.

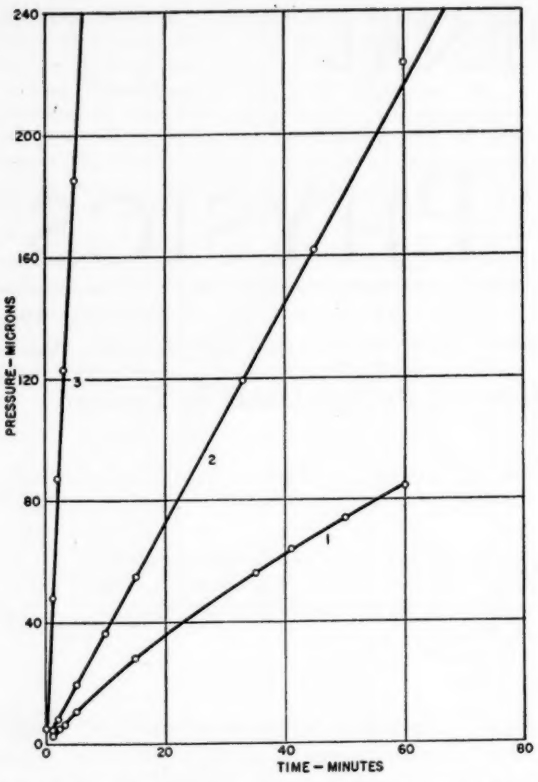

FIG. 2. Rate of reaction. Curve 1—Graphite crucible alone. Curve 2—Graphite crucible+barium oxide. Curve 3—Graphite crucible+barium oxide-powdered graphite mixture.

RESULTS

The normal progress of the reaction at 1000° with the T_1 zone cold appears in Fig. 2. The pressure increased linearly with time and fell off only moderately after repeated evacuations. The rate of reaction was highly dependent on the intimacy of contact. Gas evolution from the empty crucible, largely carbon monoxide without effect on the equilibrium, decreased considerably on repeated evacuation.

Evidence for equilibrium at 950° appears in Figs. 3 and 4. The initial point of each curve represents the time at which the evacuated system was closed off. The following rise in pressure, due to carbon monoxide, was markedly affected by the temperature T_1 of the barium reservoir, indicated at intervals along the curves. Increase of T_1 by 30° from 545° was calculated to increase the pressure of barium vapor from 0.10μ to 0.25μ.[1] As the temperature T_1 was raised the pressure dropped abruptly from more than 60μ to pressure plateaux at 29μ and 25μ in two tests. Possible complication from reaction of carbon monoxide with barium outside the T_2 zone is suggested by the anomalous drop in pressure (Fig. 3) which followed a drop in T_1 before the expected pressure rise. The somewhat lower pressure plateaux at 24μ and 16μ resulted when T_1 was held constant at 570° rather than increased suddenly to that value after accumulation of excess carbon monoxide, so that equilibrium was approached from the reverse direction. The general consistency of the results is seen by comparison of the plateau at 69±4μ for $T_1=545°$ ($p_{Ba}=0.10\mu$), followed for 50 minutes, with the average value of 25μ at $T_1=575°$ ($p_{Ba}=0.25\mu$). Corresponding values of the equilibrium constant, $K=p_{Ba}\cdot p_{CO}$, are 11.9×10^{-12} and 10.8×10^{-12} sq. atmos. respectively. The free energy change in the reduction,

$$\Delta F^0=\Delta F_{BaO}{}^0-\Delta F_{CO}{}^0=-RT\ \ln K=-61{,}200 \text{ cal.}$$

When the well-established value for $\Delta F_{CO}{}^0=-52{,}600$ cal.[2] is substituted, a rounded value for the free energy of formation of barium oxide at 1223° abs. of −114,000 cal. is obtained.

SIGNIFICANCE OF RESULTS

Establishment of the equilibrium constant within a factor of two corresponds to an uncertainty of ±1000 cal. in the free energy of formation of barium oxide. The present exploratory results indicate an internal consistency at least within this accuracy although considerable further work is necessary to establish the absolute accuracy. Complications due to side reactions: mainly reaction of barium vapor with the quartz walls and reaction of barium with carbon monoxide outside the T_2 zone appear to be less serious than might be anticipated. It is suggested that these non-equilibrium

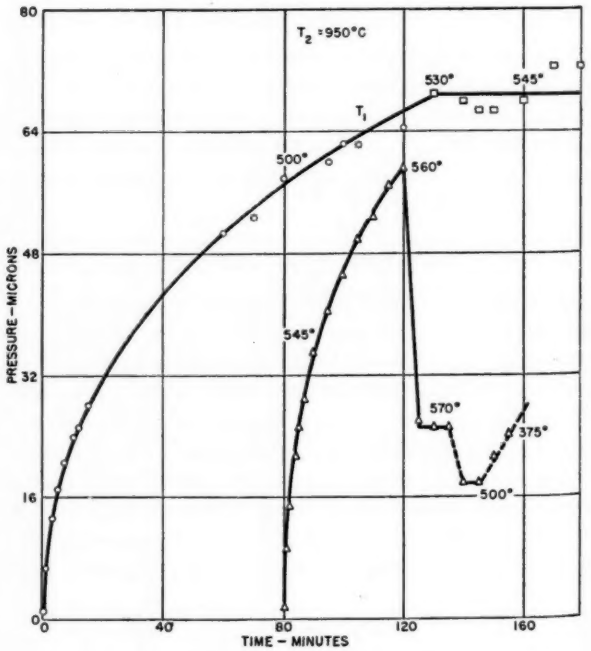

FIG. 3. Equilibrium at $p_{Ba}=0.10$ micron.

[1] Based on vapor pressure data for solid barium. E. Rudberg and J. Lempert, J. Chem. Phys. 3, 627 (1935).

[2] Calculated at 1223° abs. from equation of M. deKay Thomson, "The Total and Free Energies of Formation of the Oxides of Thirty-Two Metals" (The Electrochemical Society, New York, 1942), p. 4.

processes decrease in rate as reaction proceeds and it is only necessary that the two equilibria:

$$\mathrm{Ba}(s)=\mathrm{Ba}(g) \text{ at } T_1 \qquad (1)$$

and

$$\mathrm{BaO}(s)+\mathrm{C}(s)=\mathrm{Ba}(g)+\mathrm{CO}(g) \text{ at } T_2, \qquad (2)$$

adjust with relative rapidity to pressure changes. A possible effect of thermal diffusion on the pressure of barium vapor at T_2 is inherent in the method, but its maximum value is given by the ratio $(T_2/T_1)^{\frac{1}{2}}$.

The possibility of solid solution of carbon in barium oxide, or the incidence of barium carbide formation, must also be considered. Equilibrium at 1141° and 1295°C in the formation of barium carbide from the oxide and carbon has been reported by M. deKay Thomson.[3] The reaction was considered to be

$$\mathrm{BaO}+3\mathrm{C}=\mathrm{BaC_2}+\mathrm{CO}. \qquad (3)$$

The equilibrium pressure of carbon monoxide was found to depend upon the composition of the solid mixture and it was concluded that a single solid solution of the three solids was necessary to account for the trivariance of the system. Thomson points out that dissociation of barium carbide into its elements occurs at higher temperatures, barium deposits on the walls, and the equilibrium measured is no longer that of reaction (3). The reaction,

$$2\mathrm{BaO}+\mathrm{BaC_2}=3\mathrm{Ba}(g)+2\mathrm{CO}(g) \qquad (4)$$

was not considered. Since carbon alone reduces barium oxide below 1000°C at low pressures, reduction by barium carbide by the reaction 4 is to be expected at much lower temperatures than dissociation of the carbide into its elements. The sum of reactions (3) and (4) gives the equilibrium (2) considered in the present work. Since our temperatures are considerably lower than those usually associated with barium carbide formation and the pressures are much lower than those used by Thomson, thereby favoring removal of any combined carbon by reaction (4), complication of the low pressure reduction by barium carbide is unlikely.

[3] M. deKay Thomson, Trans. Am. Electrochem. Soc. **54**, 91 (1928).

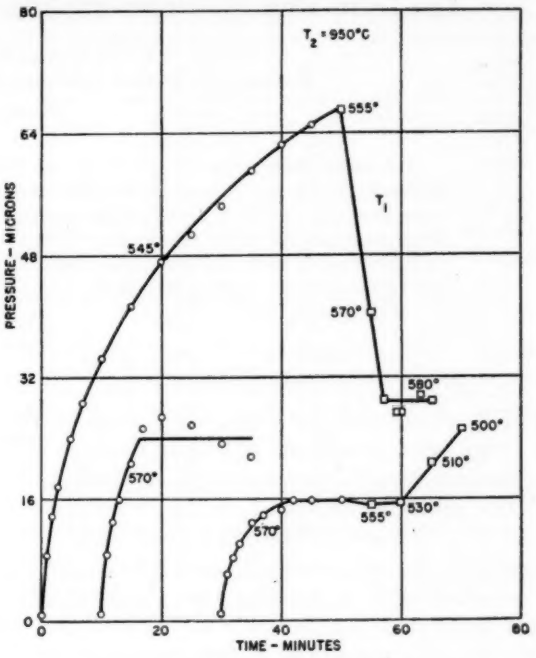

FIG. 4. Equilibrium at $p_{Ba}=0.25$ microns.

The free energy of formation of barium oxide has been estimated by White[4] by application of the third law of thermodynamics to available specific heat data. Interpolation of his calculations gives a value of $-120{,}000$ cal. at 950°C, considered to be correct within 5000 cal. Recent determination of the high temperature specific heat of barium oxide[5] increases this estimate by about 1000 cal., and narrows the range of uncertainty in the third law value, now mainly in the heat of sublimation of metallic barium at room temperature. The present direct attack on the equilibrium constant thus indicates a value higher by a factor of ten than the third law value. For such a difficult system this is most encouraging agreement. With sufficient refinement and data at a series of temperatures, the equilibrium method should provide thermochemical constants of high accuracy.

[4] A. H. White, J. App. Phys. **20**, 856 (1949).
[5] J. J. Lander, private communication for early publication in J. Am. Chem. Soc.

The Infra-Red Spectrum of Chloroacetylene and Deuterochloroacetylene*

W. S. RICHARDSON AND J. H. GOLDSTEIN†
Mallinckrodt Chemical Laboratory, Harvard University, Cambridge, Massachusetts
(Received July 10, 1950)

The vapor phase infra-red spectra of the molecules HCCCl and DCCCl have been investigated in the region 2μ to 30μ, and four of the five fundamentals have been identified for each molecule. Force constants have been calculated for the stretching modes of vibration assuming a linear structure. The bond stretching force constants have the values: $f_{CH}=5.88$, $f_{CC}=14.9$, $f_{CCl}=5.51$ all in units of 10^5 dynes/cm. The effect of resonance between the covalent structure, $H-C\equiv C-Cl$, and the structure $H-C^-=C=Cl^+$ in stiffening the carbon-chlorine bond is discussed.

I. INTRODUCTION

THE vibrational spectrum of chloroacetylene has not been previously reported. Electron diffraction measurements[1] indicate that the molecule is linear, and this result is confirmed by the microwave spectrum.[2] The carbon-chlorine internuclear distance as reported from the microwave study is 1.632A, representing a considerable shortening over the essentially covalent single bond length in CH_3Cl. This effect is probably due to resonance of the covalent structure $H-C\equiv C-Cl$, with the double-bonded chlorine structure $H-C^-=C=Cl^+$. If the latter structure is important, it is to be expected that the carbon-chlorine stretching force constant will be increased over its normal covalent value, an effect which is indeed observed. A close similarity can be expected between chloroacetylene and cyanogen chloride. In the latter molecule the carbon-chlorine bond is shortened[3] and stiffened[4] through resonance with the structure $N^-=C=Cl^+$ to an extent closely paralleling the case of chloroacetylene.

II. EXPERIMENTAL

The samples of chloroacetylene and deuterochloroacetylene were the same ones used in the investigation of their microwave spectra mentioned above. The chloroacetylene contained as an impurity about five to eight percent of *cis*-dichloroethylene, one of the reactants from which it was prepared. It was possible to separate the two somewhat by bulb-to-bulb fractionation in vacuum; but, because of the small size of the sample and the dangers involved in handling chloroacetylene, no complete separation was attempted. The deuterochloroacetylene contained less than one percent of HCCCl as judged from its spectrum and no *cis*-dichloroethylene. It did, however, show two bands (at 788 cm^{-1} and 2700 cm^{-1}) which have no apparent analogs in the HCCCl spectrum and for which there is no obvious assignment. Again the small sample did not permit any extensive attempts at purification, and crude bulb-to-bulb fractionation failed to alter the intensity of these bands with respect to those of DCCCl. It may be noted that neither of these bands can be a stretching fundamental of DCCCl.

All measurements were made in the gaseous state at pressures from 3 to 10 cm of Hg as indicated in Figs. 1 and 2. The spectra were taken in the region 2μ to 16μ with a Baird Associates, Inc., Model B (NaCl prism), infra-red recording spectrophotometer. In the region 16μ to 30μ the spectrograph described by Gershinowitz and Wilson[5] with modifications described by Hyde[6] was used with a KRS-5 prism and a 30 cm cell equipped with KBr windows. Both spectrographs were calibrated in the regions of interest with bands of common molecules whose frequencies have been well established. The dispersion of the Baird Spectrograph is relatively low from 2μ to 6μ, but by using a point by point technique rather than continuous recording, it was possible to obtain indications as to the shape of the band envelopes in this region.

III. RESULTS

Figures 1 and 2 show the spectra obtained at the pressures indicated. Bands due to chloroacetylene are marked *A*, those due to deuterochloroacetylene *B*, *cis*-dichloroethylene *C*, and the unassigned bands in the DCCCl spectrum *D*.

IV. FREQUENCY ASSIGNMENTS

A linear four atomic molecule has three non-degenerate stretching modes (Σ^+) and two doubly degenerate bending modes (π). It is to be expected that the stretching frequencies for HCCCl will fall roughly in the regions characteristic of the $H-C\equiv$ stretch ($\sim$3300 cm^{-1}), the $C\equiv C$ stretch ($\sim$2000 cm^{-1}) and the $\equiv C-Cl$ stretch (less definite than the others, but

* The research reported in this paper was made possible through support extended Harvard University by the Navy Department (ONR) under ONR Contract N5ori-76, T.O.V.
† National Research Council Predoctoral Fellow. Present address: Chemistry Department, Emory University, Emory University, Georgia.
[1] L. O. Brockway and I. E. Coop, Trans. Faraday Soc. **34**, 1429 (1938).
[2] Westenberg, Goldstein, and Wilson, Jr., J. Chem. Phys. **17**, 1319 (1949).
[3] Smith, Ring, Smith, and Gordy, Phys. Rev. **74**, 370 (1947).
[4] W. S. Richardson and E. Bright Wilson, Jr., J. Chem. Phys. **18**, 155 (1950).
[5] H. Gershinowitz and E. B. Wilson, Jr., J. Chem. Phys. **6**, 197 (1938).
[6] W. L. Hyde, thesis, Harvard University (1948).

714 cm^{-1} in ClCN[4]). The two strong bands in HCCCl at 3319 cm^{-1} and 2109 cm^{-1} must be the first two of these. They show a large and small isotopic shift respectively in DCCCl which substantiates the assignment. The small isotopic shift shown by the 756 cm^{-1} band marks it as the $\equiv C-Cl$ stretching mode. As a check we may apply the Teller-Redlich product rule[7] for the Σ^+ vibrations:

$$\frac{\omega_1\omega_2\omega_3}{\omega_1{}^i\omega_2{}^i\omega_3{}^i}=\left(\frac{M}{M^i}\cdot\frac{m^i}{m}\right)^{\frac{1}{2}}=1.403 \quad (1)$$

$$\frac{\nu_1\nu_2\nu_3}{\nu_1{}^i\nu_2{}^i\nu_3{}^i}=1.378, \quad (2)$$

where the ω's are zero-order frequencies, ν's the observed frequencies, M the molecular weight, and m the mass of the hydrogen atom in question, the superscript i denoting the deuterium compound. We note that the observed frequency ratio is about two percent smaller than the mass term which is to be expected for hydrogen-deuterium isotopic pairs because of differences in anharmonicity.[8]

The bands at 606 cm^{-1} in HCCCl and 476 cm^{-1} in DCCCl are assigned as the $H-C\equiv C$ and $D-C\equiv C$ bending modes (ν_5) respectively. The large isotopic shift substantiates the assignment. The bands at 1202 cm^{-1} and 940 cm^{-1} are close to twice these lower frequence bands and are assigned as $2\nu_5$. The other bending frequency was not observed for either molecule, and no obvious combination or overtone bands involving it were observed. The assingments are summarized in Table I.

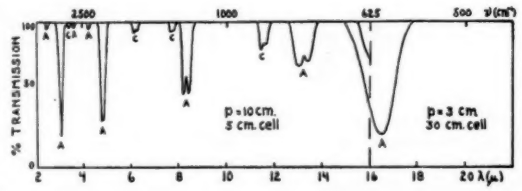

FIG. 1. The infra-red spectrum of HCCCl from 2μ to 30μ. No bands due to HCCCl were observed between 22μ and 30μ. *A* =chloroacetylene; *C*=cis-dichloroethylene.

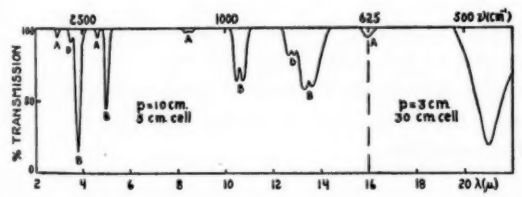

FIG. 2. The infra-red spectrum of DCCCl from 2μ to 30μ. No bands due to DCCCl were observed between 22μ and 30μ. *A* =chloroacetylene; *B*=deuterochloroacetylene; *D*=unassigned bands.

[7] See for instance, G. Herzberg, *Infra-Red and Raman Spectra of Polyatomic Molecules* (D. Van Nostrand Company, Inc., New York, 1945), p. 231 ff.

[8] See for instance, F. Halverson, Rev. Mod. Phys. **19**, 87 (1947).

TABLE I. Observed frequencies of HCCCl and DCCCl.

Designation	Species	HCCCl Freq. (cm^{-1}, vac.)	DCCCl Freq. (cm^{-1}, vac.)
ν_1	Σ^+	3319	2610
ν_2	Σ^+	2109	1979
$2\nu_5$	Σ^+	1202	941
ν_3	Σ^+	756	742
ν_5	π	606	476
ν_4	π	not obs.	not obs.

TABLE II. Force constants for HCCCl and DCCCl in units of 10^5 dynes/cm.

	From HCCCl	From DCCCl	Average
f_{CH}	5.88	6.13	—
f_{CC}	15.0	14.9	14.9_5
f_{CCl}	5.52	5.51	5.51_5

V. CALCULATION OF FORCE CONSTANTS

If we neglect all cross terms in the general quadratic potential function

$$2V=\sum_{ij} f_{ij}\Delta r_i\Delta r_j \quad (3)$$

we may write for the Σ^+ vibrations of HCCCl

$$2V=f_{CH}\Delta r^2_{CH}+f_{CC}\Delta r^2_{CC}+f_{CCl}\Delta r^2_{CCl} \quad (4)$$

where f is the force constant and Δr is the change in bond length of the bonds described by the subscripts. In principle, the six stretching frequencies observed should permit the evaluation of five force constants in Eq. (3) (i.e., the three principal force constants and two interaction constants). In practice, because of the differences in anharmonicity in the two molecules, no significant values for the interaction terms could be obtained, and we must be content with evaluation of the principal force constants independently from the two species, setting all cross terms equal to zero as in Eq. (4).

The equations which give the bond stretching force constants in terms of the normal frequencies may be put in the form:

$$\lambda_1+\lambda_2+\lambda_3=(\mu_H+\mu_C)f_{CH}+2\mu_C f_{CC}+(\mu_C+\mu_{Cl})f_{CCl} \quad (5)$$
$$\lambda_1\lambda_2+\lambda_1\lambda_3+\lambda_2\lambda_3=(\mu_C{}^2+2\mu_H\mu_C)f_{CH}f_{CC}$$
$$+(\mu_H+\mu_C)(\mu_C+\mu_{Cl})f_{CH}f_{CCl}+(\mu_C{}^2+2\mu_C\mu_{Cl})f_{CC}f_{CCl}$$
$$\lambda_1\lambda_2\lambda_3=(\mu_H\mu_C{}^2+2\mu_H\mu_C\mu_{Cl}+\mu_{Cl}\mu_C{}^2)f_{CH}f_{CC}f_{CCl}$$

where $\lambda=4\pi^2\omega^2$ and μ is the reciprocal of the mass denoted by the subscript. The values of the principal force constants obtained from the two molecules are given in Table II together with the averages for the $C\equiv C$ and $C-Cl$ force constants.

While it is not possible to evaluate any cross terms in (3), the effect of various values of the cross term between the carbon-carbon and the carbon-chlorine bonds on the values of the principal force constants was investigated. For a series of values of this interaction constant ranging from -0.6 to $+0.6\times10^5$ dynes/cm

the force constants f_{CC} and f_{CCl} were found to vary by $\pm 0.7\times10^5$ and $\pm 0.3\times10^5$ dynes/cm respectively. Effects due to other cross terms were not investigated, but it is to be expected that they will cause much smaller variations in f_{CCl} than the above term. We may somewhat arbitrarily select a value of 5.0×10^5 dynes/cm as a reasonable lower limit to f_{CCl}; this corresponding to a positive interaction constant and allowing for small variations from other sources.

VI. DISCUSSION

For an essentially covalent carbon-chlorine bond (in a molecule such as CH_3Cl) the carbon-chlorine stretching force constant has a value $\sim 3.6\times10^5$. The value of $f_{CCl} \geqslant 5.0\times10^5$ in chloroacetylene, therefore, indicates considerable stiffening of the bond. We ascribe this to resonance between the covalent structure and the double-bonded $H-C^-=C=Cl^+$. We might also expect a corresponding softening of the carbon-carbon bond, and the value of 14.9×10^5 for f_{CC} is rather lower than its value in acetylene and other molecules where such resonance cannot occur. However, it must be noted that the uncertainty in the values of the interaction terms puts the true value of f_{CC} in considerable doubt, and no valid deductions can be made from it. It is also to be expected that for a molecule which is a resonance hybrid of the above type the stretch-stretch interaction terms will be positive and at least for the one term investigated this leads to higher values of f_{CC}.

VII. ACKNOWLEDGMENT

The authors wish to express their indebtedness to Professor E. Bright Wilson, Jr., for his advice and encouragement, to Mr. A. A. Westenberg who prepared the samples of HCCCl and DCCCl and to Dr. D. M. Simpson for illuminating discussions.

THE JOURNAL OF CHEMICAL PHYSICS VOLUME 18, NUMBER 10 OCTOBER, 1950

The Intensities of Several of the Infra-Red Absorption Bands of Cyanogen and Cyanogen Chloride*

EUGENE R. NIXON** AND PAUL C. CROSS†
Metcalf Research Laboratory, Brown University, Providence, Rhode Island
(Received February 10, 1950)

Measurement of the absolute intensities of several infra-red absorption bands of cyanogen and cyanogen chloride gives the following values in cycles per cm at N.T.P.

Cyanogen	Band	Intensity
	2150 cm^{-1}	90×10^{10}
Cyanogen chloride	Band	Intensity
	714 cm^{-1}	17×10^{10}
	2214 cm^{-1}	220×10^{10}

Values of the variation in bond moments with change in bond length are calculated on the basis of bond moment additivity. This leads to widely different values of this derivative for the CN bond in the two molecules.

The infra-red spectrum of cyanogen chloride from 2 to 20 microns is reported.

INTRODUCTION

RECENTLY Wilson and Wells[1] have described an experimental method by which the intensities of infra-red absorption bands may be determined to a fair degree of accuracy even with a spectrometer of ordinary resolution. This method has been used here to measure the intensities of the 2150 cm^{-1} band of cyanogen and the 714 cm^{-1} and 2214 cm^{-1} bands of cyanogen chloride. Errors in the measurements are estimated as less than $\pm$ten percent.

In the Wilson-Wells method (and using their terminology) the integrated apparent absorption, $\mathcal{B}$, given by the equation

$$\mathcal{B} = pLB = \int (\ln T_0/T)\,d\nu \qquad (1)$$

is measured for a given band at a series of values of the product pL. In this expression p is the pressure of the absorbing gas; L is the cell length; T_0 the light transmitted by the empty cell; T the light transmitted by the sample cell; and the integration is carried over the

* Part of the material in this paper is taken from a thesis presented by Eugene R. Nixon in partial fulfillment of the requirements for the Ph.D. degree in the Graduate School of Brown University, October, 1947. The research reported here was supported in part by the ONR under Contract N6ori-88, T.O.1.

** Present address: Department of Chemistry and Chemical Engineering, University of Pennsylvania, Philadelphia, Pennsylvania.

† Present address: Department of Chemistry and Chemical Engineering, University of Washington, Seattle, Washington.

[1] E. Bright Wilson, Jr. and A. J. Wells, J. Chem. Phys. 14, 578 (1946).

width of the band. If the fine structure of the band is satisfactorily eliminated by pressure broadening and corrections are made for any atmospheric absorption or stray light, the true band intensity is then the value of B obtained by extrapolation to $pL=0$.

In a first approximation the true intensity A_k of the kth fundamental vibrational band is related to the molecular parameters by the expression

$$A_k=(N\pi/3c)\,|\partial\mathfrak{y}/\partial Q_k|^2, \qquad (2)$$

in which N is the number of molecules per unit volume, c is the velocity of light, $\mathfrak{y}$ is the dipole moment of the molecule and Q_k is the normal coordinate for the particular vibrational mode. If it is assumed that bond moments are additive and depend only upon bond lengths and if the normal coordinates are known in terms of internal coordinates, it is then possible to reduce band intensities to values of either the individual bond moments μ_i, or rates of change of bond moments with internuclear distances $(\partial\mu/\partial r)_i$.

The instrument used in this investigation was a Perkin-Elmer Spectrometer Model 12B, modified by a double beam arrangement, which allowed rapid comparison of the transmission of the filled and empty cells.

CYANOGEN

The cyanogen was prepared by the thermal decomposition of mercuric cyanide. A charge of Mallinckrodt Analytical Reagent $Hg(CN)_2$ was preheated to assure dryness, then decomposed at 550–600°. The gas evolved was passed through P_2O_5 and condensed in a dry ice trap; the crystalline condensate was twice fractionally sublimed, each time the bottom fraction (about 30 percent) being discarded.

The experimental values of the integrated apparent absorption for the 2150 cm^{-1} band are shown in Fig. 1. It can be seen that the addition of one atmosphere of nitrogen as a broadening agent produces only a minor increase in $\mathcal{B}$. This was taken to mean that for the spectrometer resolution in this spectral region the fine structure of the band is already essentially eliminated in pure cyanogen by self broadening and that the one atmosphere of nitrogen is adequate for the pressure broadening effect. It might be expected that larger values of the integrated apparent absorption would result from the use of smaller slit widths and hence greater resolving power but the scattering of the data due to experimental error obscures such a relation. Because of this scattering of experimental data, the intensity was calculated from values of $\mathcal{B}$ taken from the smooth curve in Fig. 1. These "smoothed" values of $\mathcal{B}$ determine the curve $B=\mathcal{B}/PL$ which extrapolates at $PL=0$ to an intensity of 90×10^{10} cycles per cm at N.T.P. for the 2150 cm^{-1} band.[2]

With a potential function containing only harmonic valence forces, the normal coordinate for the vibrational mode corresponding to this band, which Herzberg[3] labels ν_3, is given by $Q_3=2.32\times10^{-12}(r_1-r_2)$ where r_1 and r_2 represent changes in the two C—N distances. The assumptions of bond moment additivity then lead to $(\partial\mu/\partial r)_{CN}=\pm0.72\times10^{-10}$ (c.g.s. units), the ambiguity in sign resulting from the quadratic relation in (2).

CYANOGEN CHLORIDE

Samples of cyanogen chloride were prepared and purified according to the method of Coleman, Leeper and Schulze.[4]

Prior to intensity measurements, the infra-red spectrum of the gas in the region from 2 to 20 microns was investigated. The results of this work are given in Fig. 2 and Table I. A survey in the thallium bromoiodide prism range revealed an additional strong absorption band centering at about 390 cm^{-1}, but neither the frequency nor the intensity of this band could be de-

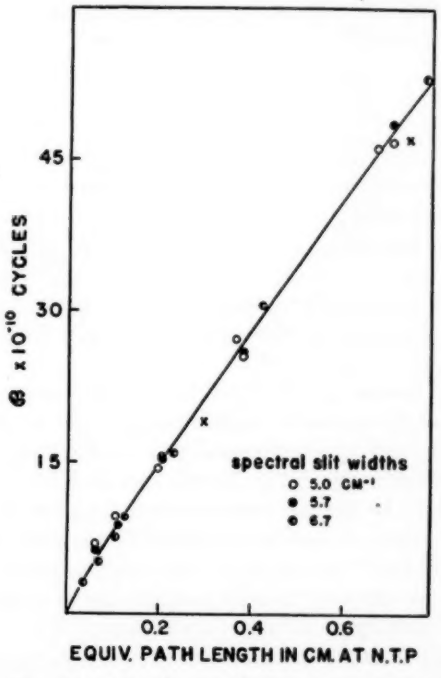

FIG. 1. Experimental values of $\mathcal{B}$, the integrated apparent absorption, for the 2150 cm^{-1} band of cyanogen as a function of the pressure of cyanogen. The circles represent determinations in which nitrogen was added to give a total pressure of one atmosphere. The x represents cases in which no broadening agent was added.

[2] There is a slight complication here in that the band at 2150 cm^{-1} overlaps a weaker one on the low frequency side. Bailey and Carson (J. Chem. Phys. 7, 859 (1939)) report the center of the weaker band at 2093 cm^{-1} and its intensity as 15 percent of that of the 2150 cm^{-1} band. It is difficult to see from the data given in their paper how they arrived at this value for the relative intensity. The present work indicates that the 2093 cm^{-1} band is much weaker than this and its contribution to the intensity of the 2150 cm^{-1} band has hence been neglected.

[3] G. Herzberg, *Infrared and Raman Spectra of Polyatomic Molecules* (D. Van Nostrand Company, Inc., New York, 1945), p. 294.

[4] *Inorganic Syntheses* (McGraw-Hill Book Company, Inc., New York, 1946), Vol. II, p. 90.

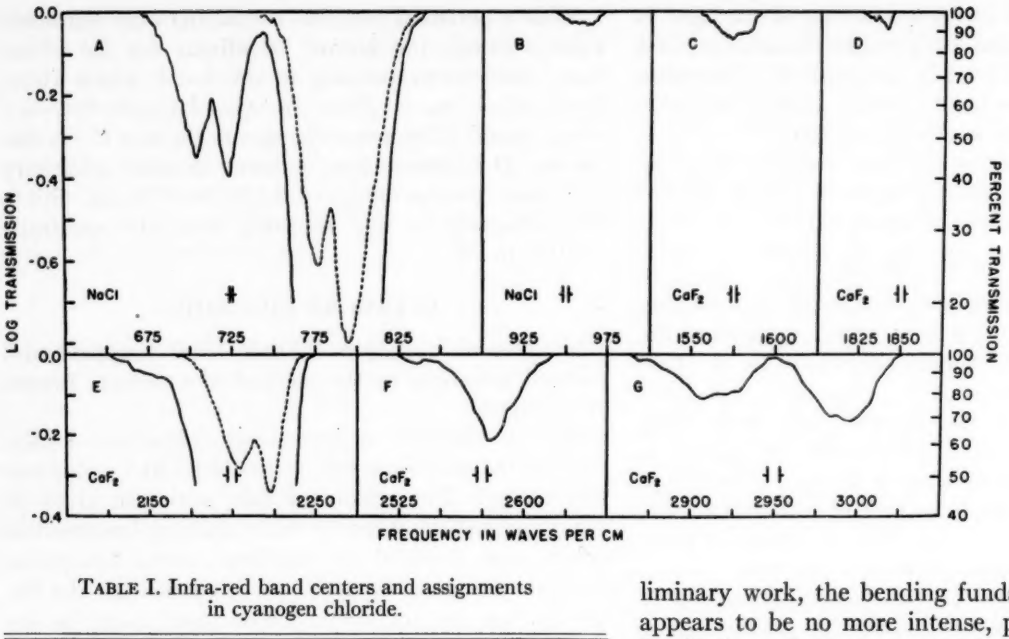

FIG. 2. Infra-red spectrum of cyanogen chloride at 25°, 10-cm path length and pressure of 45.5 cm Hg (solid line). Dashed lines represent 21.0-cm pressure in (*A*) and 3.3 cm pressure in (*E*).

TABLE I. Infra-red band centers and assignments in cyanogen chloride.

Frequency (cm^{-1})	Assignment
(390)	ν_2
714	ν_1
784	$2\nu_2$
960	?
1573	?
1840	?
2214	ν_3
2580	$\nu_3+\nu_2$
2915	$\nu_3+\nu_1$
2995	$\nu_3+2\nu_2$

termined accurately because of the presence of a considerable amount of stray radiation and the lack of a precise prism calibration.

In the Raman spectrum of liquid cyanogen chloride, West and Farnsworth[5] found strong lines at 397, 729 and 2201 cm^{-1} which they assigned as the three fundamental vibrations. A very weak line at 809 cm^{-1} they assumed to be the first overtone of the bending mode. It thus seems reasonable to assign the strong infra-red bands at 390, 714 and 2214 cm^{-1} as the three fundamentals for the gas. Table I includes these assignments given according to Herzberg's numbering.[6]

Several remarks on the spectrum of cyanogen chloride seem to be in order. First, the appearance of weak bands at 960 and 1573 cm^{-1} is almost certainly caused by impurities. One sample of the gas was prepared in which there was no trace of absorption at these frequencies. This sample was discarded, however, because it contained an estimated 0.4 percent of CO_2, the result of a slight decomposition. Second, the band at 1840 cm^{-1}, which appeared in all the samples of cyanogen chloride prepared, is unaccounted for but may be due to an impurity not readily removed by the methods of purification employed here. Thirdly, from the preliminary work, the bending fundamental ν_2(390 cm^{-1}) appears to be no more intense, possibly weaker, than $2\nu_2$ (784 cm^{-1}), but as stated before, estimation of intensities is somewhat uncertain in the 390 cm^{-1} range. Lastly it should be pointed out that there is the possibility of Fermi resonance between levels ν_1 and $2\nu_2$ and levels $\nu_3+\nu_1$ and $\nu_3+2\nu_2$. The magnitude of such resonance cannot be determined from the available data and so resonance effects have been neglected in the

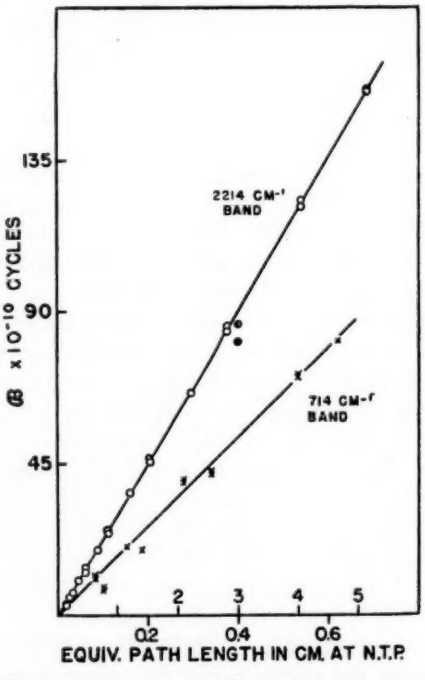

FIG. 3. Experimental values of $\mathfrak{B}$, the integrated apparent absorption, for the 714 cm^{-1} and 2214 cm^{-1} bands of cyanogen chloride as a function of the pressure of cyanogen chloride. The upper abscissa scale applies to the 714 cm^{-1} band. The open circle and x represent experiments in which nitrogen was added to give a total pressure of one atmosphere, the half-filled circle represents the case with one-half atmosphere of nitrogen; the completely filled circle the case with no foreign gas present.

[5] W. West and M. Farnsworth, J. Chem. Phys. 1, 402 (1933).
[6] See reference 3, p. 174.

TABLE II. Force constants, normal coordinates and bond moment derivatives of cyanogen chloride as a function of the interaction constant k_{12}.

k_{12}	k_1 (in units of 10^5)	k_2	L_{11}^{-1}	L_{12}^{-1} (in units of 10^{-12})	L_{21}^{-1}	L_{22}^{-1}	$(\partial\mu/\partial r)_{CCl}$ (in units of 10^{-10})	$(\partial\mu/\partial r)_{CN}$
0.0	4.93	17.05	4.96	3.01	0.524	−2.98	0.41	1.84
							0.92	1.03
0.5	4.77	17.71	4.98	2.95	0.407	−3.05	0.47	1.87
							0.86	1.08
1.0	4.63	18.34	4.99	2.86	0.294	−3.11	0.43	1.88
							0.81	1.12
5.0	4.86	22.49	4.97	2.36	0.468	3.51	0.89	2.01
							0.44	1.38

calculation of force constants and bond moment derivatives discussed below.[7]

Experimental data for the intensities of ν_1 and ν_3 are shown in Fig. 3. Again one atmosphere of nitrogen proved to be adequate for the pressure broadening effect. In the same manner as described for cyanogen, "smoothed" values of $\mathfrak{B}$ were used in the extrapolation process, leading to 17×10^{10} and 220×10^{10} (cycles per cm at N.T.P.) as the intensities of ν_1 and ν_3 respectively.

The force constants k_1 and k_2 have been calculated for several values of the interaction constant k_{12} on the basis of the potential function

$$V=\tfrac{1}{2}k_1r_1^2+k_{12}r_1r_2+\tfrac{1}{2}k_2r_2^2, \qquad (3)$$

where r_1 and r_2 are respectively the changes in the CCl and CN distances. These calculations are given in Table II, together with values of the coefficients L_{kj}^{-1} for the transformation from internal to normal coordinates.

$$Q_k=\sum_j L_{kj}^{-1}r_j. \qquad (4)$$

Calculation of bond moment derivatives in cyanogen chloride again involves sign ambiguity and for each k_{12} two numerical values of each derivative are possible. These are given in Table II, the upper set for the case in which both derivatives have the same sign (either positive or negative), the lower set for the case of opposite signs.

DISCUSSION

It has been pointed out that information aside from intensity data is necessary to establish the sign of bond moment derivatives. In the case of cyanogen chloride, Beach and Turkevich[8] have suggested that two resonating structures may be written for the molecule.

(*a*) Cl−C≡N
(*b*) $^+$Cl=C=N$^-$.

If it is assumed that the CN and CCl bond moments both have their positive ends directed toward the carbon atom, then a CCl stretch, favoring structure (*a*) and a CN stretch, favoring (*b*), lead to increased moments and hence positive signs for both derivatives. By this argument we should then adopt the upper set of values in Table II with positive signs for the bond moment derivatives.

Despite any sign considerations, however, it is seen that $(\partial\mu/\partial r)_{CN}$ has widely different numerical values in C_2N_2 and ClCN. It is reasonable to expect that bond moment derivatives should vary from molecule to molecule since the assumptions of bond moment additivity disregard the effects of induced polarization in neighboring bonds within a molecule. That $(\partial\mu/\partial r)_{CN}$ in ClCN is much greater than in C_2N_2 would indicate that the CCl bond is more polarizable than the CC bond.

[7] While the actual extent of resonance and consequent mixing of levels is undetermined, a first-order perturbation calculation, using observed intensities and frequencies, gives ±12.5 cm^{-1} as the maximum possible Fermi shift for the levels ν_1 and $2\nu_2$. In this extreme case of resonance the "unperturbed" fundamental ν_1 would fall at 727 cm^{-1} and possess zero intensity. Under these conditions force constants and bond moment derivatives would have the following values

$k_1=5.14\times10^5$ $(\partial\mu/\partial r)_{CCl}=\pm0.32\times10^{-10}$
$k_2=16.98\times10^5$ $(\partial\mu/\partial r)_{CN}=\pm1.74\times10^{-10}$

for the case in which the interaction constant, k_{12}, of expression (3) is set equal to zero. These values are to be compared with those in the first line of Table II, in which resonance involving ν_1 has been neglected.

[8] J. Y. Beach and A. Turkevich, J. Am. Chem. Soc. **61**, 299 (1939). See also C. H. Townes and B. P. Dailey, J. Chem. Phys. **9**, 788 (1949).

Substituted Ethanes. II. Raman and Infra-Red Spectra of 2,3-Dibromo-2,3-Dimethylbutane and 2,2,3,3-Tetramethylbutane*

FORREST F. CLEVELAND AND JAMES E. LAMPORT**
Spectroscopy Laboratory, Department of Physics, Illinois Institute of Technology, Chicago, Illinois
AND
RICHARD W. MITCHELL***
Department of Physics, Lynchburg College, Lynchburg, Virginia

(Received May 29, 1950)

Raman displacements and infra-red absorption wave numbers for 2,3-dibromo-2,3-dimethylbutane and 2,2,3,3-tetramethylbutane (hexamethylethane) are reported, together with depolarization factors for the Raman lines and relative intensities for both the Raman lines and the infra-red absorption bands. The spectra were obtained in both benzene and CCl_4 solutions and the infra-red measurements covered the region 400–5000 cm^{-1}. The results indicate that both molecules possess a center of symmetry and that the structure is the same in the two solvents. The dipole moment of 1.01 D. obtained by Mizushima, Morino, and Miyagawa for 2,3-dibromo-2,3-dimethylbutane in CCl_4 solution may be explained by oscillations of 48° amplitude about the equilibrium trans- position.

SAMPLES of 2,3-dibromo-2,3-dimethylbutane (*DB*) and 2,2,3,3-tetramethylbutane (*TM*) were kindly sent to us by Dr. George Calingaert, Ethyl Corporation, Detroit, Michigan, following an earlier study of some ethane-like molecules.[1]

Kahovec and Wagner[2] had obtained Raman spectral data for *DB*, as well as for the similar molecule, 2,3-dichloro-2,3-dimethylbutane (both in powdered crystalline form); and infra-red spectral data for *TM* were available both for the gaseous state[3] in the region 675–6000 cm^{-1} and for a solution[4] in the region 790–4310 cm^{-1}. Lambert and Lecomte[5] also have reported, in graphical form, the infra-red spectrum of *TM*. However, we were unable to find any previous Raman data for *TM* or any previous infra-red data for *DB*.

EXPERIMENTAL

The Raman displacements, semiquantitative relative intensities, and quantitative depolarization factors were obtained by use of previously described[6] apparatus and methods. Eastman 103-J plates were used and excitation was by Hg 4358A. The depolarization measurements for each line were made—when possible—on that spectrogram for which the densities fell on the linear portion of the *density–log intensity* curve, thus yielding greater accuracy.

The melting point of the *DB* sample was 158.5-158.7°C. Since it was a solid at room temperature, it was investigated in solution in both benzene and CCl_4. The infra-red records were obtained with a Beckman IR-2 recording spectrophotometer equipped with KBr optics. The region investigated was from 400 to 5000 cm^{-1} and the thickness of the absorbing layer was approximately 0.1 mm.

The *TM* also was a solid at room temperature and was likewise investigated in solution in benzene and CCl_4, and later in CS_2. The infra-red records for this compound were obtained by one of us (F.F.C.) in the Physics Department at Ohio State University during the summer of 1947, using a Beckman IR-2 recording spectrophotometer equipped with NaCl optics and covering the range 700–5000 cm^{-1}. Here, too, the thickness of the absorbing layer was approximately 0.1 mm. Later, the spectrum was obtained (by J. E. L.) also with a Beckman IR-2 spectrophotometer equipped with KBr optics.

The method of preparation, the purity, and the physical properties of the *TM* sample were as follows:[7] the sample was made from methyl magnesium chloride and 2,3,3-trimethyl-2-chlorobutane (triptyl chloride). This method should preclude the presence of any impurity, except perhaps a trace of triptyl chloride or triptyl alcohol. Measurements indicated that the purity was 99.93 mole percent. The freezing point was 100.63°C and the boiling point was 106.30°C.

RESULTS

2,3-Dibromo-2,3-dimethylbutane

The Raman and infra-red data obtained for *DB* are compared with the previous Raman data obtained by Kahovec and Wagner[2] for the solid state in Table I,

* Preliminary reports were made at the Houston (1947) and Chicago (1949) meetings of the American Physical Society; abstracts in Phys. Rev. **73**, 653 (1948); **77**, 740 (1950).

** Present address: Sinclair Research Laboratories, Harvey, Illinois.

*** Present address: Department of Physics, Texas Agricultural and Mechanical College, College Station, Texas.

[1] Dwight T. Hamilton and Forrest F. Cleveland, J. Chem. Phys. **12**, 249 (1944).

[2] L. Kahovec and J. Wagner, Zeits. f. physik. Chemie **B47**, 48 (1940).

[3] R. A. Oetjen and H. M. Randall, Rev. Mod. Phys. **16**, 265 (1944).

[4] American Petroleum Institute Research Project 44. National Bureau of Standards. Catalog of Infra-Red Spectral Data. No. 444, 2,2,3,3-tetramethylbutane, contributed by the Shell Development Company laboratory.

[5] P. Lambert and J. Lecomte, Ann. de physique **10**, 525, 528 (1938).

[6] Forrest F. Cleveland, J. Chem. Phys. **11**, 1, 227 (1943); **13**, 101 (1945).

[7] G. Calingaert, private communication, August 8, 1944; also Calingaert, Soroos, Hnizda, and Shapiro, J. Am. Chem. Soc. **66**, 1389 (1944).

and the infra-red percent transmission curve is shown in Fig. 1.

It seems significant that none of the infra-red absorption bands, below the region of the C−H frequencies where the dispersion and resolving power is small, corresponds to a Raman line, with the exception of the doubtful 532 cm^{-1} Raman line. This indicates that the rule of mutual exclusion holds for this molecule, which in turn means that the molecule must have a center of symmetry. If this conclusion is correct, the orientation of the two ends of the molecule with respect to each other is such that the two Br atoms are as far apart as possible for rotation about the central C−C bond, and that the methyl groups have the proper orientation for a center of symmetry.

Additional evidence in favor of a center of symmetry is the fact that the number of Raman lines observed for *DB* is less than is normal for a molecule containing 20 atoms. For example, for 1-bromohexane (*n*-hexylbromide)—which contains 20 atoms and for which no center of symmetry is possible—32 Raman lines were observed,[8] while for *DB* only 18 were found. Likewise, the number of observed infra-red bands also is less than is normal for a molecule containing 20 atoms, which implies the same conclusion.

If a center of symmetry is present, the structure of the molecule is that corresponding to the point group C_{2h}. For this structure, the selection rules predict 15 type A_g fundamentals, polarized in the Raman, forbidden in the infra-red; 12 type B_g fundamentals, depolarized in the Raman, forbidden in the infra-red; 13 type A_u fundamentals, forbidden in the Raman, parallel bands in the infra-red; and 14 type B_u fundamentals, forbidden in the Raman, perpendicular bands in the infra-red.

It is thus clear that the presence of a center of symmetry would severely restrict the number of vibrations observable in the Raman or in the infra-red spectrum. If all lines were resolved, there should be 15 polarized and 12 depolarized, or a total of 27, Raman lines corresponding to fundamental frequencies. Since only 18 Raman lines, of which 7 were polarized and 3 were depolarized, were observed in the Raman spectrum, it is evident that several lines must be unresolved, or else so weak that they escaped observation.

Only 11 infra-red bands were observed in the region below 3000 cm^{-1} where the fundamentals are expected to appear, whereas 27 fundamentals are allowed by the selection rules. Some of the missing fundamentals could correspond to unresolved bands and some to very weak unobserved bands; others no doubt fall in the non-investigated region below 400 cm^{-1}.

For the similar 2,3-dichloro-2,3-dimethylbutane (*DC*) molecule, van Arkel and Snoek[9] found a dipole moment

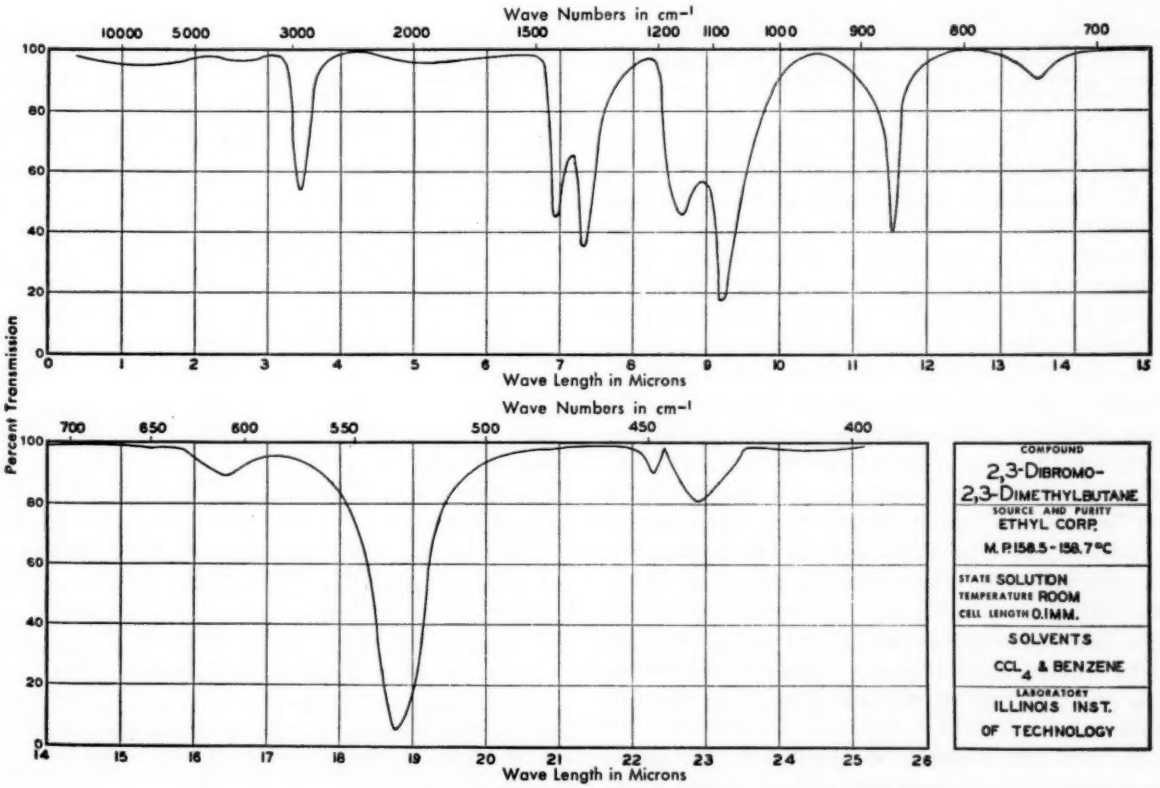

FIG. 1. Infra-red percent transmission curve for 2,3-dibromo-2,3-dimethylbutane.

[8] E. A. Crigler, J. Am. Chem. Soc. **54**, 4199 (1932).
[9] A. E. van Arkel and J. L. Snoek, Zeits. f. physik. Chemie **B18**, 159 (1932).

TABLE I. Raman and infra-red spectral data for 2,3-dibromo-2,3-dimethylbutane, $(CH_3)_2BrC-CBr(CH_3)_2$.*

Raman: Kahovec, Wagner** Solid $\Delta\nu$	I_e	Raman: Present results Solution CCl_4 $\Delta\nu$	Benzene $\Delta\nu$	I	ρ	Infra-Red: Present results Solution CCl_4 ν	Benzene ν	I_e
		178	179	100	0.51	The region below		
291	½	303	299	12	0.77	400 cm^{-1} was not		
						investigated.		
						437	437	w
						(449)	(449)	vw
			(532)	5		532	532	vvs
570	2	567	570	53	0.40			
						607	607	w
728	4	728	727	23	0.81			
						***	741	w
						868	869	vs
			892	4	*P*			
			935	3	*P*			
968	½		(966)	1				
						1088	1090	vvs
1109	4	1117	1116	14	0.58			
						1157	1160	vs
1239	½		1240	1				
			1297	1				
						1374	1380	vs
1390	90		1392	1				
1443	½		1430	2				
						1442	***	vs
2728	00		2720	1				
		2864	2868	10	0.54			
2925	3	2935	2933	21	0.07	2928	***	vs
2984	3	2985	2982	8	0.95			
		3009	3003	8				

* $\Delta\nu$ = Raman displacement in cm^{-1}; I = semiquantitative relative intensities, I_e = estimated relative intensities (s = strong, w = weak, v = very); ρ = depolarization factor; ν = the wave number in cm^{-1} corresponding to the maximum adsorption in the infra-red band; and P = apparently polarized, but too weak for quantitative measurement; and data in regard to which there is some uncertainty are enclosed in parentheses.
** See reference 2.
*** Bands covered by strong solvent bands.

of zero in CCl_4 solution, but obtained a dipole moment of 1.35D. in benzene solution. This would imply a difference in structure in the two solvents. If *DB* behaves similarly—as one would expect—differences in the spectra of the CCl_4 and benzene solutions should have been found. Examination of Table I shows that no more infra-red bands were obtained for the benzene than for the CCl_4 solution; and while 9 more Raman lines were obtained for the benzene than for the CCl_4 solution, all of the additional lines are weak and can be accounted for by the observed fact that the *DB* was about twice as soluble in benzene as in CCl_4. This is further borne out by the certainty that—whatever the structure in CCl_4—the 1430 cm^{-1} C−H deformation line should have been present; its absence must surely be attributed to the smaller concentration in this solvent. Consequently, on the basis of the Raman and infra-red spectra, there does not appear to be a difference in the structure of the *DB* molecule in the two solvents.

If the *DB* has a center of symmetry, the dipole moment (for which we could find no value in the literature) should be zero. To check this point, as well as the possibility of a difference in structure in the CCl_4 and benzene solutions, Professor Mizushima kindly offered to measure the dipole moment of the two solutions used in our spectroscopic investigation. The dipole moment obtained[10] for the *DB* in the CCl_4 solution was 1.01D. and the corresponding value in benzene solution was 1.20D., both at 25°C. Previously, Mizushima, Morino, and Higasi[11] had measured the dipole moment of 1,2-dibromoethane (*DBE*) in the same solvents and had obtained 0.86D. in the CCl_4 solution and 1.18D. in the benzene solution, both at 20°C. From this they

TABLE II. Raman and infra-red spectral data for 2,2,3,3-tetramethylbutane (hexamethylethane), $(CH_3)_3C-C(CH_3)_3$.*

Raman: Present results (solution) $\Delta\nu$	I	ρ	O.R. (gas) ν	I_e	Infra-Red: S.D.C. (solution) ν	I_e	Present results (solution) ν	I_e
385	33	0.88					The region below	
481	26						400 cm^{-1} has not	
647	80	0.10					been investigated.	
			679	vw				
			735	w				
			788	vw				
			796	m	797	6	795	m
808	vw		803	w				
819	8	0.93						
(844)	vw							
876	16	0.44			870	0		
					892	0		
923	20	0.51						
			931	m	932	4	928	m
			999	m	997	3	997	w
1005	1							
1044	3				1040	1		
1068	2							
			1184	vs	1180	10	1182	vvs
1238	20	0.74			(1235)	0		
1258	8	0.93						
			1315	vw				
1371	1				1373	10		
1389	2		1380	vs	1383		1376	vvs
1449	18	0.77			1468	10		
1475	86	0.87	1477	w	1477		1472	vvs
					(1631)	0		
					1718	3		
					1828	1		
					1965	0		
			2034	w	2035	1		
					2160	0		
			2286	vw	2295	1		
			2392	vw	2410	1		
					2555	0		
			2614	w	(2645)	0		
			2731	w	2740	1	2738	w
2879	23	0.40						
2911	63	0.29						
2936	53	0.52	2938	s	2970	10	2924	vvs
2957	100	0.50						
2972	86							
			3226	m	3205	2	3203	w
			3367	vw	(3335)	0		
			3455	w	(3415)	0		
			**3610	w				
			3871	w	3860	0		
			4153	m	4130	3	4155	w
			4323	m	4310		4377	w
			5967	vw			5814	w

* O.R. = Oetjen and Randall, reference 3; S.D.C. = Shell Development Company, reference 4; s = strong, m = medium, vw = very weak; other symbols same as in Table I.
** "Probably due to impurity in sodium chloride prism."

[10] Mizushima, Morino, and Miyagawa, private communication, February 28, 1950.
[11] Mizushima, Morino, and Higasi, Physik. Zeits. **35**, 905 (1934).

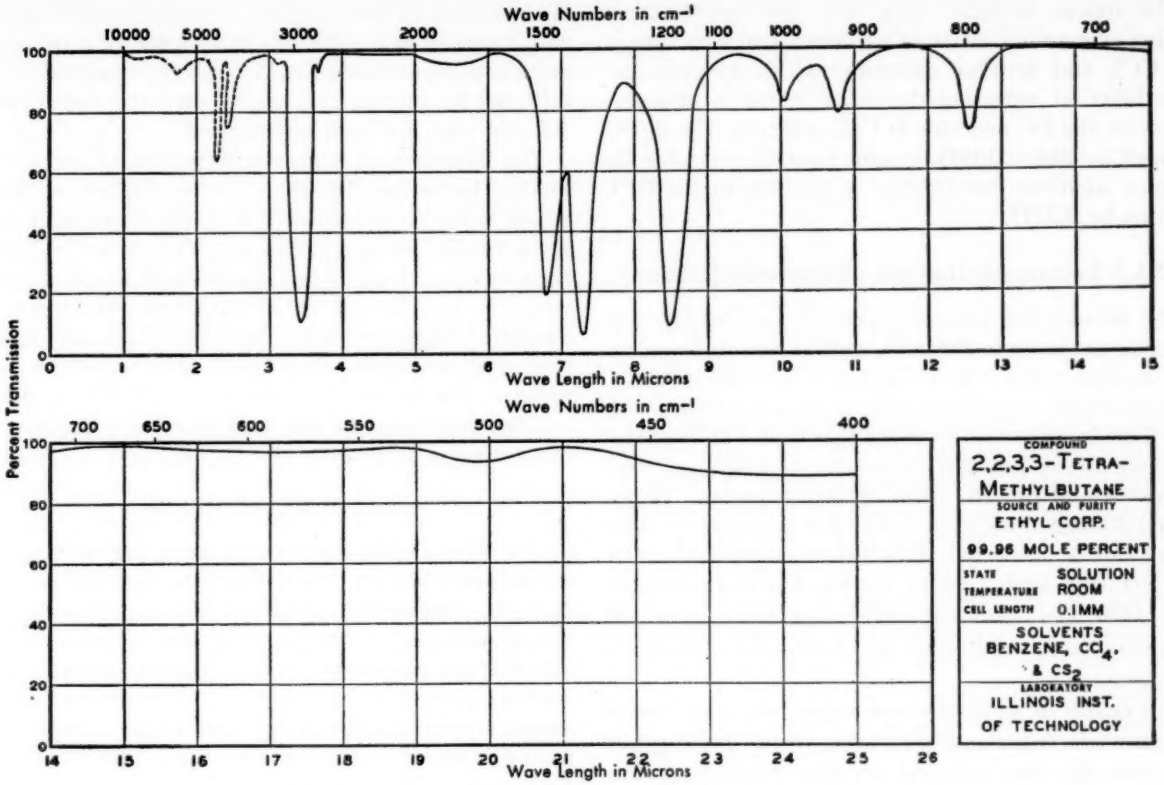

FIG. 2. Infra-red percent transmission curve for 2,2,3,3-tetramethylbutane.

concluded that the *DBE* existed in both the *trans-* (with center of symmetry) and *gauche* (120° rotation from trans position about the C−C bond) forms. Since the dipole moment of *DB* is not much different from that of the *DBE*, Mizushima, Morino, and Miyagawa conclude that—so far as the dipole moment is concerned—the *DB* molecule also seems to exist in both the *trans-* and *gauche* forms.

The spectroscopic data, on the other hand, can—as has been shown above—be interpreted on the basis of the existence of the *trans-* form alone. The number of lines observed for *DB* does not seem sufficient to indicate two forms for this molecule, since only 8 Raman lines were observed below 1100 cm^{-1} for *DB*, whereas 17 were observed in this region for the *DBE*.[12] It is, of course, possible that some of the Raman or infra-red bands may have been so weak as to escape observation. But if the *gauche* form does exist, coincident Raman and infra-red bands would be allowed by the selection rules, and—unless the concentration of this form is very small—it seems that at least some of the *gauche* bands should have been strong enough to have been observed as coincident Raman and infra-red bands. (The doubtful 532 cm^{-1} band might be such a coincidence, but this seems doubtful in view of the large intensity of the infra-red band.)

The observed dipole moment of 1.01D.—obtained in the CCl_4 solution—can be explained by assuming that all of the molecules are oscillating with harmonic motion and with equal amplitudes of 48° about the equilibrium *trans-* position. This result was obtained from the time average of the square of the dipole moment, namely

$$\mu^2 = 16(\mu_p^2/T)\int_0^{\frac{1}{4}T} \sin^2\tfrac{1}{2}[\beta_m \sin(2\pi/T)t]dt,$$

where μ is the magnitude of the observed dipole moment, μ_p is the component perpendicular to the central C−C axis of the $-CBr(CH_3)_2$ group moment, T is the period of oscillation of one group relative to the other about the central C−C axis, β_m is the maximum angular displacement from the equilibrium *trans-* ($\beta=0$) configuration, and t is the time; $\beta=\beta_m \sin(2\pi/T)t=0$ when $t=0$.[13] The value used for the C−Br and C−CH_3 bond moments were −1.5 and +0.4D., respectively, and the value obtained for μ_p was 1.79D. The moment obtained in CCl_4 solution was used, rather than that obtained in benzene solution, because abnormally large values are frequently obtained for the dipole moment of halogen compounds in benzene solution.[14] The integral was evaluated by numerical integration.

[12] See Ta-You Wu, *Vibrational Spectra and Structure of Polyatomic Molecules* (Edwards Brothers, Ann Arbor, Michigan, 1946), 2nd edition, 306–312.

[13] See R. J. W. Le Fèvre, *Dipole Moments* (Methuen and Company, Ltd., London or John Wiley and Sons, Inc., New York, 1948), 2nd Edition, p. 89.

[14] See reference 13, p. 102.

The dipole moment data, like the spectroscopic results, give no indication of a difference in structure in the CCl_4 and benzene solutions, which suggests the desirability of repeating the dipole moment measurements for the *DC* molecule in CCl_4 solution. The dipole moment for *DB* is 0.19D. less for the CCl_4 than for the benzene solution. For *DBE* it is also less in the CCl_4 solution by 0.32D.[14]

2,2,3,3-Tetramethylbutane (Hexamethylethane)

The Raman and infra-red spectral data for the *TM* molecule are given in Table II, and the infra-red percent transmission curve is shown in Fig. 2. For this molecule, 22 Raman lines were observed, as compared with 18 for *DB*. This is consistent with the fact that *TM*, containing more atoms, has 72 fundamental vibrations, as compared with 54 or *DB*. Here again the number of observed Raman lines is so small that a center of symmetry can be suspected. This suspicion is borne out by the fact that again, except for the C—H frequencies near 1450 and 2925 cm^{-1} where several unresolved lines may exist, the Raman and infra-red bands do not coincide.

If a center of symmetry does exist, the structure of the molecule is that corresponding to the point group D_{3d}. For this structure, the selection rules allow $8A_{1g}$ fundamentals, polarized in the Raman, forbidden in the infra-red; $5A_{1u}$ and $4A_{2g}$, forbidden in both Raman and infra-red; $7A_{2u}$, forbidden in the Raman, parallel bands in the infra-red; $12E_g$, depolarized in the Raman, forbidden in the infra-red; and $12E_u$, forbidden in the Raman, perpendicular bands in the infra-red.

Consequently, if the center of symmetry exists and if all lines are resolved, one would expect to observe 8 polarized and 12 depolarized Raman lines (a total of 20) and 19 infra-red bands corresponding to fundamentals. We observed 22 Raman lines, of which 8 were polarized and 5 depolarized, which is in reasonably good agreement with this expectation. A similar comparison for the infra-red bands cannot be made since the region below 400 cm^{-1} has not been investigated.

The existence of a center of symmetry for *TM* is further borne out by the electron diffraction data[15] which favor this structure. The dipole moment data are not as decisive for *TM* as for *DB*, since in the former the contribution of the carbon skeleton to the moment would be zero for any rotational isomer. However, the moment arising from the H atoms would be zero only if their orientations are such that a center of symmetry is present. The observed dipole moment[16] is only 0.1D., which is small enough to be consistent with the presence of a center of symmetry.

ACKNOWLEDGMENTS

The Hilger E518 spectrograph used for the depolarization spectrograms was obtained in part with a grant from the American Academy of Arts and Sciences, and the optical parts of the two-prism spectrograph used for the Raman displacement spectrograms were secured with a grant from the Society of the Sigma Xi. The samples were furnished by the Ethyl Corporation, Detroit, Michigan, through the courtesy of Dr. George Calingaert. The use of the Beckman IR-2 spectrophotometer at Ohio State University was at the kind invitation of Professor Harald H. Nielsen, Chairman of the Department of Physics. The authors are grateful for this assistance. Thanks also are due to Professor San-ichiro Mizushima, Tokyo University, for helpful correspondence and for permission to quote the dipole moment results.

[15] S. H. Bauer and J. Y. Beach, J. Am. Chem. Soc. **64**, 1142 (1942).
[16] L. Tiganik, Zeits. f. physik. Chemie **B13**, 425 (1931).

Oxygen and Nitrogen Isotope Effects in the Decomposition of Ammonium Nitrate*

LEWIS FRIEDMAN AND JACOB BIGELEISEN
Chemistry Department, Brookhaven National Laboratory, Upton, Long Island, New York
(Received June 28, 1950)

The isotopic composition of the products of the controlled thermal decomposition of ammonium nitrate has been studied. It has been found that small amounts of water are necessary to initiate the decomposition of ammonium nitrate. $N^{15}H_4NO_3$ has been found to yield exclusively the isomer $N^{15}N^{14}O$. Some inferences are drawn from this observation regarding the mechanism of the reaction.

Oxygen and nitrogen isotope effects accompanying the decomposition have been studied with material of "natural" isotopic composition. Satisfactory agreement is found between the experimental results and theoretical calculations.

A method for the isotopic analysis of nitrates for O^{18} is outlined.

I. INTRODUCTION

As part of a program aimed at studying the effect of isotopic substitution on chemical equilibria and the rates of chemical reactions, we have investigated the decomposition of ammonium nitrate for nitrogen and oxygen isotope effects both during the course of the reaction and at complete decomposition. In the course of our work we have made some observations which are pertinent to the mechanism of the decomposition. We have prepared a sample of N_2O containing enriched N^{15} in the end position exclusively. In view of the current status of the analysis of the vibrational spectrum of N_2O,[1] we have investigated the infrared spectrum of $N^{15}N^{14}O^{16}$. A similar and concurrent investigation of the infra-red spectrum has been carried out by Richardson and Wilson.[2] At present we are studying the infra-red spectrum of $N^{14}N^{15}O^{16}$, and the results of the spectroscopic study of these two isomers as well as their thermodynamic properties will be communicated shortly. The results of the study of the isotope effects accompanying the decomposition are presented in this paper.

II. DECOMPOSITION OF NH_4NO_3

The decomposition of ammonium nitrate has been investigated repeatedly.[3] In the temperature region between 180–300°C pure molten ammonium nitrate decomposes according to the equation

$$NH_4NO_3 \rightarrow N_2O + 2H_2O. \quad (1)$$

We wish to record here an observation which has not been described previously. A three-gram sample of J. T. Baker's "C.P. Analyzed" NH_4NO_3 was put into a glass apparatus shown schematically in Fig. 1. The sample was held at approximately 150°C and pumped overnight by the mercury diffusion pump. The system closed off from the pump was capable of maintaining a vacuum of better than 10^{-5} mm over a period of hours. During the pumping operation all of the ammonium nitrate sublimed to the cool portion of the tube above the furnace. The furnace was then raised and the temperature gradually increased over a period of hours to about 300°C. There was no decomposition detectable manometrically with the reservoir bulbs shut off from the system. The furnace was removed and a small amount of water vapor was admitted to the system. The furnace was then replaced around the tube containing the NH_4NO_3 and the decomposition commenced at about 180°C. The experiment was completely reproducible, and we find that ammonium nitrate which has been thoroughly dried does not decompose up to 300°C. A similar experiment was tried using dry N_2O. The N_2O sufficed to prevent sublimation but did not induce the decomposition.

A qualitative experiment was carried out to determine the role of the water in initiating the reaction. A small amount (4 cc at N.T.P.) of water vapor containing 1.5 percent H_2O^{18} was used to initiate the decomposition of a three-gram sample of NH_4NO_3. The reaction was continued until about 4 cc of N_2O were produced. The N_2O was examined mass spectrometrically and the O^{18}/O^{16} ratio was within 0.3 percent of that found in N_2O samples obtained from the decomposition initiated by ordinary water. From this we conclude that the water does not enter into reactions which lead directly to the formation of N_2O.

Apart from our observations on the catalytic effect of water, our experimental results on the decomposition are in agreement with those of Kretzschmar.[3c] In our experiments the water from the decomposition was removed in trap A, which was cooled to −80°C after the decomposition had been initiated by the addition of small amounts of water. The gas, non-condensable at −80°C, was 98 percent N_2O; the remainder was N_2 and may have contained some O_2.

Kummer[4] has reported some isotopic analyses of nitrogen produced by the reduction of N_2O, formed from the decomposition of 62 percent $N^{15}H_4NO_3$, by

* Research carried out under the auspices of the AEC.

[1] See G. Herzberg, *Infrared and Raman of Polyatomic Molecules* (D. Van Nostrand Company, Inc., New York, 1945), p. 174.

[2] W. S. Richardson and E. B. Wilson, Jr., J. Chem. Phys. **18**, 694 (1950).

[3] See (a) H. L. Saunders, J. Chem. Soc. **121**, 698 (1922); (b) M. S. Shah and T. M. Oza, *ibid.* 725 (1932); (c) W. Kretzschmar, Zeits. f. anorg. u. allgem. Chemie **219**, 17 (1934); (d) H. Tramm and H. Velde, Angew. Chem. **47**, 782 (1934).

[4] J. T. Kummer, J. Am. Chem. Soc. **69**, 2559 (1947).

iron at room temperature. Kummer finds 0.35 percent $N^{15}N^{15}$ in the nitrogen as against the expected 0.24 percent if the ammonium ion reacted with the nitrate ion by an N−N bond formation. If the N_2O were formed from some intermediate such as nitroxyl, Eqs. (3a) and (4a) below, the nitrogen analyzed by Kummer would contain 9.6 percent $N^{15}N^{15}$, which figure would also be expected for any mechanism in which the ammonium and nitrate nitrogen atoms become randomly mixed. His results therefore rule out the possibility that N_2O is formed by an oxidation-reduction mechanism of the type

$$NH_4^+ + NO_3^- \rightarrow NH_3OH^+ + NO_2^-, \quad (2)$$

$$NH_3OH^+ + NO_2^- \rightarrow 2NOH + H_2O, \quad (3a)$$

$$2NOH \rightarrow N_2O + H_2O, \quad (4a)$$

but they furnish no evidence for or against an alternative oxidation-reduction mechanism proceeding through hyponitrous acid.

$$NH_3OH^+ + NO_2^- \rightarrow H_2N_2O_2 + H_2O \quad (3b)$$

$$H_2N_2O_2 \rightarrow N_2O + H_2O. \quad (4b)$$

The production of N_2O from hyponitrous acid predicts equal amounts of the isomers $N^{15}N^{14}O$ and $N^{14}N^{15}O$, apart from small isotope effects, unless one postulates an unsymmetrical structure for hyponitrous acid. Most of the evidence points to the structure HONNOH for this acid.[5,6]

From Kummer's experiment it is not possible to determine which of the isomers $N^{15}N^{14}O^{16}$ or $N^{14}N^{15}O^{16}$ or whether a mixture of these isomers is formed from the decomposition of $N^{15}H_4N^{14}O_3$. By means of microwave spectroscopy, Richardson and Wilson[2] have established that $N^{15}N^{14}O^{16}$ is formed from the decomposition of $N^{15}H_4N^{14}O_3$. We have also established this fact independently with the mass spectrometer. A sample of N_2O was prepared from NH_4NO_3 containing 7.5 percent N^{15} in the NH_4^+ ion. The $N^{15}H_4NO_3$ was obtained from the Eastman Kodak Company. A 2.4-gram sample was decomposed after thorough evacuation drying and then the addition of trace amounts of water. The N_2O was collected and analyzed mass spectrometrically in a Consolidated-Nier "Isotope Ratio" mass spectrometer. The results of the analyses are given in Table I.

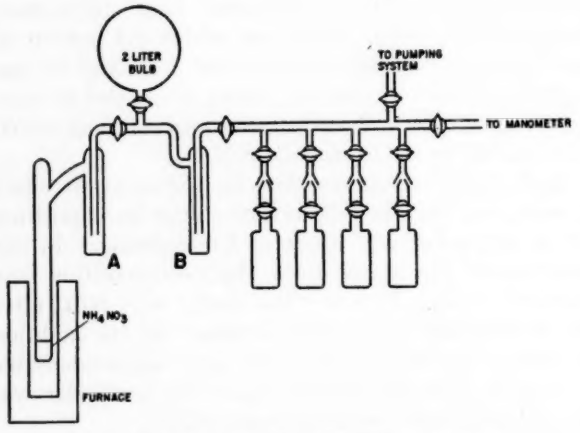

FIG. 1. Vacuum line for the decomposition of ammonium nitrate (schematic).

If the isomer $N^{15}N^{14}O^{16}$ is produced then the intensity ratio of 31/30, corresponding to the NO^+ ions, should be that due to normal N^{15} and O^{17} isotopic abundance or 0.0042.† On the other hand, if the isomer $N^{14}N^{15}O^{16}$ is produced, then the 31/30 ratio for this experiment should be 0.0830. If a mixture of the two isotopic isomers is formed, the the 31/30 ratio will measure their relative abundances. The possibility of rearrangement on electron impact in the mass spectrometer may give a value intermediate between 0.0042 and the 45/44 ratio corrected for the presence of two N atoms in N_2O, even if an authentic sample of $N^{15}N^{14}O^{16}$ were analyzed. However, fortunately such rearrangements appear to be uncommon and, where they do occur, they are usually less than 10 percent of the more normal simple rupture of chemical bonds by electron impact. It is clear from the data in Table I that our sample contains less than seven percent of the N^{15} from the NH_4^+ in the form of the isomer $N^{14}N^{15}O^{16}$. The fact that the 31/30 ratio is 0.010 rather than 0.0042 may be due either to production of $N^{14}N^{15}O$ in the course of the decomposition reaction or to production of $N^{15}O^+$ ions from $N^{15}N^{14}O$ by electron impact or a combination of both. Richardson and Wilson[2] have shown by microwave spectroscopy that no $N^{14}N^{15}O$ above that expected from the normal abundance of N^{15} in nitrate is formed in the decomposition of $N^{15}H_4N^{14}O_3$. Therefore we infer that there is a seven percent rearrangement on electron impact.

Our results, as well as those of Kummer[4] and Richardson and Wilson,[2] lead us to suggest that the decomposition of ammonium nitrate proceeds by a dehydration mechanism:

$$NH_4^+ + NO_3^- \rightarrow H_2N-NO_2 + H_2O, \quad (5)$$

$$H_2N-NO_2 \rightleftarrows HN=NO_2^- + H^+ \rightleftarrows HN=N(=O)(OH), \quad (6)$$

$$H-N=N(=O)(OH) \xrightarrow[\text{or Acid catalysis}]{\text{Basic}} N_2O + H_2O. \quad (7)$$

Reactions (6) and (7) are the mechanisms which have

[5] E. C. E. Hunter and J. R. Partington, J. Chem. Soc. 309 (1933).
[6] A. Hantzsch, Ber. 66, 1555 (1933).

† This value is calculated from the data in Table II, the "natural" abundance of O^{17}, and an average value for certain instrumental factors.

been proposed to explain the acidic[7] and basic[8] catalysis in the decomposition of nitramide. From our analyses of the N_2O formed from the decomposition of $N^{15}H_4N^{14}O_3$ and Kummer's analysis of the N_2 formed on reduction we conclude that the N—N bond is not broken in the adsorption and reduction of N_2O on catalytic iron at room temperature.

III. N^{15} AND O^{18} ISOTOPE EFFECTS IN THE DECOMPOSITION OF NH_4O_3. THE ISOTOPIC COMPOSITION OF NH_4NO_3

A. Experimental

Prior to measurement of the O^{18} isotope effect on the decomposition, we have reinvestigated and extended the exchange study of oxygen between N_2O and water. Previous investigation by density measurements on water slightly enriched in O^{18} showed no exchange between N_2O and water in 14 days at 20°C.[9] Our experiments were carried out with 1.5 percent H_2O^{18} and the N_2O was analyzed mass spectrometrically. We find 0.26 percent exchange in three days at 24±1°C between N_2O gas and liquid water. At 195±2°C we find 0.68 percent exchange in 22 hours between water vapor at a partial pressure of 0.8 atmospheres and N_2O at a partial pressure of 0.0017 atmospheres. Thus the exchange between N_2O and water is negligible under the conditions of our experiments.

It is not surprising that N_2O exchanges slowly with water. Solutions of N_2O in water show no acidic properties[10] despite the fact that N_2O is the stoichiometric anhydride of hyponitrous acid and is formed from the decomposition of the latter. Furthermore, N_2O is salted out of water by all electrolytes, including bases, except nitric acid.[10,11]

The decomposition reactions were carried out by the method described in Section II. The decomposition temperature was 220°±20°C. Temperature control was difficult because of the large heat evolved in the reaction. The N_2O formed after one percent decomposition was collected in a bulb. The reaction was then carried to completion and the N_2O and water were separated continuously by cold traps. The N_2O was purified by the use of cold traps from the small amounts of nitrogen and oxygen that arise from side reactions and analyzed as N_2O. The water was equilibrated with CO_2 and analyzed according to the method described by Cohn and Urey.[12] It does not seem feasible to obtain and analyze the water at one percent decomposition. Each sample was analyzed at least three times in a Consolidated-Nier "Isotope Ratio" mass spectrometer. The reproducibility of the analyses was better than 0.3 percent of the ratio measured.

TABLE I. Analysis of N_2O prepared from 7.5 percent $N^{15}H_4N^{14}O_3$.

Peak ratio measured	Ion	Ratio
45/44	N_2O^+	0.0869
31/30	NO^+	0.010
29/28	N_2^+	0.081

The Consolidated-Nier "Isotope Ratio" mass spectrometer is a dual collector instrument and is used to measure isotope ratios directly. In the analysis for N^{15} in N_2O, measurements can be made by measuring the 45/44 ratio directly. Analysis for O^{18} in either N_2O or CO_2 can be made by measuring the 46/44+45 ratio and correcting for the 45/44 ratio. The intercomparison of samples with nearly identical isotopic composition can be made with little error by comparison of the directly determined ratios. Samples of widely different isotopic composition were compared only after correction for incomplete resolution on the isotopic peaks of 45 and 46 from the normal peak at 44 and the relative efficiencies of collection and amplification through the two collectors. The intercomparison between O^{18}/O^{16} in N_2O and CO_2 is made here after direct experimental determination of these factors. No correction need be made for a possible mass discrimination effect because both O^{18}/O^{16} ratios are derived from 46/44 ratios. The intercomparison between N_2O samples for 45/44 and 46/44+45 is made from the uncorrected ratios. The resolution corrections and collector efficiencies remained constant during the determination of these uncorrected ratios. This was demonstrated by the reproducibility of the measurements and alternate measurements of standard samples of N_2O and CO_2.

The ratio of O^{18}/O^{16} in N_2O is given by Eq. (8).

$$\frac{O^{18}}{O^{16}}=\frac{N^{14}N^{14}O^{18}+N^{15}N^{14}O^{18}+N^{14}N^{15}O^{18}+N^{15}N^{15}O^{18}}{N^{14}N^{14}O^{16}+N^{15}N^{14}O^{16}+N^{14}N^{15}O^{16}+N^{15}N^{15}O^{16}}$$

$$=\frac{N^{14}N^{14}O^{18}}{N^{14}N^{14}O^{16}}. \quad (8)$$

The experimentally determined 46/(44+45) and 45/44 ratios are given by Eqs. (9) and (10).

$$\frac{46}{44+45}=\frac{N^{14}N^{14}O^{18}+N^{15}N^{14}O^{17}+N^{14}N^{15}O^{17}+N^{15}N^{15}O^{16}}{N^{14}N^{14}O^{16}+N^{15}N^{14}O^{16}+N^{14}N^{15}O^{16}+N^{14}N^{14}O^{17}}, \quad (9)$$

$$45/44=\frac{N^{15}N^{14}O^{16}+N^{14}N^{15}O^{16}+N^{14}N^{14}O^{17}}{N^{14}N^{14}O^{16}}. \quad (10)$$

For samples containing O^{17} close to natural abundance

[7] C. A. Marlies and V. K. La Mer, J. Am. Chem. Soc. **57**, 1812 (1935).
[8] K. J. Pederson, J. Phys. Chem. **38**, 581 (1934).
[9] Winter, Carlton, and Briscoe, J. Chem. Soc. 131 (1940).
[10] G. Geffcken, Zeits. f. physik. Chem. **49**, 301 (1904).
[11] G. Lunge, Ber. **14**, 2188 (1881), W. Knopp, Zeits. f. physik. Chem. **48**, 97 (1904); W. Manchot, M. Johrstorfer and H. Zepter, Zeits. f. anorg. Chemie **141**, 45 (1924).
[12] M. Cohn and H. C. Urey, J. Am. Chem. Soc. **60**, 679 (1938).

TABLE II. Isotopic analysis of N_2O and H_2O formed in the decomposition of ammonium nitrate.

Sample analyzed	Ratio reported	Sample No. 1	Sample No. 2	Sample No. 3	Sample No. 4
Tank CO_2	$C^{12}O^{16}O^{18}/C^{12}O_2^{16}$ Corrected	$422.4\pm0.3\times10^{-5}$	$422.0\pm0.5\times10^{-5}$		
CO_2 from H_2O equilibration	$C^{12}O^{16}O^{18}/C^{12}O_2^{16}$ Corrected	$432.7\pm0.6\times10^{-5}$	$431.8\pm0.4\times10^{-5}$		
N_2O complete reaction (t_∞)	$\frac{N^{14}N^{14}O^{18}}{N^{14}N^{14}O^{16}}$ Corrected	$212.6\pm0.2\times10^{-5}$	$212.5\pm0.5\times10^{-5}$		
N_2O One percent decomposition (t_ϵ)	$\frac{N^{14}N^{14}O^{18}}{N^{14}N^{14}O^{16}}$ Corrected		$213.5\pm0.2\times10^{-5}$		
N_2O t_ϵ	46/44+45 Uncorrected			$232.7\pm0.5\times10^{-5}$	
N_2O t_∞	46/44+45 Uncorrected			$233.8\pm0.4\times10^{-5}$	
N_2O t_ϵ	45/44 Uncorrected			$875.0\pm2.7\times10^{-5}$	$866.5\pm0.3\times10^{-5}$
N_2O t_∞	45/44 Uncorrected			$880.8\pm1.0\times10^{-5}$	$873.4\pm0.5\times10^{-5}$
	$\left(\frac{45}{44}\right)_{t_\infty}\Big/\left(\frac{45}{44}\right)_{t_\epsilon}$			1.007 ± 0.004	1.008 ± 0.001
	$\left(\frac{46}{44}\right)_{t_\infty}\Big/\left(\frac{46}{44}\right)_{t_\epsilon}$		0.9953 ± 0.003	1.0047 ± 0.004	
	$(H_2O'^8/H_2O^{16})_{t_\infty}$	$208.0\pm0.3\times10^{-5}$	$207.6\pm0.2\times10^{-5}$		
	$\left(\frac{N_2O^{18'}}{N_2O^{16}}\right)\Big/\left(\frac{H_2O^{18'}}{H_2O^{16}}\right)_{t_\infty}$	1.022 ± 0.003	1.024 ± 0.003		

we get from Eqs. (9) and (10)

$$\frac{N^{14}N^{14}O^{18}}{N^{14}N^{14}O^{16}}=\frac{46}{44+45}\left(1+\frac{45}{44}\right)-\frac{1}{4}\left(\frac{45}{44}-0.0004\right)^2-(0.0004)\frac{45}{44}. \quad (11)$$

For the analysis of water by the equilibration method of Cohn and Urey[12] we need the ratio $C^{12}O^{16}O^{18}/C^{12}O^{16}O^{16}$ and the equilibrium constant for the reaction

$$C^{12}O^{16}O^{16}(g)+H_2O^{18}(l)=C^{12}O^{16}O^{18}(g)+H_2O^{16}(l). \quad (12)$$

For CO_2 with both C^{13} and O^{17} close to natural abundance the ratio $C^{12}O^{16}O^{18}/C^{12}O^{16}O^{16}$ is given by Eq. (13).

$$\frac{C^{12}O^{16}O^{18}}{C^{12}O^{16}O^{16}}=\frac{46}{44+45}\left(1+\frac{45}{44}\right)-(0.0008)\frac{45}{44}-(0.0004)^2. \quad (13)$$

The samples of water and CO_2 were equilibrated at 24°C and the equilibrium constant (12) was taken as $2\times(1.040)$.[12–14]

The results of the analysis are given in Table II. The reproducibility of the analysis between the different samples was better than 0.3 percent of the ratio. None of the ratios reported should be considered absolute ratios because of an undetermined mass discrimination effect. There is a fortuitous agreement between our 46/44 ratio for tank CO_2 and Thode's[15] results for CO_2 equilibrated with Lake Ontario water ($422\pm1\times10^{-5}$). From the analysis of samples 2 and 3 we conclude that the O^{18} content of the N_2O does not change by more than one-half of one percent during the course of the decomposition. Thus the isotopic analysis of any sample of N_2O from the decomposition of NH_4NO_3 can be used to analyze nitrates for O^{18}. In most cases it might be preferable to analyze nitrates by analysis of the water formed in the decomposition because the precision of CO_2 analysis is in general better than N_2O analyses and N_2O pumps out of the mass spectrometer extremely slowly. Samples of N_2O with abnormal isotopic composition will introduce a memory effect because of the latter fact.

From the CO_2 and N_2O analyses performed on samples 1 and 2, the fact that tank CO_2 is in equilibrium with fresh water,[12,14] and the stoichiometry of Eq. (1), we can compare the O^{18} content of our ammonium nitrate sample with that of fresh water. We get as the average of these two samples the ratio of O^{18} to O^{16} in ammonium nitrate compared to the similar ratio in fresh water $3\times(1.032\pm0.003)$. The ammonium nitrate used in this investigation is reported to be entirely of synthetic origin.[16] Synthetic nitrates have most of their

[12] Weber, Wahl, and Urey, J. Chem. Phys. **3**, 129 (1935).
[14] H. C. Urey, J. Chem. Soc. 562 (1947).

[15] H. G. Thode, Report No. MC-57, National Research Council of Canada. McMaster University, Hamilton, Ontario (April 29, 1944). Also reported by K. T. Bainbridge to the Seventh International Solvay Congress on Chemistry. R. Stoops, Editor, *Rapports et Discussions sur Les Isotopes* (Brussells, 1948), p. 84.
[16] Private communication from Dr. J. R. Stevens, J. T. Baker Chemical Co.

oxygen derived from atmospheric oxygen, which Dole[17] has shown to be enriched in O^{18} over fresh water by 1.030. This is very close to the enrichment found in our nitrate sample. In view of the fact that nitrates do not exchange oxygen with water[18] we conclude that the fractionation in the catalytic synthesis of nitrates is small. Detailed calculations would require more extensive knowledge than is available of the actual processes in the synthesis plants.

In the intercomparison of the abundance of O^{18} in nitrous oxide and water formed from the decomposition of ammonium nitrate as determined from N_2O^{18}/N_2O^{16} and $CO^{16}O^{18}/CO_2^{16}$ respectively we have made the tacit assumption that if there is any isotope effect in the production of the parent ions by electron impact in the mass spectrometer it is the same in both cases. A theoretical estimate of the magnitude of this effect, based on the assumption that there is no isotope effect on the total ions produced by electron impact and a five percent O^{18} isotope effect on bond rupture, indicates that the O^{18}/O^{16} ratio in N_2O may be too high by as much as one percent. Therefore the assumption with regard to equal isotope effect on the production of the parent ions N_2O^+ and CO_2^+ was investigated experimentally. From the data in Table II we find that the ratio of $(N_2O^{18})/(N_2O^{16})_{t_\infty}/(H_2O^{18})/(H_2O^{16})_{\text{water}}^{\text{fresh}}$ is 1.047 ± 0.003. This ratio is based on the N_2O and tank CO_2 analyses, the equilibrium constant K_{12}, and the assumption of no difference in the electron impact isotope effect on the parent ions N_2O^+ and CO_2^+. A sample of N_2O was decomposed completely to nitrogen and oxygen in a quartz vessel at 1000°K. The O^{18} in the oxygen was compared with the O^{18} content of atmospheric oxygen by measurement of 34/32+33 ratios. As a result of this intercomparison and Dole's determination of the relative abundance O^{18} in atmospheric oxygen and fresh water by density measurements,[17] we get $(N_2O^{18})/(N_2O^{16})_{t_\infty}/(H_2O^{18})/(H_2O^{16})_{\text{water}}^{\text{fresh}}$ is equal to 1.045 ± 0.003. The agreement for this ratio as determined by the latter method, which is independent of the equilibrium constant K_{12} and the assumption concerning isotope effects in the production of parent ions, with the ratio calculated from Table II is within the limit of our experimental errors and the uncertainty in K_{12}. For the parent ions N_2O^+ and CO_2^+ we may therefore neglect any difference in the ratios N_2O^{18}/N_2O^{16} and $CO^{16}O^{18}/CO_2^{16}$ arising from isotope effects on electron impact. The agreement of the intercomparison of O^{18} in nitrous oxide and fresh water by these two methods serves as a good check on the reliability of the data in Table II.

B. Theoretical

The experimental results on the nitrogen isotope effect cannot be interpreted unambiguously. The nitrogen isotope effect measured at small amounts of reaction is an undetermined combination of two effects: N^{15} substitution in the ammonium ion and N^{15} substitution in the nitrate ion. The effect of N^{15} substitution in each ion has yet to be determined. For this reason, as well as the fact that our knowledge of the mechanism and the kinetics of the decomposition reaction is meager, no calculations of the nitrogen isotope effect have as yet been carried out.

In spite of the limitations of our knowledge of the mechanism and kinetics of the decomposition, some interesting predictions can be made about the oxygen isotope effects from some rather general models of the activated complex and the mechanism of the reaction. For the purpose of the calculations we assume that the reaction proceeds by the successive elimination of two molecules of water from one ammonium ion and one nitrate ion. The intermediate chemical species may be nitramide or some other substance. The oxygen bound to the nitrogen is assumed to be in the form of a nitro group. This mechanism is consistent with our results on the decomposition of $N^{15}H_4NO_3$. The following equations are assumed for the purpose of calculation

$$NH_4^+ + NO_3^{16-} \rightarrow NH_2NO_2^{16} + H_2O^{16}, \quad (14)$$

$$NH_4^+ + NO_2^{16}O^{18-} \rightarrow NH_2NO_2^{16} + H_2O^{18}, \quad (15)$$

$$NH_4^+ + NO_2^{16}O^{18-} \rightarrow NH_2NO^{16}O^{18} + H_2O^{16}, \quad (16)$$

$$NH_2NO_2^{16} \rightarrow N_2O^{16} + H_2O^{16}, \quad (17)$$

$$NH_2NO^{16}O^{18} \rightarrow N_2O^{16} + H_2O^{18}, \quad (18)$$

$$NH_2NO^{16}O^{18} \rightarrow N_2O^{18} + H_2O^{16}. \quad (19)$$

We shall assume that the nitramide or analogous intermediate formed in reactions (14)–(16) is present in a steady state concentration. With this assumption and the further assumption that the contributions of reactions (16) and (19) to the total amount of H_2O^{16} can be calculated without regard to isotope effects (they contribute a small fraction of the total H_2O^{16} formed), and a similar assumption with regard to the production of N_2O^{16} from $NO_2^{16}O^{18-}$, we find

$$\frac{\left(\frac{N_2O^{18}}{N_2O^{16}}\right)_{t_\infty}}{\left(\frac{H_2O^{18}}{H_2O^{16}}\right)_{t_\infty}} = \frac{2\left(\frac{k_{16}}{k_{15}+k_{16}}\right)\left(\frac{k_{19}}{k_{18}+k_{19}}\right)}{\left(\frac{k_{15}}{k_{15}+k_{16}}\right)+\left(\frac{k_{16}}{k_{15}+k_{16}}\right)\left(\frac{k_{18}}{k_{18}+k_{19}}\right)}, \quad (20)$$

and

$$\frac{\left(\frac{N_2O^{18}}{N_2O^{16}}\right)_{t_\epsilon}}{\left(\frac{N_2O^{18}}{N_2O^{16}}\right)_{t_\infty}} = \frac{k_{15}+k_{16}}{k_{14}}. \quad (21)$$

[17] M. Dole, Science **109**, 77 (1949).
[18] N. F. Hall, and O. R. Alexander, J. Am. Chem. Soc. **62**, 3455 (1940).

TABLE III. Distribution of O^{18} between N_2O and H_2O in the decomposition of ammonium nitrate.

	$\left(\frac{N_2O^{18}}{N_2O^{16}}\right)_{t_\infty} / \left(\frac{H_2O^{18}}{N_2O^{16}}\right)_{t_\infty}$
Model *A*	1.034
Model *B*	1.026
Experimental	1.023±0.003

The general theory of the effect of isotopic substitution on the rates of chemical reactions[19] leads to the relation

$$\frac{k_1}{k_2}=\frac{s_1s_2\ddagger}{s_2s_1\ddagger}\frac{K_1}{K_2}\left(\frac{m_2^*}{m_1^*}\right)^{\frac{1}{2}} \times\left[1+\sum_i^{3n-6} G(u_i)(u_{i(1)}-u_{i(2)}) - \sum_i^{3n'-6} G(u_i\ddagger)(u_{i(1)}\ddagger-u_{i(2)}\ddagger)\right] \quad (22)$$

for the ratio of the rate constants of two isotopic molecules.[20] In the comparison of k_{16} with k_{15} and k_{19} with k_{18} respectively it is to be noted that $u_{i(15)}=u_{i(16)}$ and $u_{i(18)}=u_{i(19)}$. This leads to the ratios necessary for the evaluation of Eqs. (20) and (21).

$$\frac{k_{16}}{k_{15}}=2\left(\frac{m_{15}^*}{m_{16}^*}\right)^{\frac{1}{2}}\left[1-\sum_i^{i=21} G(u_i\ddagger)_{15,16}(u_{i(16)}\ddagger-u_{i(15)}\ddagger)\right] \quad (23)$$

$$\frac{k_{19}}{k_{18}}=\left(\frac{m_{18}^*}{m_{19}^*}\right)^{\frac{1}{2}}\left[1-\sum_i^{i=12} G(u_i\ddagger)_{18,19}(u_{i(19)}\ddagger-u_{i(18)}\ddagger)\right] \quad (24)$$

$$\frac{k_{14}}{k_{15}}=3\left(\frac{m_{15}^*}{m_{14}^*}\right)^{\frac{1}{2}} \times\left[1+\sum_i^{i=6} G(u_i)_{14,15}(u_{i(14)}-u_{i(15)}) - \sum_i^{i=21} G(u_i\ddagger)_{14,15}(u_{i(14)}\ddagger-u_{i(15)}\ddagger)\right]. \quad (25)$$

The factors 2 and 3 in Eqs. (23) and (25) respectively arise from symmetry considerations. In accord with the previous discussion we take K_1/K_2 equal to unity.[19]

We now consider the implications of the fact that the oxygen content of the N_2O is the same at one percent decomposition as it is at complete decomposition. We use Eqs. (23) and (25) to evaluate the right-hand side of Eq. (21). All the factors $G(u_i\ddagger)$ are the same and we arrive at the empirical relation

$$\sum_i^{i=21} G(u_i\ddagger)(u_{i(14)}\ddagger-\tfrac{1}{3}u_{i(15)}\ddagger-\tfrac{2}{3}u_{i(16)}\ddagger) - \sum_i^{i=6} G(u_i)(u_{i(14)}-u_{i(15)}) = 0.333-\tfrac{1}{3}\left(\frac{m_{14}^*}{m_{15}^*}\right)^{\frac{1}{2}}. \quad (26)$$

The term $m_{14}^{*\frac{1}{2}}/m_{15}^*$ is less than unity and has been calculated for two models. In model *A* we simply use the reduced masses[21] of $N^{14}O^{16}$ and $N^{14}O^{18}$ for Eqs. (14) and (15) respectively. In model *B* we assume not only that one of the N−O bonds is ruptured but a water molecule is formed as the activated complex decomposes. This gives for the right-hand side of Eq. (26) 0.009±0.005 and 0.007±0.005 for models *A* and *B* respectively.

The empirical Eq. (26) leads to the conclusion, which is valid for any model, that the activated complex in the elimination of water from nitrate ion has some oxygen vibrations which are of higher frequency than the oxygen vibrations in nitrate ion. This can be readily understood if we suppose that one oxygen is loosely bound in the activated complex and at a greater distance from the nitrogen atom than the other two. From chemical considerations we would expect the effect of isotopic oxygen substitution on the difference between the free energy function for the activated complex and the free energy function for the nitrate ions to be similar to the difference in the free energy function of CO_2 and $CO_3^=$ on substitution of O^{18} for O^{16}. At 500°K this difference is 0.013.[14] This value for the left-hand side of Eq. (26) is in satisfactory agreement with the values calculated for the right hand side.

For the evaluation of Eq. (20) we must know the differences in the vibrational frequencies of activated complexes which differ from one another only in that they are isotopic isomers. We would expect this effect on the free energy function to be smaller than the free energy function which arises from direct isotopic substitution. We have seen from Eq. (26) that the latter is small, which is to be expected for competitive reactions involving oxygen isotopes at 500°K. As a first approximation we shall evaluate Eq. (20) by neglecting the contributions of the free energy functions to Eqs. (23) and (24). The results for the two models discussed above are compared with experiment in Table III. The agreement between theory and experiment is within the limit of the approximations made in $\Sigma_i G(u_i\ddagger)(u_{i(16)}\ddagger-u_{i(15)}\ddagger)$ and $\Sigma_i G(u_i\ddagger)(u_{i(19)}\ddagger-u_{i(18)}\ddagger)$ in Eq. (23) and (24) respectively.

It is clear from the calculations presented and their agreement with experiment that the principal factor

[19] J. Bigeleisen, J. Chem. Phys. **17**, 675 (1949).
[20] See Eq. 8(a) reference 19.
[21] N. B. Slater, Proc. Roy. Soc. **194**, 112 (1948).

contributing to the preference of O^{18} for N_2O over H_2O in the decomposition of ammonium nitrate is the greater frequency of rupture of $N-O^{16}$ bonds than $N-O^{18}$ bonds. In accord with theoretical expectations we find that there is little isotope effect on the equilibrium between the substrate and activated complex at 500°K.

ACKNOWLEDGMENTS

We wish to thank Dr. Joseph R. Stevens for making available to us the information on the origin of "Baker's Analyzed" ammonium nitrate. We also wish to thank Mr. W. S. Richardson and Professor E. B. Wilson, Jr., for sending us a copy of their manuscript on the infrared spectrum of $N^{15}N^{14}O^{16}$ in advance of publication.

THE JOURNAL OF CHEMICAL PHYSICS VOLUME 18, NUMBER 10 OCTOBER, 1950

Ultrasonic Velocities of Sound in Some Metallic Liquids. Adiabatic and Isothermal Compressibilities of Liquid Metals at Their Melting Points*

O. J. KLEPPA
Institute for the Study of Metals, University of Chicago, Chicago, Illinois
(Received June 2, 1950)

The ultrasonic velocities of sound at 12 mc in 12 pure liquid metals at their melting points under atmospheric pressure and in 4 equi-atomic liquid metallic mixtures have been determined by the use of the electronic pulse-circuit technique.

For the pure metals the adiabatic and isothermal compressibilities have been computed. The compressibilities were generally found to be somewhat larger than for the corresponding solids at room temperatures. A calculation of Grüneisen's γ for the liquid metals shows that this quantity, in the case of normal metals, does not change appreciably on going from the solid state at room temperature to the liquid at moderately elevated temperature. These facts support the familiar view that the liquid metals at temperatures not far above their melting points are in a "solid like" state, and that equations of state for the solid state may be applicable to such liquids.

INTRODUCTION

IN view of the experimental difficulties associated with the measurement of isothermal compressibilities at elevated temperatures, it is not surprising that such data are not generally available for liquid metals. However, the well-known relationship between velocity of sound u, density, ρ, and adiabatic compressibility, K_s

$$K_s=1/\rho u^2$$

makes an alternative approach to the problem possible, if velocities of sound can be measured. Under these circumstances we get the isothermal compressibility K_T through the relationship

$$K_T=(C_P/C_V)K_s,$$

where

$$\frac{C_P}{C_V}=\frac{1}{1-(TM\alpha^2/\rho C_P K_T)}.$$

If data are available for specific heat, C_P, and coefficient of thermal expansion, α, and with temperature, T, and atomic weight, M, fixed by the investigator, the isothermal compressibility can be derived readily by successive approximations.

With the obvious exception of mercury, reliable measurements of velocity of sound have not, to the knowledge of the author, been carried out for liquid metals. The present investigation was started in order to secure such information. In other communications the author will discuss some of the consequences of these measurements with respect to the thermodynamic properties of liquid alloy systems.

Through the development of the electronic pulse-circuit technique during and after the war, a new and experimentally simple approach has been opened up, by which velocities of sound in solids and liquids can be measured with considerable accuracy.[1] The method was previously applied by Pellam and Galt[2] in the case of a number of simple liquids at room temperatures, and more recently by Galt[3] and by Galt and Squire[4] for investigation of liquids at low temperatures.

The author has previously reported briefly[5] on the use of the same technique for the study of metallic liquids at moderately elevated temperatures. In the present paper will be given a more complete account of this work, which covers measurements at atmospheric pressure on 12 pure liquid metals at and above their melting points and on 4 equi-atomic liquid metal mixtures.

* This research has been partially supported by the ONR (Contract No. N-6ori-20-IV, NR 019 302).

[1] Cefola, Droz, Frankel, Jones, Maslach, and Teeter, Jr., MIT Radiation Laboratory Report 963 (March 1946).
[2] J. R. Pellam and J. K. Galt, J. Chem. Phys. **14**, 608 (1946).
[3] J. K. Galt, J. Chem. Phys. **16**, 505 (1948).
[4] J. K. Galt and C. F. Squire, Phys. Rev. **72**, 1245 (1947).
[5] O. J. Kleppa, J. Chem. Phys. **17**, 668 (1949).

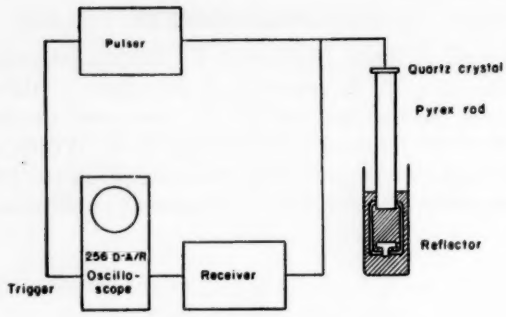

FIG. 1. Schematic diagram of apparatus.

EXPERIMENTAL

The electronic equipment used in the present investigation was assembled and in part constructed by Dr. D. Lazarus, and a more complete description of circuits, etc., has appeared elsewhere.[6] Here shall only be given in brief outline the operation of this equipment, a schematic diagram of which appears in Fig. 1.

A Du Mont 256 D-A/R oscilloscope provides triggering pulses to an external pulser and the means for accurate measurement of the time of travel of the ultrasonic pulses. The triggering pulse from the oscilloscope generates a short group of 12 mc waves in the pulser. This signal is applied to a thin x-cut quartz crystal, which is cemented by means of Phenyl Salicylate to a 15-mm diameter Pyrex rod (see below) fitted with a suitable Pyrex acoustic reflector at known distance. The electrical signal generates a short train of longitudinal acoustic pulses which travel back and forth in the Pyrex rod. The surface of the rod was roughened on a coarse grinding wheel in order to prevent incoherent reflections from the surface of the rod. Each time the sound pulse passes through the quartz crystal an electrical pulse is generated, which is applied to the receiver. After amplification and detection the initial as well as the delayed sets of pulses are displayed on the linear time base sweep of the oscilloscope. This cycle is repeated at a rate of about 2000 c.p.s.

When the measurement on liquids takes place, the lower end of the Pyrex rod with the reflector is immersed in the liquid, and a certain transmission of acoustic pulses takes place from the rod to the liquid. These pulses are reflected back by the reflector, picked up again by the Pyrex rod and in turn generate delayed electrical pulses in the quartz crystal. These are received, amplified and displayed on the oscilloscope with the original pulses through the rod. When the distance between the end of the rod and the reflector is known, the time delay between the first reflected pulse through the rod and the first pulse which has been transmitted through the liquid gives the desired velocity of sound. The total measuring range of the oscilloscope was 100 microseconds and the first reflected pulse through the rod occurred at $\sim$60 μsec. With a distance between rod and reflector of $\sim$2 cm, this allowed measurement of sound velocities of $\sim$1000 m/sec. and more.

The non-electronic part of the apparatus is shown in some detail in Fig. 2.

To the lower end of the previously mentioned Pyrex rod, *A*, which was about 16-cm long and the ends of which were ground flat and parallel, a small Pyrex reflector, *C*, was sealed by means of 3 thin Pyrex rod supports. The ground, flat side of this reflector was mounted parallel to the opposing face of the Pyrex rod. The distance between these parallel faces was accurately measured by means of a cathetometer. In the temperature range used in this investigation (up to $\sim$400°C) this distance does not change more than by about 0.1 percent, an amount which is negligible compared with other sources of error.

The liquid metal, consisting of about 25 cc, was contained in a Pyrex tube crucible, *D*, which could be raised and lowered at will by winding its supporting glass cord, *E*, on the spool, *F*. The temperature of the melt was measured by a Cromel-Alumel thermocouple, protected from the melt by a thin-walled Pyrex tube, *G*. Pyrex rod and crucible were both contained in a slightly wider Pyrex tube as indicated in the figure. Heating was by a 25-cm long resistance furnace of usual construction. Temperature control was by manual operation of a variable transformer and the temperature could easily be maintained within about $\pm$1°C for considerable periods of time.

For support, the Pyrex rod was cemented with de Khotinsky cement in the central boring of the brass top-piece, *J*. This top-piece was in turn connected with the containing Pyrex tube through a $\bar{\$}$ 45/50 ground joint.

The quartz crystal, *B*, was cemented to the top end of the Pyrex rod, and was gold sputtered for single ended connection. The arrangement of the top-piece, as well as of the contacts for the quartz crystal, will best be seen from the figure. If required, the whole top-piece could be cooled by a stream of air or water through the tubes, *K*.

Experiments were conducted in an atmosphere of nitrogen.

The main experimental difficulty was associated with obtaining a reflected signal of sufficient strength and persistence to allow measurements to take place. In preliminary work on mercury it was, for example, found that when the metal was carefully dried and filtered in the usual way, some difficulty was experienced in getting a signal through. This is believed to be due to the fact that mercury does not wet glass and that, therefore, the thin gas film between the rod and the metal prevents the transmission of the pulses. However, a few drops of mineral oil effectively reduced this "surface barrier" and gave the required signal in good strength. It was found that a layer of molten paraffin wax apparently served the same purpose at higher tempera-

[6] D. Lazarus, Phys. Rev. **76**, 545 (1949).

tures. All later experiments, except those performed on zinc, were accordingly carried out with the liquid metal contained under a layer of liquid wax or mineral oil. This wax or oil layer also gave added protection against accidental oxidation, and greatly facilitated the preparation of the liquid metals for measurement. It was found that the molten wax layer protected the metals against atmospheric oxidation, and this made the careful surface cleaning of the metals by "filtering" through a capillary prior to experiments relatively simple. This simple procedure was found to be satisfactory even for the highly reactive alkali metals.

It was generally found that with increasing temperature above 300°C the signals deteriorated and made accurate measurements difficult. This happened at temperatures somewhat below the boiling point of the wax (~400°C), and is believed to be due to a possible appearance of the "surface barrier" under these conditions at higher temperatures, although the evidence for this is not conclusive. All the measurements involving use of liquid wax were carried out below 400°C.

After unsuccessful attempts at measurement under a cover of liquid wax of the velocity of sound in liquid zinc (m.p. 420°), the measurements finally were carried out with the liquid metal covered by a layer of the eutectic mixture of LiCl and KCl. The salt melt unfortunately attacked the glass to some extent, which in turn led to gradual deterioration of the signals. In spite of this, however, it was possible to complete the measurement with the fair precision of about ±2 percent, by using a distance of 3 cm between the end of the Pyrex rod and the reflector.

A number of attempts were made to measure the velocity of sound in liquid lithium, making use of a special Pyrex apparatus which permitted the measurement to be performed when lithium was floating on top of liquid wax. Unfortunately, the lithium caused a very rapid breakdown of the glass container, and none of these attempts was therefore entirely successful. During one run, however, an approximate value for the velocity of sound at 200°C of about 3000 m/sec. was established. The error in this value is estimated to be of the order of ±10 percent. This result is in reasonable agreement with what might be expected from the trend established from the results obtained for the other alkali-metals (see below).

PRECISION OF MEASUREMENTS

Due to unavoidable pulse distortions and lack of sharpness of the leading edge, the absolute precision of the time delay measurements was generally only about ±0.15–0.20 microsecond, or about ±1 percent in the velocity measurements. In view of the absence of data for sound velocities and compressibilities for the liquid metals in question, the results obtained should still prove quite valuable. More unfortunate is the fact that this lack of precision made impossible an accurate determination of the temperature gradients of the velocities of sound in the limited temperature range of the present investigation. Such temperature gradients are reported below only as approximate values, and with due reservations.

ANALYSIS OF MATERIALS

The purity of the metals used in this investigation was checked spectrographically. The impurities found are listed in Table I.

Except for the alkali metals the total amount of impurities was thus, in all cases, of the order of 0.05 percent. The alkali metals were not of the same high quality, but even the appreciable amounts of impurities present in these metals should not affect the value of the results. If the rule of additivity (see below) is assumed, an impurity of, for example, ~1 percent of K

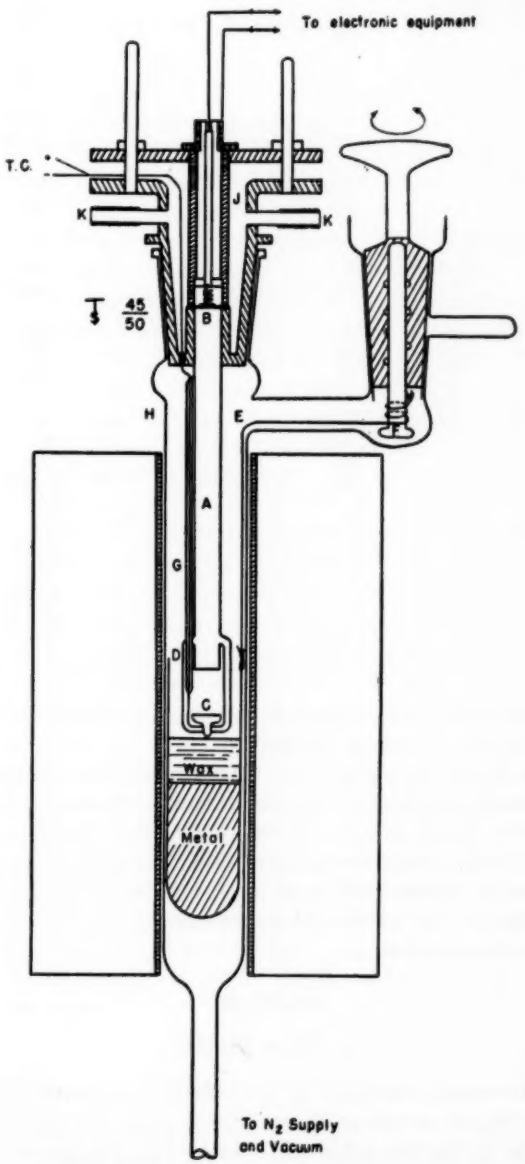

FIG. 2. Details of non-electronic part of apparatus.

TABLE I.

	Impurity	Approx. Amount (percent)
Zn:	Cd	0.005
	Pb, Si	0.002
	Fe, Mg, Ca	0.001
Ga:	Hg, Pb	0.005
	Fe, Cu, Ag	0.001
Cd:	Zn, Sb	0.01
	Pb	0.005
	Sn, Si, Cu, Ag, Fe	0.001
In:	Mg, Ca, Sn, Sb, Si	0.01
	Cu, Pb, Fe	0.002
Sn:	Pb	0.04
	Fe	0.01
	Cu, Sb	0.004
	Bi	0.002
Tl:	Mg, Ca, Si, In	0.01
	Al, Cu, Pb	0.001
Pb:	Bi	0.05
	Fe	0.01
	Sn	0.004
	Ag	0.002
Bi:	Mg, Al, Ag, Si	0.01
	Cu, Pb	0.001
Na:	Ca	1.0
	K	0.01
	Fe, Mg	0.002
K:	Na	0.5
	Rb	0.01
	Fe	0.03
Rb:	K	1.0
	Na	0.5
	Fe	0.02
	Bi	0.002
Cs:	Na	1.0
	K	0.05
	Ca	0.02
	Si	0.004
	Fe	0.002
	Al, Mg	0.001

in Rb should only increase the velocity of sound with ~6 m/sec., or about 0.5 percent.

It should be pointed out that no attempt was made to secure information on the amount of gases dissolved in the liquid metals. It is known that particularly the liquid alkali metals are able to maintain a considerable amount of gases (N_2, O_2) in solution. This represents an additional experimental uncertainty of some importance.

RESULTS

A. Pure Metals

The results obtained for the velocities of sound in the pure liquid metals at their melting points are given in Table II. In this table will also be found approximate values for the temperature gradients of the sound velocity. It was found that this gradient was of the same order of magnitude for all the metals investigated, ranging from ~ -0.3 to ~ -0.7 m sec.$^{-1}$ deg.$^{-1}$, with most of the metals showing a value of ~ -0.5. From the experimental data quoted in Table II have been computed the adiabatic and isothermal compressibilities, by use of the simple thermodynamic relations mentioned in the introduction. The required data for densities, thermal expansion coefficients and specific heats at constant pressure have been taken mainly from Landolt-Börnstein and from International Critical Tables. Finally the specific heats at constant volume have been computed for the same metals at the temperatures in question. These data are all recorded in Table III.

B. Mixtures

A series of four liquid equi-atomic mixtures of tin with cadmium, mercury, lead and bismuth was investigated, and the results are given in Table IV. In the same table will be found computed sound velocities, assuming the rule of additivity. It will be seen that this rule is only approximately valid, the deviations ranging from about -2 percent for tin-lead to about $+7$ percent for tin-mercury.

DISCUSSION

Mercury is the only liquid metal for which reliable earlier determinations of compressibilities resp. velocities of sound appear to be available. A comparison of results obtained in this investigation and earlier work for this metal has been given before.[5] Richards and Boyer[7] report for the initial compressibility of liquid gallium 4.0×10^{-6}, a result which is in disagreement with this investigation. This value for the compressibility would put liquid gallium in line with the heavy elements mercury, thallium, lead and bismuth, while the result of this investigation, 2.4×10^{-6}, is the same as for its neighbor in the periodic system liquid zinc. It should be noted also that cadmium, indium, and tin

TABLE II. Sound velocities and temperature gradients.

Metal	m.p. t°C	u (m/sec.)	$\frac{du}{dt}$ (m sec.$^{-1}$ deg.$^{-1}$, approx.)	Temp. Range m.p. to °C
Zn	420	2790±60	—	480
Ga	30	2740±50	—	50
Cd	321	2200±20	−0.5	360
In	156	2215±20	−0.5	260
Sn	232	2270±20	−0.7	380
Tl	302	1625±15	—	310
Pb	327	1790±15	−0.5	380
Bi	271	1635±15	−0.5	365
Na	98	2395±25	−0.3	235
K	64	1820±20	−0.5	160
Rb	39	1260±10	−0.4	160
Cs	29	967±10	−0.3	130

[7] T. W. Richards and S. Boyer, J. Am. Chem. Soc. 43, 294 (1921).

show very nearly the same intermediary value, between those for zinc and gallium on one hand, and mercury, thallium, lead, and bismuth on the other hand.

For three of the metals covered in the present investigation, namely, potassium, sodium, and bismuth, Bridgman[8] has measured the difference in compressibility between the solid and the liquid at the melting point. By subtracting these values from those obtained for the liquid, the compressibilities of the corresponding solids at the melting point can be obtained. These data can then be directly compared with the isothermally measured compressibilities of the solids at room temperature. The data are recorded in Table V.

As some increase in compressibility should be expected on going from room temperature to the melting point, the correlation between the data for sodium and bismuth appears to be quite satisfactory, while this is not so in the case of potassium. In view of the fact that this metal has the lowest melting point of the three and that the figures compared are obtained from three separate sets of measurements, the slight discrepancy can probably be entirely explained by the experimental uncertainties involved.

For the other metals under consideration it seems relevant to make a direct comparison with earlier results for the same metals in the solid state at room temperature. In Table VI such data for isothermal compressibilities have been tabulated with those of the present investigation.

From this table it will be seen that all metals, with the apparent exception of rubidium and cesium, show the expected increase in compressibility on going from the solid state (at room temperature) to the liquid state. The increase ranges from about 10 percent in the case of potassium to about 62 percent in the case of tin. The exceptional position of rubidium and cesium is hard to explain without assuming a very large influence of the impurities present, or a possible uncertainty in the earlier measurements. It is, for example, possible that the considerable pressure dependence of the compressibility of these metals in the low pressure range may account for a possible error in the extrapolation to zero pressure which was required in order to obtain the accepted values for the compressibility of these solids.

Recent theories of liquids have pointed to the great similarity between the solid and the liquid states, particularly for temperatures not too far above the melting point.[9] This view is supported by such facts as the small value of the heat of melting compared with the total cohesive energy, similar values for specific heats, similarity of structure, etc. To this list can now, in the case of the metals, be added the relatively small compressibility change on melting.

The most extreme statement in regard to the difference between the properties of the solid and the corresponding liquid would be to explain the difference between the two wholly in terms of the addition or removal of holes or "free volume" as we go from one state to the other.[9] Making this drastic assumption, we should be entitled to apply an equation of state developed for the solid to the liquid, and *vice versa*. Numerous attempts have been made to develop satisfactory equations of state for the solid metals. With few exceptions, however, they all seem to have elements of semi-empirical character, and we shall be satisfied here to test our point by use of the old Mie-Grüneisen theory.[10] The basis of this theory is well known: (1) Clausius' virial theorem; (2) central interatomic forces operating between pairs of atoms, due to a potential of the general type

$$\varphi(V) = -\frac{a}{V^{m/3}} + \frac{b}{V^{n/3}},$$

TABLE III. Computed data for adiabatic and isothermal compressibilities.

Metal	T°K	ρ (g cm^{-3})	$\alpha\times10^4$ (deg.$^{-1}$)	C_P	$K_s\times10^6$ (bar^{-1})	$\frac{C_P}{C_v}$	$K_T\times10^6$ (bar^{-1})	C_v**
Zn	693	6.6	1.5	7.6	1.9$_5$	1.25	2.4	6.1
Ga	303	6.09	1.2	6.8	2.1$_9$	1.08	2.4	6.3
Cd	594	8.0	1.5	7.5	2.5$_8$	1.23	3.2	6.1
In	429	7.0*	1.2*	7.0	2.9$_0$	1.12	3.2	6.2$_5$
Sn	505	6.99	1.0	6.6	2.7$_9$	1.11	3.1	5.9$_5$
Tl	575	11.0	1.4	7.1	3.4$_0$	1.21	4.1	5.8$_7$
Pb	600	10.7	1.2	6.8	2.9$_2$	1.20	3.5	5.6$_7$
Bi	544	10.1	1.2	7.2	3.7$_0$	1.15	4.2$_5$	6.2$_5$
Na	371	0.930	2.8	7.5	17.$_7$	1.12	21.$_0$	6.7
K	337	0.835	2.9	7.7	36.$_2$	1.11	40.$_2$	6.9$_4$
Rb	312	1.475	3.4	7.8	42.$_7$	1.15	49.$_1$	6.7$_8$
Cs	302	1.84	3.7	7.8	58.$_1$	1.16	67.$_3$	6.7$_2$

* Estimates.
** It should be noted that lead (!) shows a significantly lower value for C_v than the equipartition value, $3R$, while all the other metals have C_v's close to this value or, in the case of the alkali metals, considerably higher.

TABLE IV. Sound velocities in equi-atomic mixtures.

Mixture	t°C	u (m sec.$^{-1}$, exp.)	u (m sec.$^{-1}$, calc.)	du/dt (m sec.$^{-1}$ deg.$^{-1}$, exp.)
Sn-Cd	250	2205	2245	−0.6
Sn-Hg	200	1950	1815	−0.3
Sn-Bi	200	1965	1980	—
Sn-Pb	290	1975	2020	—

TABLE V. Isothermal compressibilities for solid and liquid metals at the melting point.

Metal	$K_T\times10^6$ (m.p. °C) (bar^{-1})	$(K_T{}^l - K_T{}^s)10^6$** (bar^{-1})	$K_T{}^s\times10^6$ (m.p.) (bar^{-1})	$K_T{}^s\times10^6$ (r.t.)* (bar^{-1})
K	40.$_2$ (64)	4.8	35.$_4$	36.3
Na	21.$_0$ (98)	3.4	17.$_6$	15.9
Bi	4.2$_5$ (271)	0.58	3.6$_7$	2.97

* From *Handbook of Physical Constants*, Geol. Soc. of America, Special Papers, No. 36, 1942.

[8] P. W. Bridgman, Phys. Rev. **38**, 182 (1931).

[9] J. Frenkel, *Kinetic Theory of Liquids* (Oxford University Press, London, 1946).

[10] G. Grüneisen, *Handbuch der Physik* X (1926).

TABLE VI. Isothermal compressibilities for solid and liquid metals.

Metal	$K_T \times 10^6$ (bar^{-1}) Liquid (m.p. °C)	Solid* (r.t.)	Metal	$K_T \times 10^6$ (bar^{-1}) Liquid (m.p. °C)	Solid* (r.t.)
Zn	2.4 (420)	1.69	Na	$21._0$ (98)	15.9 †
Ga	2.4 (30)	2.1	K	$40._2$ (64)	36.3
Cd	3.2 (321)	2.25	Rb	$49._1$ (39)	53.0(50°)
In	3.2 (156)	2.32	Cs	$67._3$ (29)	71.0(50°)
Sn	3.1 (232)	1.91			
Tl	4.1 (302)	3.55			
Pb	3.5 (327)	2.45			
Bi	4.2_5 (271)	2.97			

* From *Handbook of Physical Constants*, Geol. Soc. of America, Special Papers, No. 36, 1942.

† S. L. Quimby and S. Siegel, Phys. Rev. **54**, 293 (1938) have measured the compressibility of sodium single crystals by a dynamic method between 80 and 210°K and find considerably higher values for K_T. The results of this investigation give support to the earlier value measured by Bridgman.

when a, b, m, and n are constants characteristic for each metal.

Grüneisen tested this theory empirically by computing the factor

$$\gamma = \frac{\alpha V}{K_T C_V} = \frac{\alpha V}{K_S C_P}.$$

He found that for the great majority of metals γ was about 2.3. According to the theory this determines the repulsion exponent, n, which, for this value of γ for cubic crystals, will be about 12. Notable exceptions are the alkali metals, bismuth, antimony, and gallium, which all have much smaller values for γ and n.

If our assumptions above are valid, we should expect that γ does not change appreciably on going from the solid to the liquid state. Table VII will show to what extent this is actually the case.

When we consider the uncertainties involved in the accepted values for C_P and even more for α in the case of the liquid metals, the agreement must be considered very good. The only metals investigated which show a very marked change on going from the solid to the liquid state are bismuth and gallium. This change can undoubtedly be explained by the well-known structure change of these metals on melting.[11,12] It will be noted that γ for liquid bismuth and gallium falls well in line with the other heavy metals. As the compressibility of bismuth and gallium changes only about 15 percent on melting, the large change in Grüneisen's γ for these metals must be attributed largely to the abnormal increase during fusion in the coefficient of thermal expansion for these two metals.

TABLE VII. Grüneisen's γ for solid and liquid metals.

Metal	γ (liq. m.p.)	γ^* (solid)	Metal	γ (liq. m.p.)	γ^* (solid)
Zn	2.4	2.01	Na	1.1_8	1.25
Ga	2.2	1.16	K	1.1_7	1.34
Cd	2.6_0	2.19	Rb	1.4_1	1.48
In	2.3_2	2.5	Cs	1.4_1	1.29
Sn	2.2_0	2.14			
Tl	2.5_8	2.73			
Pb	2.8_0	2.73			
Bi	2.2_7	1.14			

* Mainly from G. Grüneisen, *Handbuch der Physik* **X** (1926).

ACKNOWLEDGMENTS

The author wishes to express his thanks to the following members of the staff of the Institute for the Study of Metals: to Dr. A. W. Lawson, for making the electronic apparatus available and for numerous stimulating discussions; to Dr. David Lazarus, for invaluable technical help and to Mr. L. J. Howell, for carrying out the spectrographic analysis of the materials used. He also wishes to acknowledge the loan of the gallium metal from Dr. William L. Fink of the Aluminum Company of America.

[11] J. T. Randall and H. P. Rooksby, Trans. Faraday Soc. **33**, 109 (1937).

[12] H. Menke, Physik. Zeits. **33**, 593 (1932).

An Irregularity in the Solvent Powers of Paraffins

JOEL H. HILDEBRAND
Department of Chemistry, University of California, Berkeley, California
(Received July 17, 1950)

The solubility relations of *n*-heptane with *f*-heptane, iodine, sulfur, stannic iodide, and phosphorus are all accounted for within the usual limits of accuracy for regular solution theory by a solubility parameter 8.1 instead of the value 7.45 derived from its energy of vaporization per cc. Solutions of 2,2,4-trimethyl pentane with *f*-heptane and with iodine are similarly accounted for by the empirical value 7.45 instead of 6.85. Such an adjustment for paraffins is a practical alternative to the treatment used by Simons and Dunlap for the system *n*-pentane, "pentforane," which they recently reported upon, and is, at the same time, consistent with their assumption that the exceptional behavior of paraffins is to be attributed to an irregularity in their mutual repulsions.

IT has been known for some time[1] that the solubility of iodine in paraffin hydrocarbons is somewhat less than would be expected from the theory of regular solutions using values of solubility parameters derived from heats of vaporization. Recently, Simons and Dunlap[2] have reported that the mutual solubility of *n*-pentane and *n*-perfluoropentane, "*n*-pentforane," is *less* than would be expected from the same theory. At the time this paper appeared, Benesi, Fisher, and I[3] had submitted a paper for publication in which we reported a similar discrepancy for solutions of *n*-perfluoroheptane with *n*-heptane and with 2,2,4-trimethyl pentane, "*iso*-octane." They form two liquid phases at 50° and 24°, respectively, whereas, according to theory, they should not unmix till cooled far below zero. We stated therein our conclusion that this irregularity is to be attributed to an energy rather than an entropy effect, and could be accounted for by assigning to the paraffins a larger solubility parameter than the one based upon the heat of vaporization. The purpose of this communication is to show the quantitative internal consistency that is brought into the solubility relations of *n*-heptane by so doing.

Because of the large molal volume of perfluoroheptane, (I shall call it *f*-heptane) I add the Flory-Huggins term to the regular solution equation to give the more general equation,

$$\ln a_2 = \ln \varphi_2 + \varphi_1\left(1-\frac{\mathbf{V}_2}{\mathbf{V}_1}\right)+\frac{\mathbf{V}_2\varphi_1^2(\delta_2-\delta_1)^2}{RT}. \qquad (1)$$

The equation for the critical solution temperature derived from this[3] is

$$RT_c=\frac{2\mathbf{V}_1\mathbf{V}_2}{(\mathbf{V}_1^{\frac{1}{2}}+\mathbf{V}_2^{\frac{1}{2}})^2}(\delta_2-\delta_1)^2. \qquad (2)$$

The symbols have the following meanings: a is activity referred to pure liquid, φ is volume fraction, $\mathbf{V}$ is molal volume, T_c is critical solution temperature, and δ is "solubility parameter," $(\Delta\mathbf{E}^v/\mathbf{V})^{\frac{1}{2}}$, where $\mathbf{E}$ is molal energy of vaporization and $\mathbf{V}$ is molal volume. I shall compare the solvent power of *n*-heptane with that of carbon tetrachloride for five other substances, *f*-heptane,[3] iodine,[1] sulfur,[4] stannic iodide,[5] and phosphorus,[6] which are designated as component 2. Component 1 is *n*-heptane and 1′ is carbon tetrachloride. The data used are the critical solution temperature, in the case of *f*-heptane, and the solubility of the solid form of the other substances at 25°. In these cases, the activities are those of the solid, a_2^s, referred to the supercooled liquid. Any uncertainties in the values of a_2^s are canceled out by the method of calculation used, so do not affect the comparison. Table I gives the differences, $\delta_2-\delta_1'$ and $\delta_2-\delta_1$, calculated from the solubility data for each second component and in the case of *f*-heptane, the experimental values of T_c are given in Table II, along with the values of $\mathbf{V}$ at the same temperatures.

The last row in Table I shows that all of these solutions agree in indicating that the solubility parameter of *n*-heptane should be taken as from 0.3 to 0.5 less than that of carbon tetrachloride instead of 1.15 less, as given by their energies of vaporization per cc., 7.45 and 8.6, respectively. If we assume 8.6 for carbon tetrachloride as a standard for comparison, then the value 8.1 for *n*-heptane would obviously be consistent, within the usual limits of error, with its solvent powers for all of the substances here considered. It should be remembered that a variety of disturbing factors unite to cause variations of from 0.1 to 0.2 in the δ-values for any one substance by means of Eqs. (1) and (2).

The paraffin, 2,2,4-trimethyl pentane, is, similarly, a better solvent for iodine[1] and a poorer solvent for *f*-heptane[3] than its value of $(\Delta\mathbf{E}^v/\mathbf{V})^{\frac{1}{2}}=6.85$ would lead one to expect. With iodine, $\delta_1'-\delta_1=0.7$ and with

[1] H. A. Benesi and J. H. Hildebrand, J. Am. Chem. Soc. **70**, 3978 (1948).
[2] J. H. Simons and R. D. Dunlap, J. Chem. Phys. **18**, 335 (1950).
[3] Hildebrand, Fisher, and Benesi, J. Am. Chem. Soc. (September, 1950).
[4] J. H. Hildebrand and C. L. Jenks, J. Am. Chem. Soc. **43**, 2172 (1921).
[5] M. E. Dorfman and J. H. Hildebrand, J. Am. Chem. Soc. **49**, 729 (1927). See, also, *Solubility of Nonelectrolytes* (Reinhold Publishing Corporation, New York) 1950 for the data cited in references 4–7.
[6] C. Groot and J. H. Hildebrand, J. Am. Chem. Soc., **70**, 3815 (1948).

TABLE I. Difference between solubility parameters of CCl_4 and n-C_7H_{16} from their solubility data with common solutes.

	C_7F_{16}	I_2	S_8	SnI_4	P_4
V_2		59.0	135	151	70.4
$100x_2$ in CCl_4		1.147	0.500	1.46	1.58
$100x_2$ in C_7H_{16}		0.679	0.141	0.553	1.24
$\delta_2-\delta_1'$	−2.98	5.74	4.26	3.05	5.94
$\delta_2-\delta_1$	−2.62	6.21	4.80	3.53	6.26
$\delta_1'-\delta_1$	0.36	0.47	0.54	0.48	0.32

TABLE II. Critical solution figures for n-heptane with f-heptane (2) and carbon tetrachloride (1′).

	T_c	V_1	V_1'	V_2
n-Heptane—f-heptane	332	152	—	239
Carbon tetrachloride—f-heptane	323	—	101	235

f-heptane it is −0.5. The proper value for this octane should evidently be about 7.45 instead of 6.85.

It is, of course, quite reasonable to obtain δ-values from solubility data themselves rather than from heats of vaporization. I have noted a similar displacement in the case of chloroform,[7] where a variety of solubility data are consistent with a parameter 9.0 instead of the value 9.3 from $(\Delta E^v/V)^{\frac{1}{2}}$.

The explanation offered by Simons and Dunlap in connection with their investigation of the two pentanes, *i.e.*, that hydrocarbon molecules can interpenetrate and yield a liquid with unusually small free volume seems quite reasonable. This implies that the slope of the repulsive branch of the curve of potential energy *vs.* distance in the case of paraffin molecules differs markedly from that of most other molecular species, and the repulsive branch plays a larger role in the small separations involved in mixing with another liquid than it does in the large separations involved in vaporization.

The figures cited in this paper seem to show that a simple, practical means of dealing with the solubility relations of paraffins is to derive their solubility parameters from known solubility data with a reasonable expectation that values so derived will prove applicable to new cases.

I wish to acknowledge the support of the Atomic Energy Commission in connection with the studies and calculations upon which this paper is based.

[7] J. H. Hildebrand, Chem. Revs. 44, 37 (1949).

THE JOURNAL OF CHEMICAL PHYSICS VOLUME 18, NUMBER 10 OCTOBER, 1950

LCAO Self-Consistent Field Calculation of the π-Electron Energy Levels of *cis*- and *trans*-1,3-Butadiene*

ROBERT G. PARR† AND ROBERT S. MULLIKEN
Department of Physics, University of Chicago, Chicago 37, Illinois

(Received June 6, 1950)

The π-electrons of the molecules *cis*- and *trans*-1,3-butadiene are treated by the method of antisymmetrized products of molecular orbitals, the molecular orbitals being taken as linear combinations of $2p\pi$-Slater atomic orbitals with effective charge 3.18. The *best* ground state *LCAO* molecular orbitals obtainable from these are found by application of a method recently proposed by Roothaan which is based on the variational theorem, and the π-electron energy of the ground state is calculated. Including a correction for nuclear repulsions, the *trans*- form is computed to be 0.12 ev more stable than the *cis*-form. Using the ground state orbitals to build up excited state wave functions, the energies of four singly excited singlet states and the corresponding triplet states are calculated, there resulting for the average of the lowest singlet and triplet states the excitation energy 5.4 ev for *cis*- and 5.7 ev for *trans*-, the experimental value for the lowest singlet state (probably for *trans*-) being 6.0 ev. The first ionization potential is computed to be 9.7 ev for both *cis*- and *trans*-, whereas the observed value is 9.1 ev. No extra-geometrical empirical data are used except in the calculation of ionization potentials, where the value −11.28 ev based on atomic spectroscopic data is used for the energy of a $2p\pi$-electron in a carbon atom in its valence state.

INTRODUCTION

RECENT calculations[1,2] have indicated that electronic excitation and ionization energies of unsaturated organic compounds can be computed with fair accuracy by the method of antisymmetrized products of molecular orbitals (in *LCAO* approximation) with the introduction of no extra-geometrical empirical factors. In most cases so far treated the molecular orbitals have been determined by symmetry considerations alone. In the present paper we consider a molecule (1,3-butadiene) where the orbitals can *not* be so de-

* This work was assisted in part by the ONR under Task Order IX of Contract N6ori-20 with the University of Chicago.

† Present address: Department of Chemistry, Carnegie Institute of Technology, Pittsburgh, Pennsylvania.

[1] For example, R. G. Parr and B. L. Crawford, Jr., J. Chem. Phys. 16, 526 (1948); C. C. J. Roothaan and R. G. Parr, J. Chem. Phys. 17, 1001 (1949).

[2] R. S. Mulliken, Parts II–III of "Report on molecular orbital theory," J. de Chim. Phys. 46, 497 (1949)—see 1947–8 ONR Report of University of Chicago Physics Department Spectroscopic Laboratory for English version.

termined, and apply it to the *SCF* (self-consistent field) method which Roothaan[3] has developed for simultaneous determination of orbitals and energy.[4]

Roothaan's method could (and should) be used to treat butadiene as a full 30-electron problem, but this would require numerical values for certain integrals which are not yet available.[5] It is well known, however, and it has been assumed in the treatment of other molecules mentioned above, that the unsaturation electrons in conjugated molecules such as butadiene are responsible for the lowest frequency electronic transitions, and may be profitably studied apart from the rest. Accordingly, we shall treat butadiene as a four-electron problem, replacing the 26 more tightly bound electrons by an effective potential.

We shall carry the work for *cis*- and *trans*-butadiene along side by side. This will facilitate comparison of results on the two molecules at any stage, and will provide a means for detecting arithmetic errors which may crop up. The geometry we shall assume for the carbon skeletons $C_a-C_b-C_c-C_d$ of these molecules is based upon the electron diffraction results of Schomaker and Pauling:[6] skeletons planar, $C_a-C_b-C_c$ and $C_b-C_c-C_d$ angles 124°, C_a-C_b and C_c-C_d distances 1.35A, C_b-C_c distances 1.46A.

GROUND STATE ORBITALS AND ENERGY

We consider, then, four electrons moving in the field of the single-bonded, sp^2-hybridized, completely planar structure $H_2C-CH-CH-CH_2$ forming a core with charge +4, composed of a +1 charge on each carbon atom, but no charges on the hydrogen atoms. We take as "starting orbitals" for these electrons normalized $2p\pi$-Slater *AO*'s (atomic orbitals) χ_a, χ_b, χ_c, χ_d, on the four carbon atoms, and seek two orthonormal *MO*'s (molecular orbitals) ϕ_1, ϕ_2, which are linear combinations of these starting orbitals (*LCAO*):

$$\phi_i=\sum_p C_{ip}\chi_p; \tag{1}$$

and which minimize the energy

$$E_N=\int \Psi_N^*\mathbf{H}\Psi_N d\tau \tag{2}$$

calculated from the complete four-electron Hamiltonian operator $\mathbf{H}$ and the totally antisymmetric and normalized four-electron wave function

$$\Psi_N=\frac{1}{(4!)^{\frac{1}{2}}}\begin{vmatrix}(\phi_1\alpha)^1 & (\phi_1\beta)^1 & (\phi_2\alpha)^1 & (\phi_2\beta)^1\\ (\phi_1\alpha)^2 & (\phi_1\beta)^2 & (\phi_2\alpha)^2 & (\phi_2\beta)^2\\ (\phi_1\alpha)^3 & (\phi_1\beta)^3 & (\phi_2\alpha)^3 & (\phi_2\beta)^3\\ (\phi_1\alpha)^4 & (\phi_1\beta)^4 & (\phi_2\alpha)^4 & (\phi_2\beta)^4\end{vmatrix}. \tag{3}$$

Here α and β are the two possible (orthonormal) spin functions for an electron, and $(\phi_2\beta)^3$, for example, denotes the wave function of electron 3 in the molecular orbital ϕ_2 with the spin $-(1/2)(h/2\pi)$. E_N is the total ground state energy of the four π-electrons in the field of the core.

Writing H out in the form

$$\mathbf{H}=\sum_{\nu=1}^{4}(\mathbf{T}^\nu+\mathbf{U}_c^\nu)+(1/2)\sum_{\substack{\mu,\nu=1\\ \mu\neq\nu}}^{4}(e^2/r^{\mu\nu}), \tag{4}$$

where $\mathbf{T}^\nu$ is the kinetic energy of electron ν, $\mathbf{U}_c^\nu$ is the potential energy of electron ν in the $2p\pi$-electron-less framework, e is the electronic charge, and $r^{\mu\nu}$ is the distance between electrons μ and ν, and carrying out the

TABLE I. Integrals over the atomic orbitals χ_p.[a]

Integral	Value[d,e] *cis-*	Value[d,e] *trans-*	Integral	Value[d,e] *cis-*	Value[d,e] *trans-*
Overlap integrals			Coulomb-Exchange Integrals[f]		
S_{ab}	0.27854	0.27854	$aa\|aa$	0.3914×Z	0.3914×Z
S_{bc}	0.23281	0.23281	$aa\|bb$	0.2136	0.2136
S_{ac}	0.03371	0.03371	$bb\|cc$	0.2010	0.2010
S_{ad}	0.01188	0.00218	$aa\|cc$	0.1277	0.1277
Penetration integrals[b]			$aa\|dd$	0.1083	0.0885
			$aa\|ab$	0.0834	0.0834
$a:ab$	0.0527×Z	0.0527×Z	$bb\|bc$	0.0678	0.0678
$b:bc$	0.0377	0.0377	$bb\|cd$	0.0447	0.0447
$a:bb$	0.0228	0.0228	$aa\|bc$	0.0384	0.0384
$b:cc$	0.0156	0.0156	$aa\|cd$	0.0334	0.0291
$b:ac$	0.0070	0.0070	$aa\|ac$	0.0069	0.0069
$a:ac$	0.0012	0.0012	$aa\|bd$	0.0053	0.0043
$a:bc$	0.0008	0.0008	$bb\|ac$	0.0107	0.0107
$b:cd$	0.0007	0.0007	$aa\|ad$	0.0024	0.0004
$b:ad$	0.0003	0.0004	$bb\|ad$	0.0026	0.0007
$a:cc$	0.0002	0.0002	$ab\|ab$	0.0252	0.0252
$a:ad$	0.0002	0.0000	$bc\|bc$	0.0169	0.0169
$a:bd$	0.0001	0.0000	$ab\|bc$	0.0147	0.0147
$a:cd$	0.0000	0.0000	$ab\|cd$	0.0110	0.0107
$a:dd$	0.0000	0.0000	$ab\|ac$	0.0029	0.0029
Core integrals[c]			$ab\|bd$	0.0019	0.0016
			$bc\|ac$	0.0025	0.0025
$-I_{aa}$	0.4726×Z	0.4528×Z	$ab\|ad$	0.0008	0.0001
$-I_{bb}$	0.5809	0.5809	$bc\|ad$	0.0007	0.0002
$-I_{ab}$	0.2149	0.2106	$ac\|ac$	0.0004	0.0004
$-I_{bc}$	0.1839	0.1839	$ac\|bd$	0.0003	0.0002
$-I_{ac}$	0.0312	0.0301	$ac\|ad$	0.0001	0.0000
$-I_{ad}$	0.0084	0.0026	$ad\|ad$	0.0001	0.0000

[a] The χ_p are $2p\pi$-Slater *AO*'s—see Eq. (A1).
[b] $\gamma:pq$ is an abbreviation for $(A_r:\chi_p\chi_q)$—see Eq. (A9).
[c] Energies given are relative to energy W_{2p} of a $2p\pi$-electron of a carbon atom in its valence state. ($W_{2p}=-11.28$ ev—see reference 2.)
[d] Overlap integrals are dimensionless; they are for Slater $2p\pi$-*AO*'s with $Z=3.18$ at distances indicated in text. The other integrals have dimensions of energy; their values are given in atomic units: 1 atomic unit = 13.602 ev.
[e] Values for all but the overlap integrals are the numerical entries in the table multiplied by Z (in the following, we use $Z=3.18$).
[f] $pr|qs$ is an abbreviation for $J_{pqrs}=(\chi_p\chi_r|\chi_q\chi_s)$—see Eq. (A2).

[3] C. C. J. Roothaan, Ph.D. thesis, University of Chicago (see 1948–9 ONR report for section on *LCAO SCF* method, 1949–50 ONR Report for section on application to benzene, including computation of ionization and excitation energy).
[4] See also R. S. Mulliken, "Report on molecular orbital theory," Part V, J. de Chim. Phys. **46**, 675 (1949)—see 1948–9 ONR Report for English version. A preliminary survey of the application of the present and other methods to 1,3-butadiene is given in Section 23 and Fig. 3.
[5] A systematic program for computation of integrals has been begun at the University of Chicago, but it may be several years before all of the integrals which enter *LCAO* computations on polyatomic molecules become available.
[6] V. Schomaker and L. Pauling, J. Am. Chem. Soc. **61**, 1769 (1939).

integration indicated in Eq. (2), one obtains[7]

$$E_N = 2I_1 + 2I_2 + J_{11} + J_{22} + 4J_{12} - 2K_{12}. \quad (5)$$

Here[8]

$$I_i = \int \phi_i^{*\nu}(\mathbf{T}^\nu + \mathbf{U}_c^\nu)\phi_i^\nu d\tau^\nu \quad (6)$$

$$J_{ij} = \int \phi_i^{*\nu}\phi_j^{*\mu}(e^2/r^{\mu\nu})\phi_i^\nu\phi_j^\mu d\tau^\nu d\tau^\mu, \quad (7)$$

and

$$K_{ij} = \int \phi_i^{*\nu}\phi_j^{*\mu}(e^2/r^{\mu\nu})\phi_i^\mu\phi_j^\nu d\tau^\nu d\tau^\mu, \quad (8)$$

are "core," "Coulomb," and "exchange" integrals, respectively, over the molecular orbitals ϕ_i or ϕ_i and ϕ_j. These integrals, and hence E_N, may be expressed in terms of integrals over the starting AO's χ_p through the use of Eq. (1); the results are

$$I_i = \sum_{p,q} C_{ip}^* I_{pq} C_{iq}, \quad (9)$$

$$J_{ij} = \sum_{p,q,r,s} C_{ip}^* C_{jq}^* J_{pqrs} C_{ir} C_{js}, \quad (10)$$

and

$$K_{ij} = \sum_{p,q,r,s} C_{ip}^* C_{jq}^* J_{pqsr} C_{ir} C_{js}, \quad (11)$$

where

$$I_{pq} = \int \chi_p^{*\nu}(\mathbf{T}^\nu + \mathbf{U}_c^\nu)\chi_q^\nu d\tau^\nu \quad (12)$$

and

$$J_{pqrs} = \int \chi_p^{*\nu}\chi_q^{*\mu}(e^2/r^{\mu\nu})\chi_r^\nu\chi_s^\mu d\tau^\nu d\tau^\mu \quad (13)$$

are "core" and "Coulomb-exchange" integrals over the atomic orbitals χ_p.

Evaluation of the integrals I_{pq} and J_{pqrs} is discussed in the Appendix, and leads for the molecular dimensions we are assuming to the values given in Table I. With these values known, the only unknowns remaining in Eq. (5) for the energy E_N are the coefficients C_{ip} of Eqs. (1), (9)–(11), which must be assigned values such as to make E_N a minimum subject to orthonormalization of the ϕ_i, i.e., subject to

$$\int \phi_i^{*\nu}\phi_j^\nu d\tau^\nu = \sum_{p,q} C_{ip}^* S_{pq} C_{jq} = \begin{cases} 1 & \text{if } i=j \\ 0 & \text{if } i\neq j \end{cases}, \quad (14)$$

where

$$S_{pq} = \int \chi_p^{*\nu}\chi_q^\nu d\tau^\nu \quad (15)$$

is the "overlap" integral between χ_p and χ_q. The equations which the C_{ip} must in general satisfy have been derived by Roothaan;[3] in the present case they are the homogeneous set

$$\left.\begin{aligned} &C_{ia}(L_{aa}-S_{aa}\epsilon_i)+C_{ib}(L_{ab}-S_{ab}\epsilon_i)+C_{ic}(L_{ac}-S_{ac}\epsilon_i)+C_{id}(L_{ad}-S_{ad}\epsilon_i)=0 \\ &C_{ia}(L_{ba}-S_{ba}\epsilon_i)+C_{ib}(L_{bb}-S_{bb}\epsilon_i)+C_{ic}(L_{bc}-S_{bc}\epsilon_i)+C_{id}(L_{bd}-S_{bd}\epsilon_i)=0 \\ &C_{ia}(L_{ca}-S_{ca}\epsilon_i)+C_{ib}(L_{cb}-S_{cb}\epsilon_i)+C_{ic}(L_{cc}-S_{cc}\epsilon_i)+C_{id}(L_{cd}-S_{cd}\epsilon_i)=0 \\ &C_{ia}(L_{da}-S_{da}\epsilon_i)+C_{ib}(L_{db}-S_{db}\epsilon_i)+C_{ic}(L_{dc}-S_{dc}\epsilon_i)+C_{id}(L_{dd}-S_{dd}\epsilon_i)=0 \end{aligned}\right\}. \quad (16)$$

Here the quantities L_{pq} are defined by

$$L_{pq} = I_{pq} + G_{pq}, \quad (17)$$

where the

$$G_{pq} = \sum_{i=1,2}\left[2\int \phi_i^{*\nu}\chi_p^{*\mu}(2/r^{\mu\nu})\phi_i^\nu\chi_q^\mu d\tau^\nu d\tau^\mu - \int \phi_i^{*\nu}\chi_p^{*\mu}(2/r^{\mu\nu})\phi_i^\mu\chi_q^\nu d\tau^\nu d\tau^\mu\right] \quad (18)$$

are components of the *LCAO SCF* Coulomb-exchange operator $\mathbf{G}$ for the problem. The ϵ_i are numbers which make non-trivial solutions for the C_{ip} possible; that is, the ϵ_i are solutions of the secular equation

$$\begin{vmatrix} L_{aa}-S_{aa}\epsilon & L_{ab}-S_{ab}\epsilon & L_{ac}-S_{ac}\epsilon & L_{ad}-S_{ad}\epsilon \\ L_{ba}-S_{ba}\epsilon & L_{bb}-S_{bb}\epsilon & L_{bc}-S_{bc}\epsilon & L_{bd}-S_{bd}\epsilon \\ L_{ca}-S_{ca}\epsilon & L_{cb}-S_{cb}\epsilon & L_{cc}-S_{cc}\epsilon & L_{cd}-S_{cd}\epsilon \\ L_{da}-S_{da}\epsilon & L_{db}-S_{db}\epsilon & L_{dc}-S_{dc}\epsilon & L_{dd}-S_{dd}\epsilon \end{vmatrix} = 0. \quad (19)$$

For given values of the L_{pq} and S_{pq}, there are four real roots of this equation.[3] Corresponding to each root there is a normalized molecular orbital ϕ_i, the coefficients C_{ip} in which can be found from Eqs. (14) and (16). The L_{pq} are not at first known, however, but depend upon the C_{ip} through the dependence of the G_{pq} on the occupied ϕ_i—see Eq. (18). A method of successive approximations must therefore be adopted. A set of C_{ip} values may be assumed, the G_{pq} calculated, the secular equation solved, and a new set of C_{ip} values found, and this process repeated until a "self-consistent" set of C_{ip} values is found. If the resulting orbitals are

[7] See, for example, B. L. Crawford, Jr. and R. G. Parr, J. Chem. Phys. **17**, 726 (1949), Eq. (26), or reference 2 or 3.

[8] $d\tau^\nu$ denotes the element of volume for electron ν, ϕ_i^* the complex conjugate of ϕ_i. All integrations are performed over all space.

denoted by ϕ_1, ϕ_2, ϕ_3, ϕ_4, in order of increasing energy (ϵ_i), ϕ_1 and ϕ_2 will be the ground state orbitals we are seeking, while ϕ_3 and ϕ_4 will represent some approximation to excited state orbitals (see infra).

Thus far, the fact that the χ_p are *atomic* orbitals has not been used—equations of precisely the same form would result if we began with *any* four independent orbitals. To take advantage of this fact, let us now begin again taking as starting orbitals the normalized[9] "symmetry orbitals"

$$\left.\begin{aligned}
&\sigma_1=(1/N_1)(\chi_a+\chi_d), && N_1=1.42259 \text{ for } \textit{cis}\text{-}, \ 1.41575 \text{ for } \textit{trans}\text{-}\\
&\sigma_2=(1/N_2)(\chi_b+\chi_c), && N_2=1.57023 \text{ for both } \textit{cis}\text{- and } \textit{trans}\text{-}\\
&\sigma_3=(1/N_3)(\chi_b-\chi_c), && N_3=1.23870 \text{ for both } \textit{cis}\text{- and } \textit{trans}\text{-}\\
&\sigma_4=(1/N_4)(\chi_a-\chi_d), && N_4=1.40577 \text{ for } \textit{cis}\text{-}, \ 1.41267 \text{ for } \textit{trans}\text{-}
\end{aligned}\right\}. \tag{20}$$

Defining matrix elements $S_{pq}{}^{\sigma}$ and $L_{pq}{}^{\sigma}$ in terms of the σ_q in just the way S_{pq} and L_{pq} were defined in terms of the χ_p—see Eqs. (15), (17), and (18)—we then find that the secular equation becomes simply

$$\begin{vmatrix}
L_{11}{}^{\sigma}-S_{11}{}^{\sigma}\epsilon & L_{12}{}^{\sigma}-S_{12}{}^{\sigma}\epsilon & 0 & 0\\
L_{21}{}^{\sigma}-S_{21}{}^{\sigma}\epsilon & L_{22}{}^{\sigma}-S_{22}{}^{\sigma}\epsilon & 0 & 0\\
0 & 0 & L_{33}{}^{\sigma}-S_{33}{}^{\sigma}\epsilon & L_{34}{}^{\sigma}-S_{34}{}^{\sigma}\epsilon\\
0 & 0 & L_{43}{}^{\sigma}-S_{43}{}^{\sigma}\epsilon & L_{44}{}^{\sigma}-S_{44}{}^{\sigma}\epsilon
\end{vmatrix}=0 \tag{21}$$

since matrix elements between σ_1 or σ_2 and σ_3 or σ_4 vanish.[10] The MO's ϕ_i may thus be written in the form

$$\left.\begin{aligned}
\phi_1&=d_{11}\sigma_1+d_{12}\sigma_2\\
\phi_3&=d_{31}\sigma_1+d_{32}\sigma_2\\
\phi_2&=d_{23}\sigma_3+d_{24}\sigma_4\\
\phi_4&=d_{43}\sigma_3+d_{44}\sigma_4
\end{aligned}\right\}; \tag{22}$$

where the numbering of the ϕ's anticipates the order of the roots of Eq. (21) which will actually be found;[11] where the coefficients d_{iq} satisfy the normalization conditions

$$1=\sum_{p,q} d_{ip}{}^{*}S_{pq}{}^{\sigma}d_{iq}, \quad i=1,2,3,4; \tag{23}$$

and where the ratios of the d_{iq} are equal to ratios of corresponding cofactors of the secular determinant in Eq. (21), that is,

$$\begin{aligned}
\frac{d_{11}}{d_{12}}&=-\frac{L_{12}{}^{\sigma}-S_{12}{}^{\sigma}\epsilon_1}{L_{11}{}^{\sigma}-S_{11}{}^{\sigma}\epsilon_1}, & \frac{d_{31}}{d_{32}}&=-\frac{L_{12}{}^{\sigma}-S_{12}{}^{\sigma}\epsilon_3}{L_{11}{}^{\sigma}-S_{11}{}^{\sigma}\epsilon_3},\\
\frac{d_{23}}{d_{24}}&=-\frac{L_{34}{}^{\sigma}-S_{34}{}^{\sigma}\epsilon_2}{L_{33}{}^{\sigma}-S_{33}{}^{\sigma}\epsilon_2}, & \frac{d_{43}}{d_{44}}&=-\frac{L_{34}{}^{\sigma}-S_{34}{}^{\sigma}\epsilon_4}{L_{33}{}^{\sigma}-S_{33}{}^{\sigma}\epsilon_4}.
\end{aligned} \tag{24}$$

The d_{iq}, like the C_{ip}, require an iterative method of evaluation, but they are much easier to work with.

Table II lists values of the integrals $S_{pq}{}^{\sigma}$, $I_{pq}{}^{\sigma}$ and $J_{pqrs}{}^{\sigma}$, determined from the integrals in Table I by direct insertion of Eq. (20) into the appropriate definitions.[12] From these basic integrals, the elements in the secular equation, Eq. (21), can be computed from any assumed set of values for the d_{iq}, through the use of the defining relations

$$L_{pq}{}^{\sigma}=I_{pq}{}^{\sigma}+G_{pq}{}^{\sigma} \tag{25}$$

and

$$G_{pq}{}^{\sigma}=\sum_{i=1,2}(2J_{i,\,pq}{}^{\sigma}-K_{i,\,pq}{}^{\sigma}), \tag{26}$$

TABLE II. Integrals over the symmetry orbitals σ_q.[a]

Integral	Value[c] *cis-*	Value[c] *trans-*	Integral	Value[c] *cis-*	Value[c] *trans-*
Overlap integrals			22|44	7.306	7.319
			33|44	7.438	7.445
$S_{12}{}^{\sigma}$	0.27957	0.28092	11|12	2.503	2.405
$S_{34}{}^{\sigma}$	0.28120	0.27983	22|21	3.829	2.843
Core integrals[b]			33|34	2.788	2.774
			44|43	2.594	2.504
$-I_{11}{}^{\sigma}$	20.561	19.655	11|34	2.602	2.504
$-I_{22}{}^{\sigma}$	26.834	26.834	22|34	2.718	2.705
$-I_{33}{}^{\sigma}$	22.383	22.383	33|12	2.809	2.823
$-I_{44}{}^{\sigma}$	20.320	19.516	44|12	2.493	2.408
$-I_{12}{}^{\sigma}$	9.531	9.367	12|12	0.806	0.782
$-I_{34}{}^{\sigma}$	9.126	8.923	13|13	0.343	0.363
Coulomb-exchange integrals			14|14	6.124	6.551
			23|23	4.354	4.354
11|11	10.762	10.368	24|24	0.289	0.318
22|22	12.770	12.770	34|34	0.779	0.754
33|33	13.044	13.044	13|14	1.188	1.275
44|44	10.860	10.389	23|24	0.856	0.852
11|22	7.363	7.350	13|23	0.881	0.885
11|33	7.475	7.468	14|24	1.011	1.109
11|44	10.805	10.379	12|34	0.789	0.767
22|33	12.773	12.773	13|24	0.314	0.336
			14|23	1.911	1.910

[a] The σ_q are defined in Eq. (20).
[b] See note c, Table I.
[c] Values for all but the overlap integrals are here in electron volts.

[9] The normalizing factors N_i are readily found from the overlap integrals S_{pq} given in Table I. For example, $N_2=[2(1+S_{bc})]^{\frac{1}{2}}=(2.46562)^{\frac{1}{2}}=1.57023$.

[10] This can be proved either by formal group theory or by direct computation making use of such equivalences as $S_{ab}=S_{cd}$.

[11] That the order of orbital energies is the one indicated can be seen by application of the classical criterion that energy increases with the number of nodes. As a rough approximation, the molecular orbitals for butadiene will be, in order of increasing energy,

$$\left.\begin{aligned}
&\phi_1\sim\chi_a+\chi_b+\chi_c+\chi_d\\
&\phi_2\sim\chi_a+\chi_b-\chi_c-\chi_d\\
&\phi_3\sim\chi_a-\chi_b+\chi_c-\chi_d\\
&\phi_4\sim\chi_a-\chi_b-\chi_c+\chi_d
\end{aligned}\right\}$$

and this is the order assumed in Eq. (22).

[12] For example,

$$\begin{aligned}
I_{22}{}^{\sigma}&=(1/N_2N_2)(I_{bb}+2I_{bc}+I_{cc})=(2/N_2N_2)(I_{bb}+I_{bc})\\
&=-2(0.40558)(0.7648)Z=-0.62038Z \text{ atomic unit}\\
&=-(0.62038)(3.18)(13.602)=-26.834 \text{ ev}.
\end{aligned}$$

where

$$J_{i,pq}^{\sigma}=\int \phi_i^{*\nu}\sigma_p^{*\mu}(2/r^{\mu\nu})\phi_i^{\nu}\sigma_q^{\mu}d\tau^{\nu}d\tau^{\mu}$$

$$=\sum_{r,s} d_{ir}^{*}J_{rpsq}^{\sigma}d_{is} \quad (27)$$

and

$$K_{i,pq}^{\sigma}=\int \phi_i^{*\nu}\sigma_p^{*\mu}(2/r^{\mu\nu})\phi_i^{\mu}\sigma_q^{\nu}d\tau^{\nu}d\tau^{\mu}$$

$$=\sum_{r,s} d_{ir}^{*}J_{rpqs}^{\sigma}d_{is} \quad (28)$$

are Coulomb and exchange integrals intermediate in type between the J_{ij}^{σ}, K_{ij}^{σ} and the J_{pqrs}^{σ}. This provides the starting point for solution of our problem. We assume a set of d_{iq} values, compute the L_{pq} by Eq. (25), solve Eq. (21) for the ϵ_i, solve Eqs. (23) and (24) for a new set of d_{iq} values, and repeat until self-consistency is attained. Table III gives details of the self-consistent solutions obtained in this way for *cis*- and *trans*-1,3-butadiene. Each of these solutions was found after about a dozen trials.[13,14]

From Eqs. (20) and (22) and the d_{iq} values in Table III, we obtain four orthonormal molecular orbitals, as follows:

$$\left.\begin{aligned}
\phi_1&=\begin{Bmatrix}0.3484\\0.3540\end{Bmatrix}(\chi_a+\chi_d)+\begin{Bmatrix}0.4719\\0.4687\end{Bmatrix}(\chi_b+\chi_c)\\
\phi_2&=\begin{Bmatrix}0.5106\\0.5081\end{Bmatrix}(\chi_a-\chi_d)+\begin{Bmatrix}0.4222\\0.4229\end{Bmatrix}(\chi_b-\chi_c)\\
\phi_3&=\begin{Bmatrix}0.6439\\0.6452\end{Bmatrix}(\chi_a+\chi_d)-\begin{Bmatrix}0.4662\\0.4698\end{Bmatrix}(\chi_b+\chi_c)\\
\phi_4&=\begin{Bmatrix}0.5373\\0.5343\end{Bmatrix}(\chi_a-\chi_d)-\begin{Bmatrix}0.7276\\0.7268\end{Bmatrix}(\chi_b-\chi_c)
\end{aligned}\right\}\begin{Bmatrix}\text{upper values}\\ cis\text{-}\\ \text{lower values}\\ trans\text{-}\end{Bmatrix}. \quad (29)$$

TABLE III. Self-consistent molecular orbitals for the ground state.

	Cis-	*Trans-*		*Cis-*	*Trans-*
d_{11}/d_{12} assumed	0.6690	0.6810	2, 33	6.064	6.054
d_{23}/d_{24} assumed	0.7288	0.7298	2, 44	7.756	7.442
$(d_{12})^{-2}$	1.8216	1.8464	2, 34	5.185	5.134
$(d_{24})^{-2}$	1.9410	1.9411	Matrix elements L_{pq}^{σ}[f,g]		
Coulomb integrals[a,b,e]			11	6.555	6.386
1, 11	8.525	8.359	22	2.291	2.297
1, 22	10.897	10.860	12	−5.490	−5.543
1, 12	2.760	2.721	33	9.245	9.215
1, 33	10.912	10.876	44	5.668	5.656
1, 44	8.497	8.347	34	−5.100	−5.111
1, 34	2.711	2.660	Orbital energies[f]		
2, 11	9.566	9.279			
2, 22	9.300	9.310	ϵ_1	−1.164	−1.241
2, 12	2.646	2.592	ϵ_2	1.620	1.599
2, 33	9.495	9.501	ϵ_3	14.090	14.050
2, 44	9.578	9.278	ϵ_4	17.689	17.639
2, 34	2.684	2.618	d_{11}/d_{12} found	0.6690	0.6811
Exchange integrals[a,d,e]			d_{23}/d_{24} found	0.7286	0.7299
1, 11	4.925	4.802	d_{11}	0.4957	0.5012
1, 22	9.286	9.210	d_{12}	0.7409	0.7359
1, 12	5.168	5.143	d_{31}	0.9160	0.9135
1, 33	3.122	3.102	d_{32}	−0.7320	−0.7376
1, 44	2.406	2.636	d_{23}	0.5230	0.5239
1, 34	1.579	1.610	d_{24}	0.7178	0.7177
2, 11	4.141	4.433	d_{43}	0.9013	0.9003
2, 22	1.983	1.999	d_{44}	−0.7554	−0.7548
2, 12	1.597	1.659			

[a] Values in electron volts.
[b] *i, pq* is abbreviated notation for $J_{i,pq}^{\sigma}$—see Eq. (27).
[c] Sample calculation: 1, 11 (*cis*-) = (1/1.8216) [(1)(7.363) + 2(0.6690)(2.503) + (0.6690)²(10.762)].
[d] *i, pq* is an abbreviation for $K_{i,pq}^{\sigma}$—see Eq. (28).
[e] Sample calculation: 1, 11 (*cis*-) = (1/1.8216) [(1)(0.806) + 2(0.6690)(2.503) + (0.6690)²(10.762)].
[f] Values in electron volts; energy zero W_{2p}—see Table I, Note c.
[g] *pq* is an abbreviation for L_{pq}^{σ}.

These are listed in order of increasing energy; ϕ_1 and ϕ_2 are the best *LCAO SCF* ground state *MO*'s obtainable from Slater $2p\pi$-*AO*'s with $Z=3.18$.

We can now proceed to determine the ground state energy for the four π-electrons in the field of the core. This may be computed from Eq. (5), with [compare Eqs. (9) to (11)]

$$I_i=\sum_{p,q} d_{ip}^{*}I_{pq}^{\sigma}d_{iq}, \quad (30)$$

$$J_{ij}=\sum_{p,q,r,s} d_{ip}^{*}d_{jq}^{*}J_{pqrs}^{\sigma}d_{ir}d_{js}=\sum_{q,s} d_{jq}^{*}J_{i,qs}^{\sigma}d_{js}, \quad (31)$$

and

$$K_{ij}=\sum_{p,q,r,s} d_{ip}^{*}d_{jq}^{*}J_{pqsr}d_{ir}d_{js}=\sum_{q,s} d_{jq}^{*}K_{i,qs}^{\sigma}d_{js}. \quad (32)$$

[13] The problem treated here is of course a particularly simple one. There are really only two parameters to be determined by minimization of the energy—the ratios of d_{11} to d_{12} and d_{23} to d_{24} (orthogonality and normalization conditions give all the coefficients once these two ratios are known). Further, the coupling between these parameters proves to be small, so that successive approximations to each converge more or less independently of the other.

[14] It does not appear to matter much what orbitals are assumed in the starting approximation. One can use orbitals obtained from a semi-empirical scheme, or orbitals obtained assuming completely localized bonds. The former are likely to be closer to the correct orbitals, but the latter have the advantages that they may be found without appeal to a different computational framework and that use of them permits the calculation of resonance energies with very little additional work. (This last will be discussed elsewhere.)

Equivalently, since according to Eqs. (9) to (18),[15]

$$\epsilon_i=\sum_{p,q} d_{ip}^{*}L_{pq}^{\sigma}d_{iq}=I_i+\sum_{j=1,2}(2J_{ij}-K_{ij}), \quad (33)$$

one may use the formula

$$E_N=2\epsilon_1+2\epsilon_2-J_{11}-J_{22}-4J_{12}+2K_{12}. \quad (34)$$

The result in either case is

$$E_N=\left\{\begin{matrix}4W_{2p}-49.78 \text{ ev for } cis\text{-}\\ 4W_{2p}-48.93 \text{ ev for } trans\text{-}\end{matrix}\right\}, \quad (35)$$

where W_{2p} is the energy of a $2p\pi$-electron in a carbon atom in its valence state (−11.28 ev).

EXCITED STATE ORBITALS AND ENERGIES

The π-electrons are presumably responsible for the lowest excited electronic states of butadiene. From the *MO* point of view these excited states may be thought of as the result of placing one or more of the electrons in π-*MO*'s other than the ground state orbitals ϕ_1 and ϕ_2 found above. Wave functions for such excited states cannot in general be written as single determinants, but once the excited state orbitals are known the excited state energies can be computed without much difficulty.

TABLE IV. Computed excitation energies of excited states, using *MO*'s given by Eq. (29).[a]

Energy		Excitation $\phi_1\rightarrow\phi_3$	$\phi_1\rightarrow\phi_3$	$\phi_2\rightarrow\phi_4$	$\phi_1\rightarrow\phi_4$
$\epsilon_j-\epsilon_i$	*Cis-*	12.470	15.254	16.069	18.853
	Trans-	12.451	15.291	16.040	18.880
J_{ij}	*Cis-*	9.461	9.291	9.524	10.021
	Trans-	9.315	9.218	9.429	9.956
K_{ij}	*Cis-*	2.395	2.178	2.292	1.759
	Trans-	2.551	2.087	2.169	1.828
$EV_{ij}-EN$	*Cis-*	7.799	10.319	11.129	12.350
	Trans-	8.238	10.247	10.949	12.580
$ET_{ij}-EN$	*Cis-*	3.009	5.963	6.545	8.832
	Trans-	3.136	6.073	6.611	8.924
$\bar{E}TV_{ij}-EN$[b]	*Cis-*	5.404	8.141	8.837	10.591
	Trans-	5.687	8.160	8.780	10.752

[a] All energies in electron volts.
[b] Mean of $EV_{ij}-EN$ and $ET_{ij}-EN$.

The simplest assumption we can make about the excited state orbitals is that they may be taken from the set ϕ_1, ϕ_2, ϕ_3, ϕ_4 found in our treatment of the ground state. This allows us to write down immediately approximate wave functions for excited states which are orthogonal to the ground state function of Eq. (3). For example, we may write, for the singlet excited state V_{23} resulting from excitation of an electron from ϕ_2 to ϕ_3, and for the $M_S=0$ component of the corresponding triplet state, T_{23},

$$\left.\begin{matrix}\Psi V_{23}\\ \Psi T_{23}\end{matrix}\right\}=\frac{1}{(2\cdot4!)^{\frac{1}{2}}}\begin{vmatrix}(\phi_1\alpha)^1(\phi_1\beta)^1(\phi_2\alpha)^1(\phi_3\beta)^1\\ (\phi_1\alpha)^2(\phi_1\beta)^2(\phi_2\alpha)^2(\phi_3\beta)^2\\ (\phi_1\alpha)^3(\phi_1\beta)^3(\phi_2\alpha)^3(\phi_3\beta)^3\\ (\phi_1\alpha)^4(\phi_1\beta)^4(\phi_2\alpha)^4(\phi_3\beta)^4\end{vmatrix}\mp\frac{1}{(2\cdot4!)^{\frac{1}{2}}}\begin{vmatrix}(\phi_1\alpha)^1(\phi_1\beta)^1(\phi_2\beta)^1(\phi_3\alpha)^1\\ (\phi_1\alpha)^2(\phi_1\beta)^2(\phi_2\beta)^2(\phi_3\alpha)^2\\ (\phi_1\alpha)^3(\phi_1\beta)^3(\phi_2\beta)^3(\phi_3\alpha)^3\\ (\phi_1\alpha)^4(\phi_1\beta)^4(\phi_2\beta)^4(\phi_3\alpha)^4\end{vmatrix} \quad (36)$$

with the upper (−) sign for V_{23} and the lower (+) for the T_{23}. The energies $\int\Psi^{*}\mathbf{H}\Psi d\tau$ associated with each of these wave functions can be found by straightforward integration using Eq. (4) for $\mathbf{H}$. The results are[16]

$$\left.\begin{matrix}E_{V_{23}}\\ E_{T_{23}}\end{matrix}\right\}=2I_1+I_2+I_3+J_{11}+2J_{12}+2J_{13}+J_{23}-K_{12}-K_{13}\pm K_{23}$$

$$=2\epsilon_1+\epsilon_2+\epsilon_3-J_{11}-J_{22}-4J_{12}-J_{23}+2K_{12}+K_{23}\pm K_{23} \quad (37)$$

with $+K_{23}$ for V_{23} and $-K_{23}$ for T_{23}. Hence, employing Eqs. (5) and (34) for E_N, we find

$$\left.\begin{matrix}E_{V_{23}}-E_N\\ E_{T_{23}}-E_N\end{matrix}\right\}=I_3-I_2-J_{22}-2J_{12}+2J_{13}+J_{23}+K_{12}-K_{13}\pm K_{23}$$

$$=(\epsilon_3-\epsilon_2)-(J_{23}-K_{23})\pm K_{23}$$

$$=(\epsilon_3^{(2)}-\epsilon_2)\pm K_{23}. \quad (38)$$

The last form of Eqs. (38), making use of the definition

$$\epsilon_3^{(2)}\equiv\epsilon_3-(J_{23}-K_{23}),$$

has been introduced to emphasize the fact that ϵ_3, although mathematically like ϵ_1 and ϵ_2 in being a root of the ground-state *SCF* Eq. (19), has a different physical significance. Physically, in states V_{23} and T_{23}, $\epsilon_3^{(2)}$ is much more closely an analog of ϵ_1 and ϵ_2 in representing a true orbital energy.[17] The superscript in $\epsilon_3^{(2)}$ indicates the presence of a "hole" in the ground state wave function, made by exciting a ϕ_2-electron. More generally, excitation of an electron from the $MO\phi_i$ to the $MO\phi_j$ gives rise to two excited states, one singlet and one triplet, with energies relative to the ground state given by

$$\left.\begin{matrix}E_{V_{ij}}-E_N\\ E_{T_{ij}}-E_N\end{matrix}\right\}=(\epsilon_j-\epsilon_i)-(J_{ij}-K_{ij})\pm K_{ij}$$

$$=(\epsilon_j^{(i)}-\epsilon_i)\pm K_{ij}. \quad (39)$$

[15] More simply, see reference 2, Eq. (14),—"subtractive partition."

[16] For detailed derivations see reference 3, or references 2 and 4 with due regard for reference 17.

[17] See reference 4, Section 23 (where ϵ_3 and ϵ_4 for butadiene are called "unacceptable" ϵ's), and Eqs. (21) and (22) of reference 2, where the excited-orbital ϵ's called ϵ_{pV} and ϵ_{pT} are physically significant orbital energies of the type of $\epsilon_3^{(2)}$ or $\epsilon_j^{(i)}$ of Eqs. (38) and (39) above. The latter correspond to Eq. (17a) of reference 2,

TABLE V. *LCAO* parameters α_p and β_{pq}.

Parameter	Value (ev) *cis-*	*trans-*
α_a	−5.16	−5.26
α_b	−6.32	−6.33
β_{ab}	−7.01	−6.84
β_{bc}	−3.29	−3.27
β_{ac}	−1.03	−1.03
β_{ad}	+0.44	+0.36

Excitation energies computed from these formulas for *cis-* and *trans-*1,3-butadiene are given in Table IV.

One might think that a better approximation to excited state wave functions and energies could be obtained by taking only the orbitals for *unexcited* electrons from the ground state orbitals ϕ_1 and ϕ_2 of Eq. (29), and determining better orbitals for the excited electrons than ϕ_3 and ϕ_4 of Eq. (29). This idea, however, is incorrect, since the only orbitals orthogonal to ϕ_1 and ϕ_2 of Eq. (29) and of the desired *LCAO* form are just ϕ_3 and ϕ_4 of Eq. (29),[13] and it is a prerequisite of simple energy formulas such as Eq. (39) that the molecular orbitals be orthogonal.

Nevertheless, *best SCF* orbitals for use in an excited state wave function should minimize the energy of *that* state (subject to orthogonality of the total wave function to lower state wave functions), and not be derived from a *ground* state energy-minimizing secular equation, as the Eq. (29) orbitals are. This implies that (as a result of the altered self-consistency requirements) the coefficients in the best orbitals ϕ_1 and ϕ_2 will differ somewhat from their values for the like-designated ground-state orbitals in Eq. (29); concurrently, the coefficients in the best ϕ_3 or ϕ_4 will likewise differ from the values given in Eqs. (29).

The equations for the coefficients in such a treatment are no longer as simple as Eqs. (16), but presumably they can be handled without prohibitive difficulty. We will discuss the derivation of these equations and their application to butadiene in a later paper.[18,19] We shall there also examine the so-called "ionic Hamiltonian" method of Mulliken, which works directly with the quantities $\epsilon_j^{(i)}$ in Eq. (39).

DISCUSSION

In semi-empirical *LCAO* schemes for treating butadiene, a secular equation similar in form to Eq. (19) is usually considered, but excitation energies are approximated by differences in the roots ϵ_i alone. Our discussion above in connection with Eqs. (38) and (39), and the numerical values in Table IV, show that this is not a valid way to proceed from Eq. (19) theoretically, so that our secular determinant elements L_{pq} should not be associated directly with corresponding quantities determined semi-empirically.[20] More explicitly, one may define *LCAO* parameters

$$\alpha_p \equiv L_{pp} \tag{40}$$

and[21]

$$\beta_{pq} \equiv L_{pq} - (S_{pq}/2)(L_{pp}+L_{qq}), \tag{41}$$

and relate the L_{pq} to the L_{pq}^{σ} through the use of Eqs. (20). If [2,4] one assumes

$$W_{2p} = -11.28 \text{ ev}, \tag{42}$$

one then obtains the numerical values given in Table V, but these do not refer to the same thing as semi-empirical α_p- and β_{pq}-values do.[20] The Table V values may legitimately be compared with *theoretically* determined values for other molecules,[2,4] however, and are in fact in reasonable accord with them.[20,22]

One would not expect that the ground state orbitals given in Eqs. (29) would agree quantitatively with ones obtained semi-empirically, but the agreement is in fact fairly good; up to normalizing factors Lennard-Jones, for example, found[23]

$$\begin{aligned}\phi_1 &= 0.401(\chi_a+\chi_d)+0.582(\chi_b+\chi_c)\\ \phi_2 &= 0.582(\chi_a-\chi_d)+0.401(\chi_b-\chi_c)\end{aligned} \tag{43}$$

which are almost the same as our orbitals.

Theoretical first ionization potentials $\mathcal{I}_1$ for our molecules can be computed very easily from the results in Table III. According to Mulliken,[2]

$$\mathcal{I}_1 \sim -\epsilon_2. \tag{44}$$

Hence, from Table III and Eq. (42), we find

$$\mathcal{I}_1 \sim \left\{\begin{array}{l} -W_{2p}-1.620 = 9.66 \text{ ev for } cis\text{-} \\ -W_{2p}-1.599 = 9.68 \text{ ev for } trans\text{-}\end{array}\right\}. \tag{45}$$

The experimental value (probably for *trans-*)[24] is

$$\mathcal{I}_1 \text{ (exper.)} = 9.0 \text{ ev}. \tag{46}$$

while Roothaan's ϵ's correspond to Eq. (17); Eqs. (17) and (17a) become identical for ground state ϵ's, but only for these.

[18] Just as the Roothaan *LCAO SCF* theory for a closed-shell ground state parallels the Hartree-Fock *SCF* theory for such a state, so a *LCAO SCF* theory for T and V states such as those represented by Eqs. (36) and (37) may be patterned after the corresponding Hartree-Fock theory. The latter has been given by D. R. Hartree and W. Hartree in an article on excited states of Be, Proc. Roy. Soc. **A154**, 588 (1936).

[19] Perhaps easier than separate minimization of T and V energies would be minimization of their center of gravity. The corresponding Hartree-Fock theory has been discussed by G. Shortley, Phys. Rev. **50**, 1072 (1936).

[20] See reference 4 for a discussion of the faults of the semi-empirical method, and for a discussion of the variously defined α's and β's, their meanings, their interconnections, and (see especially Table XVIII) their values in various molecules. The α's and β's in Table V are α^N's and β^N's in the notation of reference 4.

[21] See reference 2, Eq. (29).

[22] The most striking feature of our calculated β's is that non-neighbor β's are important, of our α's that α's on end and central atoms differ (cf. also reference 4, Tables XV and XVIII; and concluding section of reference 3 in 1949–50 ONR report).

[23] See. R. S. Mulliken, J. Chem. Phys. **7**, 121 (1939), Table II, for a summary of semi-empirically determined *LCAO*'s for 1,3-butadiene, and references to the literature.

[24] R. S. Mulliken, Rev. Mod. Phys. **14**, 265 (1942), corrected for new values of fundamental constants.

The agreement is very encouraging, and is similar to agreements found in similar computations on other hydrocarbon molecules.[25]

At first sight, the ground state *electronic* energy values E_N of Eq. (35) would seem to predict *cis-* to be more stable than *trans*-1,3-butadiene by 0.85 ev. This interpretation is not justified, however, since the *total* energies (say W_N) of the two isomers include internuclear repulsion terms which differ for *cis-* and *trans*-1,3-butadiene. These repulsion terms would appear as parts of the total energy $W_N{}^c$ of the π-electron-less framework, giving

$$W_N = W_N{}^c + E_N \tag{47}$$

for the total energy of the neutral molecule. Although we do not know the $W_N{}^c$ values, the *differenice* between $W_N{}^c$ for *cis-* and *trans*-forms can probably be obtained with little error by treating the core, for this purpose, as a system of four point charges $+e$ located at the centers of the four carbon atoms, and then taking

$$W_N(cis\text{-}) - W_N(trans\text{-}) = [W_N{}^c(cis\text{-}) - W_N{}^c(trans\text{-})] + [E_N(cis\text{-}) - E_N(trans\text{-})]. \tag{48}$$

It is readily seen that all the repulsion terms are the same for *cis-* and *trans-*, except for those between the end atoms *a* and *d*. With the geometrical model specified at the outset of this paper, the distance R_{ad} is 2.97A for *cis-* and 3.72A for *trans-*, giving 4.84 or 3.87 ev as the respective electrostatic repulsion energies. Taking the difference, and also using Eqs. (35) and (48), we have

$$\begin{aligned} W_N{}^c(cis\text{-}) - W_N{}^c(trans\text{-}) &= +0.97; \\ E_N(cis\text{-}) - E_N(trans\text{-}) &= -0.85; \\ W_N(cis\text{-}) - W_N(trans\text{-}) &= +0.12. \end{aligned}$$

Our prediction is then that the *trans*-form is more stable than the *cis-* by 0.12 ev. This result seems to be in agreement with the weight of experimental evidence.[24,26] It also agrees with a result obtained earlier by Mrs. C. A. Rieke and one of the writers in computations by the semiempirical *LCAO* method.[24]

So far as excitation energies are concerned, our results fall in line with those previously found for other molecules.[1,25] If the mean energy of any singlet and its corresponding triplet state is called $\bar{E}_{TV}$, then the theory [cf. Eq. (39) for butadiene] gives

$$\left.\begin{matrix} E_{V_{ij}} \\ E_{T_{ij}} \end{matrix}\right\} = \bar{E}_{TV_{ij}} \pm K_{ij}. \tag{49}$$

Just as in other cases where *LCAO* computations have been made (H_2, C_2H_4, C_6H_6), the computed singlet-triplet separations ($2K_{ij}$) are too large for butadiene, indicating that the *LCAO* method is unreliable for the computation of the K_{ij}'s, or else that other factors enter to modify Eq. (49).[27] But if, as in the other cases,[28] we use for butadiene the computed *mean* values $\bar{E}_{TV}$ (cf. last lines in Table IV) and replace K_{ij} by a reasonable estimated effective value [27] (say 0.5 ev), we obtain 5.9 and 6.2 ev for the lowest singlet excitation energies of the *cis-* and *trans*-forms, respectively, as compared with the observed value 6.0 ev.[24] The similarly obtained values 8.6 and 8.7 ev for the next lowest singlet excitation energy may be compared with the probable observed value[24] of 7.2 ev. It will be interesting to see the singlet-triplet splittings which result when T and V energies are separately minimized.[29]

There are several reasons why the numerical values we have obtained should not be regarded as final:

(1) Best orbitals and energies should really be determined by a method which includes inner shell electrons explicitly, i.e., by Roothaan's complete scheme.[3] This would incidentally remove the limitations imposed by our arbitrary assumption that the π-electron-less core consists of neutral hydrogen atoms and singly charged carbon atoms.

(2) The forms of the *AO*'s which are used in constructing the *LCAO MO*'s should themselves be determined by a variational procedure, at least for the valence *AO*'s. The Slater $2p$ *AO*'s with $Z=3.18$ which we have used might thus need to be strongly modified.[30]

(3) Approximations are necessary at the present time for the evaluations of three-center and penetration integrals (see Appendix) and orbitals and energies are sensitive to these values.

Our results should be at least semiquantitatively correct, however, and so may be regarded as a "go" sign for work with *LCAO SCF* methods on other molecules.[31]

APPENDIX: INTEGRALS

The integrals we need are overlap, Coulomb-exchange and core integrals involving the atomic orbitals χ_p, which we take in the form (in atomic units)

$$\chi_p{}^\nu = (Z^5/32\pi)^{\frac{1}{2}} z^\nu \exp(-Z r_p{}^\nu/2), \tag{A1}$$

where z^ν is the perpendicular distance of electron ν from the plane of the molecule, $r_p{}^\nu$ is the distance of that electron from the pth carbon nucleus, and the screening constant Z is taken to have the value 3.18. Numerical values are given in Table I.

Overlap integrals S_{pq} between the various χ's may be computed from well-known formulas.[32]

The Coulomb-exchange integrals J_{pqrs} which involve

[25] References 2 to 4; for a summary of values see reference 4, Table XIX.

[26] Aston, Szasz, Woolley, and Brickwedde, J. Chem. Phys. **14**, 67 (1946).

[27] Cf. reference 2, Eq. (22) and accompanying discussion.

[28] For comparison of computed and observed $\bar{E}_{TV}$ values for H_2, C_2H_4, and C_6H_6, see reference 4, Table XIX. For H_2, the true $E_V - E_T$ is known from accurate theoretical calculations; for C_2H_4 (reference 24) and for C_6H_6 [cf. Roothaan and Mulliken, J. Chem. Phys. **16**, 118 (1948)] approximate values are known from spectroscopic evidence.

[29] In the case of the Be atom, Hartree and Hartree (see reference 18) found a definite improvement when T and V energies were separately minimized. However, the improvement was not as large as would be needed in the present case.

[30] Note that the Slater $2p$ *AO*'s differ markedly from the best (*SCF*) *AO*'s of the free carbon atom [cf. e.g., Mulliken, Rieke, Orloff, and Orloff, J. Chem. Phys. **17**, 1248 (1949)].

[31] Cf. reference 4, Section 27, for some further general discussion.

[32] Cf. R. G. Parr and B. L. Crawford, Jr., J. Chem. Phys. **16**, 1049 (1948).

no more than two different χ's may be found by interpolation in a table of Parr and Crawford[32] (as slightly revised by Roothaan[33]); in a slight modification of their notation,

$$J_{pqrs} \equiv (\chi_p\chi_r|\,\chi_q\chi_s). \tag{A2}$$

The J_{pqrs}'s which involve three or more different χ's must be estimated—we have used the approximation formula (due to Sklar[34])

$$(\chi_p\chi_r|\,\chi_q\chi_s) \sim S_{pr}S_{qs}(\chi_{p'}\chi_{p'}|\,\chi_{q'}\chi_{q'}), \tag{A3}$$

where $\chi_{p'}$ is a Slater $2p\pi$-carbon AO taken as located midway between atoms p and r, $\chi_{q'}$ is a Slater $2p\pi$-AO located midway between atoms q and s, and S_{pr} and S_{qs} are overlap integrals between the indicated χ's.

Core integrals cannot be evaluated so accurately. According to Eq. (12), these are defined by

$$I_{pq} = \int \chi_p{}^{*\nu}(\mathbf{T}^\nu + \mathbf{U}_c{}^\nu)\chi_q{}^\nu d\tau^\nu, \tag{A4}$$

where $\mathbf{T}^\nu$ is the kinetic energy operator for electron ν and $\mathbf{U}_c{}^\nu$ is the potential energy for electron ν in the field of the $2p\pi$-electron-less core. The difficulty lies in the $\mathbf{U}_c{}^\nu$ term. Following Goeppert-Mayer and Sklar,[35] we assume that the hydrogen atoms may be ignored, and write $\mathbf{U}_c{}^\nu$ as a sum of contributions from the four carbon atoms, each once ionized, giving

$$\mathbf{U}_c{}^\nu = \sum_{p=1}^{4} \mathbf{U}_p{}^\nu. \tag{A5}$$

Here $\mathbf{U}_p{}^\nu$ is the potential of electron ν in the field of the pth carbon atom less its $2p\pi$-electron, and

$$\mathbf{U}_p{}^\nu = \mathbf{U}_p{}^{0\nu} - \int (e^2/r^{\mu\nu})|\,\chi_p{}^\mu|^2 d\tau^\mu, \tag{A6}$$

where $\mathbf{U}_p{}^{0\nu}$ is the potential of electron ν in the field of the *neutral* pth carbon atom, for which Goeppert-Mayer and Sklar have given an approximate expression. Using the relation

$$(\mathbf{T}^\nu + \mathbf{U}_p{}^\nu)\chi_p{}^\nu = W_{2p}\chi_p{}^\nu, \tag{A7}$$

where W_{2p} is the energy of a $2p\pi$-electron in a carbon atom in its tetravalent valence state,[22] we then obtain, relative to W_{2p} as the zero of energy,

$$I_{pq} = -\sum_{r,\neq q} [(A_r{:}\,\chi_p\chi_q) + (\chi_p\chi_q|\,\chi_r\chi_r)], \tag{A8}$$

where the quantities

$$(A_r{:}\,\chi_p\chi_q) = -\int \mathbf{U}_r{}^{0\nu}\chi_p{}^{*\nu}\chi_q{}^\nu d\tau^\nu \tag{A9}$$

are "penetration integrals." Values for two-center penetration integrals based on Goeppert Mayer and Sklar's $\mathbf{U}_r{}^{0\nu}$ may be found in the paper of Parr and Crawford;[32] for three-center penetration integrals one may employ the formula

$$(A_r{:}\,\chi_p\chi_q) \sim S_{pq}(A_r{:}\,\chi_{p'}\chi_{p'}), \tag{A10}$$

where $\chi_{p'}$ is a Slater $2p\pi$-AO located midway between atoms p and q.

---

[33] C. C. J. Roothaan (unpublished work)—see reference 5. Some of Parr and Crawford's Coulomb integrals are in error by a few units in the fourth decimal.

[34] A. L. Sklar, J. Chem. Phys. **7**, 984 (1939). For another useful but perhaps slightly less accurate formula, see Mulliken, reference 4, Eq. (154b).

[35] M. Goeppert-Mayer and A. L. Sklar, J. Chem. Phys. **6**, 645 (1938). See also reference 2 for further discussion, including an estimate of the effect of the H atoms in C_2H_4 and C_2H_2.

Ionization and Dissociation by Electron Impact: Cyanogen, Hydrogen Cyanide, and Cyanogen Chloride and the Dissociation Energy of Cyanogen

D. P. STEVENSON
Shell Development Company, Emeryville, California
(Received June 13, 1950)

The appearance potentials of CN^+ in the mass spectra of HCN and $(CN)_2$ have been remeasured and found to be $19.3_6 \pm 0.2$ and $20.3_1 \pm 0.2$ ev, respectively. Combination of the appropriate thermochemical data with the difference between these energies yields, $D(NC-CN) = 6.8_8 - 2E(Z)$ ev where Z is the state of the CN radical either $X^2\Sigma^+$ or $A^2\Pi_i$, that accompanies CN^+ from $(CN)_2$, and $E(X^2\Sigma^+) = 0.00$ ev and $E(A^2\Pi_i) = 1.13$ ev. The appearance potential of Cl^+ in the mass spectrum of ClCN has also been measured and found to be $17.8_1 \pm 0.2$ ev, which value gives $D(NC-CN) = 6.9_2 - 2E(Y)$ when combined with the spectroscopic ionization potential of the chlorine atom and the necessary thermochemical data. Here Y is the state of the CN radical that accompanies Cl^+ from ClCN. In order that the two determinations of $D(NC-CN)$ be consistent it is necessary that $Y=Z$ and then the two permissible values of $D(NC-CN)$ are $6.9_0 \pm 0.2$ ev ($Y=Z=X^2\Sigma^+$) or $4.6_4 \pm 0.2$ ev ($Y=Z=A^2\Pi_i$). These results do not permit a choice between White's determination, 6.3 ± 0.2 ev, and Pauling's estimate, 3.9 ± 0.6 ev, but do serve to eliminate from further consideration the determination by Kistiakowsky and Gershinowitz, 3.3 ev. Neither value is compatible with the 5.2 ev suggested by Glockler. However, electron impact data on ethylene and methylene radical give 5.6 ev as the upper limit to energy of dissociation of ethylene into two methylene radicals, and this can be taken as an upper limit to the dissociation energy of cyanogen, suggesting the lower of the two possible values of $D(NC-CN)$ to be correct. Corresponding to this lower value of $D(NC-CN)$, $4.6_4 \pm 0.2$ ev, the dissociation energies of H−CN and Cl−CN are $4.8_0 \pm 0.1$ and $3.6_6 \pm 0.1$ ev, respectively, and the ionization potential of CN is $14.5_6 \pm 0.2$ ev.

The specific intensities of the various ions in the mass spectra of $(CN)_2$, HCN, and ClCN characteristic of 75-volt ionizing electrons are given with reference to that of A^+ in the argon mass spectrum.

INTRODUCTION

TWO experimental determinations of the heat of dissociation of cyanogen, $D(NC-CN)$, differ by a factor of about two, 3.3 ev[1] and 6.3 ev,[2] and Pauling[3] has recently suggested the value 3.9 and Glocker[3a] has suggested 5.2 ev on theoretical grounds. Although the electron impact methods[4] of determining dissociation energies in di- and polyatomic molecules are not entirely unambiguous, when carefully applied, they do yield values which are in agreement with the results of other methods.[5] In view of the wide variety in the values of $D(NC-CN)$ which have been suggested it seemed probable that the electron impact method should at least permit selection to be made between the suggested values if it could not yield a definite value by itself.

Two independent electron impact methods of estimating $D(NC-CN)$ suggest themselves. These are the "indirect method"[4,6] employing the difference between the appearance potentials of CN^+ in the mass spectra of HCN and $(CN)_2$ in combination with the appropriate thermochemical data, and the "direct method"[6] employing the difference between the spectroscopically determined ionization potential of the chlorine atom and the appearance potential of Cl^+ in the mass spectrum of ClCN in combination with the necessary thermochemical data. To the extent that the values of a dissociation energy determined by these two methods agree, considerable confidence can be placed on the reliability of the determination.

With the foregoing facts in mind the necessary measurements on cyanogen, hydrogen cyanide, and cyanogen chloride were undertaken, and are reported in this paper.

EXPERIMENTAL

Small samples of the three compounds were prepared from J. T. Baker Chemical Company c.p. potassium cyanide. Hydrogen cyanide and cyanogen were prepared by the addition of saturated aqueous solutions of the cyanide to sulfuric acid (30 percent) and concentrated cupric sulfate solution in water, respectively. Cyanogen chloride was made by the action of chlorine, generated *in situ*, by the reaction of hydrochloric acid with potassium chlorate, on the cyanide.

The initial product in each case was contaminated with carbon dioxide resulting from the potassium carbonate impurity of the cyanide. The carbon dioxide content of the hydrogen cyanide was reduced by a vacuum distillation in which a generous portion of the sample was pumped off at −78° and discarded. No effort was made to remove this impurity from the samples of cyanogen or cyanogen chloride since carbon dioxide is incapable of giving ions that would interfere with the measurements.

Hydrogen cyanide was removed from the cyanogen and cyanogen chloride preparations by treatment with cold aqueous silver nitrate and dry zinc oxide powder, respectively. All three materials were dried with anhydrous calcium chloride.

[1] G. B. Kistiakowsky and H. Gershinowitz, J. Chem. Phys. **1**, 432 (1933).
[2] J. U. White, J. Chem. Phys. **8**, 459 (1940).
[3] L. Pauling and W. F. Sheehan, Jr., Proc. Nat. Acad. **35**, 359 (1949).
[3a] G. Glockler, J. Chem. Phys. **16**, 600 (1948).
[4] D. P. Stevenson, J. Chem. Phys. **10**, 291 (1942).
[5] For comparison of various methods applied to diatomic molecules see H. D. Hagstrum, Phys. Rev. **72**, 947 (1947), while for hydrocarbons see E. W. R. Steacie, *Atomic and Free Radical Reactions* (Reinhold Publishing Corporation, New York, 1946), pp. 76–79.
[6] J. A. Hipple and D. P. Stevenson, Phys. Rev. **63**, 121 (1943).

TABLE I. Impurities in HCN, $(CN)_2$, and ClCN samples. Percent m, mass spectrometrically determined.

Impurity	Sample HCN	$(CN)_2$	ClCN
CO_2	1.7_5	4.1	22.1
HCN	M.C.[b]	0.02	0.16
$(CN)_2$	<0.002	M.C.[b]	1.8_1
BrCN[a]	...	...	0.15
HCl	...	...	<0.05

[a] Identified and estimated from intensities of ions. $m/q=107$ and 105. Sensitivity estimated from that of ClCN (Table IV) by multiplication of the latter by the ratio of the sensitivity of krypton to that of argon (see Table IV).
[b] M.C. = Major component.

The concentration of the impurities determined mass spectrometrically, in the samples upon which the appearance potential measurements were made, are shown in Table I. Although the purity of the cyanogen chloride sample left much to be desired, the absence of hydrogen chloride assured no interference with the measurements on Cl^+, which were of primary interest.

The ionization efficiency curves from which the appearance potentials were determined from the "initial breaks,"[7] were measured by recording the appropriate region of the mass spectrum at a series of settings of the apparent ionizing electron energy starting a number of volts above the onset of observable current of the ion of interest and extending at least one volt below the onset of observable current. For the measurements on CN^+ the voltage scale was calibrated by observing the onset of observable current of Ne^+ through the simultaneous admission of neon with the HCN or $(CN)_2$. In these cases the mass spectrum was recorded each time across the range $18 \leqslant m/q \leqslant 29$. In the case of the measurements of Cl^+ the voltage scale was calibrated through simultaneous measurements on A^+ from co-admitted argon, the mass spectrum being scanned across the range, $32 \leqslant m/q \leqslant 44$. A minimum of four series of measurements were made on each ion.

The mass spectrometer used in this investigation is a Westinghouse, Type LV.[8] The mass spectra were scanned by varying the magnetic field through the appropriate range for a positive ion accelerating potential of 1000 v. A positive ion drawing out potential of 5.0 v was used throughout. The ionizing electrons (10 μa) were taken from a Wolfram filament driven and controlled as described by Hipple, Grove, and Hickam.[9] The apparent ionizing electron energy was adjusted by means of a 15-turn, $3\frac{1}{2}$-in., 50,000Ω Helipot and read on a Weston, Model 622, 1000Ω per volt meter. The guaranteed precision of this meter is ±0.5 percent at full-scale deflection and all voltage settings were made with the deflections in the upper half of the range, by selection of the proper range shunt. As judged from the reproducibility of ion current measurements in the range of their rapid increase, the voltage settings are reproducible to ±0.02 v.

TABLE II. Appearance potentials of CN^+ and Cl^+.

Molecule	Ion (I^+)	$A(I^+)$ ev	Previous measurements
HCN	CN^+	19.3_6±0.2	20.1±0.2[a]
$(CN)_2$	CN^+	20.3_1±0.2	21.3±0.3,[b] 18[c]
ClCN	Cl^+	17.8_1±0.2	—

[a] Kusch, Hustrulid, and Tate, Phys. Rev. **52**, 843 (1937).
[b] Tate, Smith, and Vaughan, Phys. Rev. **48**, 525 (1935).
[c] Dorsch and Kallman, Zeits. f. Physiks. **60**, 376 (1930).

From the agreement of the difference between the apparent appearance potentials of A^+ and Ne^+ with the difference between the spectroscopic first ionization potentials of argon (15.76 ev) and neon (21.56 ev),[10] it is concluded that the differences between appearance potentials are accurate to ±0.1 ev and the accuracy of the absolute voltage scale is ±0.2 ev.

The ionization efficiency curves from which the appearance potentials shown in Table II were deduced are shown in Fig. 1.

DISCUSSION

As was mentioned above, the appearance potentials were taken equal to the ionizing electron energy corresponding to the first detectable positive ion current, the vanishing-current method.[7] Equality of sensitivity was achieved for the ion CN^+ [both HCN and $(CN)_2$], Cl^+, and Ne^+ through the use of equal pressures of the gases in the reservoir. The much greater cross section of argon for production of A^+ than of the other gases for production of the other ions of interest was compensated for by plotting one-tenth the A^+ current observed at the same argon pressure as for the other gases. It is believed that the systematic difference between the values obtained for the appearance potentials of CN^+ and those of Tate and co-workers[11] arise from the use by the latter of the linear extrapolation method of interpreting ionization efficiency curves.[12] When the linear extrapolation method was applied to our data the appearance potentials of CN^+ were found to be 19.7_0 ±0.2 ev (HCN) and 20.8_0±0.2 ev $(CN)_2$, which agree with the previously published values[11] within the combined limits of error. Inasmuch as the appearance potentials of CN^+ in HCN and $(CN)_2$ are to be combined by difference in computing $D(NC-CN)$ (see below), the choice of method of determining the appearance potentials would have little effect on the value obtained for the dissociation energy. However, such would not be the case when the datum on Cl^+ from ClCN is employed, since this datum is to be combined with a spectro-

[7] (a) L. G. Smith, Phys. Rev. **51**, 263 (1937). (b) D. P. Stevenson and J. A. Hipple, *ibid.* **62**, 237 (1942). (c) T. Mariner and W. Bleakney, *ibid.* **72**, 807 (1947).
[8] J. A. Hipple, J. App. Phys. **13**, 551 (1942).
[9] Hipple, Grove, and Hickam, Rev. Sci. Inst. **16**, 69 (1945).
[10] C. E. Moore, *Atomic Energy Levels*. Circular C-467 of the National Bureau of Standards (1949).
[11] See Table II, references (a) and (b).
[12] See reference 7c for a thorough discussion of the probable significance of the appearance potentials deduced by the two methods.

scopically determined ionization potential rather than an electron impact appearance potential.[13] As will be seen below, the choice of the vanishing current method results in complete agreement between the two calculations of $D(NC-CN)$.

The heats of formation, $\Delta Hf°(25°C)$, of HCN (gas), $(CN)_2$ (gas), and ClCN (gas) from the elements are 1.35, 3.20, and 1.50 ev, respectively.[14] The dissociation energies, $D(A-A)$, of H_2 and Cl_2, are 4.48 and 2.48 ev,[15] respectively, and the ionization potential[10] of Cl, $I^z(Cl)$, is 13.01 ev. We may write for the electron impact induced ionization and dissociation reactions,

$$HCN+\epsilon^-\rightarrow CN^++H+2\epsilon^-;$$
$$A_1(CN^+)=D(H-CN)+I^z(CN) \quad (1)$$

$$(CN)_2+\epsilon^-\rightarrow CN^++CN(Z)+2\epsilon^-; \quad (2)$$
$$A_2(CN^+)=D(NC-CN)+I^z(CN)+E(Z),$$

where Z is the electronic state of the neutral CN radical formed in (2). From the magnitudes of $A_1(CN^+)$ and $A_2(CN^+)$ and the expected magnitudes of $I^z(CN)$, 10–15 ev, $D(H-CN)$, 4–5 ev, and $D(NC-CN)$, 3.5–6.5 ev, it follows that the H [Eq. (1)], and the CN^+ [Eqs. (1) and (2)], are in their lowest electronic states. The formation of H, $2p$, would require A_1 to be ~10 ev larger than is observed. By analogy with N_2, the first excited state of CN^+ would be expected to be 5 to 7 ev above the ground state,[16] and this too would require higher values of $A_1(CN^+)$ and $A_2(CN^+)$. However, on *a priori* grounds the neutral CN of Eq. (2) could be equally well in either the $X^2\Sigma^+$-ground state or the $A^2\Pi_i$ first excited state with $E(A^2\Pi_i)=1.13$ ev. As has been found to be satisfactory in numerous other similar cases,[6] the possibility that $A_1(CN^+)$ and/or $A_2(CN^+)$ are greater than the indicated sums is ignored.

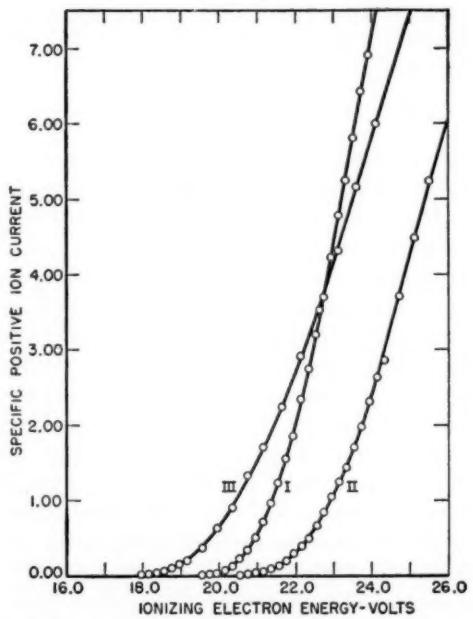

FIG. 1. Ionization efficiency curves. I. CN^+ from HCN. II. CN^+ from $(CN)_2$. III. Cl^+ from ClCN.

TABLE III. Dissociation energies of HCN, $(CN)_2$, and ClCN in ev.

Z	$E(Z)$	$D(NC-CN)$	$D(H-CN)$	$D(Cl-CN)$	$I^z(CN)$
		$(CN)_2$, and ClCN in ev.			
$X^2\Sigma^+$	0.00	$6.9_0\pm0.2$	$5.9_4\pm0.1$	$4.7_9\pm0.2$	$13.4_2\pm0.2$
$A^2\Pi_i$	1.13[a]	4.64±0.2	4.81±0.1	3.66±0.2	14.55±0.2

[a] G. Herzberg, *Molecular Spectra and Molecular Structure, I, Spectra of Diatomic Molecules* (Van Nostrand Company, Inc., New York, 1950), second edition, p. 520.

Combining Eqs. (1) and (2) with the following:

$$\tfrac{1}{2}H_2+C_{graph}+\tfrac{1}{2}N_2=HCN \qquad \Delta Hf°=1.35 \text{ ev} \quad (3)$$

$$2C_{graph}+N_2=(CN)_2 \qquad \Delta Hf°=3.20 \text{ ev} \quad (4)$$

$$H_2=2H \qquad D(H_2)=4.48 \text{ ev} \quad (5)$$

we find,

$$(CN)_2=2\,CN(Z)$$
$$\Delta H_6=4.98+2(A_2(CN^+)-A_1(CN^+))$$
$$\Delta H_6=D(NC-CN)+2E(Z) \quad (6)$$
$$\Delta H_6=6.8_8\pm0.2 \text{ ev}$$

and

$$HCN=H+CN(Z)$$
$$\Delta H_7=4.98+A_2(CN/)-A_1(CN^+)$$
$$\Delta H_7=D(H-CN)+E(Z) \quad (7)$$
$$\Delta H_7=5.9_3\pm0.1 \text{ ev}.$$

Similarly,

$$C_{graph}+\tfrac{1}{2}\,Cl_2+\tfrac{1}{2}\,N_2=ClCN$$
$$\Delta Hf°=1.50 \text{ ev} \quad (8)$$

$$Cl_2=2Cl \qquad D(Cl_2)=2.48 \text{ ev} \quad (9)$$

$$Cl=Cl^++\epsilon^-$$
$$I^z(Cl)=13.01 \text{ ev} \quad (10)$$

$$ClCN+\epsilon^-=Cl^++CN(Y)+2\epsilon^-$$
$$A_{11}(Cl^+)=D(Cl-CN)+I^z(Cl)+E(Y) \quad (11)$$

and thus

$$(CN)_2=2\,CN(Y) \qquad \Delta H_{12}=2A(Cl^+)-28.70$$
$$\Delta H_{12}=D(NC-CN)+2E(Y) \quad (12)$$
$$\Delta H_{12}=6.9_2+0.2 \text{ ev}$$

$$ClCN=Cl+CN(Y)$$
$$\Delta H_{13}=A(Cl^+)-13.01$$
$$\Delta H_{13}=D(Cl-CN)+E(Y) \quad (13)$$
$$\Delta H_{13}=4.8_0\pm0.2 \text{ ev}$$

The virtual identity of ΔH_6 and ΔH_{12} provides reasonable ground for accepting the assumption of the equality of the sums written for $A_1(CN^+)$, $A_2(CN^+)$, and $A_{11}(Cl^+)$, and further that the neutral CN formed by

[13] See reference 6 for a similar situation in the estimation of $D(CH_3-H)$ and $D(C_2H_5-H)$ from various electron impact data.

[14] *Tables of Selected Values of Chemical Thermodynamic Properties* (National Bureau of Standards). The conversion factor, 1 ev/molecule=23.06 kcal./mole, was used.

[15] G. Herzberg, *Molecular Spectra I* (Prentice-Hall, Inc., New York, 1939).

[16] L. Pauling, Zeits. f. Naturforschung **3a**, 438 (1948).

TABLE IV. Mass spectra[a] of HCN, $(CN)_2$, and ClCN. 75 ev, 55°C magnetic scan, 1000-v ion acceleration.

Ion	m/q	Ne	HCN	A	$(CN)_2$	ClCN	Kr
Kr^+	78, 80, 82, 83, 84, 86						1.61
$ClCN^+$	64, 63, 62, 61					1.51[b]	
$C_2N_2^+$	53, 52				1.22_0		
ClC^+	50, 49, 48, 47					0.0154	
Kr^{++}	39, 40, 41, 41½, 42, 43						0.290
A^+	40			1.000			
C_2N^+	39, 38				0.0175		
Cl^+	37, 35					0.0386	
$ClCN^{++}$	32, 31½, 31, 30½					0.0491	
N_2^+	28				0.0006		
HCN^+	28, 27		0.736				
$C_2N_2^{++}$	26½, 26				0.0441		
CN^+	27, 26		0.0813		0.0580	0.0179	
C_2^+	25, 24				0.0229		
A^{++}	20			0.133			
Ne^+	22, 20	0.159					
N^+	15, 14		0.0015		0.0031	0.0012	
HCN^{++}	14, 13½		0.0053				
CH^+	14, 13		0.0022				
C^+	13, 12		0.0048		0.0151	0.0058	

[a] The intensities are in arbitrary units for unit pressure gradient across the effusive "inlet leak."
[b] Ratio, $^{37}ClCN^+/^{35}ClCN^+ = 0.322 \pm 0.001$.

(2) and (11) are in the same state, i.e., $Z=Y$. Thus corresponding to the possible states of CN, we obtain for the three interrelated dissociation energies the values shown in Table III. The corresponding values of $I^z(CN)$ from Eq. (1) are also shown in Table III.

The second excited state of CN, $B^2\Sigma^+$, with the energy, $E(B^2\Sigma^+)=3.22$ ev is excluded from consideration since this would require of $D(NC-CN)$ the impossibly low value 0.4_6 ev.

Observations on the long wave limit of the continuous absorption spectrum of cyanogen chloride substantiates the possible energies of Table III, but do not permit a choice to be made between them. Badger and Woo,[16a] set 2270A as the long wave limit to the absorption of cyanogen chloride. New measurements in this laboratory permit raising this limit to 2450A. The continuous absorption, $\lambda < 2450$A, may correspond to either,

$$ClCN + h\nu \rightarrow Cl(3p^5\ ^2P_{\frac{3}{2}}^0) + CN(X^2\Sigma^+) \qquad (14)$$

or

$$ClCN + h\nu \rightarrow Cl(3p^5\ ^2P_{\frac{1}{2}}^0) + CN(A^2\Pi_i). \qquad (15)$$

If the absorption is represented by (14), the long wave limit sets 4.96 ev as the upper limit to $D(Cl-CN)$, while if (15) holds, then 3.94 ev is the upper limit to $D(Cl-CN)$. The first of these limits is consistent with the electron impact dissociation energies corresponding to $Z=X^2\Sigma^+$, while the second is consistent with the electron impact values corresponding to $Z=A^2\Pi_i$.

The value of $D(NC-CN)=6.9$ ev corresponding to $Z=X^2\Sigma^+$ is not incompatible with the experimental value due to White,[2] 6.3, while 4.6 corresponding to $Z=A^2\Pi_i$ lies within the uncertainty estimated by Pauling[3] for his theoretical value, 3.9 ± 0.6. The low experimental value of Kistiakowsky and Gershinowitz seems to be eliminated from further consideration by these data (Table III).

In neither 1,3-butadiene nor vinyl chloride does the double bond character of the single C—C or C—Cl bond result in an increase in the dissociation energy.[17,18] Thus the increases of 3.3 ev in $D(C-C)$ and 1.3 ev in $D(C-Cl)$ in the cases of cyanogen and cyanogen chloride, respectively, over the values found in ethane and methyl chloride,[17] which would be required by the larger possible value of $D(NC-CN)$, seem excessive. However, the shortening of the interatomic distances, C—C = 1.36A[18] and C—Cl = 1.67A[19] from the normal single bond values, 1.54A and 1.76A, respectively, might well be expected to be reflected in an increase in the dissociation energies. A difference in behavior of bonds to CN and C_2H_3 could easily be rationalized in the lesser possibilities of resonance stabilization of CN than of C_2H_3. Since the C—C distance in cyanogen is greater than normal double bond value,[18] 1.33A it seems reasonable to conclude that the dissociation energy of ethylene into two methylene radicals is an upper limit to the dissociation energy of cyanogen into two cyanide radicals. It is possible to calculate an upper limit to the dissociation energy of ethylene into two methylene radicals, as will be shown in the following paragraph.

Smith[7a] gives 15.7 ev as the appearance potential of CH_2^+ in the methane mass spectrum, and we may write:

$$CH_4 + \epsilon^- \rightarrow CH_2^+ + H_2 + 2\epsilon^-, \quad A_{16}(CH_2^+) = 15.7 \text{ ev} \qquad (16)$$

Langer and Hipple[20] have found the ionization potential of the methylene radical to be 11.9 ev. Combining these data with the heats of formation of methane (−0.78 ev) and ethylene (+0.54 ev) we find:

$$C_2H_4 = 2\,CH_2, \quad D(H_2C=CH_2) = 5.6 \text{ ev} \qquad (17)$$

Inasmuch as the appearance potential, $A_{16}(CH_2^+)$, is greater than or equal to the minimum energy required for (16), $D(H_2C=CH_2)=5.6$ ev is an upper limit to the energy required for the dissociation of ethylene, (17).

If we accept the conclusion that the energy of dissociation of ethylene into two methylene radicals is an upper limit to the energy required for the dissociation of cyanogen into two cyanide radicals, we conclude that the lower of the two values, $4.6_4 \pm 0.2$ ev (Table III), consistent with the electron impact data on the cyanide is the correct one. This of course requires that the cyanide radicals formed along with the cyanide ions (CN^+) or chloride ions (Cl^+) from cyanogen or cyanogen chloride are in the first excited state, $A^2\Pi_i$. It is not obvious to the author why electron impact induced transitions to levels above the dissociation limit of the states of $(CN)_2^+$ of $ClCN^+$ formed from $X^2\Sigma^+$ of CN should not be observable. It is conceivable that the internuclear distances in the states of RCN^+ ($R=Cl$ or CN) formed from CN in $X^2\Sigma^+$ are equal to or less

[16a] R. M. Badger and S. C. Woo, J. Am. Chem. Soc. **53**, 2572 (1931).

[17] D. P. Stevenson, J. Am. Chem. Soc. **65**, 209 (1943).

[18] L. Pauling, *Nature of the Chemical Bond* (Cornell University Press, Ithaca, New York, 1939), pp. 203 and 200.

[19] J. Y. Beach and A. Turcevich, J. Am. Chem. Soc. **61**, 299 (1939).

[20] A. Langer and J. A. Hipple, Phys. Rev. **69**, 691 (1946).

than those in the ground states of the RCN and that the amplitude of the oscillations of the atoms in the ground state of the RCN give an insufficient number of molecules with sufficiently small internuclear distances to permit the observation of transitions to the continuum of the lowest states of RCN$^+$.[21] A conceivable set of potential curves which would give rise to such a situation is shown in Fig. 2. It is clear (see below) that transitions to levels above dissociation limits are of limited probability since in both $(CN)_2$ and ClCN undissociated ions constitute in excess of 85 percent of the mass spectra (Table IV).

If the conclusion that the appearance potentials, $A_2(CN^+)$, and $A_{11}(Cl^+)$, are associated with the formation of CN $A^2\Pi_i$ is correct, it would follow from the explanation for the non-observance of the process yielding CN $X^2\Sigma^+$ that if a mass spectrometer of sufficiently high sensitivity were to be employed, this latter process should be observable. It is not apparent how much increase in sensitivity over that of currently available (commercial) mass spectrometers would be required.

The mass spectra of HCN, $(CN)_2$, and ClCN characteristic of 75-v ionizing electrons and 55°C deduced from the mass spectra of samples available for this investigation are given in Table IV. The mass spectra are given in mono-isotopic forms, sums over isotopic ions having been taken where necessary. The mass to charge ratio, m/q, of the ions included in these sums are recorded in the second column of Table IV.

The low dissociation probabilities of the ions of these cyanides indicate the temperature effect on the mass spectra of these compounds will be primarily that due to the change in kinetic energy $(3/2kT)$ that accompanies change in gas temperature.[22] Thus the parent ion sensitivities relative to those of the rare gases will be essentially independent of temperature, and these mass spectra should be transferable for analytical purposes to other mass spectrometers. However, due to the pronounced differences in the discrimination properties of the Westinghouse $\pi/2$-sector analyzer mass spectrometer and the Consolidated Engineering Corporation 180° mass spectrometer these data should be used with caution in the case of the latter mass spectrometer. The necessary correlation between the two types of mass spectrometer may be made through the sensitivities of the rare gases.[23]

[21] For a discussion of the effect of the motions in the ground state on the distribution of products in electron impact induced ionization and dissociation reactions, particularly of H_2 and D_2, see J. Chem. Phys. **15**, 409 (1947).

[22] D. P. Stevenson, J. Chem. Phys. **17**, 101 (1949).

[23] Dibeler, Mohler, and Reese, J. Research Nat. Bur. Stand. **38**, 617 (1947).

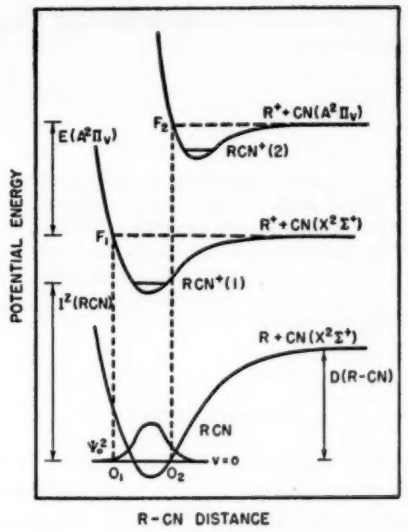

FIG. 2. Schematic potential energy curves for cyanogen and cyanogen chloride ($R-$CN). The area under Ψ_0^2 to the left of O_1F_1 measures the fraction of the molecules RCN capable of dissociating to $R^+ + CN(X^2\Sigma^+)$ while the area under Ψ_0^2 to the left of O_2F_2 measures the fraction of molecules RCN capable of dissociating to $R^+ + CN(A^2\Pi_i)$. If the area under Ψ_0^2 to the left of O_1F_1 is sufficiently small the ion current, R^+, resulting from transition to the continuum of RCN$^+$(1) may be below the limit of detection of a given mass spectrometer. The appearance potential of R^+ in the RCN mass spectrum is associated with the distance O_2F_2.

The relative contributions of the ions $(CN)_2^{++}$ and CN^+ to the observed intensity at $m/q=26$ in the cyanogen mass spectrum were calculated from the ratio of the intensity of the ion $m/q=26\frac{1}{2}$ to that of the ion, $m/q=53$ and the assumption that the isotope effects on ionization probabilities are negligible. It will be noted that in the 75-ev mass spectrum of cyanogen the current observed at $m/q=26$ is about 42 percent due to doubly charged ions.*

ACKNOWLEDGMENT

The author wishes to record his indebtedness to Dr. C. D. Wagner for the preparation and purification of the samples of the three cyanides studied, and to Drs. O. Beeck, J. W. Otvos, and J. N. Wilson for helpful discussion of various aspects of the work. Mr. D. D. Tunnicliff supervised the measurements on the ultraviolet absorption of cyanogen chloride.

* Since the above article was submitted for publication it has come to the author's knowledge that Brewer and Templeton (private communication from Professor Leo Brewer) have found from thermal data the heat of dissociation of cyanogen to be 114±10 kcal./mole (4.96±0.4 ev) in essential agreement with the electron impact value given above (June 27, 1950).

Ultrasonic Classification of Organic Liquids

GURDEVA SHARAN VERMA
Physics Department, University of Allahabad, Allahabad, India
(Received June 15, 1950)

Ultrasonic absorption in various organic liquids at four different frequencies 1.00, 1.46, 2.89, and 4.00 Mc as well as their temperature coefficient of absorption (25°C to 60°C) have been studied by ultrasonic interferometer. Liquids have been classified into four broad groups, Class I in which absorption due to changes in the heat content of the medium predominates, Class II in which absorption caused by structural changes in the quasi-crystalline structure of the liquid state predominats, Class III in which viscosity of the medium alone accounts for absorption and Class IV where absorption is not proportional to the square of the frequency.

INTRODUCTION

THE study of velocity of sound waves in the ultrasonic range of frequencies in organic liquids has thrown some light on the chemical constitution and subsequent grouping according to their properties. The study of absorption too has revealed their peculiar characteristics.

Ultrasonic absorption in various organic liquids has been studied by ultrasonic interferometer at 1, 1.46, 2.98, and 4 Mc. The temperature coefficient of absorption too has been studied. The procedure is exactly the same as followed by Fox and Rock (1937).[1] The details of apparatus have been given elsewhere.[2]

As it has been already pointed out elsewhere,[3–5] ultrasonic absorption in liquids arises due to structural changes in the quasi-crystalline structure of the liquid state as well as due to changes in the heat content of the medium and it is a question of predominance of one over the other. So far as viscous liquids are concerned, the absorption is accounted for by the viscosity of the medium alone.

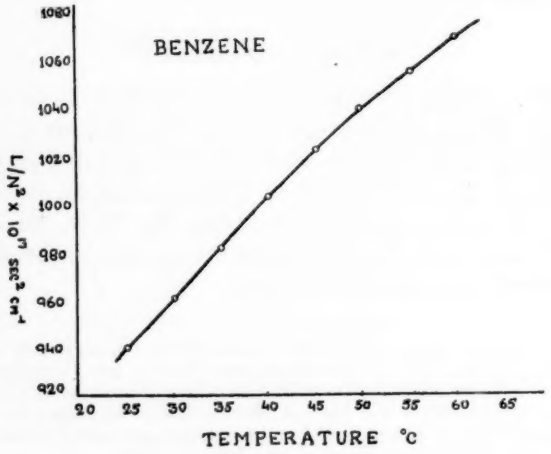

FIG. 1.

The liquids which have been studied have been placed in four broad groups, Class I in which absorption due to changes in the heat content predominates, Class II in which absorption caused by compressibility of the medium predominates; Class III where the viscosity of the medium alone is responsible for the absorption and Class IV in which absorption is not proportional to the square of the frequency. This classification is lent further support by the temperature coefficient of absorption. Liquids belonging to Class I have positive temperature coefficients of absorption whereas liquids belonging to Class II and III have negative temperature coefficients of absorption, whereas it is positive as well as negative in the case of Class IV liquids during different range of temperatures.

RESULTS

Table I shows the values of the absorption ($L/N^2 \times 10^{17}$ sec.^{2} cm^{-1}) of sound waves in the various organic liquids classed into four groups at different frequencies 1, 1.46, 2.98 and 4.00 Mc.

Table II shows the variation of L/N^2 against temperature (25°C to 60°C) for some of the representative liquids of first three classes and Table III shows the same for acetic acid.

Table III shows the variation of L/N^2 against temperature (25°C to 60°C) for acetic acid at four different frequencies 1.00, 1.46, 2.89 and 4.00 Mc.

Figures 1–5 show the plot of L/N^2 against temp-

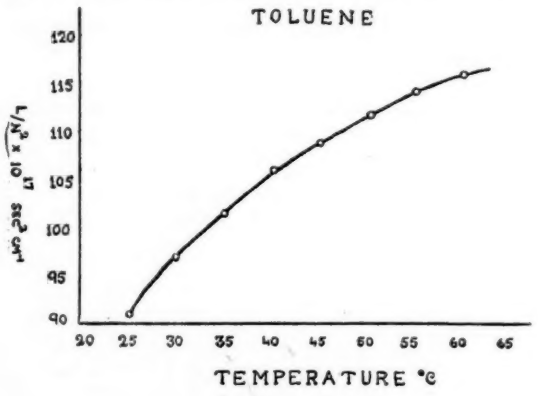

FIG. 2.

[1] F. E. Fox, Phys. Rev. **52**, 973 (1937).
[2] G. S. Verma, Proc. Nat. Acad. Sci. (Alld.), (1949).
[3] R. N. Ghosh and G. S. Verma, Sci. Ind. Res. **8**, 192 (1949).
[4] R. N. Ghosh and G. S. Verma, Ind. J. Phys. **24**, 125 (1950).
[5] G. S. Verma, Proc. Nat. Acad. Sci. (Alld.), Annual Session (50) Volume, (to be published).

TABLE I. $L/N^2 \times 10^{17}$ sec.^{2} cm^{-1}.

Class	Liquid / CS_2	1.00 Mc 8345	1.46 Mc 8416	2.89 Mc 8431	4.00 Mc 8427
I	Benzene	916	940	920	937
	Methyl iodide	818	820	816	817
	CCl_4	506	507	509	520
	Acetylene-di-chloride	436	445	437	440
	Chloroform	386	384	383	385
	Chlorobenzene	121	124	125	123
	Butyl chloride	116	115	113	116
	Heptane	86	85	84	87
	Nitrobenzene	82	83	81	85
	Toluene	92	91	93	94
	Hexane	75	77	76	78
	Xylene	76	77	76	79
	Acetone	74	66	65	68
	Ethyl bromide	63	62	64	65
II	Butyl alcohol	103	102	105	106
	Propyl alcohol	72	74	75	76
	Ethyl alcohol	52	53	56	54
	Methyl alcohol	36	38	35	39
	Water (distilled)	22.9	23.0	23.2	22.8
III	Transformer oil	105	104	103	106
	Paraffin oil	866	864	866	868
	Olive oil	1265	1256	1261	1258
IV	Acetic acid	41,000	18,000	5080	3250
	Amyl acetate	615	398	276	162
	Ethyl acetate	516	376	268	193
	Methyl acetate	468	346	235	186

erature for the above mentioned representative liquids. Figure 6 shows the same for acetic acid for the different frequencies.

DISCUSSION

Thus it may be noticed from Tables I and II that liquids such as CS_2, C_6H_6, CH_3I, CCl_4, acetylene-dichloride, $CHCl_3$, chlorobenzene, butyl chloride, heptane, nitrobenzene, toluene, hexane, xylene, acetone and ethyl bromide possess very high absorption ($L/N^2 \times 10^{17}$) of the order of 60–9000 and have positive temperature coefficient (with the exception of CCl_4) whereas water and alcohols have very low absorption of the order 20 to 60 (leaving cases of higher alcohols) and have large negative temperature coefficient of

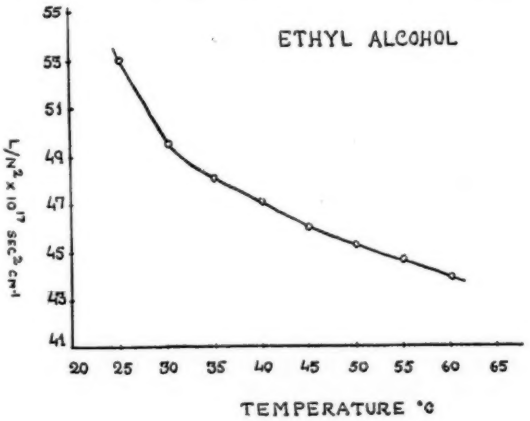

FIG. 3.

TABLE II. $L/N^2 \times 10^{17}$ (sec.^{2} cm^{-1}).

Liquid	25°C	30°C	35°C	40°C	45°C	50°C	55°C	60°C
Benzene	940	961	982	1002	1021	1038	1054	1066
Toluene	91	97	102	106	109	112	114	116
Ethyl alcohol	53.0	49.2	48	46.9	45.9	45.2	44.6	43.9
Water	23	19.4	17.6	15.5	13.5	12.2	11.1	10.3
Olive oil	1256	1026	831	706	605	525	454	414

TABLE III. Acetic acid. $L/N^2 \times 10^{14}$ (sec.^{2} cm^{-1}).

Frequency	25°C	30°C	35°C	40°C	45°C	50°C	50°C	65°C
1.00 Mc	42.3	51.2	55.5	55.4	46.7	33.6	31.9	28.8
1.46 Mc	18.7	24.8	30.6	33.2	31.6	30.8	29.3	26.1
2.89 Mc	5.1	8.6	12.4	14.8	17.4	18.6	21.3	20.2
4.00 Mc	3.4	5.6	8.2	9.8	10.9	12.3	12.9	13.6

absorption. They have been classified into two classes I and II. In the latter the absorption due to structural changes in the quasicrystalline state of the liquid *viz.* changes in the compressibility of the medium predominates, whereas in Class I liquids absorption due to changes in the heat content of the medium predominates. The changes in the compressibility ($\Delta\beta$) of the liquid medium is expressed by

$$\Delta\beta = (V/2RT)^2(\Delta V/V)^2/1+\cosh(\Delta F/RT),$$

where ΔF is the structural energy change and ΔV is the change in the molar volume V due to transition of molecules from the equilibrium state to perturbed state. The change in the heat content (ΔC cal./mole) is expressed in the form

$$\Delta C = \Delta H(\partial N/\partial T)$$

and the absorption (L) is

$$L/N^2 = \frac{2\pi^2}{V}\left[\frac{\Delta C}{C}(Cp-Cv)+\frac{\Delta\beta}{\beta}\right]\frac{k}{(\omega^2+k^2)},$$

where N is the frequency and V the velocity of sound

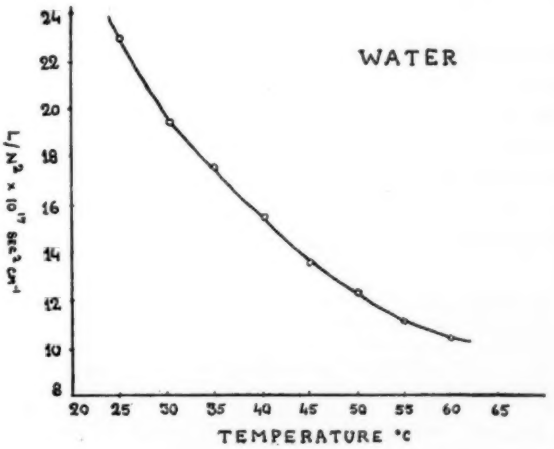

FIG. 4.

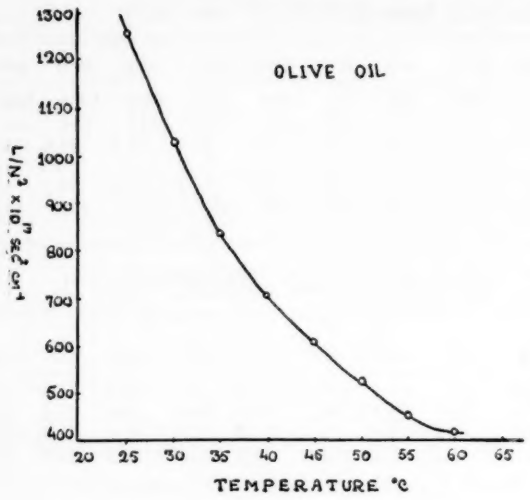

FIG. 5.

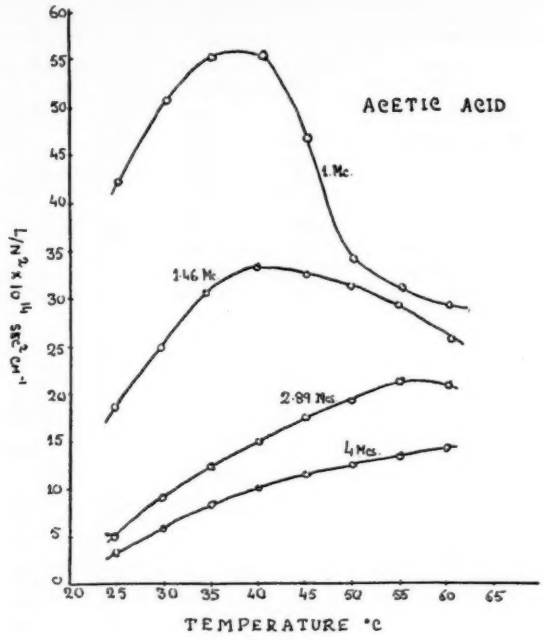

FIG. 6.

waves, C and β, the equilibrium values of specific heat and compressibility, k the equilibrium reaction rate and $\omega=2\pi N$. Taking the particular case of benzene (Class I), $V=1.3\times10^5$ cm/sec., $C=20$ cal./mole. $\Delta C\sim11$ cal./mole, $Cp-Cv=10.8$ cal./mole, $k=\cdot4\times10^{10}$ sec.; $L/N^2\times10^{17}=931$. Take the case of water (Class II), $\beta=38\times10^{-12}$, cm^2/dyne, $\Delta\beta=23\times10^{-12}$ cm^2 dyne^{-1}, $V=1.48\times10^5$ cm/sec., $k=.46\times10^{12}$ sec.; $(L/N^2\times10^{17})=17.7$.

In the case of viscous liquids such as transformer oil, paraffin oil and olive oil, etc. the absorption is of the same order as is expected by Stoke's formula $L=\frac{2}{3}\eta\omega^2/\rho v^3$ where ρ and η are the density and viscosity of the medium. These liquids also show large negative temperature coefficient of absorption.

In all the above liquids, absorption is strictly proportional to the square of the frequency, *viz.* values of L/N^2 at different frequencies are constant. But liquids containing acetate radical such methyl acetate, ethyl acetate, amyl acetate as well as acetic acid form an exception to this frequency law. They show a large variation from higher values at lower frequencies to lower values at higher frequencies. Their temperature coefficient of absorption at 4 Mc is positive but below this frequency it is positive, as well as negative which is apparent from Fig. 6.

ACKNOWLEDGMENT

I offer may sincerest thanks to Dr. R. N. Ghosh for having suggested this problem and his valuable guidance throughout the progress of the research as well as to Council of Scientific and Industrial Research (India) for Research Grant.

THE JOURNAL OF CHEMICAL PHYSICS VOLUME 18, NUMBER 10 OCTOBER, 1950

Classical Thermodynamics and Reaction Rates Close to Equilibrium

MILTON MANES,* L. J. E. HOFER,* AND SOL WELLER*
Research and Development Branch, Office of Synthetic Liquid Fuels, Bureau of Mines, Bruceton, Pennsylvania
(Received July 20, 1950)

For reversible reactions close to equilibrium the net reaction rate $(r_f - r_b)$ is shown to be proportional to ΔX, where X is any one of the thermodynamic functions, e.g., the Gibbs free energy, F, governing equilibrium under the conditions of the reaction, e.g., $(r_f - r_b) = r_f \cdot -\Delta F/RT$. The derived relationships are independent of the manner in which small displacements from equilibrium may be brought about. Equations are derived by which the magnitude of the forward (or backward) reaction rate at equilibrium may be determined with the aid of observations of the net reaction rate close to equilibrium. Since the magnitude of the former is a function of the kinetics of the reaction, measurements of the net reaction rate near equilibrium over a range of conditions may be used within specified limits to determine the kinetics of reversible reactions.

IN a recent article, Prigogine, Outer, and Herbo[1] deduced relationships between the reaction rate close to equilibrium and the "affinity," on the basis that there is an intrinsic connection between reaction rates and thermodynamic concepts. It is the purpose of this article to derive more general expressions for the reaction rate close to equilibrium on the basis of classical thermodynamics and to clarify the relations between thermodynamics and reaction rates. In keeping with classical thermodynamics, no connection between the magnitudes of reaction rates and the macroscopic thermodynamic functions will be implied, except for the acceptable but relatively trivial statements, that: (a) At equilibrium the rates of the forward and backward reactions are equal; i.e., the net reaction rate is zero, and (b) the direction of a reaction toward equilibrium is determined by the sign of the appropriate thermodynamic function as given by the Gibbs criteria.[2]

I. RELATION BETWEEN RATE AND FREE ENERGY NEAR EQUILIBRIUM

Of the various thermodynamic functions, such as F, A, S, and E, we shall choose the Gibbs free energy, F, to illustrate the sort of relationships between net reaction rate and the thermodynamic functions which may be derived from statements (a) and (b). The term "reaction rate" will refer in all cases to a single over-all reaction. For any given over-all reaction it will not be necessary to know whether it takes place in one or in several steps nor will it be necessary to specify the mechanism in any way. In systems where several reactions are simultaneously taking place as, for example, in the case of a pure substance at its triple point, it will be necessary to specify which reaction is under discussion, for example, the solid-gas reaction.

If ΔF denotes the change in the total free energy of the system per mole of reacting component when a small amount of reaction takes place, we may in general express ΔF in terms of n independent variables

$$\Delta F = \Delta F(a, b, \cdots n), \tag{1}$$

where the variables are the temperature, pressure, and the individual activities of each of the molecular species which are written in the over-all reaction. For example, for a homogeneous reaction involving C molecular species[3] in an inert medium $n = C+2$. We shall call these variables the "thermodynamic variables." The net reaction rate, r, for a reversible reaction may be expressed in terms of these same variables and some added ones,

$$r = r(a, b, \cdots n; u \cdots z), \tag{2}$$

where $u \cdots z$ represent what will be denoted as the "non-thermodynamic" variables, the ones which affect the reaction rate but not the position of equilibrium.[4] According to statement (a), any set of values of $a \cdots n$ which makes ΔF vanish will also make r vanish, irrespective of the values of $u \cdots z$. Let us now consider a system at one of the many possible states of equilibrium, i.e., let us choose a particular set, $a_i, b_i \cdots n_i$, such that

$$\Delta F(a_i \cdots n_i) = 0; \quad r(a_i \cdots n_i; u_i \cdots z_i) = 0. \tag{3}$$

Let us now go to any neighboring state of equilibrium by making arbitrary differential changes in the values of $a_i \cdots (n-1)_i$ in such a manner that $\delta(\Delta F) = 0$ and $\delta r = 0$. The change in the remaining variable is now determined by these arbitrary changes and the constraint to equilibrium conditions, the system having $(n-1)$ degrees of freedom. The total number of atoms in the

* Physical Chemist, Bureau of Mines, Research and Development Branch, Office of Synthetic Liquid Fuels, Bruceton, Pa.

[1] Prigogine, Outer, and Herbo, J. Phys. Colloid Chem. **52**, 321 (1948).

[2] This statement appears to be identical with the DeDonder inequality, $Av T > 0$. See reference 1.

[3] Since the reaction is not necessarily restricted to equilibrium one considers every molecular species which appears in the stoichiometric equation. This is in contrast to the procedure in determining the number of components in the Gibbs Phase Rule where the constraint to equilibrium reduces the number of independent variables.

[4] Examples of non-thermodynamic variables are: the area of catalyst surface or of the gas-solid interface in gas-solid reactions, catalyst poisons, and type of catalyst.

system need not remain constant. We can now write

$$\delta(\Delta F)=\frac{\partial(\Delta F)}{\partial a}\delta a+\cdots+\frac{\partial(\Delta F)}{\partial(n-1)}\delta(n-1)+\frac{\partial(\Delta F)}{\partial n}\delta n=0, \quad (4)$$

and

$$\delta r=\frac{\partial r}{\partial a}\delta a+\cdots+\frac{\partial r}{\partial(n-1)}\delta(n-1)+\frac{\partial r}{\partial n}\delta n+\frac{\partial r}{\partial u}\delta u+\cdots+\frac{\partial r}{\partial z}\delta z=0, \quad (5)$$

where

$$\delta n=-\left(\frac{\partial(\Delta F)}{\partial n}\right)^{-1}\sum_{a}^{n-1}\left(\frac{\partial(\Delta F)}{\partial n_i}\delta n_i\right). \quad (6)$$

Since at equilibrium the reaction rate will be zero, irrespective of the values of the non-thermodynamic variables, we may also write,

$$\left(\frac{\partial r}{\partial u}\right)_{a\cdots n}=0; \quad \left(\frac{\partial r}{\partial z}\right)_{a\cdots n}=0, \text{ etc.} \quad (7)$$

Therefore Eq. (5) becomes,

$$\delta r=\frac{\partial r}{\partial a}\delta a+\cdots+\frac{\partial r}{\partial n}\delta n=0.^{5} \quad (8)$$

If now we eliminate the last terms from the simultaneous Eqs. (4) and (8) we get,

$$0=\left[\left(\frac{\partial(\Delta F)}{\partial a}\right)\left(\frac{\partial r}{\partial n}\right)-\left(\frac{\partial r}{\partial a}\right)\left(\frac{\partial(\Delta F)}{\partial n}\right)\right]\delta a+\cdots+\left[\left(\frac{\partial(\Delta F)}{\partial(n-1)}\right)\left(\frac{\partial r}{\partial n}\right)-\left(\frac{\partial r}{\partial(n-1)}\right)\left(\frac{\partial(\Delta F)}{\partial n}\right)\right]\delta(n-1). \quad (9)$$

This equation can be true for arbitrary values of $\delta a\cdots\delta(n-1)$ only if each of the coefficients is equal to zero. Equating each of these to zero, we get

$$\frac{\partial r/\partial a}{[\partial(\Delta F)]/\partial a}=\cdots=\frac{\partial r/\partial n}{[\partial(\Delta F)]/\partial n}, \quad (10)$$

or,

$$\left(\frac{\partial r}{\partial(\Delta F)}\right)_{(b\cdots n)}=\cdots=\left(\frac{\partial r}{\partial(\Delta F)}\right)_{(a\cdots(n-1))}=x(a_i\cdots n_i;\ u_i\cdots z_i) \quad (11)$$

where x is a proportionality factor which depends on the particular values of all the variables, but which is independent of the manner in which the differential change in ΔF arises. Since the partial derivatives $\partial r/\partial a$ etc., and $[\partial(\Delta F)]/\partial a$ etc., are determined by the functions r and ΔF in Eqs. (1) and (2), Eq. (11) must also hold for differential changes from equilibrium in which $d(\Delta F)$ and dr are other than zero. Writing the equations for the total differentials of r and ΔF, and substituting from Eq. (11) we have, for a change in $(a\cdots n)$,

$$dr=x\frac{\partial(\Delta F)}{\partial a}da+\cdots+x\frac{\partial(\Delta F)}{\partial n}dn+\frac{\partial r}{\partial u}du\cdots+\frac{\partial r}{\partial z}dz, \quad (12)$$

$$d(\Delta F)=\frac{\partial(\Delta F)}{\partial a}da+\cdots+\frac{\partial(\Delta F)}{\partial n}dn. \quad (13)$$

Near equilibrium, the dependence of the *net* reaction rate on the non-thermodynamic variables, as shown by Eq. (7), becomes negligible.[6] Therefore, for small variations from equilibrium resulting from small changes in any or all of the thermodynamic variables,

$$r=x(a_i\cdots n_i;\ u_i\cdots z_i)\cdot\Delta F. \quad (14)$$

The sign of x is given by statement (b) as being opposite to the sign of ΔF.

It follows from Eq. (14) that under the conditions where the stated assumptions hold, the net rate near equilibrium is directly proportional to the free energy change. Moreover, the proportionality factor will be the same for a given set of equilibrium conditions no matter which of the thermodynamic variables (e.g., activities, temperature, etc.) are changed.

Equation (14) shows the limitations of the thermodynamic approach. Since x depends on factors which are not determined by thermodynamics, one cannot by Eq. (14) calculate absolute rates from thermodynamic data. The dependence of x on the particular conditions of a given state of equilibrium will best be discussed in a later paragraph, after the physical significance of this quantity has been discussed.

The proportionality factor, x, appears to be identical with the "angular coefficient" of Prigogine *et al.*[1] The derivation given here is more general than the one given by these authors in that x is independent, for a given set of equilibrium conditions, of the manner in which the equilibrium is disturbed. Prigogine *et al.* did indeed find this to be the case in their experiments, but considered it to be in excess of theory.

It should be emphasized at this point that the relationships thus far deduced follow in a formal sense from the fact that r and ΔF vanish together and would hold for any two functions similarly related. Under the proper conditions, therefore, as determined by the

[5] In both Eqs. (4) and (8) it is understood that a total number of $(n-1)$ variables may be arbitrarily varied, but that one is not otherwise limited. For example one could just as well have varied $b\cdots n$ arbitrarily and let δa be determined by the constraint of equilibrium.

[6] It is assumed that we are dealing with equilibria where the forward and reverse reactions take place at a finite rate and that no discontinuities appear in the region under discussion.

Gibbs criteria for equilibrium, the same type of relationship would hold, for example, for ΔA, ΔE, ΔH, ΔS. The form of the free energy and rate functions will presently be examined and will be found to yield additional information.

II. THERMODYNAMICS AND RELATIONS BETWEEN THE RATE LAWS FOR THE FORWARD AND REVERSE REACTIONS

If the respective rate laws for the forward and reverse reactions are to apply over a given range of conditions, it is necessary that they do not contradict the thermodynamic description of equilibrium as stated in (a) and (b). Therefore these rate functions must satisfy the condition that for every set of the concentrations[7] of the individual components which satisfies the expression for the equilibrium constant, K, the values of the forward and reverse reactions obtained by substitution of these quantities into the rate law must be equal. Gadsby, Hinshelwood, and Sykes[8] derived what were considered to be necessary relationships between the opposing rate laws. The concluded, in effect, that for the single-phase reaction

$$aA+bB+\cdots\rightleftharpoons mM+nN+\cdots, \tag{15}$$

the rate laws for the forward and reverse reactions would have to obey the relationship,

$$\frac{r_f}{r_b}=\frac{k_f(A)^a(B)^b\cdots}{k_b(M)^m(N)^n\cdots}, \quad \text{where} \quad \frac{k_f}{k_b}=K. \tag{16}$$

In this equation the exponents of the individual concentrations are identical with the stoichiometric coefficients in (15). According to these conclusions, the rate law for the reaction in one direction determines the rate law for the opposing reaction and therefore the complete kinetics of the system. For example, if the forward rate law is of the form,

$$r_f=\frac{k_f(A)^\alpha(B)^\beta\cdots(M)^\xi(N)^\zeta\cdots}{\psi_f[(A),(B),\cdots(M),(N),\cdots]}, \tag{17}$$

where the exponents $\alpha, \beta\cdots\xi, \zeta\cdots$ are to be determined experimentally and ψ is some complicated function,[9] then the reverse rate law must have the form

$$r_b=\frac{k_b(A)^{\alpha-a}(B)^{\beta-b}\cdots(M)^{m+\xi}(N)^{n+\zeta}\cdots}{\psi_b[(A),(B),\cdots(M),(N),\cdots]}, \tag{18}$$

where $k_f/k_b=K$ and $\psi_f\equiv\psi_b$.

The derivation of Gadsby, Hinshelwood, and Sykes[8] contains, as one step, the reasoning that if F_1 and F_2 (Eqs. (30) and (31), reference 8) are some functions of the concentrations of the reaction components, and if F_1/F_2 has a constant value at every set of equilibrium conditions, then $F_1\equiv F_2$. We shall see that this statement, on which the derivation of Eq. (16) is based, is not necessarily true in the general case. Equation (16) therefore does not hold for the general case. For example, from the standpoint of thermodynamics we could write Eq. (15) as

$$qaA+qbB+\cdots=qmM+qnN+\cdots, \tag{19}$$

where q is any positive quantity. Substitution of the new coefficients qa, qb, etc. into Eq. (16) leads to a new relationship for every value of q. Furthermore, one can show that different relationships between the opposing rate laws (different q's) may apply in conceivable cases under different conditions. Consider for example the hypothetical reaction,

$$A_2+\tfrac{1}{2}B_2=A_2B,$$

$$\text{where at equilibrium } K=\frac{(A_2B)}{(A_2)(B_2)^{\frac{1}{2}}} \tag{20}$$

and which proceeds by the mechanism,

$$B_2\rightleftharpoons B+B, \tag{21}$$

$$A_2+B\rightleftharpoons A_2B. \tag{22}$$

If reaction (21) is rate controlling one would have the rate laws

$$r_f=k_f(B_2), \quad r_b=\frac{k_f(A_2B)^2}{K^2(A_2)^2}, \tag{23}$$

while if reaction (22) were rate controlling one would find

$$r_f=k_f(A_2)(B_2)^{\frac{1}{2}}, \; r_b=k_f/K(A_2B). \tag{24}$$

Both of these pairs of rate laws satisfy the conditions of equilibrium. Both cannot be simultaneously represented by the results of Gadsby, Hinshelwood, and Sykes.[8] Furthermore, some rate functions may exist which satisfy equilibrium conditions but which cannot be made to fit Eq. (16), no matter how one wrote the stoichiometric equation. Consider the case where reaction (20) is proceeding by the mechanisms leading to (23) and (24), where both mechanisms are operating simultaneously, in which case,

$$r_f=k_f'(B_2)+k_f''(A_2)(B_2)^{\frac{1}{2}} \tag{25}$$

---

[7] We shall assume activity coefficients equal to unity.

[8] Gadsby, Hinshelwood, and Sykes, Proc. Roy. Soc. (London) 187, 129 (1946).

[9] The erroneous practice of writing the rate law for a reaction as $r_f=k_f(A)^a(B)^b\cdots$ for the general case, i.e., of assuming that the Guldberg-Waage law of mass action holds generally, appears in the literature from time to time in spite of its implication that the kinetics of a reaction may in general be determined from the stoichiometric equation and without experiment. The assumption of the Guldberg-Waage law for the general case has been used to derive the correct expression for the equilibrium constant. This is in itself no proof of the correctness of the assumption. One notes that Eqs. (17) and (18) also yield the correct expression for the equilibrium constant, without in general satisfying the Guldberg-Waage law.

and

$$r_b=\frac{k_f'(A_2B)^2}{K^2(A_2)^2}+\frac{k_f''}{K}(A_2B). \tag{26}$$

These rate laws satisfy the conditions of equilibrium for any values of k' and k'', but could not fit Eq. (16) no matter how one wrote the stoichiometric equation.

We shall now derive relationships between the opposing rate laws. Rather than deriving the necessary relationships for the general case we shall enumerate some of the relationships which fulfill the requirements of equilibrium, and discuss their physical significance and range of applicability. Let us express the rate laws for the opposing reactions in Eq. (15) as

$$r_f=G_f[(A), (B), \cdots (M), (N), \cdots] \tag{27}$$

and

$$r_b=G_b[(A), (B), \cdots (M), (N), \cdots] \tag{28}$$

where G_f and G_b are some algebraic functions of the concentrations. These functions are assumed to describe the actual rate laws for the reaction and are therefore at the outset independent of any arbitrary formulation of Eq. (15). Let us, for convenience in notation, consider that the coefficients $a, b, \cdots m, n, \cdots$ represent the smallest integral coefficients for the reaction. The only restriction set by thermodynamics on G_f and G_b is that at every state of equilibrium,

$$\frac{r_f}{r_b}=\frac{G_f}{G_b}=1, \tag{29}$$

and that $r_f/r_b>1$ when $\Delta F<0$. In order to fulfill this condition it is sufficient to assume, for example, that

$$\frac{G_f}{G_b}=\frac{k_f}{k_b}\left[\frac{(A)^a(B)^b\cdots}{(M)^m(N)^n\cdots}\right]^z, \quad \text{where} \quad \frac{k_f}{k_b}=K^z \tag{30}$$

where z has any constant positive value. As an example of two such rate laws we may consider the functions,

$$G_f=\frac{k_{1f}(A)^{\alpha_1}(B)^{\beta_1}\cdots(M)^{\xi_1}(N)^{\zeta_1}\cdots}{\psi_1[(A), (B), \cdots (M), (N), \cdots]} + \frac{k_{2f}(A)^{\alpha_2}(B)^{\beta_2}\cdots(M)^{\xi_2}(N)^{\zeta_2}\cdots}{\psi_2[(A), (B), \cdots (M), (N), \cdots]}+\cdots \tag{31}$$

$$G_b=\frac{k_{1f}}{K^z}\frac{(A)^{\alpha_1-za}(B)^{\beta_1-zb}\cdots(M)^{zm-\xi_1}(N)^{zn-\zeta_1}}{\psi_1[(A), (B), \cdots (M), (N), \cdots]} + \frac{k_{2f}}{K^z}\frac{(A)^{\alpha_2-za}(B)^{\beta_2-zb}\cdots(M)^{zm-\xi_2}(N)^{zn-\zeta_2}\cdots}{\psi_2[(A), (B), \cdots (M), (N), \cdots]} +\cdots, \tag{32}$$

where the exponents $\alpha_1, \beta_1, \cdots \alpha_2, \beta_2 \cdots, \xi_1, \cdots$ are in general unknown and to be determined experimentally, and are unrelated to each other, and the functions ψ_1 and ψ_2 are also unrelated functions which may contain additive terms, *e.g.*,

$$\psi_1=1+k_A(A)+k_B(B)+\cdots. \tag{33}$$

Equation (30) will apply to any pair of rate laws, each of which may be a sum of functions of the concentrations, provided that for each such function in one rate law there is a corresponding one in the opposing rate law such that the pair fulfills Eq. (30) and provided further that the value of z is the same throughout. Assumption (30) therefore applies to reactions where several mechanisms may be simultaneously active. This assumption does not cover the general case, but will be found to have a wide range of applicability. For example, it will include all of the mechanisms listed by Yang and Hougen[10] for surface-catalyzed gas-phase reactions. One notes further that if assumption (30) applies, the value of z is determined by the order of both rate laws in any single component.

It should be pointed out that much more complicated rate functions than (31) and (32) could conceivably be found. In the first place, the individual additive terms of the rate functions could be related in pairs through Eq. (30) but with different values of z. An example of such a case has been shown. Furthermore, if each such pair of functions has a complicated denominator, such as ψ, it does not follow from thermodynamics that these denominators be identical, but only that they be equal at equilibrium. If they are not identical, then Eq. (30) will not hold. It may be expected in the general case that at equilibrium, each additive term in a complicated rate function becomes equal to its counterpart in the opposing rate function. We may expect this to be the case because the position of equilibrium is not changed by the arbitrary "freezing" of any mechanism.

If the reaction is written in the usual manner with the lowest integral stoichiometric coefficients it is most unlikely that z would be other than a small integer or its reciprocal, and, in most cases z will probably be equal to unity, in which case the implicit assumptions of Gadsby, Hinshelwood, and Sykes[8] give the correct results. This unproved assertion is based on the concept that chemical reactions take place between discrete particles, and on the well-founded belief that multiple collisions are rarely rate controlling. These matters must be beyond the scope of classical thermodynamics, which does not take into account the particulate nature of matter.

III. RELATIONS BETWEEN THE NET REACTION RATE, GROSS REACTION RATE, AND FREE ENERGY NEAR EQUILIBRIUM

We shall now limit ourselves to the widely applicable, but nevertheless special case of reversible reactions where assumption (30) holds. For this case one may derive relationships whereby the kinetics may be deter-

[10] K. H. Yang and O. A. Hougen, Chem. Eng. Prog. **46**, 146 (1950).

mined by measurements close to equilibrium. Equation (30) may be written

$$\ln\frac{r_f}{r_b}=z\left[\ln K(T)-\ln\frac{(M)^m(N)^n\cdots}{(A)^a(B)^b\cdots}\right]=-z\cdot\frac{\Delta F}{RT},^{11} \quad (34)$$

Where K and ΔF refer to reaction (15). Near equilibrium,

$$\ln\frac{r_f}{r_b}=\frac{r_f-r_b}{r_f}, \quad (35)$$

and therefore, near equilibrium,

$$r_f-r_b=-z\cdot r_f(\Delta F/RT). \quad (36)$$

It follows from Eq. (36) that if one plots the observed net reaction rate against $-\Delta F/RT$ the slope is equal to $zr_f(=zr_b)$, and is therefore proportional to the gross reaction rate, or equal to it if $z=1$. It has already been demonstrated that this slope is independent of the manner in which any small displacements from equilibrium take place. This now fits well with the physical explanation of the slope, since the gross reaction rate for a given state of equilibrium should indeed be independent of the manner in which one approaches it.

Equation (36) is independent of the mechanism of the reaction within the stated assumptions. However, in keeping with its derivation from thermodynamics, it does not in any way specify the magnitude of the forward rate, r_f. Now r_f does not have one unique value for any given reaction but can take on any of a range of values for different conditions of equilibrium. The dependence of the reaction rate r_f at any particular state of equilibrium on the temperature and concentrations which are found at that state is given specifically by the same rate law which governs the reaction rate away from equilibrium. Conversely, if the reaction is observed near equilibrium over a range of temperatures and concentrations, the individual values of r_f under each separate set of such conditions serve to determine the rate law in exactly the same manner as if similar observations were made away from equilibrium. The relations expressed in Eq. (36) therefore yield a method whereby, at least in principle, one may determine the kinetics of a reversible reaction from a series of observations under different conditions of equilibrium. Furthermore, within the range of proximity to equilibrium where Eq. (36) holds, only one determination of r_f-r_b and $\Delta F/RT$ is required to determine the corresponding $z\cdot r_f$ for each equilibrium, since all the lines represented by Eq. (36) pass through the origin.

We shall now take a hypothetical reaction, first to illustrate the crucial importance of specifying the particular equilibrium under discussion, then to illustrate the manner in which Eq. (36) may be specifically applied to the study of kinetics. Let us assume a surface-catalyzed gas reaction,

$$A+B\rightleftarrows C+D$$

at a total pressure of 1 atmosphere. We shall also assume that at the temperature T, $K=1$, and that the temperature dependence of the equilibrium constant is known. It is further assumed that the rate law for the forward reaction, and the corresponding rate law for the reverse reaction which must be consistent with it are, respectively

$$r_f=k_f p_A \quad \text{and} \quad r_b=\frac{k_f}{K}\frac{p_C p_D}{p_B} \quad (37)$$

and $k_f=k_b=1$ sec.$^{-1}$ The rate laws for the forward and reverse reactions are related to each other by Eq. (30), where $z=1$. As an example, three equilibrium compositions may be considered as follows:

Composition	p_A	p_B	p_C	p_D
I	0.25 atmos.	0.25 atmos.	0.25 atmos.	0.25 atmos.
II	0.28	0.22	0.28	0.22
III	0.01	0.81	0.09	0.09

The gross reaction rate, $r_f=r_b$, for each composition is found by substitution of the corresponding partial pressures in the rate law, giving for compositions I, II, and III the respective values for r_f of 0.25, 0.28, and 0.01 atmos./sec. The wide variation between these values illustrates the dependence of r_f on the particular state of equilibrium. The necessity of specifying the equilibrium is also shown graphically by Fig. 1, in which

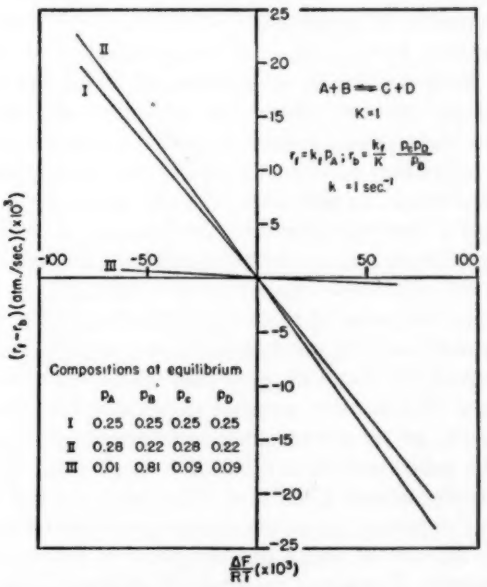

FIG. 1. The dependence of the plot of (r_f-r_b) *versus* $\Delta F/RT$ on the specific state of equilibrium; three separate plots near three equilibrium compositions for the same hypothetical reaction under otherwise identical conditions.

[11] It follows from the form of this equation that the *relative* rates of the forward and reverse reactions are determined by the thermodynamic functions under all conditions where the equation applies. We shall confine ourselves here to the region close to equilibrium.

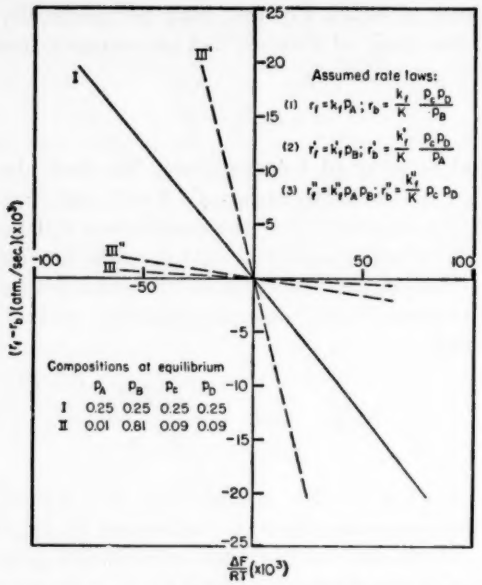
Assumed rate laws:
(1) $r_f = k_f p_A$; $r_b = \frac{k_f}{K} \frac{p_C p_D}{p_B}$
(2) $r_f' = k_f' p_B$; $r_b' = \frac{k_f'}{K} \frac{p_C p_D}{p_A}$
(3) $r_f'' = k_f'' p_A p_B$; $r_b'' = \frac{k_f''}{K} p_C p_D$
Compositions at equilibrium
p_A p_B p_C p_D
I 0.25 0.25 0.25 0.25
II 0.01 0.81 0.09 0.09
$(r_f - r_b)$(atm./sec.)(x10^3)
$\frac{\Delta F}{RT}$(x10^3)

FIG. 2. Application of Eq. (36) to determination of rate laws. The solid line represents an "actual" determination for composition I. The three dashed lines show expected plots for composition III on the assumption of three different rate laws consistent with I.

calculated values of $r_f - r_b$ are plotted against $\Delta F/RT$ $(= -\ln(p_C p_D/p_A p_B))$ for the isothermal approach to equilibria I, II, and III. As expected, the slopes at the origin are equal to the corresponding values of r_f and are opposite in sign, and each line is characteristic for the corresponding equilibrium state. Over the small displacement from equilibria for which they were plotted the lines show only a slight curvature.

Special emphasis has been put upon the necessity for specifying equilibrium conditions because the article by Prigogine *et al.*[1] contains an essentially similar plot for a number of experiments carried out at constant temperature for a number of compositions, not all of which went to the same equilibrium. The net rate, $(r_f - r_b)$ was plotted against the "affinity" without regard for the separate equilibria, although the necessity of the restriction to identical equilibrium is implicit in their derivation as well as in the one given here. The fact that a linear relationship was found at all may be considered fortuitous and explainable on the basis that, under the described experimental conditions, a relatively narrow range of gross equilibrium reaction rates was encountered. Figure 1 shows how two rather close-lying equilibria, I and II, give lines which are not very far apart. If a narrow range of slopes is encompassed, the results of an erroneously unrestricted plot may easily be misconstrued as lying on a single line.

For compositions I, II, and III, similar curves with identical slopes at the origin would of course be found by any manner of small displacement of equilibrium. For example, if one had maintained constant composition and varied the temperature, one would obtain the same slopes at the origin for any assumption as to the temperature dependence of the forward reaction rate, which, however, would have to be subject to the restriction that the temperature dependence of the forward and backward reaction rates are related to each other through the temperature dependence of the free energy change. Prigogine *et al.*[1] did study net reaction rates both at constant temperature and at constant composition. Unfortunately, the individual series of experiments were carried out on different catalysts and cannot be compared. The present derivation leads, of course, to the necessity that similar experiments under otherwise identical conditions and based on the same state of equilibrium should yield identical slopes at the origin for variation of composition, or temperature, or both.

We shall now illustrate the application of Eq. (36) to the determination of a rate law. Let us assume that we have observed the slope zr_f for composition I and that, as before, it is equal to 0.25 atmos. per sec. Let us further assume that rate law (37) is one of three possible rate laws, the other two being,

$$r_f' = k_f' p_B, \quad r_b' = \frac{k_f'}{K} \frac{p_C p_D}{p_A}, \quad (k_f' = 1 \text{ sec.}^{-1}) \quad (38)$$

and

$$r_f'' = k_f'' p_A p_B, \quad r_b'' = \frac{k_f''}{K} p_C p_D,$$

$$(k_f'' = 4 \text{ atmos.}^{-1} \text{ sec.}^{-1}) \quad (39)$$

both of which are consistent with the observation on composition I. One expects, on the basis of each of these rate laws, that the slopes which will be found for composition III will be, $zr_f = 0.01$, $zr_f' = 0.81$, and $zr_f'' = 0.032$ atmos./sec. The corresponding lines are shown in Fig. 2, and show how a distinction can be made between rate laws. One sees, therefore, that rate measurements close to equilibrium are not essentially different from any other kind of rate measurement and that no information is derivable from the outlined method that is not derivable, at least in principle, from classical kinetics.

The value of z need not be known in order to determine the rate law, since a knowledge of the relative reaction rates under different conditions suffices for this purpose. However, the method has the limitation, in principle, that the value of z cannot be determined by measurements differentially close to equilibrium. For example, one cannot by this method distinguish between the rate laws

$$r_f = k_f p_A$$

and

$$r_f = k_f p_A \left(\frac{p_A p_B}{p_C p_D} \right)^y \quad (40)$$

where y may have any constant value, since the expression in parenthesis is always a constant at equilibrium.

Although in practice the distinction between rate laws such as (38) and (39) may be expected to be much more important, the fact remains that the complete kinetics of the reaction and the absolute magnitude of r_f would in principle require some measurements other than at equilibrium.

The problem arises as to how one would make rate measurements close to equilibrium, which will be discussed here only briefly. Prigogine *et al.*[1] studied the catalytic hydrogenation of benzene to cyclohexane by passing their non-equilibrium mixtures very rapidly over the catalyst so that all of the catalyst was in effect presented with the same gas composition. This method measures, in effect, instantaneous reaction rates. In cases where the velocity of the reaction rates makes such measurements inconvenient, the integration of the reaction rate over a range becomes very simple. All reactions close to equilibrium (taking ΔF as the appropriate function) may be considered from Eq. (36) to be first order in ΔF. If we express the reaction rate, for example, in terms of the rate of disappearance of one of the components, we can rewrite Eq. (36) as

$$r=-\frac{1}{a}\frac{d(A)}{dt}=-\frac{r_f}{RT}z\cdot\Delta F, \tag{41}$$

which, by multiplying both sides by $d(\Delta F)/d(A)$ and rearranging, becomes

$$\frac{d\ln\Delta F}{dt}=\frac{a}{RT}\cdot\frac{d(\Delta F)}{d(A)}\cdot zr_f. \tag{42}$$

The term $d(\Delta F)/d(A)$ is a function of the composition and remains constant over a small extent of reaction, making Eq. (42) easily integrated. This term is, of course, the total differential and includes the effect on ΔF of the reaction of all the components.

For homogeneous gas reactions, one may, in principle, displace equilibrium by changes in pressure or temperature and measure the rate at which the reaction follows a sudden change in conditions, or possibly a time dependent change in conditions. Measurements of this type may possibly be of advantage in studying reactions in rocket nozzles.

THE JOURNAL OF CHEMICAL PHYSICS VOLUME 18, NUMBER 10 OCTOBER 1950

The Cataphoresis of Spherical Particles in Strong Fields

F. Booth
Department of Theoretical Physics, King's College, London, England
(Received June 16, 1950)

The problem of determining the rate of cataphoresis of a solid spherical particle in an electrolyte when relaxation effects are neglected, is solved completely by using Oseen's equations. The bearing of the results on the usual methods of finding zeta-potentials from cataphoretic velocities is discussed.

I. INTRODUCTION

In 1931 Henry[1] obtained a formula for the electrophoretic velocity of solid conducting spheres in an electrolyte. The treatment involved three simplifications; the Debye-Hückel approximation was applied to the double layer of the sphere, relaxation effects were neglected and the inertia terms in the equations of motion for the electrolyte dropped. In the following note we shall retain the first two approximations and examine the effect of the inertia terms on the rate of cataphoresis. The question we are to discuss is closely related to a classical problem in hydrodynamics, namely, the calculation of the drag on a solid sphere moving with uniform velocity through an infinite viscous fluid. The solution of this problem when the inertia terms are neglected was given by Stokes in 1845. When the inertia terms are not ignored the solution is difficult since the equations are non-linear. The most exhaustive analysis is due to Goldstein[2] and we shall make considerable use of his work in what follows. The two papers containing his calculations will be denoted in future by the symbols $G(a)$ and $G(b)$.

By analogy with the drag problem we would expect the correction of Henry's result due to the inertia terms to be small provided that $Ua\eta\ll 1$, where U is the cataphoretic velocity, a the particle radius and η the coefficient of viscosity for the electrolyte. This condition is generally satisfied in cataphoresis measurements. Nevertheless it is of interest to examine precisely the effect of the inertia terms, since, owing to the double layer, the flow distribution round the particle in our problem is quite different from that round an uncharged sphere dragged through a fluid. We shall show that the relation between the velocity U and the field strength E may be written in the form

$$U=\sum_{\nu=1}^{\infty}(\epsilon E\zeta)^{\nu}a^{\nu-1}\eta^{1-2\nu}W_{\nu}, \tag{1}$$

where ϵ is the dielectric constant of the electrolyte, ζ the zeta-potential and the W_ν are functions of the ratio of a

[1] D. C. Henry, Proc. Roy. Soc. London **A33**, 106 (1931).
[2] S. Goldstein, Proc. Roy. Soc. **A123**, 216 and 225 (1929).

to the double layer thickness, and of the conductivities of particle and electrolyte. A general method for the evaluation of the W_ν functions is given, but the first three terms only of (1) will be examined in detail.

II. PRESSURE AND VELOCITY DISTRIBUTION

We require the steady velocity of translation of a charged solid sphere in an infinite electrolyte, when a field E is applied. The problem is equivalent to that of finding the velocity at infinity U, which must be imparted to the fluid for the sphere to remain stationary. Choosing the center of the sphere as origin, the equations of motion and continuity are

$$\eta \operatorname{curl}\operatorname{curl}\mathbf{v}+(\mathbf{v}\cdot\operatorname{grad}\mathbf{v})=-\operatorname{grad}p-\rho\operatorname{grad}\Psi \quad (2)$$

$$\operatorname{div}\mathbf{v}=0 \quad (3)$$

where $\mathbf{v}$ is the fluid velocity, p the pressure, ρ the charge density and Ψ the electrostatic potential. We make the usual assumption that the electrolyte can be regarded as incompressible. To solve (2) and (3) we shall adopt Oseen's method[3] and write the equations in the form

$$\eta \operatorname{curl}\operatorname{curl}\mathbf{u}+U(\partial\mathbf{u}/\partial x)=-\operatorname{grad}p-\rho\operatorname{grad}\Psi \quad (4)$$

$$\operatorname{div}\mathbf{u}=0, \quad (5)$$

where $\mathbf{v}=U+\mathbf{u}$, and x is measured in the direction of U.

The appropriate general solutions of (4) and (5) when $\rho=\Psi=0$, are, in spherical polar coordinates (r, θ, α),

$$u_r^*=-\sum_{n=0}^{\infty}(n+1)\frac{A_nP_n(\mu)}{r^{n+2}}+\tfrac{1}{2}e^{\mu\xi}\sum_{n=0}^{\infty}B_n[\chi_n'(\xi)-\mu\chi_n(\xi)]P_n(\mu)$$

$$u_\theta^*=-\sin\theta\sum_{n=1}^{\infty}\frac{A_nP_n'(\mu)}{r^{n+2}}-\tfrac{1}{2}e^{\mu\xi}\sin\theta\sum_{n=0}^{\infty}B_n\chi_n(\xi)\left[\frac{P_n'(\mu)}{\xi}-P_n(\mu)\right] \quad (6)$$

$$u_\alpha^*=0$$

$$p^*=-U\frac{\partial}{\partial x}\sum_{n=0}^{\infty}\frac{A_nP_n(\mu)}{r^{n+1}} \quad (7)$$

where $\mu=\cos\theta$, $\xi=kr$, $k=U/2\eta$. A_n and B_n are integration constants, and the χ_n functions are defined in $G(b)$. To find the general solutions of (4) and (5) when ρ and Ψ are not zero, we must find particular integrals of (4), add them to (6) and (7) and determine A_n and B_n from the boundary conditions for $\mathbf{u}$ and p.

To determine ρ and Ψ, we have first Poisson's equation

$$\Delta\Psi=-\frac{4\pi}{\epsilon}\rho.$$

Also, following Henry, we have, if relaxation effects are ignored

$$\Psi=\Psi_1(r)+\Phi(,r\ \theta),$$

where

$$\Psi_1(r)=\frac{a\zeta}{r}e^{\kappa(a-r)}. \quad (8)$$

κ is defined by the equation

$$\kappa^2=\frac{4\pi e^2\sum_{i=1}^{s}n_iz_i^2}{\epsilon kT}$$

n_i being the concentration of the ions of type i far from the particle, z_i their valency.

$$\Phi(r,\theta)=-Er\cos\theta(1+\lambda a^3/r^3),\quad \lambda=\frac{\sigma-\sigma'}{2\sigma+\sigma'} \quad (9)$$

σ being the specific conductivity of the electrolyte, σ' that of the particle.

Let

$$p_1=p-\int_r^{\infty}\rho\frac{d\Psi_1}{dr}dr, \quad (10)$$

then (4) gives

$$\nabla^2p_1=-\frac{\partial\Phi}{\partial r}\frac{d\rho}{dr} \quad (11)$$

By the usual methods a particular integral for p_1 is

$$p_1=\frac{\epsilon E\zeta}{4\pi r}\cos\theta C_0(\alpha)$$

where $\alpha=\kappa r$,

$$C_0(\alpha)=be^{b-\alpha}\left[1+\frac{1}{\alpha}+\lambda b^3\left(-\frac{1}{2\alpha^2}+\frac{1}{6\alpha}-\frac{1}{12}+\frac{\alpha}{12}-\frac{\alpha^2e^{\alpha}}{12}E_i(\alpha)\right)\right] \quad (12)$$

and $b=\kappa a$.

Now consider the particular integrals for u_r and u_θ. Writing

$$\mathbf{w}'=e^{-kx}\operatorname{curl}\mathbf{u}, \quad (13)$$

the curl of (4) gives

$$(\operatorname{curl}\operatorname{curl}+k^2)\mathbf{w}'=-\frac{e^{-kx}}{\eta}\operatorname{curl}(\rho\operatorname{grad}\Phi). \quad (14)$$

[3] Oseen, Arkiv. f. Mathematik. **6**, No. 129 (1911).

Since the motion is symmetrical about the θ-axis both w_r' and w_θ' are zero. For the particular integral of w_α' we assume

$$w_\alpha' = \sin\theta \sum_{n=1}^{\infty} C_n(r) P_n'(\mu) \tag{15}$$

where the C_n are functions of r only. We find for $C_n(r)$

$$C_n(r) = \frac{(-1)^n \epsilon E}{2\pi^2 \eta (2n+1)^2} \times \int_r^\infty r\psi_n(kz)[\psi_n(kz)\chi_n(kr) - \psi_n(kr)\chi_n](kz) \times \left[1 + \frac{\lambda a^3}{z^3}\right] \frac{d\Psi_1(z)}{dz} dz. \tag{16}$$

This expression is obtained by substituting (15) in (14) and equating coefficients of like powers of $\sin\theta P_n'$. For e^{-kz} we have

$$e^{-kz} = \sum_{n=0}^{\infty} (-1)^{n+1} \frac{\psi_n(\xi)}{\xi} P_n'(\mu). \tag{17}$$

where the ψ_n functions are defined in $G(b)$. The integral of (16) is convergent provided that $\kappa > 2k$ or $b > 2ka = 2\xi_0$. This condition imposes no serious restriction; for we shall eventually see that our result is mainly of interest for the case $b \gg 1$, that is for a thin double layer. On the other hand the use of Oseen's equations implies the restriction that Ua/η or ξ_0 is not very large.

For the calculation of U it is convenient to express the C_n as series in ascending powers of k or ξ. We accordingly expand the exponentials $e^{\pm kz}$ and $e^{\pm kr}$ in the expressions for ψ_n and χ_n before carrying through the integration. It is easily verified that C_n is of order k^{n-1} in k. Put

$$e^{\mu\xi} P_m'(\mu) = \sum_{n=1}^{\infty} X_{n,m}(\xi) P_n'(\mu). \tag{18}$$

Then we find

$$(\mathrm{curl} u)_\alpha = \sin\theta \sum_{n=1}^{\infty} D_n(r) P_n'(\mu), \tag{19}$$

where

$$D_n(r) = \sum_{m=1}^{\infty} X_{n,m}(\xi) C_m(r). \tag{20}$$

The D_n functions are easily obtained from formula (51) of $G(b)$ for the $X_{n,m}(\xi)$, together with (16) for the C_n. For example

$$D_1 = \sum_{m=1}^{\infty} \frac{3m(m+1)}{2(2m+1)} \frac{\psi_m(\xi)}{\xi} C_m(r). \tag{21}$$

It is convenient to express the D_n functions in powers of ξ. We accordingly set

$$D_n(r) = \frac{\epsilon E \zeta \kappa}{4\pi\eta} \sum_{m=0}^{\infty} D_{n,m}(\alpha) \xi^m. \tag{22}$$

If we now let

$$u_\theta = \sin\theta \sum_{n=1}^{\infty} U_{\theta,n}(r) P_n'(\mu), \tag{23}$$

$$u_r = \sum_{n=0}^{\infty} U_{r,n}(r) P_n(\mu), \tag{24}$$

the equations to determine $U_{r,n}(r)$ and $U_{\theta,n}(r)$ are respectively

$$\frac{dU_{\theta,n}}{dr} + \frac{U_{\theta,n}}{r} + \frac{U_{r,n}}{r} = D_n(r), \tag{25}$$

$$\frac{dU_{r,n}}{dr} + 2\frac{U_{r,n}}{r} + \frac{n(n+1)}{r} U_{\theta,n} = 0. \tag{26}$$

The first equation follows from (19), the second from (5) since by symmetry u_α vanishes. The solutions of (25) and (26) are

$$U_{r,n} = \frac{n(n+1)}{(2n+1)} \times \int_r^\infty \left[\left(\frac{r}{z}\right)^{n-1} - \left(\frac{z}{r}\right)^{n+2}\right] D_n(z) dz, \tag{27}$$

$$U_{\theta,n} = -\frac{1}{(2n+1)} \times \int_r^\infty \left[(n+1)\left(\frac{r}{z}\right)^{n-1} + n\left(\frac{z}{r}\right)^{n+2}\right] D_n(z) dz. \tag{28}$$

We have now completely determined the particular integrals for p, u_r and u_θ; it only remains to add them to the general integrals (6) and (7) and to fix the constants A_n and B_n. The boundary conditions at infinity are automatically satisfied; the condition of no slip at the particle surface gives the constants. Since the calculation follows that of $G(b)$ closely we omit details and state the conclusion. We find for the B_n the following equations

$$\frac{1}{2} \sum_{m=0}^{\infty} \lambda_{n,m} B_m = -3U - U_{r,1}(a) + 2U_{\theta,1}(a) \quad n=1$$

$$= (n+1)U_{\theta,n}(a) - U_{r,n}(a) \quad n>1 \tag{29}$$

where the $\lambda_{n,m}$ coefficients are defined in $G(b)$, Eq. (19). Solving for the B_n by means of (58) to (60) of $G(b)$ for

the $\lambda_{n,m}$, we find

$$B_0=\frac{\xi_0}{\pi}\Big[U\Big(3+\frac{9}{4}\xi_0+\frac{183}{80}\xi_0^2\Big)+\frac{\epsilon E\zeta}{4\pi\eta}(F_{1,0}(b)+\tfrac{3}{4}\xi_0F_{1,0}(b)+\xi_0^2\Big\{\frac{61}{80}F_{1,0}(b)-\frac{6}{5}F_{2,1}(b)+F_{1,2}(b)\Big\}\Big)\Big]+O(\xi_0^4),$$

$$B_1=\frac{\xi_0^3}{\pi}\Big[-U+\frac{\epsilon E\zeta}{6\pi\eta}F_{2,1}(b)\Big]+O(\xi_0^4),$$

$$B_2=O(\xi_0^5), \tag{30}$$

where

$$F_{n,m}(\alpha)=(n+1)\alpha^{n-1-m}\int_\alpha^\infty D_{n,m}(z)z^{1+m-n}dz. \tag{31}$$

Equations (30) give the B_n coefficients to the order in ξ_0 we require and since the A_n are not needed we can now proceed to calculate U.

III. CATAPHORETIC VELOCITY

The rate of electrophoresis is obtained by equating the total force due to the fluid stresses over the surface, to the electrostatic force due to the action of the external field on the surface charge. The electrostatic force is simply the field strength E multiplied by the total charge on the surface. This follows easily since we ignore relaxation and therefore assume that the double layer remains spherically symmetrical. The force caused by the fluid stresses may be divided into two parts, the first arising from the general integrals (6) and (7), the second from the special integrals for $\mathbf{u}$ and p. The first contribution is given by Eq. (27) of $G(a)$ and Eq. (55) of $G(b)$, the second by direct calculation. We finally obtain the following rather complicated relation for ζ in terms of U.

$$\zeta\Big[b+1-\frac{2b}{3}D_{1,0}(b)-\frac{1}{3}C_0(b)+\frac{1}{2}F_{1,0}(b)+\frac{3}{16}F_{1,0}(b)\Big(\frac{aU}{\eta}\Big)+\Big\{\frac{61}{640}F_{1,0}(b)+\frac{1}{10}F_{2,1}(b)+\frac{1}{8}F_{1,2}(b)-\frac{1}{6}bD_{1,2}(b)\Big\}\Big(\frac{aU}{\eta}\Big)^2+O(U^3)\Big]=-\frac{6\pi\eta U}{\epsilon E}\Big[1+\frac{3}{8}\frac{aU}{\eta}-\frac{19}{320}\Big(\frac{aU}{\eta}\Big)^2+O(U^3)\Big]. \tag{32}$$

This formula can be rearranged to give U in terms of ζ and we obtain a series of the form given in (1), the W_r functions being functions of b and λ only. The first term of (1) is simply Henry's formula. For a given zeta-potential, field strength and double layer thickness it is easy to show from (1) that the correction to Henry's formula is the greater the larger the radius a. Hence we would expect that for the cases of interest the double layer thickness is small compared with the radius. For this case we only need the limiting values of the W_r for b large. Series (1) now becomes

$$U=\frac{\epsilon E(1+\lambda)\zeta}{6\pi\eta}\times\Big[1+\frac{67}{11{,}520\pi^2}\Big(\frac{a\epsilon E\zeta(1+\lambda)}{\eta^2}\Big)^2+O(\zeta Ea)^3\Big]. \tag{33}$$

From (33) it is obvious that the correction is more important the larger the radius, the zeta-potential and the field strength. Also it is most important for non-conducting particles since in this case λ achieves its maximum value of $\frac{1}{2}$. It is easy to see from (33) that the correction will be quite small in the usual experimental determinations unless exceptionally strong fields are used. For example, if we take particles with a zeta-potential of 200 millivolts at room temperature, then we find that for the correction to be greater than 10 percent the product Ea must be greater than 200 volts. This result confirms in detail that Henry's neglect of the inertia terms is legitimate.

Nevertheless, if the experimental difficulties associated with strong fields could be overcome, the agreement or lack of it between (32) or (33) and the experimental data might serve as a check on the usual interpretations of cataphoresis measurements by the use of the Smoluchowski or Henry theories. For example, in Henry's theory and in the present calculations, it is assumed that at the surface of the particle there is an abrupt change from a fluid of viscosity η to a rigid solid, the change occurring when the potential is ζ. This may not be true; it is quite possible that there is a continuous increase in η with the potential in the ionic atmosphere. But from measurements of cataphoretic velocities and similar electrokinetic effects, as interpreted by the usual theories, it is impossible to decide whether this is true or false since ζ is really an unknown variable. Now if a considerable variation of η occurred in the range of interest, the method we have given would break down. But it is reasonable to assume that in this case, the dependence of U on E would be different from what we have found. The value of ζ which satisfied Henry's equation for *weak* fields would not then satisfy (1) or (33) for *strong* fields.

Correlation of Ionic and Atomic Radii with the Heat of Hydration

W. D. ROBERTSON
*Institute for the Study of Metals, University of Chicago, Chicago, Illinois**
(Received June 28, 1950)

It is shown that Pauling's ionic and atomic radii may be correlated with the ionic heat of hydration in a manner which provides a method of intercomparison of the different radii and demonstrates their self-consistency. The correlation also indicates significant differences between ionic and atomic radii which may be interpreted in terms of the ion-dipole interaction theory of solutions.

IDEALLY the energy obtained by hydration of an ion of charge ze and radius r is given by the Born formula[1]

$$\frac{z^2e^2}{2r}\left[1-\frac{1}{D}\right]. \tag{1}$$

However, since the field near the ion exceeds the saturation field of the dielectric (water), (1) is an inadequate expression for the hydration energy. Bernal and Fowler[2] have proposed an expression by means of which the necessary corrections may be evaluated from the experimentally determined heat of hydration, U.

$$U=\frac{D-1}{2D}\frac{z^2e^2}{R}+npP(r)-u. \tag{2}$$

R is an effective radius inside which the energy is that of ionic coordination while outside it is that of dipole interaction of water; n is the coordination number, $P(r)$ is the potential energy of ion-dipole interaction which may be calculated and p is a correction term including the repulsion between ion and water molecule, van der Waal's attraction, the change of the dipole moment in the field of the ion and the mutual potential energy of the water molecules; u is a small term representing the electrostatic energy of disoriented water molecules. The individual correction terms are not readily calculated nor is the radius R; but (2) may be put in the form

$$U=a+bP(r) \tag{3}$$

and the constants evaluated empirically by plotting the experimental values of U *versus* the calculated potential energy, $P(r)$, from which b and a are obtained for different values of z and n.

In the above treatment, Goldschmidt's[3] empirical crystallographic radii were used in the calculation of $P(r)$ as being more directly applicable than Pauling's ionic radii.[4] The reason for this choice is not obvious and the method of plotting does not show clearly the interrelationships existing between the different ions and between the various possible radii. The fact that the ionization energy differs from the heat of hydration by only a few percent indicates that, in effect, the function of the dielectric is to return electrons to the ion which may justify the use of Pauling's semi-empirical atomic or covalent radii.[5]

Figure 1 shows that in fact there is a relationship between Pauling's univalent ionic radii and the heat of hydration; further, Fig. 2 demonstrates that there is an equally close relationship between Pauling's single bond atomic radii and the same heats of hydration, obtained from independently measured quantities through the Born-Haber cycle and the partition of energy between the potassium ion and the fluoride ion in accordance with Bernal and Fowler's method.[2]

In plotting the data, experimental heats of hydration have been used wherever possible; where adequate data were lacking, the calculated values of Bernal and Fowler were used; to tie down critical points in the absence of other data, the ionization energy was used, corrected in proportion to the difference between the observed heat of hydration and the ionization energy for similar ions.

The most obvious characteristic of both correlations is the self-consistency of the data and the convenient

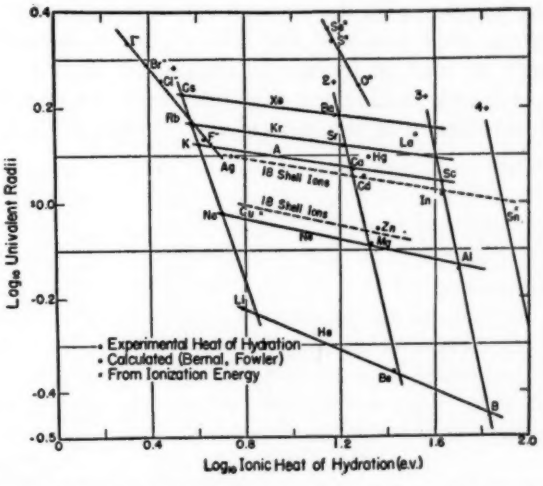

FIG. 1. Univalent ionic radii *versus* the ionic heat of hydration.

* Present address: Hammond Metallurgical Laboratory, Yale University, New Haven, Connecticut.

[1] M. Born, Zeits. f. Physik **1**, 45 (1920).

[2] J. D. Bernal and R. H. Fowler, J. Chem. Phys. **1**, 531 (1933).

[3] V. M. Goldschmidt, *Geochemische Verteilungsgesetze der Elemente*, VII *and* VIII (Oxlo, 1927).

[4] L. Pauling, *The Nature of the Chemical Bond*, 2nd edition (Cornell University Press, Ithaca, 1940), p. 343.

[5] L. Pauling, J. Am. Chem. Soc. **69**, 542 (1947).

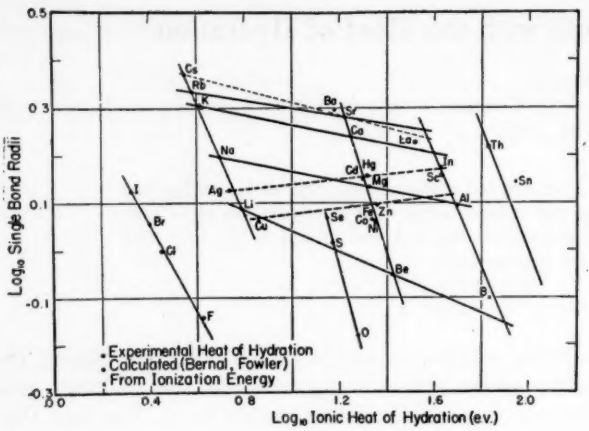

FIG. 2. Single bond atomic radii *versus* the ionic heat of hydration.

form in which the interrelationships between different ions, radii, and charge are displayed.

Considering ionic radii first, Fig. 1, the slope is -1.5 for positive ions and -0.6 for the negative halide ions, indicating that the heat of hydration is proportional to $r^{-\frac{3}{2}}$ and $r^{-\frac{3}{5}}$ for positive and negative ions respectively, instead of r^{-1} as indicated by the simple Born formula. This effect should be compared with the corresponding atomic radii, Fig. 2, in which the slope is -1 for both positive and negative ions. For all ions having the rare gas electron configuration, the heat of hydration increases in proportion to the square of the charge at constant radius. The eighteen electron shell ions and mercury do not fall on the main lines characteristic of the rare gas ions but appear to approach the lines more closely as the charge increases; for example, in the series silver, cadmium and indium, the latter coincides with the line for boron and aluminum. This effect should be compared with the plot of atomic radii where both types of ions fall on the same lines.

The lines for single bond atomic radii, Fig. 2, approach unit slope for both negative and positive "ions." This, together with the above mentioned correlation of eighteen shell ions and the relationship of ionization energy to heat of hydration, apparently justifies the use of atomic radii rather than ionic radii. Further, the self-consistency of the radii is very evident with, perhaps, two exceptions, namely, barium and lanthanum. The heat of hydration for lanthanum should probably be given less weight than that for barium since it was obtained by calculation and it does not fall exactly where it should on either the atomic or ionic plot. But, considering the two sets of data, it appears probable that the atomic radii for barium and lanthanum are too small; an increase of 0.26A in both cases is required to bring them into conformity with the other atomic radii.

The valence assigned by Pauling to transition elements and succeeding elements in the table of atomic radii, based on magnetic criteria, has not been considered in plotting the data. It is interesting to note that in each case the points for silver, cadmium, zinc, iron, cobalt, nickel, and indium fall on, or very near, lines characteristic of ions with normal, integral valence.

While the validity of the procedure is not immediately apparent, extrapolation of the line for univalent positive ions to the hydration energy of the hydrogen ion, 12 ev, gives 0.55A as an effective atomic radius. The same procedure indicates a value of 0.26A as the ionic radius of the hydrogen ion. It should be observed that geometric considerations for the packing of spheres require a cation-anion ratio of 0.225 to 0.414 for stability of tetrahedral coordination; taking the radius of the water molecule as 1.4A and the above atomic radius of hydrogen gives a radius ratio of 0.39 which is well within the limits of tetrahedral stability. Alternatively, the radius ratio for the apparent ionic radius is 0.18, indicating a triangular coordination of water molecules which is not in accord with the known structure.

In conclusion it may be said that the method of plotting assembles a mass of data in a manner which permits immediate correlation and intercomparison. It also demonstrates the self-consistency of the data. Whether more fundamental concepts regarding the nature of the ion-dipole interaction can be deduced from the characteristics of the plots, particularly from the differences resulting from the use of ionic or atomic radii, remains to be demonstrated by more detailed consideration.

This work was supported in part by Army Air Force Contract No. AF 33(038)-6534.

The Accommodation Coefficients of Gases on Platinum as a Function of Pressure

LLOYD B. THOMAS AND ROBERT E. BROWN
Chemical Laboratory, University of Missouri, Columbia, Missouri
(Received June 26, 1950)

The accommodation coefficients of nine gases on platinum at various temperatures in six different tubes are presented as a function of pressure. In all cases the accommodation coefficients show a constant value as the pressure is lowered toward zero, which is in contradiction to results reported by Amdur and co-workers. Reasons for disagreement are suggested and criticism of an earlier paper from this laboratory is answered. Presumably specially reliable values of the accommodation coefficients of argon and krypton taken in Tube *B* are given and this tube and method of operation are described in detail.

INTRODUCTION

UPON examination of assembled measurements of the accommodation coefficients of gases on platinum by various investigators,[1–3] one is disturbed by the wide variation in the reported values. This is not too surprising, perhaps, when one considers the rather insidious opportunities for error in measurement of the coefficient, superimposed on the fact that one is dealing with a very sensitive surface phenomenon that may be markedly affected by adsorbed layers formed sometimes quite slowly from traces of impurities in the system or from the gas itself under investigation. These latter effects have not been subject to reproducible control especially from laboratory to laboratory since vacuum techniques ranging from modern procedures with all glass systems, liquid air traps, baking facilities, etc., to use of bell jars have been used by investigators in obtaining the reported values. Recently another possible explanation of much of the variation in reported values may be seen in the phenomenon reported by Amdur and co-workers[4] who have found the accommodation coefficients of all ten gases investigated to show a marked pressure dependence. In a second paper Amdur[5] has developed a theory which fits his observed accommodation coefficients as a function of pressure and, after revising several of the most radically low values of reference 4, finds the following general behavior. In the neighborhood of 0.1 mm and for a range above the values are essentially constant. Below this, the values fall off with increasing rate as the pressure is lowered. The greatest decrease is with krypton and xenon whose accommodation coefficients fall almost fifty percent when the pressure is lowered to about 0.008 mm (lowest used) and apparently would continue to fall at lower pressure. The other eight gases show similar but smaller drops in their accommodation coefficients. If such is the true behavior of the coefficients, there is little reason to expect agreement between investigators' reported results since the values are obtained over a variety of pressures, usually in the region of variation (below 0.1 mm).

Thomas and Olmer[5a] state: "Runs were made in two ways with results in good agreement. In the first method the pressure of the gas was varied from zero to a maximum of 0.05 mm and the filament and heaters brought to balance at the original temperature after each addition of gas. The power loss varied linearly with pressure and the slope of the line gave the power loss per unit pressure, which was used to determine the accommodation coefficient." The pressure range quoted above lies in the region of rapid accommodation coefficient change in references 4 and 5, so the quoted statement is in definite disagreement with the findings of references 4 and 5. Measurements supporting the above quotation from reference 1 may be found in a number of papers, e.g. Knudsen,[6] Mann,[7] Soddy and Berry.[8] It seems imperative to examine this disagreement further and the purpose of this paper is to present sets of accommodation coefficient measurements in which behavior with pressure may be observed and perhaps elucidated.

EXPERIMENTAL

The data presented in this paper have been obtained from six different tubes of several types which have been operated by four investigators. The work on krypton and argon in Tube *B* is considered by us to be the most reliable and since this type of tube has not been described previously it is shown in Fig. 1. Tubes *C* to *G* will be briefly identified at the end of this section. Tube *B* is designed to give a flat temperature distribution over the full length of the filament and thus eliminate end losses of heat from the filament and hence need for attempted correction. This is accomplished by bringing the platinum blocks (Fig. 1) to the same temperature as the filament through adjustment of the current through the heaters of platinum wound on glass and mounted on the tungsten leads in the side tubes. The heaters are supplied by alternating current from filament windings of twin transformers powered by a

[1] Thomas and Olmer, J. Am. Chem. Soc. **65**, 1036 (1943).
[2] Grilly, Taylor, and Johnston, J. Chem. Phys. **14**, 435 (1946).
[3] Kennard, *Kinetic Theory of Gases* (McGraw-Hill Book Company, Inc., New York, 1938).
[4] Amdur, Jones, and Pearlman, J. Chem. Phys. **12**, 159 (1944).
[5] I. Amdur, J. Chem. Phys. **14**, 339 (1946).
[5a] See reference 1, p. 1039.
[6] Knudsen, Ann. d. Physik **34**, 629 (1911).
[7] Mann, Proc. Roy. Soc. **A146**, 780 (1934).
[8] Soddy and Berry, Proc. Roy. Soc. **A83**, 254 (1910).

constant voltage transformer and are individually controlled by rheostat arrangements capable of fine adjustment. The thermocouples were calibrated over the range used against N.B.S. calibrated thermometers and their e.m.f.'s were read on a L & N White Double Potentiometer to within one microvolt. The power losses from the filament and its resistance are obtained by reading to five figures on a L & N Type K-2 potentiometer the fall in potential across the filament using the potential leads attached to the blocks and the fall in potential across a standard ohm resistor in series with the filament. The filament temperature is obtained from its R_0 value and the temperature coefficient of resistance. This was carefully determined over the range used in a special tube and thermostat using N.B.S. calibrated thermometers ($\alpha=0.00388$). Tube *B* was operated immersed in a stirred kerosene filled thermostat (0.03°) held at 32°C. Frequent checks of the power loss in vacuum and the R_0 value of the filament were made in order to guard against sporadic changes in the filament surface or electrical characteristics which are occasionally observed. It is to be emphasized that the balancing of the thermocouples and filament temperature and measurement of the power expended has been done with care using precision instruments read to accuracies which are about 100-fold as great as may be had with deflection meters which are often used in this kind of work.

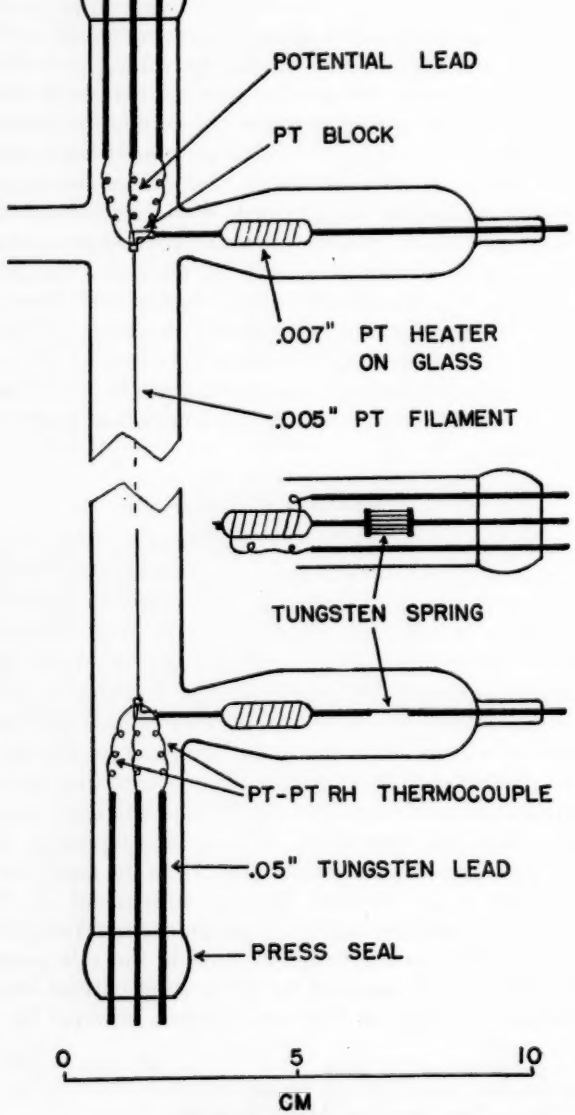

FIG. 1. Tube *B*.

The high vacuum system was all glass and mercury except for the tube elements and employed a mercury condensation pump, mercury cut-offs, and a liquid air trap between the last cut-off and the measuring tube. One cut-off, open only when gases were admitted, led to a "lock" system between two mercury seal stopcocks, manometer, and manifold with supply of gases held in flasks with mercury seal stopcocks to contain the gases after opening by the usual glass enclosed magnetic breaking slugs. The inert gases were of highest purity obtainable from Airco. The tube was occasionally baked and the system torched and the filament flashed some hours before each set of measurements to take reasonable precaution to minimize accumulation of adsorbed impurities in the system. All measurements were taken with liquid air on the trap excluding mercury vapor and other condensable gases from the sample under investigation. The greatest source of inaccuracy in measurement of the coefficients is the pressure reading. Two McLeod gauges of different types employing 300-ml bulbs and exceedingly carefully calibrated capillaries of Fisher and Porter standard bore tubing were attached to the system and both were usually read to establish the pressures. The two gauges seldom differed by as much as 0.25 micron on the same gas samples. Each gauge was self-consistent upon successive reading to about ± 0.05 micron. It appears that the pressure readings regularly fall within ± 2.5 percent of the mean value in the least favorable range used (below 5 microns) and within ± 0.5 percent in higher ranges.

The other tubes used in obtaining data presented in this paper are described below. Tube *C* had a filament consisting of 42 cm of 0.0175-cm diameter platinum in a hairpin loop with 0.0025-cm potential leads attached 6 cm from the ends. Tube *D* contained a 25-cm filament of 0.0125-cm diameter platinum placed along the axis of the cylindrical envelope and used 0.0025-cm potential leads 5 cm from filament ends. Tube *E* consisted of a hairpin loop of 0.00375-cm platinum 22 cm in length and it was operated in a bridge circuit with a potentiometer to measure the voltage across the filament to get the power loss. Tube *F* is of loop construction with 32 cm of 0.010-cm platinum with 0.0025-cm potential leads attached 4.5 cm from the ends. Tube *G* is of hairpin loop construction with heater ends as described in reference 1. The electrical measurements on all tubes except Tube *F* were made in similar manner to Tube *B*.

EXPERIMENTAL RESULTS AND DISCUSSION

The accommodation coefficient values are presented in the nineteen curves of Figs. 2, 3, and 4 and include, as specified on the graphs, values for krypton, argon, neon, helium, hydrogen, nitrogen, oxygen, carbon monoxide, and mercury. In the parentheses on the graphs following the gas designation are given approximate ΔT (filament temperature minus wall temperature) values for the points of each curve and the tube, designated by letter, in which the measurements were taken and which are described in the preceding section. The wall temperatures are in all cases close to 32°C.

Reports of present day work on accommodation coefficients should contain, we believe, enough description of the method of taking data and enough indication of the accuracy of the measurements to allow the reader to judge the validity of the work. With this in view we have selected a typical point for argon, $\Delta T = 100°$ in Tube B, at 0.026 mm and give the preparation procedure, the data taken, and the calculations made in obtaining the point. The filament surface is cleaned by heating to a bright orange with the system open to the pumps. Argon is admitted and regulated to the desired pressure and the filament is run for about 15 hours at moderate temperature (about 200°C). During the first part of the 15 hours the accommodation coefficient rises but is quite stable toward the end of the period and thereafter. The filament and blocks are then brought to the desired temperatures within a tolerance of ±0.15° at 100° and ±0.06° at 7° by a series of successive adjustments of fine control rheostats interspersed with filament and thermocouple temperature measurements. This can be done in approximately one hour. The set of measurements shown in Table I is then taken. Calculated quantities and previously determined quantities necessary to complete the calculations are interspersed in the table with the data taken at this time.

For the purpose of this paper, which is to show the pressure dependence of the accommodation coefficient at low pressure, it seems sufficient to show the points by plotting on the graphs only. However, we feel that the values for argon and krypton obtained with Tube B merit consideration among the most reliably determined values in the literature and present in Table II the numerical values of these together with the corresponding pressures as plotted in Figs. 2 and 3.

The accommodation coefficient values in Table II calculated as indicated in Table I using the assumption that the temperature of the molecules incident upon the filament is that of the wall begin to decrease noticeably above approximately 20 microns. To obtain a value for the accommodation coefficient in each case we have taken the average of the values above the dotted lines in Table II, excluding the questioned values indicated, and the results are shown at the end of the respective columns.

It is seen from inspection of Figs. 2 and 3 that the accommodation coefficients in all sets presented for each

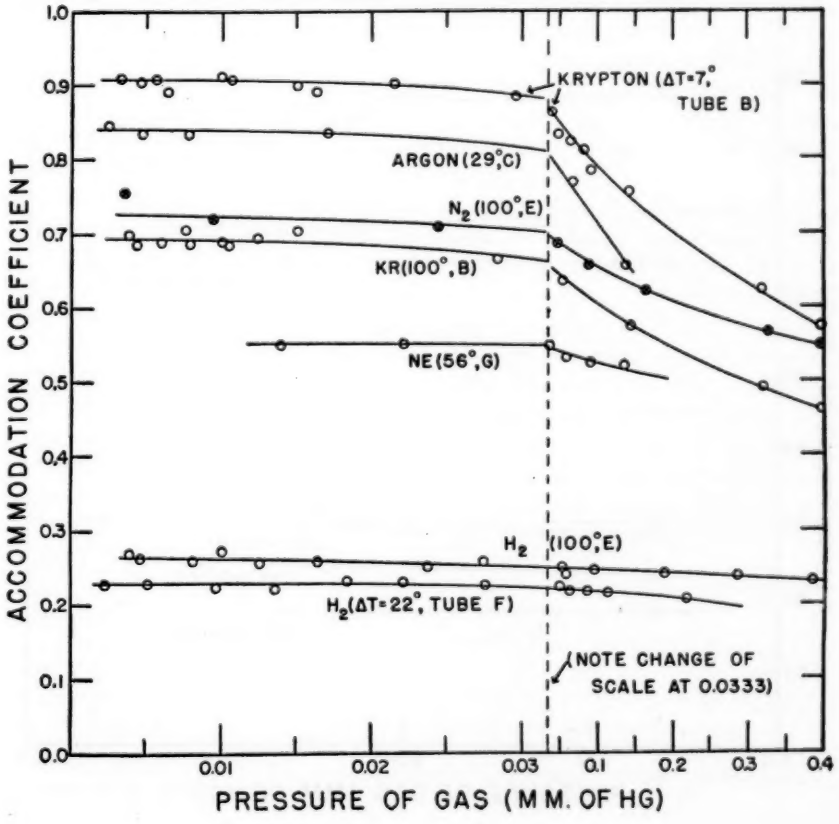

FIG. 2. Accomodation coefficients as a function of pressure. (Assumptions in the calculation method begin to fail above 0.02 mm.)

of the nine gases are essentially constant in the range of applicability of the free molecule heat conduction method of calculation in a tube of cylindrical symmetry using a filament of diameter small compared to the mean free path in the gas. The lower apparent values at higher pressures are not real values for the accommodation coefficient and are given in this way to show for each of the gases and tubes of Fig. 2 the permissible range of application of the assumption that the temperature of the incident molecules is that of the wall. If adequate theory of heat conduction in cylindrical symmetry were available for the pressure range immediately above the "free molecule" range, no doubt essentially the same accommodation coefficient values would be obtained from the data in the compressed scale portion of Fig. 2. Conversely, a possible use of the data in the compressed scale region is to test such theory. We note here that the factors which tend toward a large temperature jump also act, as would be expected, to diminish the slope of the curves of Fig. 2 which is readily seen in the compressed scale portions. These factors are low accommodation coefficient and large temperature gradient in the gas at the surface of the filament. The latter increases as the filament diameter decreases. The filament diameters for the tubes are $C=0.007''$, $B=0.005''$, $G=0.004''$, $E=0.0015''$. The flattest curve—no apparent change in slope up to the maximum pressure—is for hydrogen which has small accommodation coefficient in Tube E which has the smallest diameter filament. The steepest curve is for argon which has high accommodation coefficient in Tube C which has the largest filament.

The results here shown are in complete disagreement with those of Amdur and co-workers[4,5] at the lower pressures. Our measurements are extended in many cases to less than half the minimum pressures used by Amdur and in no case are diminished accommodation coefficient values obtained except as attributable to experimental variation due to diminished accuracy of the pressure measurement. The electrical measurements as used are capable of much greater accuracy than required for these low pressure measurements as is indicated by the curves of Fig. 4. These curves are for mercury vapor which has about half the ability to conduct heat from a platinum filament as does argon and the pressure range covered is 0.2 to 1.5 microns which is less than one tenth the pressures used for the permanent gases. The consistency of these points is seen to be about as good as for the permanent gases and the reason is considered to be that the vapor pressures can be controlled accurately and determined by thermometer and vapor pressure tables (I.C.T. used with thermal transpiration corrections applied) as accurately as the McLeod gauge can be read in the higher range. Even down to the lowest pressure here (0.2 micron) there has been no apparent dip in the accommodation coefficient value. Amdur shows for all the eight gases common to his work and the present paper accommodation coefficients which fall from his steady values (at higher pressure) most of

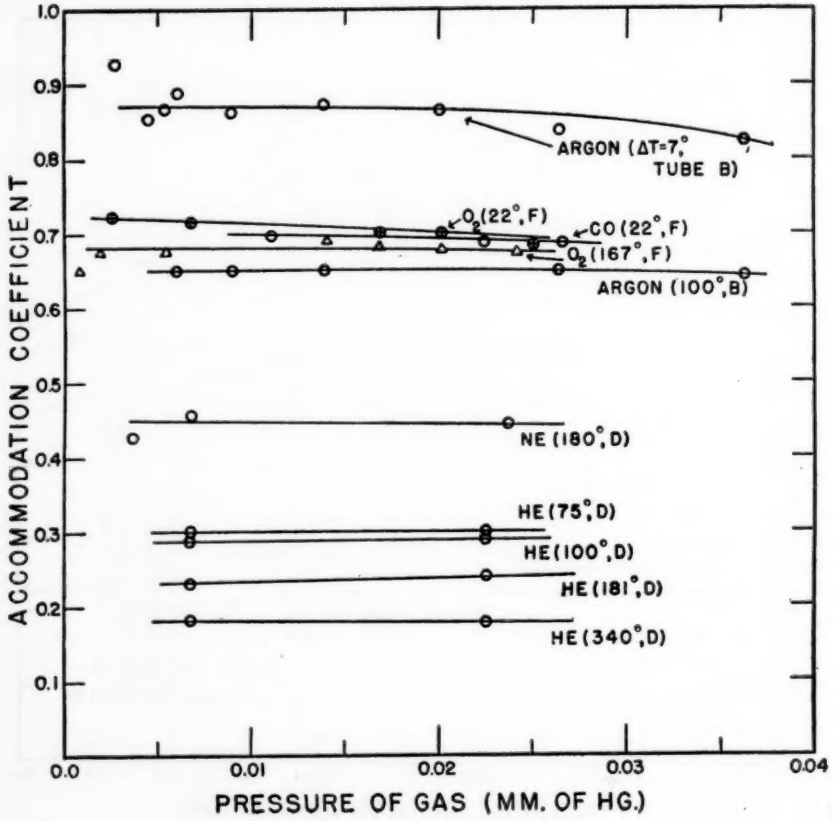

FIG. 3. Accomodation coefficients as a function of pressure.

which are not far from our flat values at low ΔT and low pressure, to an average of about 0.7 of these steady values with the greatest drop shown for krypton which falls to 0.51 of his α_∞. Amdur's ΔT values are lower than the minimum presented in this paper and we have considered it possible that one might have the phenomena described by him showing up at this lower ΔT but we have checked this quite carefully in several runs with ΔT of the order of two degrees. Our results with this ΔT show no indication of a decrease in the accommodation coefficient although erratic low and high values appear. Curves for these ΔT's are not included because we consider this pushes the apparatus too far into an unfavorable range of operating conditions.

Since we were confronted with the phenomenon of the pressure dependence of the accommodation coefficient as described in references 4 and 5 which was contrary to our earlier experience and since we set out to search for the phenomenon and were unable to find indications of it in any of the experiments tried and have had the advantage of knowing what to look for, we naturally attribute the disagreement to error in the work of references 4 and 5. We cannot hope to attempt a detailed criticism of the method on the basis of our knowledge of the apparatus but would like to suggest the following points as open to question.

The experiments were done in a vessel constructed of brass and solder and it was operated in a bell jar, which technique could not be regarded as clean from a vacuum standpoint and would not allow baking or freeing from mercury vapor. The conductivity gauge used was not designed for accommodation coefficient measurement and lacked the simplicity desirable to avoid a patchwork of assumptions and corrections. One might question the completeness of temperature stationing of the Mycalex block hung in the filament loop or of the filament threaded through the loop or of the comparison filament strung between the mica sheets in the flattened cylinder. The pressures were obtained by expansion from a high measured pressure in a small volume to a low pressure in the large bell jar. Adsorption after expansion into the large volume following partial desorption of the extensive surfaces upon evacuation could render Boyle's law inapplicable and would give low accommodation coefficients as observed at low pressure. The bridge current, which enters as the second power in the power loss measurement, was read on a deflection meter. The great dependence upon the accuracy of this meter is indicated at the bottom of p. 341, reference 5, where it is said that recalibration of the meter after publishing reference 4 resulted in a 1 percent revision of the current, yet this apparently changed the accommodation coefficient value of xenon from 0.108 to 0.469 at the lowest pressure used and of krypton from 0.232 to 0.445. The constants of the platinum filament needed to calculate the temperature distribution and end losses of the filament, i.e., resistivity, thermal conductivity, and radius, are obtained through a series of relationships involving the

TABLE I. Sample data and calculations for argon ($\Delta T=100°$, Tube B), at 0.026 mm.

(a)	Potential fall across filament between potential leads	0.24526 volts
(b)	Potential fall across standard ohm in series with the filament (also the current through the filament)	0.079818 volts
(c)	Power loss of filament by gas conduction and radiation given by $(a)\times(b)$	0.0195762 watts
(d)	Resistance of filament given by $(a)/(b)$	3.0727 ohms
(e)	Power loss of filament in vacuum at resistance value of (d) as previously determined	0.0048545 watts
(f)	Power loss due to gas conduction, given by $(c)-(e)$	0.0147217 watts
(g)	R_0 (frequent determination made by limiting zero current extrapolation method at bath temperature and calculated to 0°C)	2.0324 ohms
(h)	Temperature of filament from (d) and (g) through $R=R_0(1+0.00388t)$	131.92°C
(i)	Temperature of bath (by calibrated 0.1 degree thermometer)	31.94°C
(j)	$\Delta T=(h)-(i)$	99.98°
(k)	Pressure measurements (0.02625, 0.02640, 0.02640, 0.02652) Av	0.02639 mm
(l)	Area of filament (from mass and length and density of Pt.)	0.9754 cm²
(m)	Energy conducted by gas per unit area of filament per unit ΔT per unit pressure (micron) per unit time (second)	57.203 ergs
(n)	Calculated value of (m) in same units assuming temperature equilibrium of argon atoms with the wire $A=(Cv/R+\frac{1}{2})\times(R/2\pi MT)^{\frac{1}{2}}$	88.192 ergs
(o)	Accommodation coefficient, $(m)/(n)$	0.6486

Matthiessen rule and the Wiedemann-Franz law and the values obtained depend on the temperature coefficient of resistance measurement, $\alpha=0.00363$. Direct measurement in this laboratory agrees well with the resistivity 9.83×10^{-6} ohm cm and the temperature coefficient $\alpha=0.0039$ which are commonly given for high grade platinum rather than with the 10.694 and 0.00363 values used in reference 4.

Amdur *et al.*[4] devote most of page 166 to pointing out an "error" in reference 1 which should be discussed briefly here. Apparently the authors of reference 4 have taken the expressions 242(b) and 241(c) on page 317 of reference 3, which apply to conduction between parallel plates, as applying to conduction from a small diameter filament in a much larger diameter tube. In picking the example of the treatment of mercury to criticize they have chosen the one least open to doubt. At the lower pressures of the measurements on mercury the mean free path is much larger than the average radius of the tube. If one wishes to obtain an estimate of the average

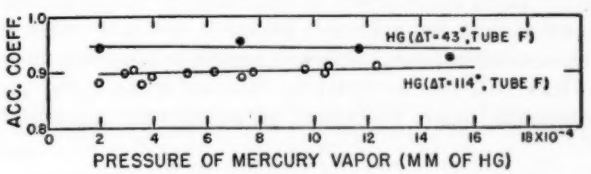

FIG. 4. Accomodation coefficients of mercury vapor as a function of pressure.

TABLE II. Accommodation coefficients of Kr and A taken in Tube *B*.

Krypton ($\Delta T = 7°$) A.C.	Pressure (microns)	Krypton ($\Delta T = 100°$) A.C.	Pressure (microns)	Argon ($\Delta T = 7°$) A.C.	Pressure (microns)
0.909	3.28	0.699	3.86	0.929 ?	2.74
0.902	4.60	0.686	4.40	0.852	4.48
0.908	5.58	0.689	6.00	0.866	5.38
0.891	6.41	0.748 ?	7.07	0.899	6.04
0.912	9.91	0.705	7.56	0.863	8.91
0.906	10.59	0.686	7.96	0.872	13.8
0.898	15.07	0.685	8.04	.....	
0.891	16.4	0.689	10.05	0.865	20.04
0.905	21.9	0.684	10.30	0.836	26.39
.....		0.693	12.34	0.824	36.24
0.885	29.61	0.703	15.07	0.8695 Av	
0.863	38.76	.....			
0.831	49.08	0.665	28.44	Argon ($\Delta T = 100°$)	
0.824	64.32	0.634	53.22		
0.810	80.94	0.574	141.8	A.C.	Pressure
0.781	89.22	0.492	319.8		
0.755	141.8	0.418	556.2	0.649	6.04
0.624	319.8	0.6919 Av		0.648	8.91
0.500	556.2			0.649	13.86
0.9024 Av				.....	
				0.649	26.39
				0.640	36.24
				0.6487 Av	

temperature of the gas for mercury he should roughly (neglecting the accommodation coefficient) use an average temperature of the filament and wall, each weighted with its area in the vessel, which would for reference 1 give an average temperature of the order of 1/500 of the ΔT added to the temperature of the wall. But the fact that the hot mercury atoms are headed away from the filament and even if they make occasional collisions they still will have velocity persistence away from the filament, together with the fact that one is interested only in the atoms coming toward the filament made the 1/500 of ΔT too much to add to the wall temperature. Further rendering the error innocuous is the fact that this temperature appears to the one-half power in the calculation. For the other gases at higher pressure the problem is more serious and has been considered by ourselves and others. It seems clear experimentally that the assumption of the temperature of the molecules incident upon the filament (and the average temperature of the gas) being that of the wall is valid over the pressure range covered by the flat portion of curves as in Figs. 2 and 3. Presumably there would be no changes of slope of these curves from the lowest measured pressures to the axis of zero pressure (and this is supported by the behavior of mercury, Fig. 4) and the ideas concerning the average temperature applicable to mercury as indicated above would be applicable to the permanent gases at very low pressure. However, the same value of the accommodation coefficient would be obtained up to at least 0.02 mm as would be obtained in the extremely attenuated state. Therefore, the assumption concerning the temperature must be essentially correct. This criterion of flatness of the accommodation coefficient *vs.* pressure curves was used in reference 1 and we do not agree with reference 4 that all or any values reported in reference 1 are grossly incorrect due to taking the temperature of the wall as the average temperature of the gas.

The falling off of the accommodation coefficient with increasing filament temperature is seen by inspection of Figs. 2, 3, and 4. (The two curves for hydrogen are not comparable. Tube *E* was made to serve as a Pirani gauge and no attempt was made to obtain the temperature coefficient or the dimensions of the filament at the time the data were taken. These were later estimated, tentative coefficients calculated, and one point for nitrogen was adjusted to a reasonable accommodation coefficient by a factor. This same factor was then used on all data for nitrogen and hydrogen taken with this tube. The points of these two curves are not independent "absolute" values but should show very accurately any changes of the accommodation coefficient with pressure and therefore are included in this paper.) It is apparent that the fall of the coefficients is more marked for the inert gases than for oxygen or mercury which is possibly due to the lighter binding of adsorbed inert gas molecules to the surface. We have indications that quantitatively reproducible measurements of this variation with temperature are particularly elusive for the inert gases. That the behavior is a specific surface effect and not due to faulty assumptions or experimental measurement is shown by observations taken on an evaporated aluminum surface. Mr. J. W. Faust of this laboratory, whose measurements in Tube *D* we have used, has observed that the accommodation coefficients are essentially constant with increasing filament temperature for helium and argon on an aluminum surface evaporated on the platinum filament of Tube *D*.

In conclusion we wish to assert that the accommodation coefficient has been a theoretically interesting concept with useful applications even though, as knowledge of it progressed, it has been found to depend in a complex way on a number of factors. Yet, if the observations presented in this paper are sustained, its most important simplicity is still maintained, i.e., the accommodation coefficient keeps a steady value as the pressure is reduced toward zero.

We wish to acknowledge with appreciation the support given this work by the Office of Naval Research and to express thanks for the contributions of J. W. Faust, F. J. Olmer, E. J. Rodekohr, W. M. Hubbard, and E. F. Cave to the work. We thank Professor J. L. Morrison of the University of Alberta, and Professor K. F. Herzfeld of Catholic University for comments on the work.

Harmonic Oscillator Contributions to the Thermodynamic Functions*

P. TORKINGTON
British Rayon Research Association, Barton Dock Road, Urmston, Lancashire, England
(Received July 3, 1950)

Tables giving the harmonic oscillator contributions to the specific heat, internal energy and free energy functions directly, for frequencies in the range 100 to 3600 cm^{-1}, at nine standard temperatures, have been drawn up.

THE available tables[1] for computing harmonic oscillator contributions to thermodynamic functions are tabulated for values of ν/T from 0.10 to 10.0. In the present tables (Tables I–III), the contributions from any frequency can be looked up directly for the nine temperatures usually chosen. The specific heat tables are worked out to intervals of 10 cm^{-1} from 100 to 1000 cm^{-1}, 20 cm^{-1} from 1000 to 1800 cm^{-1}, and 50 cm^{-1} from 1800 to 3600 cm^{-1}. The values in heavy type were calculated directly from the existing tables;[1] intermediate values were obtained by careful interpolation, using adjusted differences. The intervals in the internal and free energy tables are 50 cm^{-1} from 100 to 500 cm^{-1}, 100 cm^{-1} from 500 to 1800 cm^{-1}, and 200 cm^{-1} from 1800 to 3600 cm^{-1}. For each temperature, the second column contains the differences, and the third column contains the mean increments $\frac{1}{2}[\phi(\nu-10)-\phi(\nu+10)]$ in the function ϕ for $\Delta\nu=10$ cm^{-1} at each frequency. The specific heat tables are given in full since this is the best function for checking vibrational assignments and estimating barrier heights resisting internal torsions. The condensed tables for the internal and free energy functions, if properly used, should be accurate enough for most purposes. Calculation of the contributions from the twelve modes of tetrachloroethylene[2] gave results (for the totals) to within 0.0005 for C, and 0.001 for $(E^0-E_0{}^0)/T$ and $(F^0-F_0{}^0)/T$ of the values obtained using the tables in Taylor and Glasstone.[1] The relatively large contributions from the low frequencies is responsible for the lower accuracy in the internal and free energies.

Harmonic oscillator contributions, and hence contributions from anharmonic internal torsions, can thus now be rapidly evaluated, facilitating calculations for polyatomic molecules. It seemed unnecessary to simplify the calculation of barrier heights.[3,4]

TABLE I. Harmonic oscillator contributions to the specific heat in calories per degree per mole.

cm^{-1} \ °K	273.15	298.15	300	400	600	800	1000	1200	1500
100	**1.9415**	**1.9488**	**1.9493**	**1.9655**	**1.9772**	**1.9815**	**1.9834**	**1.9844**	**1.9853**
110	321	409	415	610	752	803	827	839	850
120	219	323	330	562	731	790	819	834	847
130	9109	229	238	510	708	776	810	828	843
140	8991	129	139	454	683	762	801	822	839
150	**1.8866**	**1.9022**	**1.9033**	**1.9393**	**1.9655**	**1.9747**	**1.9791**	**1.9815**	**1.9834**
160	733	8909	8921	328	625	731	780	808	829
170	592	789	803	260	594	714	769	800	824
180	445	663	678	188	562	696	757	791	819
190	291	531	548	112	528	676	744	782	813
200	**1.8130**	**1.8394**	**1.8412**	**1.9033**	**1.9493**	**1.9655**	**1.9731**	**1.9772**	**1.9807**
210	7962	251	271	8951	455	634	717	762	801
220	788	8103	8124	865	415	612	703	752	794
230	608	7948	7971	775	373	588	688	741	787
240	422	788	813	681	329	563	672	730	780

* This work has been carried out as part of the program of fundamental research undertaken by the British Rayon Research Association.

[1] E. B. Wilson, Jr., Chem. Rev. **27**, 17 (1940); with corrected constants: S. C. Schumann and M. L. Schwartz in the section by J. G. Aston, of Taylor and Glasstone's *Physical Chemistry*, (D. Van Nostrand Company, Inc., New York and London: MacMillan and Company, London, 1942) Vol. I, Atomistics and Thermodynamics.

[2] P. Torkington, Trans. Faraday Soc. **45**, 445 (1949).

[3] K. S. Pitzer, J. Chem. Phys. **5**, 469 (1937); K. S. Pitzer and W. D. Gwinn, J. Chem. Phys. **10**, 428 (1942).

[4] B. L. Crawford, Jr., J. Chem. Phys. **8**, 273 (1940).

TABLE I.—*Continued.*

°K / cm^{-1}	273.15	298.15	300	400	600	800	1000	1200	1500
250	**1.7232**	**1.7624**	**1.7651**	**1.8582**	**1.9284**	**1.9537**	**1.9655**	**1.9719**	**1.9772**
260	7036	455	483	481	237	511	638	707	764
270	6835	281	311	377	189	484	620	695	756
280	629	7133	7135	270	139	456	602	682	748
290	419	6922	6955	159	087	426	583	669	739
300	**1.6206**	**1.6735**	**1.6770**	**1.8047**	**1.9033**	**1.9394**	**1.9563**	**1.9655**	**1.9731**
310	5988	545	582	7931	8978	362	543	641	722
320	766	352	391	812	921	329	522	626	712
330	541	155	6196	691	862	296	500	611	702
340	313	5955	5998	567	802	262	477	595	692
350	**1.5083**	**1.5751**	**1.5796**	**1.7440**	**1.8742**	**1.9225**	**1.9454**	**1.9580**	**1.9682**
360	4851	546	592	311	679	188	430	564	671
370	617	338	386	179	615	151	406	547	660
380	381	5126	5176	7045	549	113	381	529	649
390	4144	4913	4965	6908	482	074	356	511	638
400	**1.3905**	**1.4700**	**1.4753**	**1.6770**	**1.8412**	**1.9033**	**1.9330**	**1.9493**	**1.9626**
410	665	485	540	630	341	8992	303	474	614
420	425	268	325	487	269	950	275	455	602
430	3182	4051	4109	343	196	907	246	435	589
440	2940	3831	3891	196	122	863	216	415	576
450	**1.2697**	**1.3610**	**1.3671**	**1.6047**	**1.8047**	**1.8818**	**1.9188**	**1.9394**	**1.9563**
460	455	388	451	5897	7970	772	158	373	550
470	2213	3167	231	745	892	726	128	352	536
480	1971	2945	3011	592	813	679	097	330	522
490	730	723	2790	437	733	631	065	308	508
500	**1.1490**	**1.2501**	**1.2569**	**1.5281**	**1.7651**	**1.8582**	**1.9033**	**1.9285**	**1.9493**
510	251	279	349	5123	568	532	9000	262	478
520	1014	2059	2130	4964	484	481	8967	238	463
530	0778	1839	1911	805	398	429	933	214	447
540	544	620	693	645	311	377	899	189	431
550	312	401	475	485	223	324	864	164	415
560	1.0082	1183	258	324	134	270	828	139	398
570	0.9854	0965	1041	4162	7044	215	792	113	381
580	628	748	0825	3999	6953	160	755	087	364
590	404	533	611	835	862	104	717	061	347
600	**0.9183**	**1.0320**	**1.0398**	**1.3671**	**1.6770**	**1.8047**	**1.8680**	**1.9033**	**1.9330**
610	8964	1.0108	1.0187	506	677	7989	642	9006	312
620	747	0.9897	0.9977	341	582	931	603	8978	294
630	533	689	769	176	486	872	564	950	276
640	321	584	564	3011	390	812	524	922	257
650	8112	280	361	2845	293	752	483	893	238
660	7907	9078	9160	679	195	691	442	864	219
670	705	8879	8961	514	6096	629	400	834	199
680	507	682	764	348	5997	566	358	804	179
690	312	487	570	183	897	503	315	773	159
700	**0.7119**	**0.8295**	**0.8378**	**1.2018**	**1.5796**	**1.7440**	**1.8272**	**1.8742**	**1.9139**
710	6929	8105	188	1854	695	376	228	711	118
720	742	7917	8000	690	593	311	184	680	097
730	559	732	7815	527	490	245	139	648	076
740	379	550	633	364	386	179	094	616	055
750	203	370	453	201	282	112	048	583	033
760	6031	193	275	1039	177	7045	8002	550	9011
770	5863	7018	7100	0877	5072	6978	7955	516	8989
780	699	6846	6928	716	4966	910	908	482	967
790	538	678	759	556	860	841	861	448	944

TABLE I.—*Continued.*

cm⁻¹ \ °K	273.15	298.15	300	400	600	800	1000	1200	1500
800	**0.5379**	**0.6511**	**0.6592**	**1.0398**	**1.4753**	**1.6770**	**1.7813**	**1.8413**	**1.8922**
810	224	347	428	240	646	700	765	378	899
820	5072	187	267	1.0083	539	629	716	343	876
830	4923	6029	6109	0.9926	431	558	667	307	852
840	778	5874	5953	770	323	487	618	271	828
850	636	721	800	615	215	415	568	235	804
860	497	572	650	461	4107	343	518	198	780
870	361	426	503	308	3998	270	467	161	755
880	229	283	359	157	889	196	416	123	730
890	4100	142	218	9008	780	122	364	085	705
900	**0.3974**	**0.5004**	**0.5080**	**0.8860**	**1.3671**	**1.6047**	**1.7312**	**1.8047**	**1.8680**
910	851	4869	4944	713	562	5972	260	8009	654
920	731	736	811	567	452	897	207	7970	628
930	614	607	681	423	342	821	154	931	602
940	500	480	553	280	232	745	100	892	576
950	389	355	428	8139	122	669	7046	852	549
960	281	234	306	7999	3012	592	6992	812	522
970	176	4114	186	861	2902	515	937	772	495
980	3073	3998	4069	724	791	437	882	732	468
990	2972	885	3955	588	680	359	827	691	441
1000	**0.2874**	**0.3774**	**0.3843**	**0.7453**	**1.2569**	**1.5281**	**1.6770**	**1.7651**	**1.8413**
1020	689	560	627	7189	348	5125	658	568	357
1040	514	356	421	6930	2127	4968	544	484	300
1060	349	3162	225	676	1908	810	429	399	242
1080	194	2977	3038	429	689	650	313	312	184
1100	**0.2047**	**0.2801**	**0.2860**	**0.6188**	**1.1471**	**1.4488**	**1.6196**	**1.7224**	**1.8125**
1120	1908	633	691	5954	254	326	6078	135	064
1140	777	476	531	726	1038	4163	5958	7045	8002
1160	655	326	379	504	0823	3999	837	6955	7940
1180	541	184	235	289	610	835	715	863	877
1200	**0.1434**	**0.2050**	**0.2099**	**0.5080**	**1.0398**	**1.3671**	**1.5592**	**1.6770**	**1.7813**
1220	333	1922	1969	4877	1.0188	507	468	676	748
1240	239	802	847	680	0.9980	342	344	581	683
1260	152	688	732	489	773	177	219	486	617
1280	1071	582	624	305	568	3011	5093	390	550
1300	**0.0993**	**0.1482**	**0.1522**	**0.4127**	**0.9365**	**1.2845**	**1.4966**	**1.6293**	**1.7483**
1320	921	387	425	3955	9163	679	839	195	415
1340	854	296	333	789	8964	513	711	6097	346
1360	792	212	247	628	767	348	583	5998	277
1380	734	133	167	473	571	183	454	898	207
1400	**0.0679**	**0.1059**	**0.1091**	**0.3323**	**0.8378**	**1.2018**	**1.4324**	**1.5797**	**1.7136**
1420	628	0990	1020	178	8187	1854	194	696	7064
1440	581	924	0953	3039	7999	690	4064	593	6991
1460	537	862	890	2905	814	526	3933	490	918
1480	496	805	831	776	632	363	802	386	844
1500	**0.0458**	**0.0750**	**0.0775**	**0.2651**	**0.7453**	**1.1200**	**1.3671**	**1.5281**	**1.6770**
1520	423	699	722	531	276	1038	540	177	695
1540	391	651	673	416	7101	0877	408	5072	620
1560	362	606	627	306	6928	717	276	4966	544
1580	335	564	584	200	758	557	143	860	468
1600	**0.0310**	**0.0525**	**0.0544**	**0.2099**	**0.6592**	**1.0398**	**1.3010**	**1.4753**	**1.6391**
1620	286	489	507	2002	429	240	2877	646	313
1640	264	455	472	1909	268	1.0083	745	539	235
1660	244	423	439	820	6110	0.9927	613	432	156
1680	235	394	409	734	5955	772	481	324	6077

TABLE I.—*Continued.*

cm^{-1} \ °K	273.15	298.15	300	400	600	800	1000	1200	1500
1700	**0.0207**	**0.0367**	**0.0381**	**0.1652**	**0.5802**	**0.9618**	**1.2349**	**1.4216**	**1.5997**
1720	190	342	355	572	652	465	217	108	917
1740	175	317	330	495	505	313	2085	4000	836
1760	161	295	307	422	360	161	1953	3891	755
1780	148	274	285	353	219	9010	821	781	674
1800	**0.0136**	**0.0254**	**0.0265**	**0.1286**	**0.5080**	**0.8860**	**1.1690**	**1.3671**	**1.5592**
1850	111	208	218	135	4747	496	1363	396	386
1900	091	173	181	1001	430	8140	1038	3120	5177
1950	074	144	151	0882	4128	7792	0716	2845	4966
2000	**0.00585**	**0.0119**	**0.0125**	**0.0775**	**0.3843**	**0.7453**	**1.0398**	**1.2569**	**1.4753**
2050	472	098	103	678	576	7123	1.0084	294	540
2100	381	081	085	594	323	6802	0.9773	2020	324
2150	308	067	070	520	3084	490	465	1746	4107
2200	**0.00248**	**0.00550**	**0.00578**	**0.0454**	**0.2860**	**0.6188**	**0.9161**	**1.1472**	**1.3890**
2250	199	449	474	397	649	5895	8860	1200	670
2300	159	370	392	347	452	613	570	0930	450
2350	128	305	323	304	269	342	282	664	230
2400	**0.00103**	**0.00250**	**0.00265**	**0.0265**	**0.2099**	**0.5080**	**0.8000**	**1.0398**	**1.3010**
2450	082	203	216	231	1940	4826	7723	1.0134	2790
2500	066	167	178	201	789	583	453	0.9876	570
2550	053	136	145	174	647	350	187	619	351
2600	**0.00042**	**0.00111**	**0.00118**	**0.0151**	**0.1519**	**0.4127**	**0.6928**	**0.9365**	**1.2130**
2650	034	090	096	130	400	3911	675	9112	1910
2700	027	074	079	113	289	706	429	8864	690
2750	021	061	065	098	186	510	6189	619	471
2800	**0.00017**	**0.00049**	**0.00053**	**0.00852**	**0.1091**	**0.3323**	**0.5953**	**0.8378**	**1.1255**
2850		40	43	736	1003	3141	726	8141	1039
2900		32	35	635	0920	2970	506	7907	0823
2950		26	28	550	844	807	291	678	610
3000		**0.00021**	**0.00023**	**0.00474**	**0.0775**	**0.2651**	**0.5080**	**0.7453**	**1.0398**
3050				410	710	504	4878	233	1.0188
3100				354	651	362	682	7015	0.9980
3150				306	596	227	489	6801	773
3200				**0.00265**	**0.0544**	**0.2099**	**0.4305**	**0.6593**	**0.9568**
3250				227	497	1982	4128	389	363
3300				196	454	869	3956	6189	9161
3350				169	416	758	789	5994	8960
3400				**0.00145**	**0.0381**	**0.1652**	**0.3627**	**0.5802**	**0.8761**
3450				125	348	553	471	614	667
3500				107	318	459	320	431	578
3550				092	290	370	176	253	489
3600				**0.00079**	**0.0265**	**0.1286**	**0.3038**	**0.5080**	**0.8000**

TABLE II. Harmonic oscillator contributions to the internal energy function, $(E^0-E_0^0)/T$, (in calories per degree per mole).

cm^{-1} \ °K	273.15			298.15			300			400			600			800			1000			1200			1500		
100	1.510		43	1.546			1.549		40	1.651		32	1.758		22	1.814		17	1.847		14	1.870		11	1.892		9.1
		205			192			191			152			107			83			67			56			45	
150	1.304		39	1.354			1.357		36	1.499		29	1.651		21	1.731		16	1.780		13	1.814		11	1.847		9.0
		183			174			173			142			102			80			65			55			45	
200	1.121		35	1.180			1.184		33	1.357		27	1.549		20	1.651		16	1.715		13	1.758		11	1.802		8.9
		163			156			156			131			98			76			64			54			44	
250	0.958		31	1.024			1.029		30	1.226		25	1.451		19	1.575		15	1.651		13	1.704		11	1.758		8.8
		143			139			139			122			93			76			62			53			43	
300	0.815		27	0.885			0.889		27	1.104		23	1.357		18	1.499		15	1.589		12	1.651		10	1.715		8.6
		126			124			123			112			89			72			60			52			43	
350	0.689		23	0.761			0.766		23	0.992		21	1.269		17	1.427		14	1.529		12	1.599		10	1.672		8.4
		109			110			110			103			84			70			59			51			42	
400	0.580		21	0.651			0.656		21	0.889		20	1.184		16	1.357		14	1.470		12	1.548		10	1.630		8.3
		94			95			96			94			80			67			57			50			41	
450	0.486		17	0.556			0.560		18	0.795		18	1.104		16	1.290		13	1.413		11	1.499		9.8	1.589		8.1
		81			84			83			86			76			65			56			48			40	
500	0.405		15	0.472			0.477		16	0.709		16	1.029		15	1.226		13	1.357		11	1.451		9.6	1.549		8.0
		127			135			136			149			140			122			106			94			79	
600	0.278		10	0.337			0.341		12	0.560		14	0.889		13	1.104		12	1.251		10	1.357		9.1	1.470		7.7
		90			99			100			121			124			112			100			89			76	
700	0.188		7.4	0.238			0.241		8.5	0.439		11	0.766		12	0.992		11	1.152		9.7	1.268		8.6	1.394		7.5
		62			73			73			98			109			103			94			84			73	
800	0.126		5.1	0.165			0.168		6.0	0.341		8.7	0.656		10	0.889		9.7	1.058		9.1	1.184		8.2	1.321		7.2
		43			51			52			78			96			94			87			80			70	
900	0.0829		34	0.114			0.116		4.3	0.263		6.8	0.560		9.2	0.795		8.9	0.971		8.5	1.104		7.8	1.251		6.8
		287			36			36			61			83			86			82			76			67	
1000	0.0542		23	0.0776			0.0796		30	0.202		5.4	0.477		7.8	0.709		8.2	0.889		7.8	1.028		7.3	1.184		6.6
		190			251			256			48			73			78			76			72			64	
1100	0.0352		16	0.0525			0.0540		21	0.154		4.4	0.404		6.8	0.631		7.4	0.813		7.3	0.957		6.8	1.120		6.3
		126			172			176			37			63			71			71			68			62	
1200	0.0226		9	0.0353			0.0364		15	0.116		3.2	0.341		5.8	0.560		6.8	0.743		6.8	0.889		6.5	1.058		6.0
		81			118			120			28			54			64			66			64			59	
1300	0.0145		7	0.0235			0.0244		10	0.0875		25	0.287		4.9	0.496		6.0	0.677		6.3	0.826		6.2	0.999		5.7
		53			78			82			219			46			57			61			60			56	
1400	0.00916		42	0.0157			0.0162		6	0.0656		19	0.241		4.2	0.439		5.4	0.616		5.8	0.766		5.8	0.943		5.4
		337			53			55			167			39			51			56			56			54	
1500	0.00579		26	0.0104			0.0107		4	0.0489		14	0.202		3.6	0.387		4.8	0.560		5.4	0.709		5.5	0.889		5.2
		214			36			36			125			33			46			52			53			51	
1600	0.00365		17	0.00680			0.00711		30	0.0364		11	0.168		3.2	0.341		4.3	0.509		4.9	0.656		5.1	0.838		5.0
		137			234			244			94			28			41			48			50			49	
1700	0.00228		10	0.00446			0.00467		20	0.0270		9	0.140		2.5	0.300		3.9	0.461		4.5	0.607		4.7	0.789		4.7
		85			155			162			70			24			37			44			46			46	
1800	0.00143		6	0.00291			0.00305		13	0.0200		6	0.116		2.1	0.263		3.4	0.418		4.2	0.560		4.5	0.743		4.5

TABLE II.—*Continued.*

cm⁻¹ \ °K	273.15	298.15	300	400	600	800	1000	1200	1500
	88	127	174	93	37	61	77	83	87
2000	0.000553 25	0.00124	0.00131 55	0.0107 35	0.0795 15	0.202 2.7	0.341 3.5	0.477 3.9	0.656 4.1
	340	72	76	50	255	48	64	73	78
2200	0.000213 10	0.000517	0.000548 23	0.00575 18	0.0540 10	0.154 2.1	0.277 2.9	0.404 3.5	0.579 3.7
	132	302	319	270	176	37	53	63	70
2400	0.000081 3.9	0.000215	0.000229 10	0.00305 10	0.0364 7	0.116 1.6	0.225 2.4	0.341 2.9	0.509 3.3
	51	126	134	144	120	29	44	54	62
2600	0.000030 1.4	0.000089	0.000095 4.3	0.00161 5	0.0244 5	0.0875 12	0.181 1.9	0.287 2.5	0.446 2.9
	18	53	56	77	81	219	36	46	56
2800	0.000012	0.000036	0.000039 1.7	0.000845 27	0.0163 4	0.0656 9	0.145 1.6	0.241 2.1	0.391 2.6
		21	23	404	56	167	29	39	49
3000		0.000015	0.000016 0.8	0.000441 14	0.0107 3	0.0489 7	0.116 1.3	0.202 1.8	0.341 2.4
				212	36	125	23	34	44
3200				0.000229 7.6	0.00711 17	0.0364 5	0.0927 10	0.168 1.6	0.297 2.1
				110	244	95	191	28	38
3400				0.000119 3.9	0.00467 10	0.0269 4	0.0736 8	0.140 1.3	0.259 1.8
				58	162	69	152	24	34
3600				0.000061 2.0	0.00305 6	0.0200 3	0.0584 7	0.116 1.1	0.225 1.6

TABLE III. Harmonic oscillator contributions to the free energy function, $-(F^0-E_0^0)/T$, (in calories per degree per mole).

cm⁻¹ \ °K	273.15	298.15	300	400	600	800	1000	1200	1500
100	1.775 152	1.908	1.918 155	2.379 165	3.071 177	3.584 180	3.994 181	4.334 183	4.754 185
	573	590	591	641	692	719	737	749	760
150	1.202 87	1.318	1.327 91	1.738 100	2.379 108	2.865 116	3.257 119	3.585 122	3.994 124
	350	365	367	411	461	486	503	514	527
200	0.852 56	0.953	0.960 59	1.327 67	1.918 78	2.379 83	2.754 86	3.071 88	3.467 90
	232	246	247	289	335	361	375	386	396
250	0.620 38	0.707	0.713 41	1.038 49	1.583 58	2.018 63	2.379 66	2.685 68	3.071 71
	162	174	175	212	256	280	296	306	317
300	0.458 27	0.533	0.538 30	0.826 37	1.327 45	1.738 50	2.083 53	2.379 56	2.754 57
	116	127	127	164	203	225	240	251	259
350	0.342 19	0.406	0.411 22	0.662 28	1.124 36	1.513 45	1.843 44	2.128 45	2.495 47
	84	94	95	124	164	186	200	210	222
400	0.258 15	0.312	0.316 16	0.538 22	0.960 30	1.327 36	1.643 37	1.918 38	2.273 41
	63	71	72	99	134	156	170	180	190
450	0.195 11	0.241	0.244 12	0.439 18	0.826 25	1.171 30	1.473 31	1.738 33	2.083 35
	47	55	55	79	113	133	146	155	165

TABLE III.—*Continued.*

cm^{-1} \ °K	273.15	298.15	300	400	600	800	1000	1200	1500
500	0.148	0.186	0.189	0.360	0.713	1.038	1.327	1.583	1.918
	8.1	73	9.6	14	20	25	27	29	31
	62		74	116	175	212	238	256	275
600	0.0861	0.113	0.115	0.244	0.538	0.826	1.089	1.327	1.643
	46	44	5.8	9.3	15	18	21	22	24
	357		45	77	127	162	186	202	221
700	0.0504	0.0960	0.0702	0.167	0.411	0.664	0.903	1.124	1.422
	27	267	34	6.2	11	14	16	18	20
	208		268	52	95	126	147	164	181
800	0.0296	0.0423	0.0434	0.115	0.316	0.538	0.756	0.960	1.241
	16	163	21	4.3	8.2	11	13	15	16
	122		167	35	72	99	120	134	152
900	0.0174	0.0260	0.0267	0.0797	0.244	0.439	0.636	0.826	1.089
	9.3	100	13	29	6.3	8.8	11	12	14
	71		102	244	54	79	98	113	129
1000	0.0103	0.0160	0.0165	0.0553	0.190	0.360	0.538	0.713	0.960
	5.4	61	8.0	20	4.7	7.1	8.8	10	12
	42		63	169	42	64	81	94	109
1100	0.00605	0.00987	0.0102	0.0384	0.148	0.296	0.457	0.619	0.851
	31	377	5.0	14	3.6	5.7	7.4	8.7	10
	249		39	117	33	52	68	81	95
1200	0.00356	0.00610	0.00631	0.0267	0.115	0.244	0.389	0.538	0.756
	20	235	3.0	9.8	2.6	4.7	6.2	7.4	8.7
	145		242	81	25	42	56	68	82
1300	0.00211	0.00375	0.00389	0.0186	0.0900	0.202	0.333	0.470	0.674
	11	143	19	7.0	22	3.8	5.2	6.3	7.7
	87		148	56	195	35	48	59	72
1400	0.00124	0.00232	0.00241	0.0130	0.0705	0.167	0.285	0.411	0.602
	6.5	89	11	4.7	17	3.1	4.4	5.4	6.7
	51		91	40	152	28	41	51	64
1500	0.000732	0.00143	0.00150	0.00904	0.0553	0.139	0.244	0.360	0.538
	37	55	7.5	32	13	2.6	3.7	4.7	5.9
	301		58	273	119	24	34	44	55
1600	0.000431	0.000878	0.000920	0.00631	0.0434	0.115	0.210	0.316	0.483
	22	335	44	23	10	2.2	3.2	4.1	5.2
	174		348	192	93	19	31	38	50
1700	0.000257	0.000543	0.000572	0.00439	0.0341	0.0957	0.180	0.278	0.433
	13	208	27	16	9.0	18	2.7	3.5	4.7
	105		219	133	74	160	25	34	44
1800	0.000152	0.000335	0.000353	0.00306	0.0267	0.0797	0.155	0.244	0.389
	8	205	16	11	5.7	15	2.3	3.1	4.2
	97		116	156	102	244	40	54	73
2000	0.000055	0.000130	0.000137	0.00150	0.0165	0.0553	0.115	0.190	0.316
	2.7	79	7	5	4.1	10	1.7	2.4	3.3
	36		83	77	63	169	29	42	59
2200	0.000019	0.000051	0.000054	0.000727	0.0102	0.0384	0.0858	0.148	0.257
	1.0	31	2.6	26	2.4	7.0	13	1.9	2.6
	11		33	374	39	117	218	33	47
2400	0.000007	0.000020	0.000021	0.000353	0.00631	0.0267	0.0640	0.115	0.210
	0.4	12	1.0	13	15	4.8	9.3	1.4	2.1
	5		13	180	242	81	162	25	38
2600	0.000002	0.000008	0.000008	0.000173	0.00389	0.0186	0.0478	0.0900	0.172
	0.1	5	0.4	6	8	3.3	7.0	11	1.7
			5	86	148	56	121	195	32
2800		0.000003	0.000003	0.000087	0.00241	0.0130	0.0357	0.0705	0.140
		2	0.2	3	6	2.4	5.2	8.6	1.4
			2	44	91	40	90	152	25
3000		0.000001	0.000001	0.000043	0.00150	0.00904	0.0267	0.0553	0.115
			0.1	1.5	5	16	3.9	6.8	1.1
				22	58	273	67	119	20
3200				0.000021	0.000918	0.00631	0.0200	0.0434	0.0945
				0.7	23	12	2.9	5.3	9.2
				11	346	192	50	94	168
3400				0.000010	0.000572	0.00439	0.0150	0.0340	0.0777
				0.5	14	8	2.2	4.1	7.6
				5	219	133	38	73	137
3600				0.000005	0.000353	0.00306	0.0112	0.0267	0.0640
				0.2	8	5	1.6	3.2	6.2

Transport Properties of Dense Media. I. Thermal Diffusion in Isotopic Mixtures of Gases

W. L. Robb and H. G. Drickamer
University of Illinois, Urbana, Illinois
(Received June 19, 1950)

Based on Meixner's thermodynamics for irreversible processes, and the work of Haase, an equation for the thermal diffusion ratio α, which can be evaluated from the equation of state, is presented.

Using van der Waals' equation, α's are calculated in the critical region and compared with data for ethane-xenon. The equation reproduces all the essential features of the experimental results.

Calculations made for a mixture of isotopes indicate that the effect of pressure on α cannot be attributed to selective clustering.

Nomenclature

A, B, C = phenomenological coefficients
a, b = van der Waals' constants
$c_i = \rho_i/M_i$
D = diffusion coefficient
f = fugacity
$\bar{H}_i$ = partial molar enthalpy of component i
$\bar{H}_i^*$ = partial molar enthalpy of comp. i in standard state
$\mathbf{J}_i$ = flux of component i
$\mathbf{J}_u$ = flux of heat
M_i = molecular weight of component i
$\bar{M}$ = mean molecular weight
p = pressure
R = gas constant
T = temperature
T_r = reduced temperature T/T_c
T_c = critical temperature
$\bar{V}_i$ = partial molar volume of i
$\bar{V}$ = mean molar volume
x_i = mole fraction of component i
α = thermal diffusion ratio
λ = thermal conductivity
μ_i = chemical potential of component i
ρ_i = mass per unit volume of component i
ρ = mean density of system
ρ_r = reduced density $= \rho/\rho_c$
ρ_c = critical density

THE thermodynamics of irreversible processes as developed by Meixner[1-3] and de Groot[4] permits the prediction of relationships which must exist among the transport coefficients of a nonuniform mixture. Haase[5] has extended this to the actual calculation of transport properties. The method has the disadvantage of not giving absolute values, but it is possible to predict the changes with pressure and temperature in dense gases, and even in liquids, where the kinetic theory is not yet applicable. It is the purpose of this paper to compare calculated and experimental thermal diffusion coefficients in the critical region.

Let us consider a binary mixture with a temperature and concentration gradient, omitting, for the time being, any gradient in the pressure or in an externally applied force. Then, following Haase, the flux of component one can be written

$$\mathbf{J}_1=\frac{\bar{M}}{M_1M_2}\left\{AT\left[\operatorname{grad}\frac{\mu_2'}{T}-\operatorname{grad}\frac{\mu_1'}{T}\right]-\frac{B}{T}\operatorname{grad}T\right\}. \quad (1)$$

Now define

$$\mu_1'=\frac{\mu_1}{M_1}. \quad (2)$$

From thermodynamics

$$T\left[\operatorname{grad}\frac{\mu_1}{T}\right]_p=\frac{\partial\mu_1}{\partial x_1}\operatorname{grad}x_1-\frac{\bar{H}_1}{T}\operatorname{grad}T, \quad (3)$$

$$x_1\frac{\partial\mu_1}{\partial x_1}+x_2\frac{\partial\mu_2}{\partial x_2}=0. \quad (4)$$

Then the flux equations can be written

$$\mathbf{J}_1=-\mathbf{J}_2=-\frac{A(c_1+c_2)\bar{M}^3}{x_2M_1^2M_2^2\rho}\frac{\partial\mu_1}{\partial x_1}\left\{\operatorname{grad}x_1-x_1x_2\left[\frac{\left(\frac{\bar{H}_1}{m_1}-\frac{\bar{H}_2}{m_2}\right)AM_1M_2-BM_1M_2}{A\bar{M}x_1\frac{\partial\mu_1}{\partial x_1}}\right]\frac{1}{T}\operatorname{grad}T.\right\} \quad (5)$$

Comparing this with the flux equation in kinetic theory terms

$$\mathbf{J}_1=(c_1+c_2)\left[-D\left(\operatorname{grad}x_1-\alpha x_1x_2\frac{1}{T}\operatorname{grad}T\right)\right], \quad (6)$$

$$D=\frac{A\bar{M}^3}{x_1x_2M_1^2M_2^2}x_1\frac{\partial\mu_1}{\partial x_1}, \quad (7)$$

$$\alpha=\frac{A(\bar{H}_1M_2-\bar{H}_2M_1)-BM_1M_2}{A\bar{M}x_1\frac{\partial\mu_1}{\partial x_1}}. \quad (8)$$

[1] J. Meixner, Ann. d. Phys. (5) **39**, 333 (1941).
[2] J. Meixner, Ann. d. Phys. (5) **43**, 244 (1943).
[3] J. Meixner, Zeits. f. Physik Chemie **B53**, 235 (1943).
[4] S. R. de Groot, Thesis, Amsterdam 1945.
[5] R. Haase, Zeits. f. Physik **127**, 1 (1949).

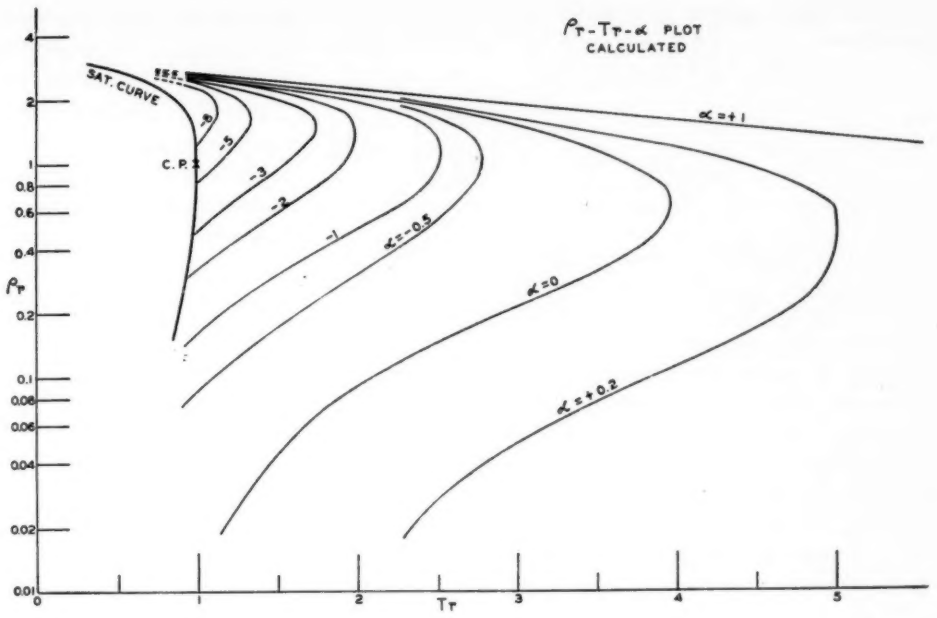

FIG. 1. Calculated plot of T_r *versus* ρ_r for constant α.

From known thermodynamic relationships[6]

$$x_1\frac{\partial\mu_1}{\partial x_1}=RT\left[1+x_1x_2\frac{\partial^2\ln f}{\partial x_1^2}\right] \tag{9}$$

$$\bar{H}_1=\bar{H}_1^*-RT^2\left[\frac{\partial\ln f}{\partial T}+x_2\frac{\partial}{\partial T}\frac{\partial\ln f}{\partial x_1}\right]. \tag{10}$$

For perfect gases we can write

$$\alpha_0=\frac{\bar{H}_1^*M_2-\bar{H}_2^*M_1}{\bar{M}RT}-\left(\frac{B}{A}\right)_0\frac{M_1M_2}{RT}. \tag{11}$$

α_0, the thermal diffusion ratio for an ideal gas, is calculable from the kinetic theory using the Lennard-Jones model and Enskog's equations. If we now assume that the ratio B/A is independent of the state of the system (it can be shown from diffusion data that A varies as much between different ideal gas mixtures as it does between gas and liquid), the value of α can be calculated for any system for which the equation of state is known.

Haase[5] has made the calculation for gas describable in terms of the second virial coefficient, and has shown that α is pressure dependent, but his equations fail to reproduce the phenomena found[7,8] in the critical region.

If we consider now a van der Waals' gas the fugacity is

$$\ln f=\ln RT+\frac{b}{\bar{V}-b}-\ln(\bar{V}-b)-\frac{2a}{RT\bar{V}}. \tag{12}$$

In a gas mixture we can set

$$\bar{V}=x_1\bar{V}_1+x_2\bar{V}_2, \tag{13a}$$

$$b=b_1x_1+b_2x_2, \tag{13b}$$

$$a=a_{11}x_1^2+2a_{12}x_1x_2+a_{22}x_2^2, \tag{13c}$$

$$a_{12}=(a_1a_2)^{\frac{1}{2}}.$$

For the first approximation let us consider a mixture of isotopes. This simplifies the results as a, b, and $\bar{V}$ are independent of x.

Then

$$x_1\frac{\partial\mu_1}{\partial x_1}=RT, \tag{14}$$

$$\bar{H}_1=\bar{H}_2=H^*-\left[\left(\frac{2a}{\bar{V}^2}-\frac{RT\bar{V}}{(\bar{V}-b)^2}\right)\times\left\{\frac{RT}{p-\frac{a}{V^2}+\frac{2ab}{V^3}}\right\}+RT+\frac{2a}{\bar{V}}\right], \tag{15}$$

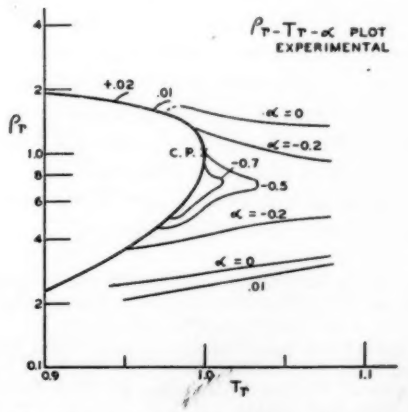

FIG. 2. Plot of experimental T_r *versus* ρ_r for constant α.

[6] F. T. Wall and G. Stent, J. Chem. Phys. **17**, 1112 (1949).
[7] Pierce, Duffield, and Drickamer, J. Chem. Phys. **18**, 950 (1950).
[8] Giller, Duffield, and Drickamer, J. Chem. Phys. **18**, 1027 (1950).

$$\alpha=\alpha_0-\frac{(M_2-M_1)}{\bar{M}}\left[\left(\frac{2a}{\bar{V}^2}-\frac{RT\bar{V}}{(\bar{V}-b)^2}\right)\times\left[\frac{1}{p-\frac{a}{\bar{V}^2}+\frac{2ab}{\bar{V}^3}}\right]+1+\frac{2a}{RT\bar{V}}\right]. \quad (16)$$

Now the experimental data in the critical region are for the system ethane-xenon. The van der Waals' constants for these gases do not differ greatly. To the first approximation we can consider these as a mixture of isotopes of molecular weights 133 and 30, using α_0 evaluated from kinetic theory.

Figure 1 is a plot of T_r *versus* ρ_r with lines of constant α. Figure 2 shows the results of experiment. It can be seen that the calculated curves reproduce all the essential features of the experiment. While the agreement is entirely qualitative nevertheless it seems very remarkable that the double sign change in α with increasing density could be predicted using no empirical constants.

It is of particular interest to note that this calculation has been made for a mixture of isotopes. In the original papers[7,8] the phenomenon was attributed to a selective clustering of the ethane molecules. No such selective clustering would be conceivable among isotopes, so that this seems rather to be a phenomenon of molecular interaction explainable directly from kinetic theory. It is hoped that the consideration of ternary collisions now being undertaken by Kirkwood and Hirschfelder will permit the prediction of the pressure coefficient of thermal diffusion.

It is planned to treat thermal diffusion in nonisotopic mixtures, diffusion and thermal conductivity in dense gases, and transport properties of van der Waals' liquids in later papers.

THE JOURNAL OF CHEMICAL PHYSICS VOLUME 18, NUMBER 10 OCTOBER, 1950

The Infra-Red Spectrum of Acetylene*

E. E. Bell and H. H. Nielsen
Ohio State University, Columbus, Ohio

(Received June 29, 1950)

New measurements of the infra-red absorption spectrum of acetylene between 16 and 2.5μ have established many new bands. A cooling experiment has demonstrated that the central line of the parallel band $\nu_4^1+\nu_5^1$ (1328.18 cm^{-1}) belongs to a difference band, $2\nu_4^0+\nu_5^1-\nu_4^1$ (1328.46 cm^{-1}). Resolution sufficient to distinguish the center of the fundamental ν_3 (3282.5 cm^{-1}) from the combination band $\nu_2+\nu_4^1+\nu_5^1$ (3295.56 cm^{-1}) has been obtained. An interesting $\Pi_u-\Pi_g$-band, identified as $\nu_1+\nu_5^1-\nu_4^1$, is shown. Frequencies of the infra-red inactive fundamentals are derived and many anharmonic coefficients are evaluated. Diagrams of the absorption regions and tables of the line frequencies are included.

ACETYLENE is known to be a linear, symmetrical molecule. Because of its simplicity and small moment of inertia, a large amount of experimental and theoretical work has been done with respect to its infra-red absorption spectrum. Expressions for the vibration-rotational energy levels have been obtained through second-order contributions by Shaffer and Nielsen.[1] Assignments of bands and numerical evaluations of the anharmonicity constants have been made by many workers.[2] Experimentally, the photographic infra-red bands have been well measured, and the Raman spectrum of the liquid has been obtained. The bolometric infra-red bands of acetylene have been measured with high dispersion by Levin and Meyer.[3]

This early work of Levin and Meyer left several questions unanswered. A parallel-type band, $\nu_4^1+\nu_5^1$, seemed to have an absorption line at the center, suggestive of a Q branch.[4] This line was also observed later by Nielsen and Williams.[5] The work of Levin and Meyer did not allow an accurate determination of the center of the ν_3-fundamental band because of the interference of an overlapping band.

A more extensive measurement of this region of the

* A part of the material of this paper was presented at the Symposium on Molecular Structure and Spectroscopy at Ohio State University, in Columbus, Ohio (June, 1947).

[1] W. H. Shaffer and A. H. Nielsen, J. Chem. Phys. **9**, 847 (1941).

[2] Note the many references given by G. Herzberg, *Infrared and Raman Spectra of Polyatomic Molecules* (D. Van Nostrand Company, Inc., New York, 1945).

[3] Levin and Meyer, J. Opt. Soc. Am. **16**, 137 (1928).

[4] In agreement with G. Herzberg (see reference 2) the vibrational frequencies will be designated as follows:
ν_1, species Σ_g^+, about 3373 cm^{-1}, parallel vibration in which the C atoms are approaching while the H atoms are separating.
ν_2, species Σ_g^+, about 1974 cm^{-1}, parallel vibration in which the CH groups vibrate against each other.
ν_3, species Σ_u^+, about 3282 cm^{-1}, parallel vibration in which the C atoms are moving together against the H atoms.
ν_4, species Π_g, about 613 cm^{-1}, perpendicular vibration in which the C atoms move opposing each other and H atoms move against each other.
ν_5, species Π_u, about 731 cm^{-1}, perpendicular vibration in which the C atoms move together against the H atoms.

[5] A. H. Nielsen and D. Williams, Phys. Rev. **59**, 911A (1941).

infra-red spectrum of acetylene has now been made and the results will be given in this paper.

The notation used to designate the anharmonic coefficients is that used by Shaffer and Nielsen. The vibrational energy of acetylene is given by

$$G_V=G_0+\sum_{n=1}^{5}\omega_n(V_n+g_n/2)+\sum_{n=1}^{5}x_{nn}(V_n+g_n/2)^2+\sum_{n=1}^{5}\sum_{n'>n=1}^{5}x_{nn'}(V_n+g_n/2)(V_{n'}+g_{n'}/2)+\sum_{k=4}^{5}X_{kk}(l_k^2-1),$$

where V_n is the vibrational quantum number associated with the normal frequency ω_n, and g_n is the degree of degeneracy of the mode ω_n. $g_1=g_2=g_3=1$ and $g_4=g_5=2$. l_k is the quantum number associated with the internal angular momentum arising from the twofold degenerate vibrations and may assume the values $\pm V_k, \pm(V_k-2), \cdots\pm1$ or 0. The values of $G_0, x_{nn}, x_{nn'}$, and X_{kk} are given in terms of the generalized force constants in the paper by Shaffer and Nielsen.

The rotational energy of acetylene is

$$F_R=B_V[J(J+1)-l^2], \quad l=l_4+l_5$$

where J is the quantum number associated with the total angular momentum and may have integral values such that $J\geqslant|l_4+l_5|$ and the centrifugal stretching term is omitted because it was not of significance in this molecule. It is to be noted that the band frequencies are $G_V'-G_V''$ and these do not correspond to the positions of the Q branches (or band centers, where $\Delta J=0$) unless $\Delta l=0$.

EXPERIMENTAL

The absorption bands were measured with an automatic recording vacuum grating instrument.[6] The gratings were calibrated by measuring several orders of two strong mercury arc emission lines near 1μ. The measured wave-lengths of the absorption lines in this paper are the wave-lengths in vacuum obtained directly without correction, by making all band measurements with the spectrograph evacuated. The records of the bands were obtained on a Speedomax recorder and were marked at every 10 min. of arc of the grating position (sometimes every 5 min.). The frequency, in cm^{-1}, at these calibration points was computed. The frequencies of the lines were obtained by interpolation between the calibration points. Repeated measurements extending over several months time indicated that the measurements were consistent within one-tenth cm^{-1} for the lines tested. Measurements to one-hundredth of a wave number were used with the combination principles to obtain band centers, etc., and some frequencies will be given to this accuracy, even though all frequencies are of questionable absolute accuracy even in the fifth significant figure.

The acetylene used in these measurements was made by the action of water on calcium carbide. No special precautions were made to assure the purity of the acetylene used. The gas was passed through drying towers filled with calcium chloride before it was admitted to the absorption cell. The absorption cells each contained a small boat of anhydrous phosphorus pentoxide to remove the last traces of water vapor. By preevacuation

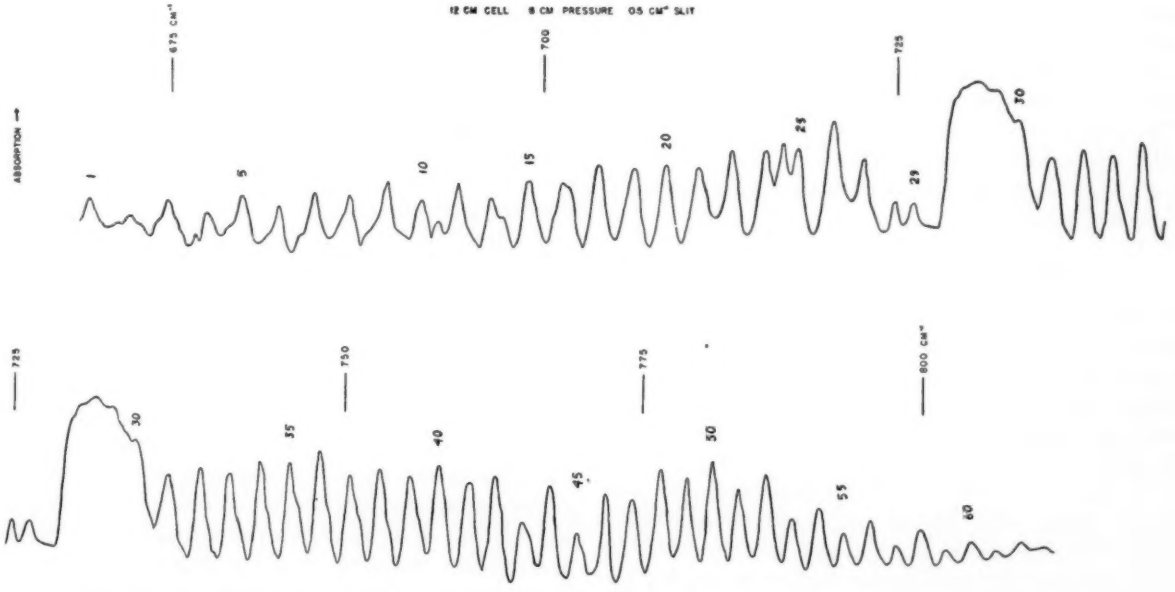

FIG. 1. The ν_5^1-band of acetylene as measured with the 1800 lines per inch grating. For the values of the line frequencies see Table I.

[6] Bell, Noble, and Nielsen, Rev. Sci. Inst. **18**, 48 (1947).

TABLE I. The ν_5^1-band frequencies, see Fig. 1.

Line No.	ν_5^1	cm^{-1}	Line No.	ν_5^1	cm^{-1}
1	P (25)	670.67	31	R (2)	736.98
2	P (24)	673.02	32	R (3)	738.97
3	P (23)	675.34	33	R (4)	741.27
4	P (22)	677.83	34	R (5)	743.58
5	P (21)	680.02	35	R (6)	746.01
6	P (20)	682.39	36	R (7)	748.36
7	P (19)	684.75	37	R (8)	750.81
8	P (18)	687.07	38	R (9)	753.33
9	P (17)	689.54	39	R (10)	755.53
10	P (16)	691.66	40	R (11)	757.96
11		692.81	41	R (12)	760.40
12	P (15)	694.19	42	R (13)	762.70
13	P (14)	696.46	43	R (14)	764.93
14		697.20	44	R (15)	767.23
15	P (13)	698.88	45	R (16)	769.45
16	P (12)	701.26	46	R (17)	771.84
17		701.58	47	R (18)	774.14
18	P (11)	703.68	48	R (19)	776.53
19	P (10)	706.00	49	R (20)	778.88
20	P (9)	708.34	50	R (21)	781.20
21	P (8)	710.47	51	R (22)	783.50
22	P (7)	713.01	52	R (23)	785.87
23	P (6)	715.44	53	R (24)	788.23
24		716.67	54	R (25)	790.63
25	P (5)	717.75	55	R (26)	792.94
26	P (4)	720.27	56	R (27)	795.31
27	P (3)	722.46	57	R (28)	797.57
28	P (2)	724.72	58	R (29)	799.87
29		726.13	59	R (30)	802.04
30	R (1)	734.24	60	R (31)	804.53

of the gas generating system and the cell, atmospheric carbon dioxide was eliminated from the absorption cell.

The absorption bands shown in this paper were traced from the original records in such a manner as to eliminate most of the drift of the thermocouple (a "dc" amplification system was used as described in reference 6). Some of the peculiar intensities on the middle of the R branch of Fig. 1 were introduced by shifting the foreprism while this portion of the spectrum was being recorded. For the other bands a single setting of this prism was used for the whole range.

The values for the band centers, for B'', and for $B'-B''$ were obtained by use of the combination principles[7] in the bands for which the rotational lines were well-enough resolved.

EXPERIMENTAL RESULTS

In describing the results it will be convenient to indicate the absolute value of the quantum number l by the usual superscript appended to the frequency. For example, the notation $\nu_5^1+2\nu_4^0-\nu_4^1$ will mean the vibrational frequency for a transition from a lower state with $V_4=1$, $|l_4|=1$ to a state with $V_5=1$, $|l_5|=1$, $V_4=2$, $|l_4|=0$, all other vibrational quantum numbers being zero. The active fundamental band regions will be discussed first and the derived values of the infra-red inactive, but Raman active, fundamentals will be given. The combination bands will be discussed in the order of increasing frequencies. Finally the derived results and anharmonic coefficients will be discussed.

THE FUNDAMENTAL BANDS AND FREQUENCIES

ν_5^1-Band

Of the five fundamental frequencies of acetylene only ν_3 and ν_5^1 are observed in the infra-red spectrum. The appearance of the ν_5^1-band, which has a frequency of 730.74 cm^{-1}, is shown in Fig. 1, and the line frequencies are given in Table I. The lines in Table I are numbered to correspond with the line numbers in Fig. 1. A combination principle applied to the P and R branch lines gives a Q branch position of 729.56 cm^{-1}. If this band were the ν_5^1, $(\Pi_u-\Sigma_g)$, band only, it would consist of a strong central Q branch and P and R branches with alternating intensities and a missing P (1) line. That this absorption region consists of more than the ν_5^1-band is easily seen. Line No. 24 at 716.67 cm^{-1} is identified as the Q branch of the difference band $\nu_4^1+\nu_5^1-\nu_4^1$, $(\Sigma_u^-,\ \Sigma_u^+-\Pi_g)$, with $l=0$ in the upper state. The vibrational frequency for this difference band is therefore 715.49 cm^{-1}. The band $\nu_4^1+\nu_5^1-\nu_4^1$, $(\Delta_u-\Pi_g)$, with $l=2$ in the upper state would be expected to produce a Q branch (weaker relative to its P and R branch lines than the Σ_u^-, $\Sigma_u^+-\Pi_g$-band Q branch) with a frequency $4B''$ smaller than line No. 24. A Q branch at this expected position, 712.06 cm^{-1}, is not seen in the spectrum except in disturbing the resolution of lines No. 21 and No. 22. The bands $2\nu_5^{2,0}-\nu_5^1$, $(\Delta_g, \Sigma_g^+-\Pi_u)$, would also lie in this region of the spectrum. The Q branch of the $2\nu_5^0-\nu_5^1$-band adds to the intensity of line No. 26 and the Q branch of $2\nu_5^2-\nu_5^1$ is at 730 cm^{-1} and hence is masked by the Q branch of ν_5^1. The assignment of these bands is consistent with anharmonic coefficients x_{55} and X_{55} which are obtained from bands in the region of $3\nu_5^1$. The frequency $2\nu_5^0-\nu_5^1$ is therefore 719.09 cm^{-1} with a Q branch at 720.27 cm. The presence of bands other than ν_5^1 in this spectrum is also indicated by the presence of line No. 29 which is not at the right position to be a P (1) line of the ν_5^1 [the P (1) line should have zero intensity], by the lack of proper three to one intensity alternation in the lines of the P and R branches, and by the presence of satellites on the R branch lines near the center of the band.

A combination principle applied to the lines in the P and R branches gives a value $B'-B''=-0.0008$ cm^{-1}. The convergence of the Q branch, however, is consistent with a positive value of $B'-B''$. This may be understood in the following manner.* The levels in the upper state are split by an l-type doubling. These component states have, effectively, two different B' values which we shall designate by $B_\pm'$. The lines in the P and R branches are due to transitions from the normal vibration state to the lower components in the upper state. The components of the Q branch, however, are due to transitions from the normal state to the upper component states.

[7] See reference 2, p. 340 ff.

* *Note added in proof:* this anomaly has been discussed by G. Herzberg in Rev. Mod. Phys. **14**, 219 (1942).

The quantities $B_{\pm}'$ are equal to $B_{\pm}'=B'\pm\Delta$ where B' are the B_v given by Shaffer and Nielsen and where Δ for a state $V_5=|l_5|=1$ is equal[8] to $B(B/\omega_5)[1+\Sigma_{s'}\zeta_{5s'}{}^2 4\omega_5{}^2/(\omega_{s'}{}^2-\omega_5{}^2)]$. It is readily verified that $\zeta_{53}{}^2=1$ and $\zeta_{51}{}^2=\zeta_{52}{}^2=0$ so that Δ reduces to $B(B/\omega_5)[1+4\omega_5{}^2/(\omega_3{}^2-\omega_5{}^2)]$. Insertion of the constants B_1, ω_5, and ω_3 into Δ leads to a value $\Delta=0.0023$ cm^{-1}. The value $B'-B''=-0.0008$ referred to earlier is in reality $B_-'-B''$. From the definition of B_+' we have that $B_+'-B''=B_-'-B''+2\Delta$. We obtain, therefore, $B_+'-B''=+0.0038$ cm^{-1} which is positive as indicated by the convergence of the Q branch.

ν_3-Band

The fundamental ν_3, $(\Sigma_u{}^+-\Sigma_g{}^+)$, which has a frequency of 3282.5 cm^{-1}, is shown in Fig. 2. This band is overlapped by the combination band $\nu_2+\nu_4{}^1+\nu_5{}^1$, $(\Sigma_u{}^+-\Sigma_g{}^+)$. The resolution is sufficient to separate these two bands as is indicated by the schematic diagram of the two bands shown in Fig. 2. The relative intensities of the two bands in the schematic spectrum were chosen to approximate the observed spectrum by giving the combination band twice the intensity of the fundamental. The $B'-B''$ values for these bands, given in Table XI, cannot be accurate because of the inability to measure the frequencies of the lines of either band without interference from the lines of the other band. The line frequencies for these two bands are given in Table II. It is strange that the intensity of the fundamental should appear weaker than the combination band and it is possible that these assignments may have to be interchanged. A test of the validity of the assignment may be obtained from the anharmonic constants after the band $\nu_2+\nu_4{}^1-\nu_5{}^1$ or the band $\nu_2+\nu_5{}^1-\nu_4{}^1$ is observed. The $\nu_2+\nu_4{}^1-\nu_5{}^1$-band was not observed with our instrument with a 30-in. cell containing acetylene at atmospheric pressure. In view of the anharmonic constants, as presently evaluated (see later), it seems that it would be possible to invert this assignment of ν_3 and $\nu_2+\nu_4{}^1+\nu_5{}^1$.

The band $\nu_3+\nu_4{}^1-\nu_4{}^1$, $(\Pi_u-\Pi_g)$, is expected at 3270.7 cm^{-1} and may therefore be adding to the intensity of line No. 27 at 3270.9 cm^{-1}. Line No. 27 is not significantly larger than one would expect without the addition of the Q branch of $\nu_3+\nu_4{}^1-\nu_4{}^1$. One of the components of $\nu_2+2\nu_4{}^{0,2}+\nu_5{}^1-\nu_4{}^1$, $(2\Pi_u,\ \Phi_u-\Pi_g)$, is expected at 3286.6 cm^{-1} and the Q branch probably adds to distort the intensities of lines No. 38 and No. 39.

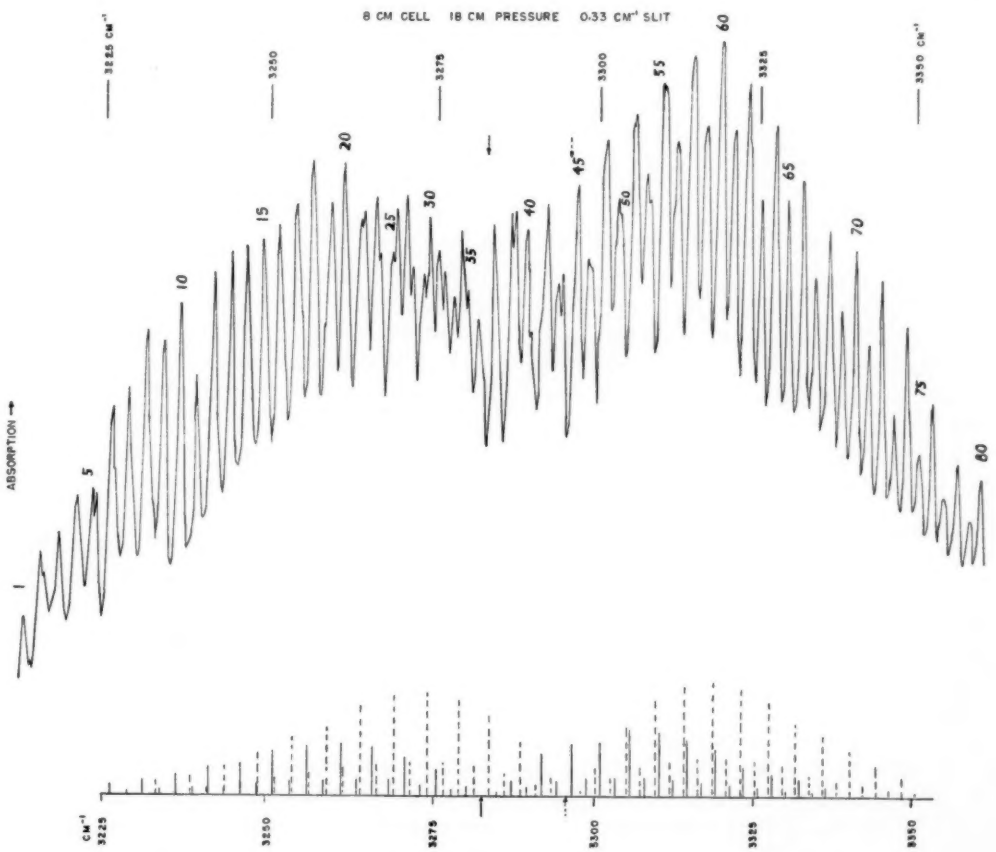

FIG. 2. The ν_3- and $\nu_2+\nu_4{}^1+\nu_5{}^1$-bands of acetylene as measured with the 7500 lines per inch grating. The values of the line frequencies are given in Table II.

[8] H. H. Nielsen, Phys. Rev. **77**, 130 (1950).

TABLE II. The ν_3- and $\nu_2+\nu_4^1+\nu_5^1$-band frequencies, see Fig. 2.

Line No.	ν_3	$\nu_2+\nu_4^1+\nu_5^1$	cm^{-1}	Line No.	ν_3	$\nu_2+\nu_4^1+\nu_5^1$	cm^{-1}
1	P (28)		3213.5	41	R (2)		3289.4
2	P (27)		3215.8	42	R (3)		3291.7
3	P (26)		3218.7	43		P (1)	3293.2
4	P (25)		3221.2	44	R (4)		3294.1
5	P (24)		3223.7	45	R (5)		3296.4
6	P (23)		3226.3	46		R (0)	3297.9
7	P (22)		3228.8	47	R (6)		3298.6
8	P (21)		3231.6	48	R (7)		3300.8
9	P (20)		3234.0	49		R (2)	3302.5
10	P (19)		3236.6	50	R (8)		3303.1
11	P (18)		3239.2	51		R (3)	3304.2
12	P (17)		3241.7	52	R (9)		3304.7
13	P (16)	P (21)	3244.2	53		R (4)	3307.2
14	P (15)	P (20)	3246.5	54	R (10)		3307.8
15	P (14)	P (19)	3249.0	55		R (5)	3309.7
16	P (13)	P (18)	3251.5	56	R (11)		3310.0
17	P (12)	P (17)	3254.0	57	R (12)	R (6)	3311.9
18	P (11)	P (16)	3256.3	58	R (13)	R (7)	3314.3
19	P (10)	P (15)	3259.1	59	R (14)	R (8)	3316.6
20	P (9)	P (14)	3261.2	60	R (15)	R (9)	3318.8
21	P (8)		3263.6	61	R (16)	R (10)	3321.0
22		P (13)	3264.2	62	R (17)	R (11)	3323.3
23	P (7)		3265.8	63	R (18)	R (12)	3325.3
24		P (12)	3266.5	64	R (19)	R (13)	3327.6
25	P (6)		3268.4	65	R (20)	R (14)	3329.8
26		P (11)	3269.1	66	R (21)	R (15)	3332.0
27	P (5)		3270.9	67	R (22)	R (16)	3334.0
28		P (10)	3271.4	68	R (23)	R (17)	3336.2
29	P (4)		3273.0	69	R (24)	R (18)	3338.3
30		P (9)	3273.9	70	R (25)	R (19)	3340.4
31	P (3)		3275.3	71		R (20)	3342.7
32		P (8)	3276.2	72		R (21)	3344.7
33	P (2)		3277.5	73		R (22)	3346.7
34		P (7)	3278.7	74		R (23)	3348.8
35	P (1)		3279.8	75		R (24)	3350.7
36		P (6)	3281.3	76		R (24)	3352.8
37		P (5)	3283.6	77		R (25)	3354.9
38		P (4)	3286.2	78		R (26)	3356.9
39	R (1)		3287.0	79		R (27)	3359.1
40		P (3)	3288.5	80		R (28)	3360.9

ν_1-, ν_2-, ν_4^1-Frequencies

No other fundamental bands of acetylene are infrared active. The fundamental Raman frequencies of acetylene gas may be obtained from some difference bands which will be discussed later. These fundamental frequencies are the following: $\nu_1=3373.2$ cm^{-1}, $\nu_2=1974.0$ cm^{-1}, and $\nu_4^1=613.3$ cm^{-1}.

COMBINATION BANDS

$\nu_1-\nu_5^1$-Band

A weak perpendicular band with a frequency of 1243.3 cm^{-1} has a Q branch which may be seen among the P branch lines of the $\nu_4^1+\nu_5^1$-band as shown in Fig. 3. This band must be $\nu_1-\nu_5^1$, $(\Sigma_g^+-\Pi_u)$. The majority of the lines seen on the two sides of the Q branch must be associated with the $\nu_4^1+\nu_5^1$-band. The Q branch peak which was taken for the band center, as marked in the Fig. 3, is at 1244.5 cm^{-1}.

$\nu_4^1+\nu_5^1$-Band

A very intense summation band is found at 1328.18 cm^{-1}, which is identified as $\nu_4^1+\nu_5^1$, $(\Sigma_u^+-\Sigma_g^+)$. This should be a parallel-type band with no Q branch and alternating intensities. The experimentally obtained band, Fig. 4C appears to have a line at the center and does not have the expected three to one intensity alternation in the rotation lines. The record shown in Fig. 4B was obtained by placing dry ice around the absorption cell, except at the windows, and thereby reducing the temperature to about -75°C. The record of Fig. 4C was obtained with the same instrumental conditions (slit widths, etc.) after the dry ice had sublimed away and the cell has warmed up to room temperature. It is easily seen that the central line, which is marked by an arrow in Fig. 4, is temperature sensitive. The alternating intensity is more marked in the cooled sample. We conclude that there must be a difference band in this region which arises from an excited $V_4=1$ or $V_5=1$ state, because the intensity of a difference band would be reduced by cooling, i.e., by reducing the number of molecules in the initial thermally excited level.

This difference band, with a Q branch in the center of the $\nu_4^1+\nu_5^1$-band, is found to be one of the two bands $2\nu_4^{0,2}+\nu_5^1-\nu_4^1$, $(2\Pi_u-\Pi_g)$, with a central Q branch at 1328.46 cm^{-1}. The center of the $\nu_4^1+\nu_5^1$-band is at 1328.18 cm^{-1} as found by a combination principle applied to the rotational lines of the cooled gas record, Fig. 4B. The fact that the 1328.46-cm^{-1} Q branch is not quite at the center of the $\nu_4^1+\nu_5^1$-band was apparent on the original records. The bands $2\nu_4^0+\nu_5^1-\nu_4^1$ and $2\nu_4^2+\nu_5^1-\nu_4^1$ would be of the same type, $(\Pi_u-\Pi_g)$, but not at the same position because of the $X_{44}l_4^2$ term in the vibrational energy of the two upper states would be different. A difficulty of assignment of this band will be reviewed later in the discussion of anharmonicity coefficients. The addition of a band of the $\Pi_u-\Pi_g$-type together with $\nu_4^1+\nu_5^1$ seems to explain the apparent intensities of the main lines in this region of the spectrum. The appearance of a $\Pi_u-\Pi_g$-type band is shown in Fig. 9.

The record shown in Fig. 4A was made with a cell whose windows had not been fogged by the dooling procedure. The additional lines seen between the main lines are difficult to explain. The most abundant expected isotope, $H^1-C^{12}\equiv C^{13}-H^1$, would be asymetrical and would not show the apparent intensity alternations which these minor lines seem to show. The difference bands $2\nu_4^{0,2}+\nu_5^1-\nu_4^1$, discussed above, and the difference bands $\nu_4^1+2\nu_5^{0,2}-\nu_5^1$, $(\Pi_g-\Pi_u)$, also would not show this intensity alternation. The very weak bands $\nu_3-\nu_2(\Sigma_u^+-\Sigma_g^+)$, and $\nu_2+\nu_4^1+\nu_5^1-\nu_2$, $(\Sigma_u^+-\Sigma_g^+)$, while of the proper type, would be expected to have a center in the P branch near 1310 and 1320 cm^{-1}. There are some additional lines in the P branch, but good records of them were not obtained. An isotope band might account for these additional P branch lines.

The line frequencies for the $\nu_4^1+\nu_5^1$-band are given in Table III. The combination relations applied to the

lines of the cooled gas records give $B''=1.1769$ cm^{-1} and $B'-B''=+0.003$ cm^{-1}.

The upper state level $V_5=1$, $V_4=2$ which is involved in producing the central line in the $2\nu_4^{0,2}+\nu_5^1-\nu_4^1$-band has been measured in transitions from the ground state, see Fig. 5 and the next paragraph. The value of the lower state level $V_4=1$ has been derived from several difference bands. From the knowledge of the upper and lower levels it is possible to predict the position of the Q branch of the $2\nu_4^{0,2}+\nu_5^1-\nu_4^1$-band. The predicted[9] value is 1328.4 cm^{-1} compared with the experimental value of 1328.46 cm^{-1}.

$2\nu_4^{2,0}+\nu_5^1$-Band

There are two Q branches with frequencies 1940.52 and 1960.66 cm^{-1} shown in Fig. 5. It is natural to identify these as $2\nu_4^0+\nu_5^1$, $(\Pi_u-\Sigma_g^+)$, and $2\nu_4^2+\nu_5^1$, $(\Pi_u-\Sigma_g^+)$, which would immediately give the value of the separation $4X_{44}$ as ± 20.14 cm^{-1} with a sign depending upon which of the two ways the assignment is made. There is difficulty with both ways, however, as will be seen later when an evaluation of the constant X_{44} is made. The difference bands $3\nu_4^{3,1}+\nu_5^1-\nu_4^1$, $(\Sigma_u^+, \Sigma_u^-, 2\Delta_u-\Pi_g)$, and $2\nu_4^{2,0}+2\nu_5^{2,0}-\nu_5^1$, $(2\Sigma_g^+, \Sigma_g^-, 2\Delta_g-\Pi_u)$ will also lie in this region. A cooling experiment to determine whether either one of the two Q branches in this region belonged to a difference band was inconclusive but seemed to indicate that it did not. An investigation of the possible vibrational resonance interactions and coriolis interactions has not disclosed any reasonable explanation for a shift in the positions of these bands.

TABLE III. The $\nu_4^1+\nu_5^1$-band frequencies, see Fig. 4.

Line No.	$\nu_4^1+\nu_5^1$	cm^{-1}	Line No.	$\nu_4^1+\nu_5^1$	cm^{-1}
1	P (20)	1282.3	21		1328.46
2	P (19)	1284.6	22	R (0)	1330.6
3	P (18)	1286.8	23	R (1)	1333.0
4	P (17)	1289.0	24	R (2)	1335.3
5	P (16)	1291.2	25	R (3)	1337.7
6	P (15)	1293.5	26	R (4)	1340.1
7	P (14)	1295.8	27	R (5)	1342.4
8	P (13)	1298.0	28	R (6)	1344.9
9	P (12)	1300.3	29	R (7)	1347.1
10	P (11)	1302.7	30	R (8)	1349.7
11	P (10)	1304.9	31	R (9)	1352.1
12	P (9)	1307.2	32	R (10)	1354.4
13	P (8)	1309.5	33	R (11)	1356.9
14	P (7)	1311.8	34	R (12)	1359.3
15	P (6)	1314.2	35	R (13)	1361.8
16	P (5)	1316.4	36	R (14)	1364.2
17	P (4)	1318.7	37	R (15)	1366.6
18	P (3)	1321.1	38	R (16)	1369.1
19	P (2)	1323.5	39	R (17)	1371.5
20	P (1)	1325.8	40	R (18)	1373.9

No resonance would be expected to induce infra-red activity in a band here either. The line frequencies are given in Table IV, and $B'-B''=0.0032$ cm^{-1} for the lines associated with the 1940.52-cm^{-1} Q branch. A tentative assignment of $2\nu_4^0+\nu_5^1$ to the stronger Q branch gives this band a vibrational frequency of 1941.70 cm^{-1}.

$3\nu_5^1$-Band

A perpendicular band attributed to $3\nu_5^1$, $(\Pi_u-\Sigma_g^+)$, is found with a frequency of 2170.84 cm^{-1} and is shown

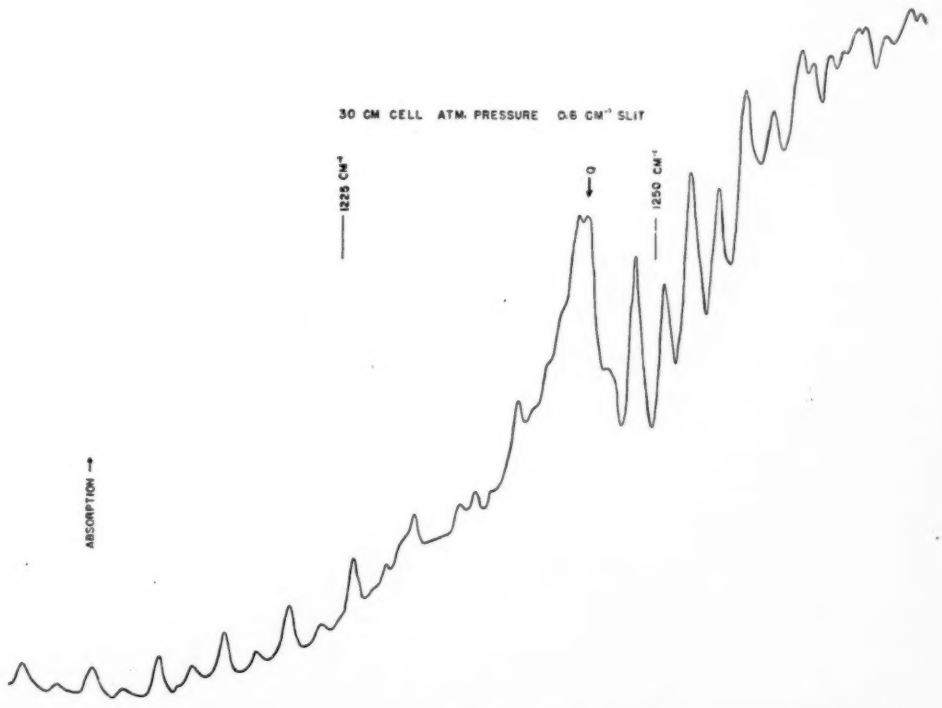

FIG. 3. The $\nu_1-\nu_5^1$-band Q branch as measured with the 3600 lines per inch grating.

[9] The $2\nu_4^{2,0}+\nu_5^1-\nu_4^1$-band was used together with the $\nu_4^1+\nu_5^1$-band to obtain one experimental value of the $V_4=1$ level, but the $V_4=1$ level could be obtained from other pairs of bands and thus predict the position of the Q branch $2\nu_4^{0,2}+\nu_5^1-\nu_4^1$.

in Fig. 6. The intensity alternation shows very well in this band. The value of $B'-B''$ equal to 0.0020 cm^{-1} and the band center of 2169.67 cm^{-1} were obtained from the combination relations. The line frequencies are given in Table V. There are several extra lines in the spectrum whose intensities relative to the other lines seemed to be decreased by cooling. Among these lines are Nos. 17 and 22, which are undoubtedly Q branches of difference bands. The difference bands which may be expected in this region are $\nu_4^1+3\nu_5^{3,1}-\nu_4^1$, $(\Sigma_u^-,\ \Sigma_u^+,\ 2\Delta_u-\Pi_g)$, and $4\nu_5^{2,0}-\nu_5^1$, $(\Sigma_g^+,\ \Delta_g-\Pi_u)$. Anharmonic constants derived from other bands indicate that the Q branch of $3\nu_5^1+\nu_4^1-\nu_4^1$ would be near 2122 cm^{-1}. Near this position there is no obvious Q branch. The expected position of $4\nu_5^0-\nu_5^1$ is near 2151 cm^{-1} so we believe that line No. 17, which occurs at 2152.0 cm^{-1}, is of the Q branch of this band. Thus the frequency of $4\nu_5^0-\nu_5^1$ is 2150.8 cm^{-1}. The line No. 22 is chosen as the Q branch of $4\nu_5^2-\nu_5^1$ because the bands ν_5^1, $3\nu_5^1$, $4\nu_5^0-\nu_5^1$, and $4\nu_5^2-\nu_5^1$ give values for the anharmonic constants x_{55} and X_{55} which are consistent with the assignment of $2\nu_5^0-\nu_5^1$. The frequency $4\nu_5^2-\nu_5^1$ is taken to be 2165.0 cm^{-1}. It is not possible to interchange the assignments of $4\nu_5^2-\nu_5^1$ and $4\nu_5^0-\nu_5^1$ without leading to an inconsistancy in the anharmonic constants.

$3\nu_4^1+\nu_5^1$-Band

A weak parallel band attributed to $3\nu_4^1+\nu_5^1$, $(\Sigma_u^+-\Sigma_g^+)$, is found at the edge of the 3.7μ absorption group. Figure 7 shows this band and the overlapping of the lines of the 3.7μ bands on the high frequency side. Only a few of the weak lines show in the record because of the poor resolution, and therefore it is difficult to find the center. The center has been chosen as 2556.5 cm^{-1} as indicated in Fig. 7. The center might very well be $4B$ larger than this value. The frequencies of the lines are given in Table VI.

$\nu_1-\nu_5^1$-, $\nu_3-\nu_4^1$-, $\nu_2+\nu_4^1+\nu_5^1-\nu_4^1$-, and $\nu_2+\nu_5^1$-Bands

Four distinct Q branches are found in the 2700-cm^{-1} region as shown in Fig. 8. The frequencies of these lines are given in Table VII. These bands are: $\nu_1-\nu_5^1$, $(\Sigma_g^+-\Pi_u)$, with a Q branch at 2643.69 cm^{-1} and a frequency of 2642.51 cm^{-1}; $\nu_3-\nu_4^1$, $(\Sigma_u^+-\Pi_g)$, with a Q branch at 2670.33 cm^{-1} and a frequency of 2669.15 cm^{-1}; $\nu_2+\nu_4^1+\nu_5^1-\nu_4^1$, $(\Sigma_u^-,\ \Sigma_u^+-\Pi_g)$ with a Q branch at 2683.09 cm^{-1} and a frequency of 2681.81 cm^{-1}; and $\nu_2+\nu_5^1$, $(\Pi_u-\Sigma_g^+)$, with a Q branch at 2702.46 cm^{-1} and a frequency of 2703.63 cm^{-1}. The Q branch of the band $\nu_2+\nu_4^1+\nu_5^1-\nu_4^1$, $(\Delta_u-\Pi_g)$, with $l=2$ in the upper state, is expected at a frequency $4B$ less than 2683.09 cm^{-1}. A strong absorption at this position is not seen in the records. The Q branch of the band $\nu_2+2\nu_5^0-\nu_5^1$, $(\Sigma_g^+-\Pi_u)$, is thought to be at 2691.7 cm^{-1}, line No. 48, and thus the frequency would be 2690.5 cm^{-1}. This is conjecture, however, since the Q branch does not tower over the other lines of the spectrum. Such a position for

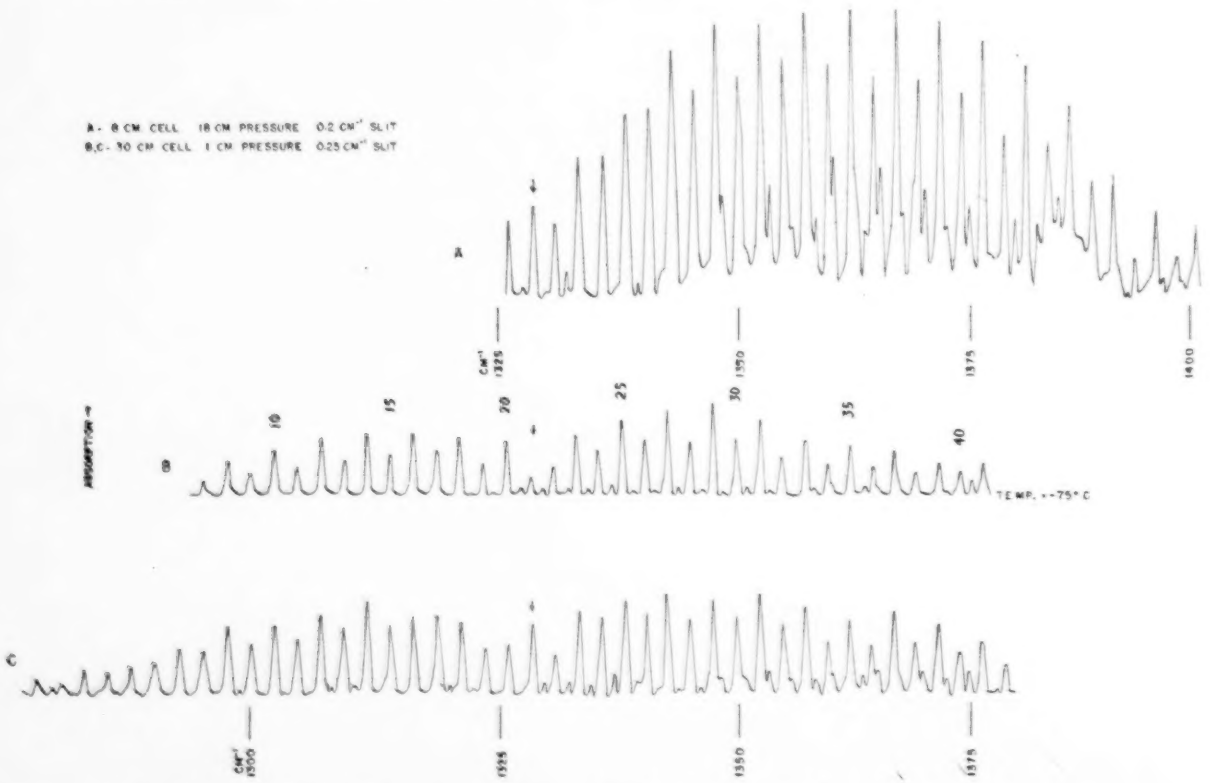

FIG. 4. The $\nu_4^1+\nu_5^1$-band of acetylene as measured with the 3600 lines per inch grating. The values of the line frequencies are given in Table III.

TABLE IV. The $2\nu_4^0+\nu_5^1$-band frequencies, see Fig. 5.

Line No.	$2\nu_4^0+\nu_5^1$		cm^{-1}	Line No.	$2\nu_4^0+\nu_5^1$		cm^{-1}
1	P (19)		1896.4	31	R (7)		1959.6
2	P (17)		1901.1	32			1960.66
3			1902.7	33	R (9)		1964.2
4	P (16)		1903.4	34		R (1)	1964.9
5	P (15)		1906.2	35	R (10)		1966.7
6			1907.4	36		R (2)	1967.2
7	P (14)		1908.2	37	R (11)		1969.0
8	P (13)		1910.1	38		R (3)	1969.7
9	P (12)		1912.5	39	R (12)		1971.5
10	P (11)		1914.8	40	R (13)		1973.8
11			1916.1	41		R (5)	1974.6
12	P (10)		1917.4	42	R (14)		1976.2
13			1918.8	43		R (6)	1977.0
14	P (9)		1919.6	44	R (15)		1978.7
15			1920.7	45		R (7)	1979.5
16	P (8)		1921.8	46	R (16)		1980.8
17	P (7)		1924.1	47		R (8)	1981.7
18	P (6)		1926.3	48	R (17)		1983.2
19	P (5)		1928.9	49		R (9)	1984.5
20		P (13)	1930.4	50		R (10)	1986.6
21	P (4)		1931.3	51	R (19)		1988.0
22	P (3)		1933.4	52		R (11)	1989.4
23		P (11)	1935.0	53	R (21)		1993.6
24	Q		1941.17	54		R (13)	1994.3
25	R (1)		1945.8	55		R (14)	1996.0
26	R (3)		1950.1	56	R (23)		1997.4
27			1952.2	57		R (15)	1999.5
28	R (5)		1954.9				
29	R (6)		1957.2				
30			1957.4				

TABLE V. The $3\nu_5^1$-band frequencies, see Fig. 6.

Line No.	$3\nu_5^1$	cm^{-1}	Line No.	$3\nu_5^1$	cm^{-1}
1	P (23)	2115.8	26		2174.8
2	P (21)	2121.1	27		2175.7
3	P (20)	2123.4	28	R (2)	2176.5
4	P (19)	2125.6	29	R (3)	2179.0
5	P (18)	2128.1	30		2180.1
6	P (17)	2130.3	31	R (4)	2181.4
7	P (16)	2132.5	32	R (5)	2183.9
8	P (15)	2134.8	33	R (6)	2186.4
9	P (14)	2137.1	34	R (7)	2188.8
10	P (13)	2139.4	35	R (8)	2191.2
11	P (12)	2141.7	36	R (9)	2193.6
12	P (11)	2144.0	37	R (10)	2195.9
13	P (10)	2146.3	38	R (11)	2198.3
14		2147.0	39	R (12)	2200.8
15	P (9)	2148.5	40	R (13)	2203.0
16	P (8)	2150.9	41	R (14)	2205.4
17		2152.0	42	R (15)	2207.9
18	P (7)	2153.2	43	R (16)	2210.2
19	P (6)	2155.6	44	R (17)	2212.6
20	P (5)	2158.0	45	R (18)	2214.8
21	P (4)	2160.3	46	R (19)	2217.4
22		2161.5	47	R (20)	2219.8
23	P (3)	2162.6	48	R (21)	2222.1
24	Q	2170.19	49	R (22)	2224.7
25	R (1)	2173.9	50	R (23)	2226.8

$\nu_2+2\nu_5^0-\nu_5^1$ would be in good agreement with the anharmonic constants, however. Confidence in the choice of the $V_4=1$ and $V_5=1$ as the lower levels for the bands in this region is gained by noting that $\nu_1-\nu_5^1$ is apparently reduced in intensity relatively more by cooling than either $\nu_3-\nu_4^1$ or $\nu_2+\nu_4^1+\nu_5^1-\nu_4^1$. This is expected since $V_5=1$ is a higher energy level than $V_4=1$. In compensating for the drift of the thermocouple the base line of the cooled records has been somewhat distorted.

$\nu_1+\nu_5^1-\nu_4^1$-Band

A beautiful example of a $\Pi_u-\Pi_g$-band is found at 3480.51 cm^{-1}. This band lies in a region where it may be seen without interference by other bands. The appearance of this band is shown in Fig. 9, and the line frequencies are given in Table VIII. The outstanding features of this band are the weak Q branch, the missing P (1) and R (1) lines, and the lack of intensity alterna-

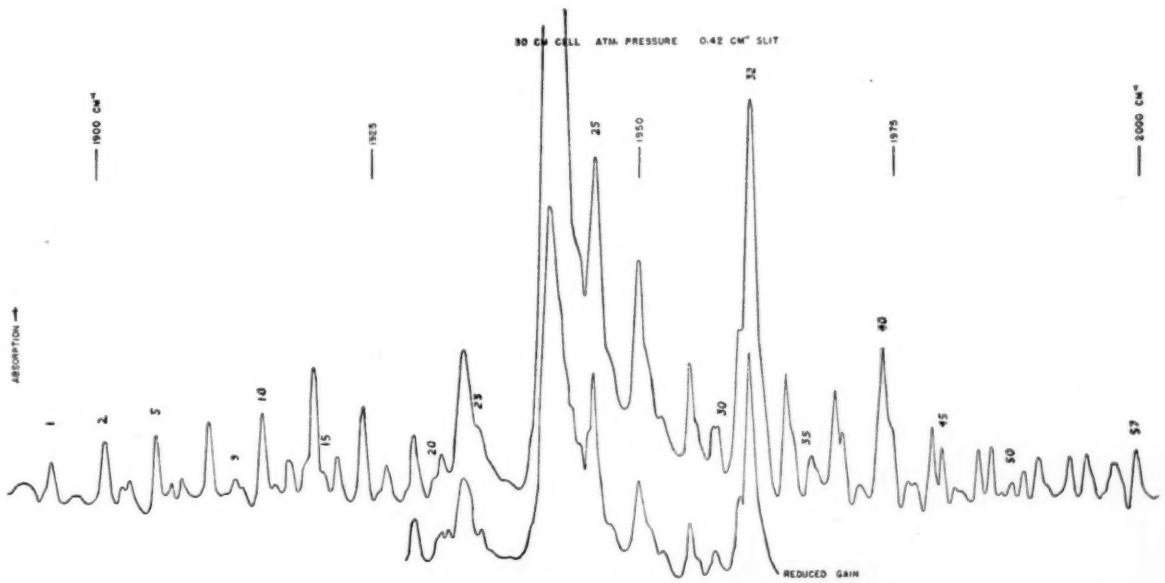

FIG. 5. The $2\nu_4^{2,0}+\nu_5^1$-band region of acetylene as measured with the 7500 lines per inch grating. The values of the line frequencies are given in Table IV.

TABLE VI. The $3\nu_4^1+\nu_5^1$-band frequencies, see Fig. 7.

Line No.	$3\nu_4^1+\nu_5^1$	cm^{-1}	Line No.	$3\nu_4^1+\nu_5^1$	cm^{-1}
1	P (17)	2520.1	12		2563.5
2	P (15)	2524.0	13	R (3)	2565.9
3	P (13)	2528.1	14		2568.2
4	P (11)	2532.0	15	R (5)	2571.0
5	P (9)	2536.2	16		2573.6
6	P (7)	2540.5	17	R (7)	2576.0
7	P (5)	2544.8	18		2578.9
8	P (3)	2549.4	19	R (9)	2580.9
9	P (1)	2554.0	20		2584.5
10	R (0)	2558.9	21	R (11)	2586.0
11	R (1)	2562.0	22		2590.0

tion. The lack of the P (1) and R (1) lines follows from the fact that there is no $J=0$ level in either the upper or lower state. The lack of the three-to-one intensity alternation is a result of the fact that each P branch line and each R branch line is the superposition of a weak line and a strong line (split by l-type doubling which is too small to be resolved). This band must be assigned to $\nu_1+\nu_5^1-\nu_4^1$.

$\nu_3+\nu_4^1$-, $\nu_2+2\nu_4^{2,0}+\nu_5^1$-Bands

Two absorption regions are shown in Fig. 10. The separation of the lines of the bands $\nu_2+2\nu_4^{2,0}+\nu_5^1$, $(2\Pi_u-\Sigma_g^+)$, and $\nu_3+\nu_4^1$, $(\Pi_u-\Sigma_g^+)$, is indicated by the predicted bands shown in Fig. 10 and in Table IX. The predicted bands were drawn with the intensity of the $\nu_3+\nu_4^1$-band equal to three-fourths the intensity of the $\nu_2+2\nu_4^{2,0}+\nu_5^1$-band. The fact that $\nu_3+\nu_4^1$ is weaker

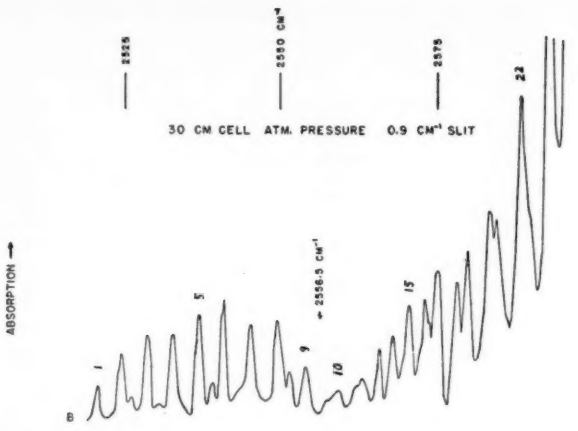

FIG. 7. The $3\nu_4^1+\nu_5^1$-band of acetylene as measured with the 7500 lines per inch grating. The values of the line frequencies are given in Table VI.

than $\nu_2+2\nu_4^{2,0}+\nu_5^1$ is as disturbing as the fact that the ν_3-band is weaker than the $\nu_2+\nu_4^1+\nu_5^1$-band. The center of the $\nu_3+\nu_4^1$-band is at 3882.81 cm^{-1} and the center of the $\nu_2+2\nu_4^{2,0}+\nu_5^1$-band is at 3898.81 cm^{-1} so that the frequencies are 3883.97 and 3899.97 cm^{-1}, respectively. Another possible assignment would, of course, be that these two bands could be the two components $\nu_2+2\nu_4^0+\nu_5^1$ and $\nu_2+2\nu_4^2+\nu_5^1$. The value of X_{44} resulting from this reassignment would be in good agreement with some other data. We prefer, however, to leave the assignment unchanged and have a band to attribute to $\nu_3+\nu_4^1$. The value of $B'-B''$ is -0.0067

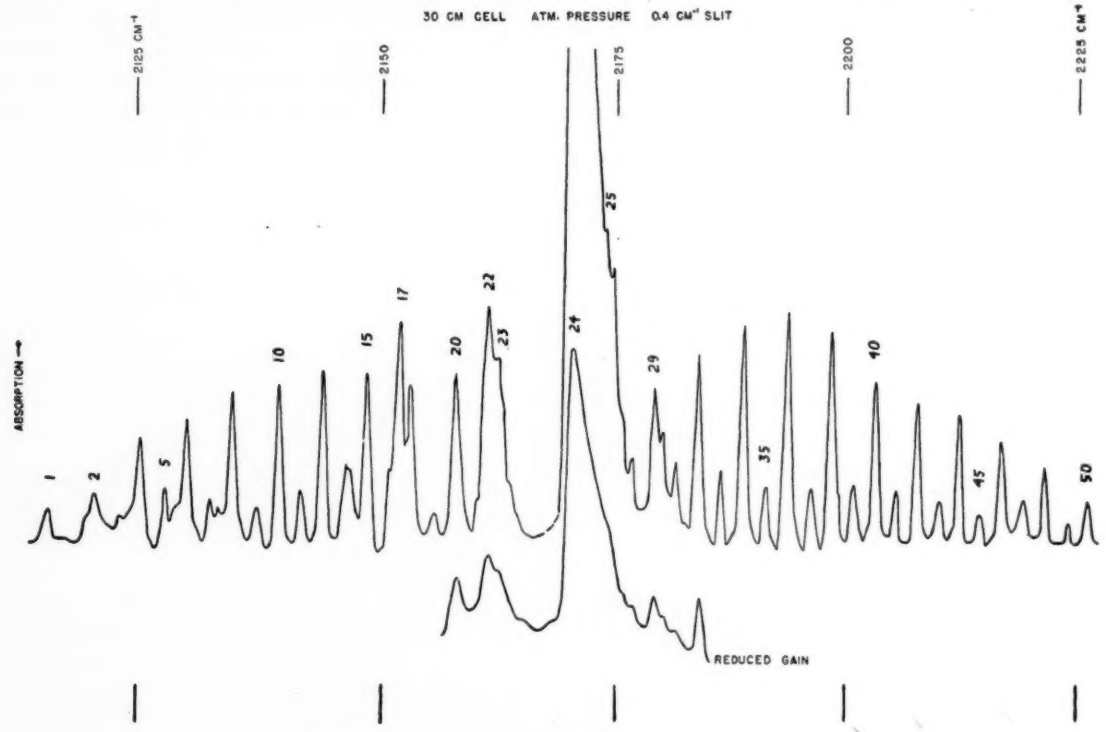

FIG. 6. The $3\nu_5^1$-band of acetylene as measured with the 7500 lines per inch grating. The values of the line frequencies are given in Table V.

cm^{-1} for the $\nu_3+\nu_4^1$-band and -0.0074 cm^{-1} for the $\nu_2+2\nu_4^{2,0}+\nu_5^1$-band.

$\nu_1+\nu_4^1+\nu_5^1-\nu_4^1$-, $\nu_1+\nu_5^1$-Bands

The high frequency absorption region shown in Fig. 10 is identified as the combination of the bands $\nu_1+\nu_4^1+\nu_5^1-\nu_4^1$, $(\Sigma_u^-, \Sigma_u^+, \Delta_u-\Pi_g)$, with Q branch near 4080 cm^{-1} and $\nu_1+\nu_5^1$, $(\Pi_u-\Sigma_g^+)$, with a Q branch at 4092.75 cm^{-1}. The rotation lines associated with the $\nu_1+\nu_5^1$-band are easily identified after reducing the intensity of the $\nu_1+\nu_4^1+\nu_5^1-\nu_4^1$-band by cooling the gas. This is shown in Fig. 10 also. The frequencies are given in Table X. The vibrational frequency of $\nu_1+\nu_5$ is 4093.92 cm^{-1} and the value of $B'-B''$ is -0.0078 cm^{-1}.

The $\Sigma_u^{\pm}-\Pi_g$-component of $\nu_1+\nu_4^1+\nu_5^1-\nu_4^1$ (with $l=0$ in the upper state) was thought to give rise to a Q branch at 4080.86 cm^{-1} and have a frequency 4079.7 cm^{-1}, line No. 126. The $\Delta_u-\Pi_g$-components (with $l=2$ in the upper state) would have a Q branch at 4076.3 cm^{-1}, line No. 124, and thus the same vibrational frequency of 4079.7 cm^{-1}. At the Symposium on Molecular Structure and Spectroscopy at Ohio State University, Columbus, Ohio (June 13, 1950), R. M. Talley and A. H. Nielsen reported on recently measured C_2H_2 absorption bands in the 4000- to 7000-cm^{-1} region.

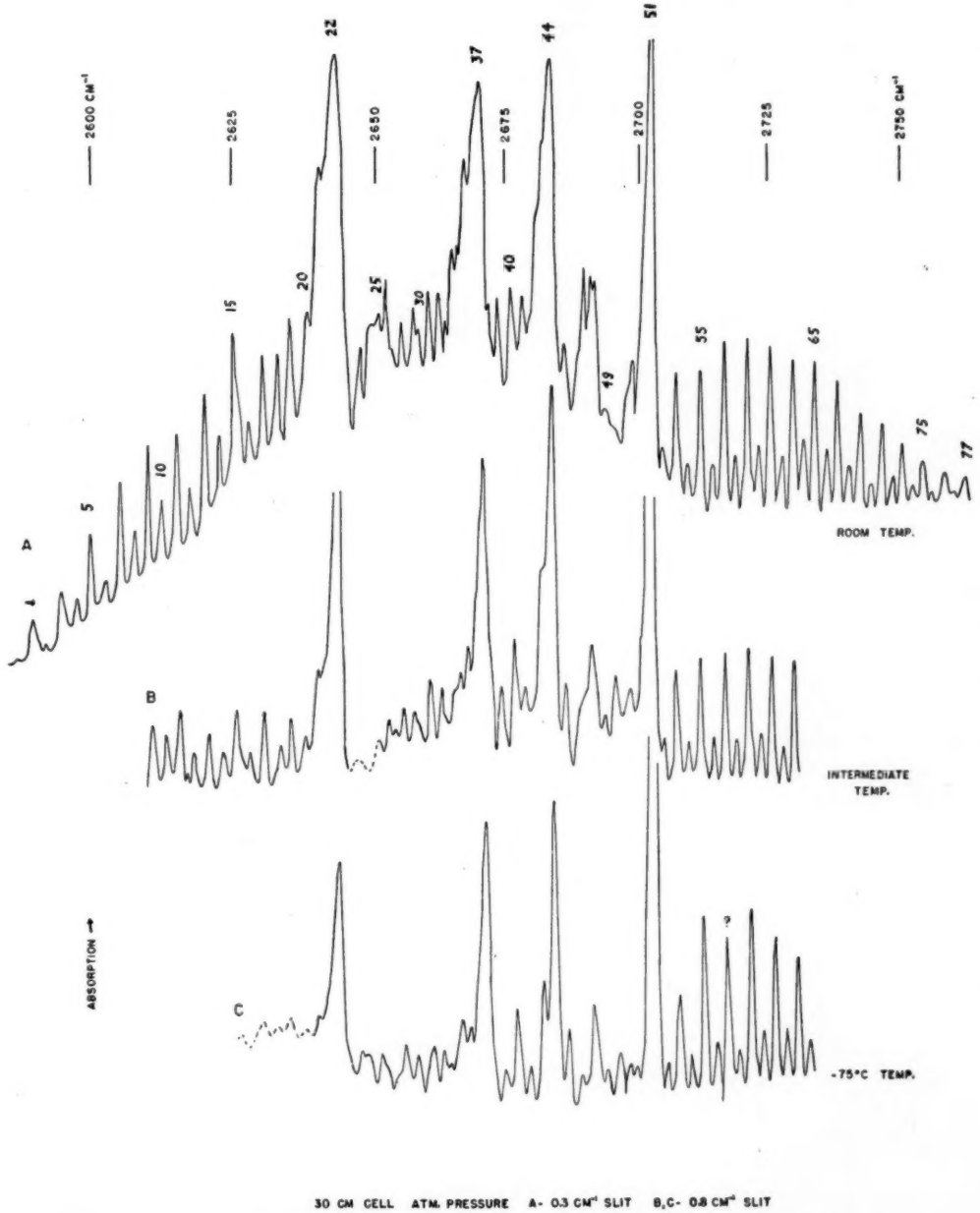

FIG. 8. The $\nu_1-\nu_5^1$-, $\nu_3-\nu_4^1$-, $\nu_3+\nu_4^1+\nu_5^1-\nu_4^1$-, and $\nu_3+\nu_5^1$-bands of acetylene as measured with the 7500 lines per inch grating. The values of the line frequencies are given in Table VII.

TABLE VII. The $\nu_2+\nu_5^1$-band frequencies, see Fig. 8.

Line No.	$\nu_2+\nu_5^1$		cm^{-1}	Line No.	$\nu_2+\nu_5^1$		cm^{-1}
1			2589.8	39			2673.8
2			2591.9	40	P (11)		2676.2
3			2594.7	41			2678.3
4			2597.5	42			2680.6
5			2600.0	43	P (9)		2681.4
6			2602.7	44		Q	2683.09
7			2605.3	45	P (7)		2686.6
8			2607.6	46			2689.6
9			2610.2	47	P (5)		2690.9
10			2612.7	48			2691.7
11			2615.3	49			2693.8
12			2617.8	50			2699.0
13			2620.4	51	Q		2702.46
14			2622.9	52	R (0)		2704.9
15			2625.5	53	R (1)		2707.3
16			2628.1	54	R (2)		2709.6
17			2630.4	55	R (3)		2711.8
18			2632.9	56	R (4)		2714.2
19			2635.2	57	R (5)		2716.4
20			2638.3	58	R (6)		2718.5
21			2640.2	59	R (7)		2720.7
22		Q	2643.69	60	R (8)		2723.0
23			2648.0	61	R (9)		2725.3
24			2649.9	62	R (10)		2727.5
25			2651.3	63	R (11)		2729.7
26			2652.8	64	R (12)		2731.9
27			2654.0	65	R (13)		2734.1
28	P (19)		2655.7	66	R (14)		2736.3
29			2657.6	67	R (15)		2738.5
30			2658.5	68	R (16)		2740.6
31	P (17)		2660.3	69	R (17)		2742.8
32			2662.5	70	R (18)		2744.9
33			2663.6	71	R (19)		2746.9
34			2665.0	72	R (20)		2748.9
35	P (15)		2665.9	73	R (21)		2751.2
36			2667.2	74	R (22)		2753.1
37		Q	2670.33	75	R (23)		2755.2
38			2672.1	76	R (25)		2759.0
				77	R (27)		2762.9

In this work was a parallel band at 4673.2 cm^{-1} attributed to $\nu_1+\nu_4^1+\nu_5^1$. The Q branches at 4076.3 and 4080.86 cm^{-1} cannot, therefore, be $\nu_1+\nu_4^1+\nu_5^1-\nu_4^1$. The Q branch at 4061.0 cm^{-1}, line No. 119 in Fig. 10, must be one of the difference band Q branches. The other Q branch would be expected at 4056.4 cm^{-1}, between lines No. 117 and No. 118, and is not seen in the records. In order to accommodate these new data the

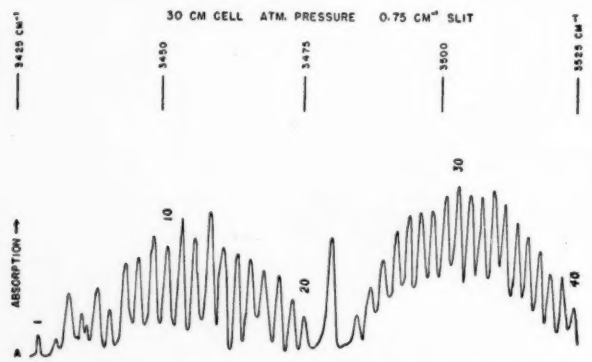

FIG. 9. The $\nu_1+\nu_5^1-\nu_4^1$-band ($\Pi_u-\Pi_g$) of acetylene as measured with the 7500 lines per inch grating. The values of the line frequencies are given in Table VIII.

TABLE VIII. The $\nu_1+\nu_5^1-\nu_4^1$-band frequencies, see Fig. 9.

Line No.	$\nu_1+\nu_5^1-\nu_4^1$	cm^{-1}	Line No.	$\nu_1+\nu_5^1-\nu_4^1$	cm^{-1}
1	P (21)	3428.4	21	Q	3480.58
2	P (20)	3430.9	22	R (1)	3485.2
3	P (19)	3433.8	23	R (2)	3487.3
4	P (18)	3436.2	24	R (3)	3489.7
5	P (17)	3438.7	25	R (4)	3492.1
6	P (16)	3441.1	26	R (5)	3494.4
7	P (15)	3443.9	27	R (6)	3496.5
8	P (14)	3446.1	28	R (7)	3498.8
9	P (13)	3448.8	29	R (8)	3501.1
10	P (12)	3451.3	30	R (9)	3503.3
11	P (11)	3453.9	31	R (10)	3505.5
12	P (10)	3456.3	32	R (11)	3507.6
13	P (9)	3458.9	33	R (12)	3509.8
14	P (8)	3461.3	34	R (13)	3512.0
15	P (7)	3463.7	35	R (14)	3514.2
16	P (6)	3466.2	36	R (15)	3516.3
17	P (5)	3468.7	37	R (16)	3518.5
18	P (4)	3471.2	38	R (17)	3520.6
19	P (3)	3473.6	39	R (18)	3522.7
20	P (2)	3475.7	40	R (19)	3524.9

original assignments have been denoted with question marks in Tables XI and XII and the new assignment is marked by parentheses.

The extra intensity of line No. 148 at 4140.35 cm^{-1} is attributed to Q branch of $\nu_2+3\nu_5^1$. The frequency of $\nu_2+3\nu_5^1$ is, then, 4141.5 cm^{-1}.

A summary of the bands observed is presented in Table XI. The value of l_4 for states in which $V_4=2$ has been labeled as zero for lack of evidence contrariwise. The centers of bands for which $B'-B''$ are given where obtained from a combination principle. Very weak bands of questionable intensity and assignment are labeled with a "w."

DERIVED RESULTS

The inactive infra-red fundamentals are fairly well determined by several difference bands. ν_4^1 may be found as follows: (the parentheses about a frequency combination is used to denote an observed frequency or a derived fundamental):

$$(\nu_4^1)=(\nu_3)-(\nu_3-\nu_4^1)=613.35 \text{ cm}^{-1}$$
$$(\nu_4^1)=(\nu_1+\nu_5^1)-(\nu_1+\nu_5^1-\nu_4^1)=613.41 \text{ cm}^{-1}$$
$$(\nu_4^1)=(\nu_2+\nu_4^1+\nu_5^1)-(\nu_2+\nu_4^1+\nu_5^1-\nu_4^1)=613.75 \text{ cm}^{-1}$$
$$(\nu_4^1)=(\nu_5^1+2\nu_4^0)-(\nu_5^1+2\nu_4^0-\nu_4^1)=613.24 \text{ cm}^{-1}$$
$$(\nu_4^1)=(\nu_4^1+\nu_5^1)-(\nu_4^1+\nu_5^1-\nu_4^1)=612.69 \text{ cm}^{-1}.$$

The value 613.3 cm^{-1} has been chosen as the value of ν_4^1, but the evidence is that ν_4^1 is slightly higher than this. The two other infra-red inactive frequencies are determined as follows:

$$(\nu_2)=(\nu_2-\nu_5^1)+(\nu_5^1)=1974.0 \text{ cm}^{-1}$$

and

$$(\nu_1)=(\nu_1-\nu_5^1)+(\nu_5^1)=3373.2 \text{ cm}^{-1}.$$

The fundamental Raman frequencies are in good agreement with the frequencies given by other observers.[2]

TABLE IX. The $\nu_3+\nu_4^1$- and $\nu_2+2\nu_4^0+\nu_5^1$-band frequencies, see Fig. 10.

Line No.	$\nu_3+\nu_4^1$	$\nu_2+2\nu_4^0+\nu_5^1$	cm^{-1}	Line No.	$\nu_3+\nu_4^1$	$\nu_2+2\nu_4^0+\nu_5^1$	cm^{-1}
1		P (35)	3792.2	29		Q	3882.55
2		P (33)	3797.9	30	P (5)	R (1)	3886.8
3		P (31)	3803.6	31		R (2)	3889.8
4		P (29)	3809.1	32	P (3)	R (3)	3891.9
5		P (27)	3814.8	33	P (2)	R (4)	3894.1
6		P (26)	3817.7	34			3898.85
7		P (25)	3820.1	35	R (0)	R (7)	3901.1
8		P (24)	3822.6	36	R (1)	R (8)	3903.4
9		P (23)	3825.6	37	R (2)	R (9)	3905.7
10		P (22)	3827.3	38	R (3)	R (10)	3908.1
11		P (21)	3830.9	39	R (4)	R (11)	3910.2
12		P (20)	3833.2	40	R (5)	R (12)	3912.8
13		P (19)	3836.1	41	R (6)	R (13)	3914.7
14		P (18)	3638.7	42	R (7)		3917.0
15		P (17)	3841.3	43		R (15)	3918.7
16		P (16)	3843.4	44	R (9)		3921.7
17		P (15)	3846.3	45		R (17)	3922.8
18	P (20)	P (14)	3848.2	46	R (11)		3925.9
19	P (19)	P (13)	3851.2	47		R (19)	3927.0
20	P (18)	P (12)	3853.4	48	R (13)		3930.5
21	P (17)	P (11)	3856.2	49	R (15)		3934.1
22	P (16)	P (10)	3858.5	50	R (16)		3936.6
23	P (15)	P (9)	3861.2	51	R (17)		3938.8
24	P (13)	P (7)	3866.7	52	R (19)		3942.9
25			3868.4	53	R (20)		3944.9
26	P (11)	P (5)	3871.6	54	R (21)		3946.8
27		P (3)	3875.5	55	R (23)		3950.9
28	P (9)	P (2)	3877.8	56	R (25)		3954.8

TABLE X. The $\nu_1+\nu_5^1$-band frequencies, see Fig. 10.

Line No.	$\nu_1+\nu_5^1$	cm^{-1}	Line No.	$\nu_1+\nu_5^1$	cm^{-1}
100	P (33)	4007.9	127	P (3)	4085.8
101	P (31)	4013.4	128	Q	4092.56
102	P (30)	4015.9	129	R (1)	4097.4
103	P (29)	4018.5	130	R (2)	4099.9
104	P (28)	4021.2	131	R (3)	4102.0
105	P (27)	4023.9	132	R (4)	4104.1
106	P (26)	4027.0	133	R (5)	4106.6
107	P (25)	4029.7	134	R (6)	4108.8
108	P (24)	4032.2	135	R (7)	4110.9
109	P (23)	4034.7	136	R (8)	4113.1
110	P (22)	4037.6	137	R (9)	4115.3
111	P (21)	4040.3	138	R (10)	4117.5
112	P (20)	4042.7	139	R (11)	4119.8
113	P (19)	4045.5	140	R (12)	4121.9
114	P (18)	4048.1	141	R (13)	4124.1
115	P (17)	4050.8	142	R (14)	4126.0
116	P (16)	4053.4	143	R (15)	4128.0
117	P (15)	4055.9	144	R (16)	4130.2
118	P (14)	4058.5	145	R (17)	4132.4
119	P (13)	4061.0	146	R (18)	4134.4
120	P (12)	4063.3	147	R (19)	4136.5
121	P (11)	4066.2	148	R (21)	4140.35
122	P (10)	4068.7	149	R (23)	4144.5
123	P (9)	4071.0	150	R (25)	4148.1
124	P (7)	4076.3	151	R (27)	4152.1
125	P (6)	4078.2	152	R (29)	4156.2
126	P (5)	4080.9	153	R (31)	4159.9

Numerous anharmonic coefficients may be determined from these data. Table XII gives the relations used to obtain the values of some of the coefficients. Because of the inaccuracies of the measurements these anharmonic coefficients may have a large percentage error. The most serious difficulty which arises from a consideration of the anharmonic constants revolves about the assignment of the $2\nu_4^{2,0}+\nu_5^1$-band. The upper vibration level consists of two Π_u-components and a Φ_u-component. Both of the Π_u-components will be infra-red active in transitions from the ground state

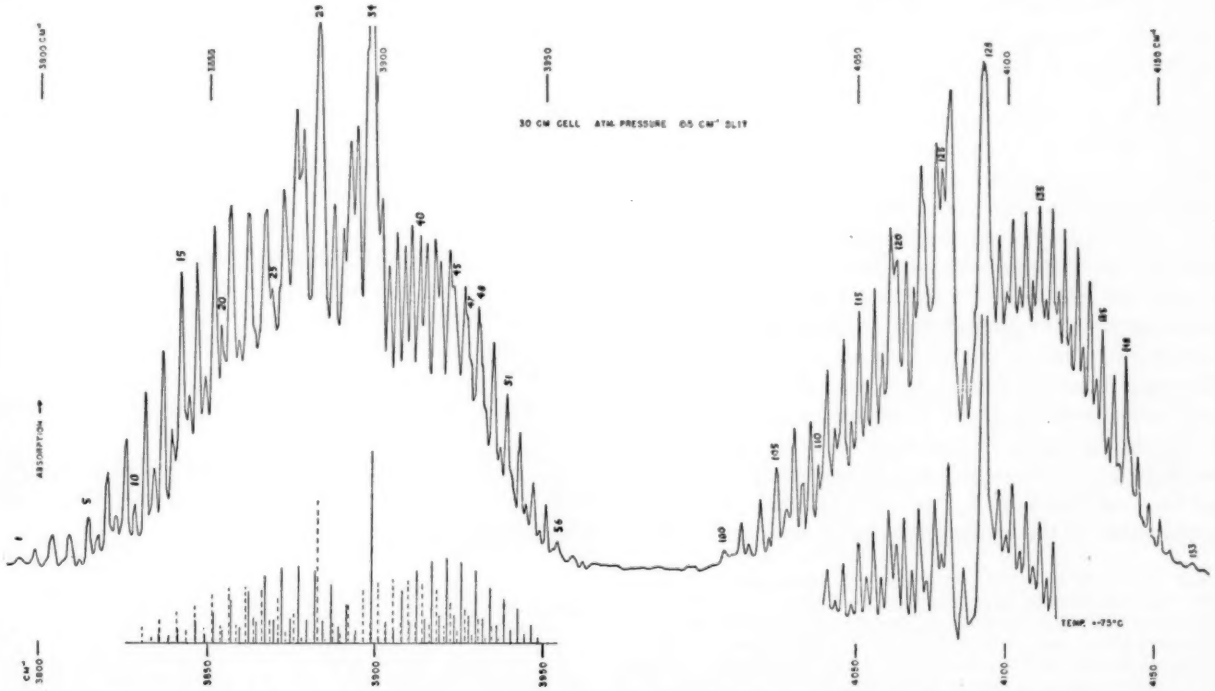

FIG. 10. The $\nu_3+\nu_4^1$-, $\nu_1+2\nu_4^{2,0}+\nu_5^1$-, $\nu_1+\nu_4^1+\nu_5^1-\nu_4^1$-, and $\nu^1+\nu_5^1$-bands of acetylene as measured with the 7500 lines per inch grating. The values of the line frequencies are given in Tables IX and X.

TABLE XI. Band assignments and frequencies.

Band	Band center cm^{-1}	Band frequency cm^{-1}	$B'-B''$ cm^{-1} or remarks	Figure
Fundamental bands				
ν_4^1	—	613.3	Derived	
ν_5^1	729.56	730.74		1
ν_2	—	1974.0	Derived	
ν_3	3285.5	3282.5	−0.0043	2
ν_1	—	3373.2	Derived	
Combination bands				
$\nu_4^1+\nu_5^1-\nu_4^1$	712.06(?)	715.49	$\Delta_u-\Pi_g$; w	1
$\nu_4^1+\nu_5^1-\nu_4^1$	716.67	715.49	Σ_u^-, $\Sigma_u^+-\Pi_g$	1
$2\nu_5^0-\nu_5^1$	720.27	719.09	w	1
$\nu_1-\nu_5^1$	1244.5	1243.3		3
$\nu_4^1+\nu_5^1$	1328.18	1327.18	+0.003	4
$2\nu_4^0+\nu_5^1-\nu_4^1$	1328.46	1328.46		4
$2\nu_4^0+\nu_5^1$	1940.52	1941.70	+0.0032	5
$2\nu_4^2+\nu_5^1$(?)	1960.66	1961.84		5
$3\nu_5^1$	2169.67	2170.84	+0.0020	6
$4\nu_5^0-\nu_5^1$	2152.0	2150.8		6
$4\nu_5^2-\nu_5^1$	2161.5	2165.0		6
$3\nu_4^1+\nu_5^1$	2556.5	2556.5		7
$\nu_1-\nu_5^1$	2643.69	2642.51		8
$\nu_3-\nu_4^1$	2670.33	2669.15		8
$\nu_2+\nu_4^1+\nu_5^1-\nu_4^1$	2683.09	2681.81		8
$\nu_2+2\nu_5^0-\nu_5^1$	2691.7	2690.5	w	8
$\nu_2+\nu_5^1$	2702.46	2703.63	−0.0079(?)	8
$\nu_3+\nu_4^1-\nu_4^1$	3270.9	3270.9	w	2
$\nu_2+2\nu_4^0+\nu_5^1-\nu_4^1$	3286.6	3286.6	w	2
$\nu_2+\nu_4^1+\nu_5^1$	3295.56	3295.56	−0.0050	2
$\nu_1+\nu_5^1-\nu_4^1$	3480.51	3480.51	−0.0068	9
$\nu_3+\nu_4^1$	3882.81	3883.97	−0.0067	10
$\nu_2+2\nu_4^0+\nu_5^1$	3898.81	3899.97	−0.0074	10
$\nu_1+\nu_4^1+\nu_5^1-\nu_4^1$(?)	4076.3	4079.7	$\Delta_u-\Pi_g$; w	10
$\nu_1+\nu_4^1+\nu_5^1-\nu_4^1$(?)	4080.86	4079.7	Σ_u^-, $\Sigma_u^+-\Pi_g$; w	10
$\nu_1+\nu_5^1$	4092.75	4093.92	−0.0078	10
$\nu_2+3\nu_5^1$	4140.35	4141.53	w	10
$(\nu_1+\nu_4^1+\nu_5^1-\nu_4^1)$	(4061.0)	(4059.9)	$(\Sigma_u^-, \Sigma_u^+-\Pi_g$; w)	10

TABLE XII. Evaluation of anharmonic coefficients.

		cm^{-1}
1:	$(\nu_4^1+\nu_5^1)-(\nu_4^1)-(\nu_5^1)=x_{45}$	$=-15.86$
2:	$(2\nu_4^0+\nu_5^1-\nu_4^1)-(\nu_4^1+\nu_5^1)=x_{45}+2x_{45}-2X_{44}$	$=+0.28$
3:	$(3\nu_4^1+\nu_5^1)-3(\nu_4^1)-(\nu_5^1)=3x_{45}+6x_{44}-2X_{44}$	$=-14.13$
4:	$(2\nu_4^0+\nu_5^1)-2(\nu_4^1)-(\nu_5^1)=2x_{45}+2x_{44}-2X_{44}$	$=-15.63$
5:	$(\nu_1+\nu_4^1+\nu_5^1-\nu_4^1)-(\nu_1+\nu_5^1)=x_{14}+x_{45}$	$=-14.22?(-34.02)$
6:	$(\nu_2+\nu_4^1+\nu_5^1-\nu_4^1)-(\nu_2+\nu_5^1)=x_{24}+x_{45}$	$=-21.82$
7:	$(\nu_2+\nu_5^1)-(\nu_2)-(\nu_5^1)=x_{25}$	$=-1.11$
8:	$(\nu_1+\nu_5^1)-(\nu_1)-(\nu_5^1)=x_{15}$	$=-10.02$
9:	$(\nu_3+\nu_4^1)-(\nu_3)-(\nu_4^1)=x_{34}$	$=-11.83$
10:	$(\nu_2+3\nu_5^1)-(\nu_2+\nu_5^1)-2(\nu_5^1)=2x_{25}+6x_{55}-2X_{55}$	$=-23.98$
11:	$(4\nu_5^0-\nu_5^1)-(3\nu_5^1)=6x_{55}-2X_{55}$	$=-20.04$
12:	$(4\nu_5^2-\nu_5^1)-(4\nu_5^0-\nu_5^1)=4X_{55}$	$=+14.2$
13:	$(\nu_2+3\nu_5^1)-(\nu_2)-(3\nu_5^1)=3X_{25}$	$=-3.31$
14:	$(3\nu_5^1)-3(\nu_5^1)=6x_{55}-2X_{55}$	$=-21.38$
15:	$(\nu_2+\nu_4^1+\nu_5^1)-(\nu_2)-(\nu_4^1+\nu_5^1)=x_{24}+x_{25}$	$=-6.62$

$x_{14}=+1.64?(-18.16)$ $x_{15}=-10.02$
$x_{24}=-5.96,\ -5.52$ $x_{25}=-1.1$
$x_{34}=-11.83$ $x_{45}=-15.86$
$x_{44}=+4.38$ $x_{55}=-2.17$
$X_{44}=-3.74$ $X_{55}=+3.55$

and the Π_u-components will differ by $2X_{44}$ cm^{-1} in vibrational energy. One would expect, therefore, that the two strong Q branches seen in Fig. 5 might be the $2\nu_4^0+\nu_5^1$, $(\Pi_u-\Sigma_g^+)$, at 1940.52 cm^{-1}, and $2\nu_4^2+\nu_5^1$, $(\Pi_u-\Sigma_g^+)$, at 1960.66-cm^{-1}, bands with a separation $4X_{44}=+20.14$ cm^{-1}. The evaluation of $4X_{44}$ from other bands gives a value of -15 cm^{-1}. An interchange of the assignments of these two bands would give $4X_{44}=-20.14$ cm^{-1}. This interchange would also demand that the 1328.46-cm^{-1} Q branch should belong to $2\nu_4^2+\nu_5^1-\nu_4^1$ because the 1941.70-cm^{-1} frequency must arise from a transition from the ground state to the upper level of the 1328.46-cm^{-1} band. (ν_4^1 is well established by other difference bands as 613.3 cm^{-1}, and the 1328.46-cm^{-1} band is quite evidently a difference band with $V_4=1$ in the initial state.) The result of this interchange would be an evaluation of $4X_{44}$ from bands other than $2\nu_4^{2,0}+\nu_5^1$ of +7.5 cm^{-1}. Even a $4B$ change in the assigned value of the center of $3\nu_4^1+\nu_5^1$, see Fig. 7, which is used in this computation, would not improve the situation. The fact that only one band of the type $2\nu_4^{2,0}+\nu_5^1-\nu_4^1$ appears in the 7.5μ region, see Fig. 4, is also strange.

The interchange of the assignments of ν_3 and $\nu_2+\nu_4^1+\nu_5^1$ would necessitate the interchange in the assignments of $\nu_3-\nu_4^1$ and $\nu_2+\nu_4^1+\nu_5^1-\nu_4^1$ because of the known value of ν_4^1. The band $\nu_2+\nu_5^1$ seems well established, however, as the only temperature-insensitive band in the 2700-cm^{-1} region. The resulting value of the anharmonic constant x_{24}, through relation No. 6 in Table XII, would be -18.62 cm^{-1}. This reasonably small value for the anharmonic constant x_{24}, a likewise small value from x_{34} from relation No. 9 in Table XII, and a reasonably consistent value of x_{25} from relations Nos. 13 and 15 would not prevent an interchange of the assignments of ν_3 and $\nu_2+\nu_4+\nu_5^1$. The fact that ν_3 is less intense than $\nu_2+\nu_4^1+\nu_5^1$, that $\nu_3+\nu_4^1$ is less intense than $\nu_2+2\nu_4^0+\nu_5^1$, and that $\nu_3-\nu_4^1$ is less intense than $\nu_2+\nu_4^1+\nu_5^1-\nu_4^1$ is not taken as sufficient evidence in itself to warrant an interchange of the assignments as previously given.

The value of B'' as determined by the combination principles from the data in any of these bands will be poor because of the fact that all bands are more or less spoiled by the overlapping of other bands. The data from the cooled gas run, Fig. 4, curve C, were used to obtain a value $B''=1.1769$ cm^{-1}. This is in good agreement with previously obtained values. The values of $B'-B''$ which were obtained are given in Table XI. Needless to say, we cannot place much faith in these values.

Mr. Bell would like to acknowledge the help received from the National Research Council which enabled him to carry on this research.

The Third Virial Coefficient for Non-Polar Gases

R. Byron Bird, Ellen L. Spotz, and J. O. Hirschfelder
Naval Research Laboratory and Department of Chemistry University of Wisconsin

(Received July 10, 1950)

The third virial coefficient for non-polar gases has been calculated with great accuracy by means of punched-card techniques. The Lennard-Jones potential, with inverse twelfth-power repulsion and inverse sixth-power attraction, was used in the calculations. Excellent agreement between our computations and those of Kihara was obtained at very high temperatures; in the moderate temperature region our calculations agree moderately well with those of Montroll and Mayer and those of de Boer and Michels. A comparison with experimental data indicates fairly good agreement for the approximately spherical molecules argon, methane, and nitrogen. In other cases there are discrepancies suggesting deviations from the form of the interaction energy which we assumed. There is considerably difficulty in obtaining accurate third virial coefficients from the equation of state data. A method is suggested whereby the third virial coefficients for mixtures of gases may be estimated. The functions which are tabulated should be particularly useful for extrapolating the equation of state to very high temperatures, where no experimental data are available. The zero-pressure derivative of the Joule-Thomson coefficient with respect to pressure provides additional means for comparing our tabulated functions with experimental data, and the deviations are consistent with those discovered by comparison of the third virial coefficients themselves.

A. CALCULATION OF THE THIRD VIRIAL COEFFICIENT FOR PURE GASES

THE third virial coefficient, $C(T)$, is the temperature-dependent coefficient of the V^{-2} term in the expansion of the compressibility:

$$pV/RT=1+B(T)/V+C(T)/V^2+\cdots \qquad (1)$$

By statistical mechanics[1] or the kinetic theory of gases[2] it is possible to show how $C(T)$ depends upon the intermolecular potential energy, $E(r)$. For our calculations we have used the Lennard-Jones potential:

$$E(r)=4\epsilon[(r_0/r)^{12}-(r_0/r)^6] \qquad (2)$$

in which ϵ is the maximum energy of attraction and r_0 is that value of the intermolecular separation, r, for which $E(r)=0$. These parameters may be obtained from experimental second virial or transport coefficient data (see reference 4). A substantial justification for the use of Eq. (2) is the excellent agreement which is obtained between experimental values of the transport coefficients and those calculated no the basis of the Lennard-Jones potential.[3–8]

There have been in the past three evaluations of the third virial coefficient for the Lennard-Jones potential; the results of these calculations, as well as our own, are pictured in Fig. 1. de Boer and Michels,[2] using their expression for the third virial coefficient derived from the pair distribution function, performed a very careful graphical integration over that temperature range where experimental data were available,—i.e., from $\tau=1$ to $\tau=4$ (τ is the reduced temperature obtained by dividing the temperature in °K by ϵ/k). Montroll and Mayer[9] performed a numerical integration over approximately the same range, using a form of the integral which involves rapidly oscillating integrands and does not seem to us to be particularly adaptable for numerical integration. Although the integrals used by de Boer and Michels can be shown to be mathe-

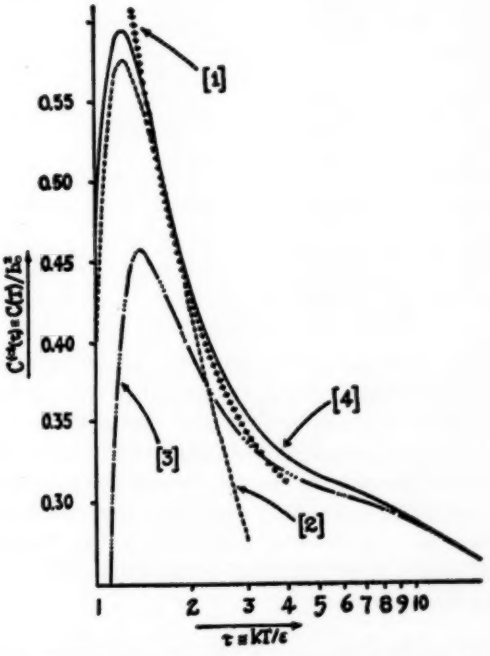

FIG. 1. Comparison of calculated curves of the third virial coefficient. (1) Calculation of de Boer and Michels from pair distribution function; (2) calculation of Montroll and Mayer from statistical mechanics; (3) calculation of Kihara using series expansion technique; and (4) punched-card calculations described in this work. Curves (3) and (4) agree almost exactly above $\tau=10$.

[1] J. E. Mayer and M. G. Mayer, *Statistical Mechanics* (John Wiley and Sons, Inc., New York, 1940).
[2] J. de Boer and A. Michels, Physica **6**, 97 (1939).
[3] Hirschfelder, Bird, and Spotz, J. Chem. Phys. **16**, 968 (1948).
[4] Hirschfelder, Bird, and Spotz, Chem. Rev. **44**, 205 (1949).
[5] K. E. Grew, J. Chem. Phys. **18**, 149L (1950).
[6] E. R. S. Winter, Trans. Faraday Soc. **46**, 81 (1950).
[7] M. Kotani, Proc. Phys. Math. Soc. Japan, **24**, 76 (1942).
[8] T. Kihara and M. Kotani, Proc. Phys. Math. Soc. Japan **25**, 602 (1944).
[9] E. W. Montroll and J. E. Mayer, J. Chem. Phys. **9**, 626 (1941).

TABLE I. A tabulation of the third virial coefficient and its derivatives for the Lennard-Jones potential.

$\tau = kT/\epsilon \qquad b_0 = (2/3)\pi N r_0^3$

$C(T) = b_0^2 C^{(0)}(\tau)$

$C^{(1)}(\tau) = \tau [dC^{(0)}/d\tau] \quad C^{(2)}(\tau) = \tau^2 [d^2C^{(0)}/d\tau^2]$

(Note: Values of $C^{(0)}$ which are marked with an asterisk * were calculated by punched-card methods; intermediate values were obtained by interpolation. $C^{(1)}$ and $C^{(2)}$ were obtained by differentiation of the interpolating functions.)

τ	$C^{(0)}(\tau)$	$C^{(1)}(\tau)$	$C^{(2)}(\tau)$
0.70	−3.37664*	28.68	−220
0.75	−1.79197	18.05	−140
0.80	−0.84953	11.60	−92.1
0.85	−0.27657	7.561	−62.1
0.90	+0.07650	4.953	−42.7
0.95	0.29509	3.234	−29.8
1.00	0.42966*	2.078	−21.0
1.05	0.51080	1.292	−14.9
1.10	0.55762	0.7507	−10.6
1.15	0.58223	0.3760	−7.52
1.20	0.59240*	+0.1159	−5.29
1.25	0.59326	−0.0646	−3.66
1.30	0.58815	−0.1889	−2.46
1.35	0.57933	−0.2731	−1.57
1.40	0.56831*	−0.3288	−0.910
1.45	0.55611	−0.3641	−0.420
1.50	0.54339	−0.3845	−0.050
1.55	0.53059	−0.3943	+0.224
1.60	0.51803*	−0.3963	0.427
1.65	0.50587	−0.3929	0.572
1.70	0.49425	−0.3858	0.680
1.75	0.48320	−0.3759	0.755
1.80	0.47277	−0.3643	0.806
1.85	0.46296	−0.3516	0.837
1.90	0.45376	−0.3382	0.854
1.95	0.44515	−0.3245	0.859
2.00	0.43710*	−0.3109	0.856
2.10	0.42260	−0.2840	0.830
2.20	0.40999	−0.2588	0.794
2.30	0.39900	−0.2355	0.749
2.40	0.38943	−0.2142	0.700
2.50	0.38108*	−0.1950	0.651
2.60	0.37378	−0.1777	0.602
2.70	0.36737	−0.1621	0.557
2.80	0.36173	−0.1482	0.514
2.90	0.35675	−0.1358	0.473
3.00	0.35234*	−0.1247	0.439
3.10	0.34842	−0.1148	0.400
3.20	0.34491	−0.1060	0.369
3.30	0.34177	−0.09826	0.340
3.40	0.33894	−0.09133	0.313
3.50	0.33638	−0.08510	0.288
3.60	0.33407	−0.07963	0.266
3.70	0.33196	−0.07462	0.246
3.80	0.33002	−0.07024	0.277
3.90	0.32825	−0.06634	0.210
4.00	0.32662*	−0.06286	0.194
4.10	0.32510	−0.05989	0.183
4.20	0.32369	−0.05709	0.169
4.30	0.32238	−0.05458	0.156
4.40	0.32115	−0.05237	0.145
4.50	0.32000	−0.05040	0.134
4.60	0.31891	−0.04865	0.125
4.70	0.31788	−0.04712	0.116
4.80	0.31690	−0.04579	0.108
4.90	0.31596	−0.04461	0.100
5.0	0.31508*	−0.04359	0.0934
6.0	0.30771*	−0.03893	0.0449
7.0	0.30166	−0.03989	0.0258
8.0	0.29618*	−0.04231	0.0192
9.0	0.29103	−0.04529	0.0183
10.0	0.28610*	−0.04825	0.0199
20.0	0.24643*	−0.06437	0.0502
30.0	0.21954	−0.06753	0.0654
40.0	0.20012	−0.06714	0.0717
50.0	0.18529*	−0.06566	0.0742
60.0	0.17347	−0.06388	0.0750
70.0	0.16376	−0.06203	0.0748
80.0	0.15560	−0.06025	0.0741
90.0	0.14860	−0.05857	0.0732
100.0	0.14251*	−0.05700	0.0722
200.0	0.10679	−0.04599	0.0619
300.0	0.08943	−0.03970	0.0547
400.0	0.07862*	−0.03551	0.0496

matically equivalent,[10,11] their numerical results are somewhat different. A third calculation was performed by Kihara,[12] who employed a very clever series expansion technique, somewhat analogous to the method used by Lennard-Jones in his integration of the second virial coefficient; this interesting approach was called to our attention as the present work was being concluded. Kihara shows how the third virial coefficient may be written in the form:

$$C(T) = r_0^6 \sum_{j=0}^{\infty} K_j \tau^{-(j+1)/2}. \tag{3}$$

The K_j are complicated double integrals which are temperature-independent; however, for j-values beyond about $j=12$, the integrals admit analytic evaluation. Between $\tau=1$ and $\tau=4$, Kihara's results are not in agreement with the other calculations; this disagreement is probably due to the fact that the K_j were not evaluated with a high degree of accuracy. In the high temperature region (from $\tau=10$ to $\tau=100$), Kihara's equation gives values for $C(T)$ which agree almost perfectly with our punched-card calculations.

From statistical mechanics[1] it can be shown that the third virial coefficient, for gases composed of monotomic molecules with spherical potential fields, is given by the integral:

$$C(T) = -(1/3V) \int \cdots \int f_{12} f_{23} f_{31} d\omega_1 d\omega_2 d\omega_3 \tag{4}$$

in which $f_{ij} = [\exp(-E(r_{ij})/kT) - 1]$, the r_{ij} represent the intermolecular distances in a cluster of three colliding molecules, and the $d\omega_i$ are the cartesian coordinates of the ith molecule. In the derivation of this ex-

[10] R. B. Bird, Ph.D. thesis, University of Wisconsin (1950).
[11] R. B. Bird and E. L. Spotz, University of Wisconsin CM-599, Project NOrd 9938 (10 May 1950).
[12] T. Kihara, J. Phys. Soc. Japan, 3, 265 (1948).

pression the force between any two molecules is assumed to be independent of the location of the third molecule in the cluster. For the purpose of punched-card calculations, it was found convenient to transform the integral in Eq. (6) into the form:

$$C(T)/b_0^2=C^{(0)}(\tau)=18M(\tau)-6[L(\tau)]^3 \quad (5)$$

in which

$$b_0=\tfrac{2}{3}\pi N r_0^3; \quad \tau=kT/\epsilon \quad (6)$$

$$M(\tau)=\int_0^\infty\int_0^\infty g(\tau,z_1)g(\tau,z_2)Q[\tau,(z_1+z_2)]dz_1dz_2 \quad (7)$$

$$Q(\tau,w)=\int_w^\infty g(\tau,z)dz \quad (8)$$

$$L(\tau)=Q(\tau,0)=\int_0^\infty g(\tau,z)dz \quad (9)$$

$$g(\tau,z)=z[\exp(-E(z)/kT)-1]. \quad (10)$$

The integration variables, z_i, are the intermolecular distances expressed in units of r_0. The integration of $L(\tau)$ can be accomplished analytically:

$$L(\tau)=\sum_{j=0}^{\infty}(12j!)^{-1}\Gamma[(3j-1)/6](4/\tau)^{(3j+1)/6}. \quad (11)$$

The summation converges quite rapidly, particularly at high temperatures, and can be evaluated by punched-card methods in several steps. No integration of the M-integral in closed form was discovered; hence, standard numerical cubature techniques were employed, the integrand being evaluated essentially at 10,000 points on the z_1z_2-plane for 17 values of the reduced temperature. The occurrence only of the functions g and Q and their symmetrical appearance in the M-integral made the form of the third virial coefficient given in Eq. (5) particularly well-suited for numerical integration by punched-card methods; in this work, IBM's 602-A (Calculating Punch) and auxiliary equipment were used. Details of the calculations have been given elsewhere.[10,11]

In Table I are presented our values of the third virial coefficient and its temperature derivatives for over seventy values of the reduced temperature, τ, from $\tau=0.7$ to $\tau=400$. The functions tabulated are $C^{(0)}$, $C^{(1)}$, and $C^{(2)}$; $C^{(0)}$ was defined in Eq. (5), and $C^{(1)}$ and $C^{(2)}$ are defined by:

$$C^{(j)}(\tau)=\tau^j[d^jC^{(0)}/d\tau^j] \quad j=1,2. \quad (12)$$

The mechanical accuracy of the $C^{(j)}$-functions is approximately: $C^{(0)}$, 1 part in 5000; $C^{(1)}$, 1 part in 1000; and $C^{(2)}$, 1 part in 500. The seventeen values of $C^{(0)}$ which were calculated by punched-card methods are marked with asterisks in Table I. The intermediate values of $C^{(0)}$ were obtained by interpolation. The tables of $C^{(1)}$ and $C^{(2)}$ were then prepared by differentiating the interpolating functions.

B. COMPARISON OF CALCULATED AND EXPERIMENTAL THIRD VIRIAL COEFFICIENTS

A comparison of the calculated third virial coefficients with the experimental values of Michels and coworkers is given in Table II and summarized graphically in Fig. 2. The "experimental values" of $C(T)$ listed in Table II are obtained in the following manner: one fits the experimental values of pV/RT with a power series in $(1/V)$ like that shown in Eq. (1), using, however, only a finite number of terms in the curve fit; the coefficient of the $(1/V^2)$-term is then assumed to be the third virial coefficient. Different values of $C(T)$ are of course obtained when polynomials of different degrees are used to represent the compressibility; the degrees of the polynomial curve fits for the various gases are indicated in Table II.

Because of the sensitivity of the third virial coefficient to the assumed form of the potential, discrepancies between calculated and experimental results were expected. Fairly satisfactory agreement was found for the approximately spherical molecules argon, methane, and nitrogen; the calculated values of $C(T)$ for the cylindrical molecules carbon dioxide, ethylene, and ethane are in marked disagreement with the experimental values; also, for the light gases hydrogen, deuterium, and helium distinct discrepancies are observed. We shall now discuss more fully the gases studied, in decreasing order of goodness of agreement.

(a) Argon, Methane, and Nitrogen (Fairly Good Agreement)

For these gases reasonably satisfactory agreement between calculated and experimental results can be re-

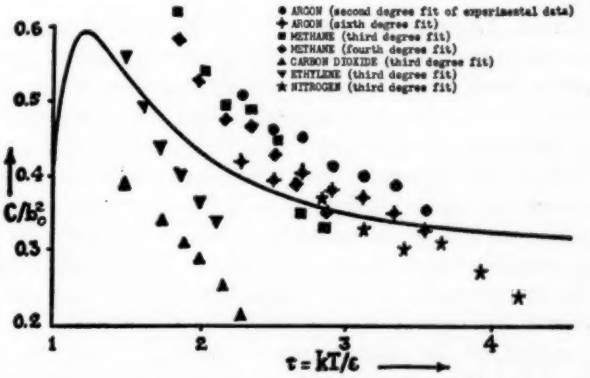

FIG. 2. Comparison of experimental third virial coefficients with values calculated from the Lennard-Jones potential. Reduced third virial coefficients are plotted against reduced temperatures, the basis for the reduction being the force constants, r_0 and ϵ/k, derived from experimental second virial coefficients. The solid curve represents the function $C^{(0)}(\tau)$ tabulated in Table I. The experimental points are represented by the symbols as shown in the legend on the figure. Not shown are the experimental points for ethane (which are large and negative) and those for hydrogen, deuterium and helium (which are available only for very high values of the reduced temperature).

TABLE II. Comparison of calculated and experimental second and third virial coefficients. The force constants used were obtained from experimental second virial coefficients. The number in parenthesis following B_{exp} and C_{exp} indicates the degree of the polynomial which was used to fit the experimental data. The units of the various quantities concerned are: r_0(A), ϵ/k(°K), b_0(cm³/mole), $B(T)$(cm³/mole), and $C(T)$(cm⁶/mole²).

Gas (Force Consts.)	T(°C) →	0	25	50	75	100	125	150
Argon[a]	$B_{exp}(2)$	−21.45	−15.75	−11.24	−7.25	−4.00	−1.18	1.38
	$B_{exp}(6)$	−21.12	−15.48	−11.05	−7.14	−3.89	−1.08	1.42
r_0= 3.405	B_{calc}	−21.49	−15.93	−11.16	−7.28	−3.98	−1.14	1.31
b_0= 49.804								
ϵ/k=119.75	$C_{exp}(2)$	1270	1160	1130	1040	1000	970	880
	$C_{exp}(6)$	1050	990	1020	960	920	880	830
	C_{calc}	990	950	910	880	860	850	830
Methane[b]	$B_{exp}(3)$	−54.1	−43.4	−34.7	−27.9	−21.7	−16.1	−11.5
	$B_{exp}(4)$	−53.9	−43.3	−34.6	−27.7	−21.6	−16.4	−11.6
r_0= 3.817	B_{calc}	−53.9	−43.4	−34.7	−27.5	−21.3	−16.1	−11.6
b_0= 70.16								
ϵ/k=148.2	$C_{exp}(3)$	3050	2620	2430	2410	2230	1750	1660
	$C_{exp}(4)$	2870	2620	2370	2340	2140	2000	1770
	C_{calc}	2290	2140	2030	1940	1870	1810	1770
Nitrogen[c, d]	$B_{exp}(3)$	−10.3	−4.71	−0.28	3.20	6.56	9.45	12.3
	B_{calc}	−10.1	−4.71	−0.27	3.42	6.56	9.25	11.6
r_0= 3.698								
b_0=63.78	$C_{exp}(3)$	1540	1320	1220	1260	1080	960	690
ϵ/k=95.05	C_{calc}	1460	1410	1380	1350	1330	1317	1300
Carbon dioxide[e, f]	$B_{exp}(3)$	−151.2	−123.6	−103.5	−86.7	−73.7	−62.2	−52.2
	B_{calc}	−147.3	−123.4	−104.1	−87.5	−74.1	−62.2	−52.1
r_0= 4.486								
b_0=113.9	$C_{exp}(3)$	5610	4930	4930	4430	4150	3620	3050
ϵ/k=189	C_{calc}	7230	6790	6390	6020	5730	5470	5260
Ethylene[g]	$B_{exp}(3)$		−140.6	−118.1	−99.9	−85.1	−72.6	−62.1
	B_{calc}		−139.3	−118.1	−100.3	−85.4	−72.6	−61.7
r_0= 4.507								
b_0=115.5	$C_{exp}(3)$		7640	6740	6000	5470	4990	4670
ϵ/k=199.2	C_{calc}		7260	6840	6450	6120	5830	5600
Hydrogen*[h]	$B_{exp}(2)$†	13.7	13.8	14.2	14.8	14.7	14.9	15.1
	$B_{exp}(2)$‡	13.8	14.1	14.6	14.9	15.2	15.4	15.6
r_0= 2.92	$B_{exp}(3)$	13.5	13.6	13.9	14.1	14.5	14.3	14.5
b_0=31.409	B_{calc}**	13.6	14.2	14.7	15.1	15.3	15.4	15.5
ϵ/k=36.77								

ported. The experimental $C(T)$ values for argon and methane are somewhat higher than the calculated ones, while those for nitrogen are somewhat lower. For all three gases, the experimental points seem to exhibit a somewhat steeper slope than the calculated curve. This is also consistent with the disagreements between calculated and experimental Joule-Thomson coefficients, as will be discussed presently. This discrepancy is probably due to the incorrectness of the assumed form for the potential. If the experimental data were sufficiently accurate we could use the discrepancy as a function of the temperature to determine the correct shape of the potential. However, in the present case only qualitative conclusions can be formulated.*[13]

(b) Carbon Dioxide, Ethylene, and Ethane (Poor Agreement for Ellipsoidal Molecules)

Even in the second virial coefficient (which is relatively insensitive to the form of the potential), the ellipsoidal nature of molecules is evident, for the curvature of the observed $B(T)$ curve is somewhat different from that of the theoretical one (which is based on spherical molecules). Corner[14] has shown that the curvature of the theoretical curve may be made more nearly like the experimental one by using the Lennard-Jones potential, but essentially taking into account the fact that the force constants must be functions of the orientations of the pairs of colliding molecules. Thus, force constants obtained by fitting the experimental second virial data with the values of $B(T)$ obtained from the Lennard-Jones potential are really "average" force

* Kihara, see reference 12, has suggested that perhaps the potential function should have a slightly steeper repulsive region and that the "soup-bowl" part of the function (i.e., that portion of the curve representing negative potential energy of interaction) should be a little wider. He arrived at this conclusion because the experimental $C(T)$ curves seem to resemble more the shape of the $C(T)$ curve which one obtains for a square-well potential (reference 13)—which has an infinitely steep repulsion and a very wide "soup-bowl."

However, the square-well potential is so far from reality that it is difficult to evaluate the strength of this argument.

[13] T. Kihara, Nippon Sugaku-Buturigakukaisi **17**, 11 (1943) (In Japanese).

[14] J. Corner, Proc. Roy. Soc. **A192**, 275 (1948).

TABLE II.—*Continued*

Gas (Force Consts.)	T(°C) →	0	25	50	75	100	125	150
	$C_{exp}(2)$†	(420)	(660)	(690)	(530)	(710)	(690)	(760)
	$C_{exp}(2)$‡	420	410	400	390	380	370	350
	$C_{exp}(3)$	(920)	(1160)	(1110)	(1420)	(960)	(1500)	(1410)
	C_{calc}**	300	290	290	290	280	280	280
Deuterium*[j]	$B_{exp}(2)$†	13.0	13.5	13.8	14.2	14.4	14.8	14.8
	$B_{exp}(2)$‡	13.2	13.8	14.2	14.7	14.9	15.1	15.4
r_0= 2.92	$B_{exp}(3)$	13.0	13.2	12.9	13.2	13.6	13.9	14.2
b_0=31.409	B_{calc}**	13.0	13.7	14.2	14.6	14.9	15.0	15.2
ϵ/k=36.77								
	$C_{exp}(2)$†	(710)	(780)	(800)	(820)	(830)	(850)	(870)
	$C_{exp}(2)$‡	390	390	380	370	360	360	350
	$C_{exp}(3)$	(2250)	(950)	(2140)	(2340)	(1900)	(1820)	(1730)
	C_{calc}**	300	290	290	290	280	280	280
Helium*[k]	$B_{exp}(3)$	11.9	11.7	11.6	11.4	11.3	11.2	11.1
	B_{calc}**	11.6	11.6	11.5	11.4	11.3	11.3	11.2
r_0= 2.56								
b_0=21.165	$C_{exp}(3)$	76	72	72	95	91	94	110
ϵ/k=10.16	C_{calc}**	102	99	97	94	93	90	89
Ethane[m]	$B_{exp}(2)$	−200	−135	−126				
	B_{calc}	−161	−138	−118				
r_0= 3.954								
b_0= 78	$C_{exp}(2)$	−37300	−72100	−30900				
ϵ/k=243	C_{calc}	+3464	+3607	+3546				

* Force constants given by de Boer and Michels, Physica **5**, 945 (1938); these constants were obtained by taking into account quantum effects.
** Quantum effects were taken into account in the calculation of B but *not* for the calculation of C.
† Quadratic fit good in range from 9–31 amagat density units.
‡ Quadratic fit good in range from 9–132 amagat density units, probably the best fit for purposes of comparison with the calculated results.
[a] Michels, Wijker, and Wijker, Physica **15**, 627 (1949).
[b] A. Michels and G. W. Nederbragt, Physica **2**, 1000 (1935).
[c] Michels, Wouters, and de Boer, Physica, **1**, 587 (1934).
[d] Michels, Wouters, and de Boer, Physica **3**, 585 (1936).
[e] A. Michels and C. Michels, Proc. Roy. Soc. **A153**, 201 (1936).
[f] A. Michels and C. Michels, Proc. Roy. Soc. **A160**, 348 (1937).
[g] A. Michels and M. Geldermans, Physica **9**, 967 (1942).
[h] A. Michels and M. Goudeket, Physica **8**, 347 (1941).
[i] A. Michels and M. Goudeket, Physica **8**, 353 (1941).
[k] A. Michels and H. Wouters, Physica **8**, 923 (1941).
[m] A. Michels and G. W. Nederbragt, Physica **6**, 656 (1939).

constants—averaged in the sense of two body collisions. Similarly fitting the experimental $C(T)$ values with the functions in Table I would give a set of "average" force constants—averaged in the sense of three-body collisions (we shall call these r_{0c} and ϵ_c/k). There is no reason why the two sets of average force constants should be the same. Figure 2 shows a comparison between calculated and experimental third virial coefficients based on the force constants, ϵ/k and r_0, determined from the experimental second virial coefficients. A simple translation of the experimental points upward and to the left would bring them into substantial agreement with the theoretical curve. This indicates that the ellipsoidal molecules at high pressures behave as though r_0 were slightly smaller and ϵ/k were slightly larger. Or, in other words, the third virial coefficient integral emphasizes three-molecule collisions in which the molecules are lined up with their long axes more or less parallel.

This tendency towards alignment has previously been discussed by Hirschfelder *et al.*,[15] who have pointed out that such a phenomenon explains why b_0 is anomalously large for ellipsoidal molecules. For many non-polar, spherical molecules, $b_0 \doteq 0.68 V_c$[16,17] (V_c is the critical volume in the same units as b_0). For ellipsoidal molecules, however, the b_0 values obtained from second virial coefficient data are considerably larger than $0.68 V_c$; this is explainable, since in the critical state the ellipsoidal molecules are packed together like cigars while in the dilute gas the molecules sweep out spherical cavities the diameters of which correspond to the length of the long axis of the molecule.

Consequently in order to use Table I for making the second pressure correction to the equation of state for gases composed of ellipsoidal molecules, the set of force constants, r_{0c}, and ϵ_c/k should be employed. The values of these force constants (along with the values of the

TABLE III. Force constants from second and third virial coefficients for ellipsoidal molecules.

Gas	b_0/V_c	Force constants from second virial coefficients r_0	ϵ/k	Force constants from third virial coefficients r_{0c}	ϵ_c/k
Carbon dioxide	1.25	4.486	189	4.11	221
Ethylene	0.92	4.507	199.2	4.30	211

[15] Hirschfelder, McClure, Curtiss, and Osborne, NDRC Report No. A-116 (November 22, 1942).

[16] Buehler, Wentorf, Hirschfelder, and Curtiss, University of Wisconsin CM-565, Project NOrd 9938 (3 February 1950).

[17] J. E. Lennard-Jones and A. F. Devonshire, Proc. Roy. Soc. **A165**, 1 (1938).

TABLE IV. Tabulation of the function, $A(\tau)$, for estimating third virial coefficients for gaseous mixtures.

$(C_{ijk})_{L.J.} = (C_{ijk})_{S.W.} A(\tau_{ij}) A(\tau_{jk}) A(\tau_{ik})$

τ	$A(\tau)$	τ	$A(\tau)$
1.00	0.71099	3.50	0.86275
1.05	0.74603	3.60	0.86259
1.10	0.76746	3.70	0.86233
1.15	0.78196	3.80	0.86198
1.20	0.79246	3.90	0.86157
1.25	0.80047	4.00	0.86109
1.30	0.80684	4.10	0.86055
1.35	0.81206	4.20	0.85996
1.40	0.81649	4.30	0.85931
1.45	0.82032	4.40	0.85863
1.50	0.82369	4.50	0.85792
1.55	0.82671	4.60	0.85717
1.60	0.82947	4.70	0.85640
1.65	0.83199	4.80	0.85560
1.70	0.83432	4.90	0.85478
1.75	0.83648	5.00	0.85394
1.80	0.83851	6.00	0.84502
1.85	0.84041	7.00	0.83580
1.90	0.84219	8.00	0.82692
1.95	0.84388	9.00	0.81857
2.00	0.84545	10.0	0.81075
2.10	0.84834	20.00	0.75449
2.20	0.85091	30.0	0.71957
2.30	0.85315	40.0	0.69443
2.40	0.85510	50.0	0.67488
2.50	0.85678	60.0	0.65893
2.60	0.85823	70.0	0.64549
2.70	0.85944	80.0	0.63391
2.80	0.86043	90.0	0.62374
2.90	0.86123	100.0	0.61468
3.00	0.86185	200.0	0.55663
3.10	0.86231	300.0	0.52415
3.20	0.86261	400.0	0.50186
3.30	0.86278		
3.40	0.86283		

ratio b_0/V_c) for several ellipsoidal molecules are given in Table III. While these choices of force constants (r_{0c} and ϵ_c/k) are by no means unique, these values would probably be more proper for extrapolation to high temperatures than those obtained from the second virial coefficient.

It is interesting to note the negative values of the third virial coefficient of ethane as given in Table II. No other experimental data is known to the authors which substantiate the negative region of the theoretical $C(T)$ curve. The values for ethane correspond to third virial force constants which differ from the second virial ones in the same manner as in the case of CO_2 and other cigar-shaped molecules. Unfortunately there are not enough experimental data to determine r_{0c} and ϵ_c/k for ethane.

(c) Hydrogen, Deuterium, and Helium (Poor Agreement)

For these molecules it is known from the direct quantum-mechanical calculation of the interaction potential, that the energy of repulsion does not increase as rapidly with decreasing separation as would be indicated by our inverse twelfth power.[18–20] Furthermore, the quantum correction to the third virial coefficients may not be negligible for the temperature range under consideration. On these accounts the poor agreement with out calculations is not surprising.

In the case of hydrogen and deuterium there was considerable difficulty in obtaining the third virial coefficients from the raw experimental data. Different methods of fitting the experimental values led to values of $C(T)$ differing by several hundred percent. On this account the difference between the third virial coefficients of H_2 and D_2 cannot be used to determine the quantum corrections quantitatively; however, the third virial coefficient values for D_2 would seem to be roughly 10 percent smaller than for H_2 at 0°C and about equal to 150°C.

It is difficult to interpret the comparison for helium given in Table II. The experimental third virial coefficients have a distinct upward trend, while the calculated $C(T)$ values are monotone decreasing; the two sets of values are of very nearly the same order of magnitude. The unusually high values of the experimental third virial coefficients in the third-degree polynomial fit for the four highest temperatures may be related to the fact that the corresponding experimental fourth virial coefficients (as given by the series fit) are given as negative. According to Mayer[1] and Harrison[21] the fourth virial coefficient must be positive in this temperature region; the curve-fitting which produces a negative fourth virial coefficient would tend to distort the third virial coefficient values. Similar behavior has been noted in connection with the curve-fitting of the data for other gases.

C. THE THIRD VIRIAL COEFFICIENT FOR MIXTURES OF GASES

For a mixture of f components, the third virial coefficient is given by:[22]

$$C(T)_{\text{mixture}} = \sum_{u=1}^{f} \sum_{v=1}^{f} \sum_{w=1}^{f} C_{uvw}(T) x_u x_v x_w \qquad (13)$$

in which x_u is the mol fraction of the uth component. The functions $C_{uvw}(T)$ are third virial coefficients calculated on the basis of clusters of three colliding molecules, 1, 2, 3, of chemical species u, v, w respectively. The separation between molecules 1 and 2 is r_{12} and the potential energy of interaction between them is $E^{uv}(r_{12})$, the superscript "uv" indicating that the potential energy depends upon the chemical species of the molecules 1 and 2. Then if we define $f_{12}{}^{uv}$ by the relation:

$$f_{12}{}^{uv} = \{\exp[-E^{uv}(r_{12})/kT] - 1\} \qquad (14)$$

[18] J. C. Slater, Phys. Rev. **32**, 349 (1928).
[19] G. Gentile, Zeits. f. Physik **63**, 795 (1930).
[20] J. de Boer, Physica **9**, 363 (1942).
[21] S. C. F. Harrison, doctoral dissertation, Johns Hopkins University (1938).
[22] J. E. Mayer, J. Phys. Chem. **43**, 71 (1939).

we can write, analogously to Eq. (4):

$$C_{uvw}=-(1/3V)\int\cdots\int f_{12}{}^{uv}f_{23}{}^{vw}f_{31}{}^{wu}d\omega_1 d\omega_2 d\omega_3. \quad (15)$$

The functions C_{uvw} are the same for any permutations of the indices and $C_{uuu}(T)$ is the third virial coefficient for the pure uth component.

Kihara[13] has shown that the functions C_{uvw} may be evaluated in closed analytical form for a three-constant "square-well" potential of the form:

$$\begin{aligned} E^{uv}(r_{12})&=\infty \quad \text{for} \quad r_{12}<r_0{}^{uv}\\ E^{uv}(r_{12})&=-d^{uv} \quad \text{for} \quad r_0{}^{uv}<r_{12}<R^{uv}r_0{}^{uv}\\ E^{uv}(r_{12})&=0 \quad \text{for} \quad R^{uv}r_0{}^{uv}<r_{12} \end{aligned} \quad (16)$$

in which the superscripts indicate force constants, d, r_0, and R, characteristic of the interaction between molecules of the uth and vth species. Using this potential energy function, C_{uvw} can be expressed by:

$$\begin{aligned} 3C_{uvw}=&I(0)-[I(1.1)\Delta_{uv}+I(1.2)\Delta_{uw}+I(1.3)\Delta_{vw}]\\ &+[I(2.1)\Delta_{uv}\Delta_{uw}+I(2.2)\Delta_{uv}\Delta_{vw}+I(2.3)\Delta_{uw}\Delta_{vw}]\\ &-[I(3)\Delta_{uv}\Delta_{uw}\Delta_{vw}] \end{aligned} \quad (17)$$

in which

$$\Delta_{uv}=(\exp(d^{uv}/kT)-1) \quad (18)$$

and

$$\begin{aligned} I(0)&=W(r_0{}^{uv}, r_0{}^{uw}, r_0{}^{vw})\\ I(1.1)&=W(R^{uv}r_0{}^{uv}, r_0{}^{uw}, r_0{}^{vw})-I(0)\\ I(1.2)&=W(r_0{}^{uv}, R^{uw}r_0{}^{uw}, r_0{}^{vw})-I(0)\\ I(1.3)&=W(r_0{}^{uv}, r_0{}^{uw}, R^{vw}r_0{}^{vw})-I(0)\\ I(2.1)&=W(R^{uv}r_0{}^{uv}, R^{uw}r_0{}^{uw}, r_0{}^{vw})\\ &\quad -[I(0)+I(1.1)+I(1.2)]\\ I(2.2)&=W(R^{uv}r_0{}^{uv}, r_0{}^{uw}, R^{vw}r_0{}^{vw})\\ &\quad -[I(0)+I(1.1)+I(1.3)]\\ I(2.3)&=W(r_0{}^{uv}, R^{uw}r_0{}^{uw}, R^{vw}r_0{}^{vw})\\ &\quad -[I(0)+I(1.2)+I(1.3)]\\ I(3)&=W(R^{uv}r^{uv}, R^{uw}r^{uw}, R^{vw}r^{vw})\\ &\quad -[I(0)+\sum_{k=1}^{3}I(1,k)+\sum_{k=1}^{3}I(2,k)]. \end{aligned} \quad (19)$$

The function, $W(a, b, c)$, which occurs in the formulas for the I's, is:

$$W(a,b,c)=(\pi^2/18)\begin{bmatrix} a^6+b^6+c^6+18a^2b^2c^2\\ \quad +16(b^3c^3+c^3a^3+a^3b^3)\\ -9\{a^4(b^2+c^2)+b^4(c^2+a^2)\\ \quad +c^4(a^2+b^2)\}\end{bmatrix}$$

when

$$\begin{aligned} a&\leqslant b+c\\ W(a,b,c)&=(16\pi^2/9)b^3c^3 \quad \text{when} \quad a\geqslant b+c. \end{aligned} \quad (20)$$

It would be very difficult to calculate exactly the C_{uvw} for the Lennard-Jones potential; however, they may be estimated, if we make use of the above results for the square-well potential. It is first necessary to modify the square-well potential so that it will contain only the two arbitrary parameters, $r_0{}^{uv}$ and ϵ^{uv}, which appear in the Lennard-Jones potential. This may be accomplished by letting $R^{uv}=1.8$ and $d^{uv}=0.56\epsilon^{uv}$; for this particular choice of constants, the second virial coefficients calculated on the basis of this two-constant square-well potential agrees over a remarkably wide temperature range with that calculated on the basis of the Lennard-Jones potential.†[10, 11, 13, 23]

Let us now define a function, $A(\tau)$, such that its cube is the ratio of $C(T)$ for a pure gas (the uth component) calculated for the Lennard-Jones potential to $C(T)$ calculated for the two-constant square-well potential:

$$(C_{uuu}(T))_{\text{L.J.}}=(C_{uuu}(T))_{\text{S.W.}}(A(\tau_u))^3 \quad (21)$$

in which τ_u is the reduced temperature for the uth component. As a result of the above discussion, it

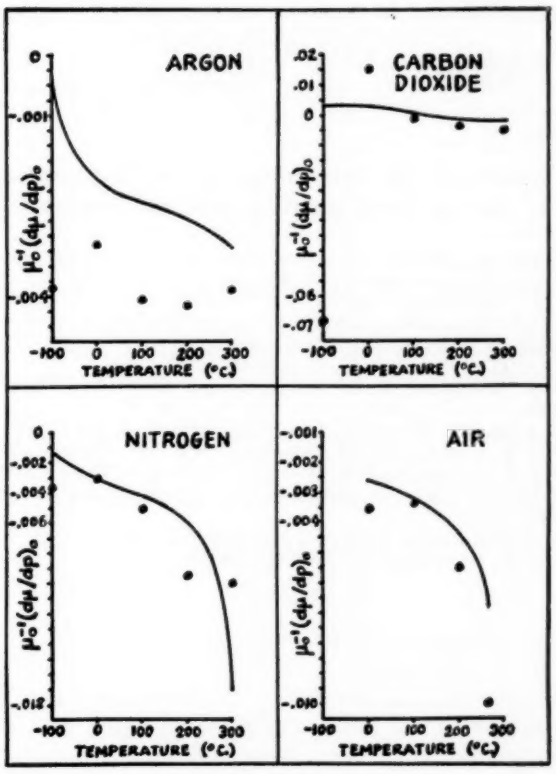

FIG. 3. Comparison of zero-pressure derivatives of the experimental Joule-Thomson *versus* pressure curves with calculated results. The solid lines represent the values of $\mu_0{}^{-1}(d\mu/dp)_0$ calculated from Eq. (23); the dots represent the corresponding experimental quantities.

† The second virial coefficient for a square-well potential is, (see reference 18),

$$B(T)=b_0[1-(R^3-1)\Delta]$$

where b_0 is expressed in terms of the square-well r_0.

[23] Hirschfelder, Ewell, and Roebuck, J. Chem. Phys. **6**, 205 (1938).

would seem fairly reasonable to write then for the "non-diagonal" terms, $(C_{uvw}(T))_{\text{L.J.}}$:

$$(C_{uvw}(T))_{\text{L.J.}}=(C_{uvw}(T))_{\text{S.W.}}(A(\tau_{uv})A(\tau_{uw})A(\tau_{vw})) \quad (22)$$

where the τ_{uv} are reduced temperatures referred to the force constants ϵ^{uv}/k, between pairs of dissimilar molecules; the A-function is slowly-varying in τ and is given in Table IV. The validity of the assumption of Eq. (22) cannot be justified until there are available good experimental data for the equation of state of mixtures of gases which contain reasonably spherical molecules.‡[24,25] Meanwhile, Eq. (22) should provide a possible method for estimating the high temperature compressibilities for gaseous mixtures.

D. JOULE-THOMSON COEFFICIENTS

Joule-Thomson coefficients (μ) have been accurately measured as functions of pressure and temperature by Roebuck and his co-workers.[26–30] The zero pressure slope of the μ *vs.* pressure curve (i.e., $(d\mu/dp)_0$) is related to the first temperature derivative of the third virial coefficient in the following manner:

$$\mu_0^{-1}(d\mu/dp)_0=(b_0/RT)(B^{(1)}-B^{(0)})^{-1}\times\begin{bmatrix}C^{(1)}-2C^{(0)}+2(B^{(0)})^2\\-2B^{(0)}B^{(1)}+\mu_0B^{(2)}R/b_0\end{bmatrix}, \quad (23)$$

in which μ_0 is the zero-pressure Joule-Thomson coefficient and the functions $B^{(j)}(\tau)$ are the dimensionless derivatives of the second virial coefficient, defined (analogously to Eq. (12)) as:

$$B^{(0)}(\tau)=B(T)/b_0; \quad B^{(j)}(\tau)=\tau^j[d^jB^{(0)}/d\tau^j]. \quad (24)$$

Tables of the functions $B^{(j)}$ have been presented elsewhere.[10,11]

As an additional check with experiment, $\mu_0^{-1}(d\mu/dp)_0$ values from experiment and from Eq. (23) have been compared. This comparison is exhibited graphically in Fig. 3. For argon, the calculated curve is definitely higher than the experimental points; this corresponds to the fact that in this temperature region $C_{\text{calc}}^{(0)}<C_{\text{exp}}^{(0)}$ and $C_{\text{calc}}^{(1)}>C_{\text{exp}}^{(1)}$ (as can be seen in Fig. 2). The two effects are additive in producing an error in $\mu_0^{-1}(d\mu/dp)_0$. For carbon dioxide and nitrogen, however, $C_{\text{calc}}^{(0)}>C_{\text{exp}}^{(0)}$ and $C_{\text{calc}}^{(1)}>C_{\text{exp}}^{(1)}$, these two effects tend to cancel one another. And, indeed, for these gases the experimental points do not all fall below the calculated curve as they did for argon. It would thus seem that the discrepancies between calculated and experimental Joule-Thomson coefficients are reasonably consistent with the differences between calculated and observed third virial coefficients.

The authors wish to express their indebtedness to Mrs. Marjorie Herrick, University of Wisconsin Computing Service, who directed the punched-card calculations in this work. Generous thanks are also due the computing section of the University of Wisconsin Naval Research Laboratory, who helped with the preliminary calculations and the preparation of the final tables: Marjorie Leikvold and Ruth Shoemaker (directors), Mary Nordling, Phyllis Rood, Ruth Schmidt, Alice Epstein, Dorothy Campbell, and Eugene Haugh. We should also like to acknowledge the assistance of Professor Charles F. Curtiss with whom we have had many interesting and helpful discussions.

Finally, the authors wish to acknowledge the financial support of the Naval Bureau of Ordnance under Contract NOrd 9938. One of the authors, R. Byron Bird, desires to thank the Wisconsin Alumni Research Foundation for financial assistance.

‡ The only data on gaseous mixtures which seemed sufficiently accurate for comparison with theoretical calculations were those on N_2-H_2 mixtures (see reference 19) and those on $CH_4-C_2H_6$ mixtures (see reference 20). However, pure H_2 does not give good agreement with the theory, and in the other mixture, the data for pure C_2H_6 are not sufficiently complete.

[24] R. Wiebe and V. L. Gaddy, J. Am. Chem. Soc. **60**, 2300 (1938).
[25] A. Michels and G. W. Nederbragt, Physica **6**, 656 (1939).
[26] J. R. Roebuck and H. Osterberg, Phys. Rev. **48**, 450 (1935).
[27] J. R. Roebuck and H. Osterberg, Phys. Rev. **46**, 785 (1934).
[28] Roebuck, Murrell, and Miller, J. Am. Chem. Soc. **64**, 400 (1942).
[29] J. R. Roebuck, Proc. Am. Acad. **60**, 537 (1925).
[30] J. R. Roebuck, Proc. Am. Acad. **64**, 287 (1930).

Fluorescence Studies of Some Simple Benzene Derivatives in the Near Ultraviolet:*† II. Toluene and Benzonitrile

ARNOLD M. BASS‡
Department of Physics, Duke University, Durham, North Carolina
(Received July 24, 1950)

The fluorescence spectra of toluene and benzonitrile have been studied using various sources of excitation. In both cases, discrete spectra have been observed in the near ultraviolet. The spectrum of toluene shows about 100 bands while that of benzonitrile shows about 140 bands. In both cases, there is good agreement with the absorption spectra. Progressions are noted and assignments are made for some of the vibrations in accordance with the symmetry properties of the molecules.

INTRODUCTION

IN a preceding paper[1] (hereafter denoted by I) a method was described for observing the fluorescence spectra of some benzene derivatives. In the present paper, the results obtained by applying the same method to excite fluorescence in toluene ($C_6H_5CH_3$) and benzonitrile (C_6H_5CN) will be described.

The fluorescence of toluene was studied previously by Marsh[2] in 1923. He found that excitation of toluene vapor by light from a mercury arc produced a discrete fluorescence spectrum in the near ultraviolet. Most of these bands had been observed before in emission in a Tesla discharge through toluene vapor.[3] After the present research was completed a paper appeared by Asundi and Padhye[4] in which the emission studies in an electric discharge through toluene were considerably extended. It will be seen later that their interpretation and ours coincide in general for the bands observed in emission and fluorescence. Toluene has been studied quite carefully with regard to its Raman spectrum[5,6] infra-red absorption spectrum,[7] and ultraviolet absorption spectrum.[8–11] Recently the phosphorescence of toluene in solid alcohol solution has also been investigated.[12]

No fluorescence data have been found for benzonitrile vapor. McVicker, Marsh and Stewart[3] reported a continuous background in the region 2740–3490A in a Tesla discharge with a few indistinct bands superimposed. Benzonitrile has been investigated in the Raman effect,[13,14] in infra-red[7,15] and in ultraviolet[9,16,17] absorption.

In both toluene and benzonitrile as well as in other substances, Schüler and Woeldike[18–21] have observed and discussed the appearance of discrete emission spectra produced as a result of electron impact in a hollow cathode discharge.

EXPERIMENTAL DETAILS

The details of the experimental arrangement were given in I. To summarize the method, fluorescence was excited using light from a mercury arc and also from high voltage condensed sparks between electrodes of different materials. The spark was operated at 10,000 v and 1 kw with a capacitor of 0.025 μf.

In order to control the exciting wave-length region, cut-off filters of organic solutions were used in conjunction with Corning glass filters. The fluorescence spectra were photographed with a Bausch and Lomb medium quartz spectrograph having a dispersion of about 9.5A per mm in the region under observation. The slit widths used ranged from 10 to 300 microns and exposure times, on Eastman II-0 plates, ranged correspondingly from 120 to 6 hours.

EXPERIMENTAL RESULTS

Toluene

In the recent work on the ultraviolet absorption spectrum of toluene,[10] the 0, 0 band was found to be a doublet at 37477 and 37480 cm^{-1} (about 2667.5A). In addition, toluene has strong absorption bands at 37993.6 cm^{-1} (2635.4A), and 38441.3 cm^{-1} (2600.6A). For exciting

* Based on a portion of a thesis submitted in partial fulfillment of the requirements for the degree of Doctor of Philosophy in the Graduate School of Arts and Sciences of Duke University, 1949.

† This investigation was assisted by the ONR under Contract N6ori-107, Task Order I, with Duke University.

‡ Present address: Laboratory for Insulation Research, Massachusetts Institute of Technology, Cambridge, Massachusetts.

[1] A. M. Bass and H. Sponer, J. Opt. Soc. Am. **40**, 389 (1950).
[2] J. K. Marsh, J. Chem. Soc. London **123**, 3315 (1923).
[3] McVicker, Marsh, and Stewart, J. Chem. Soc. London **123**, 2147 (1923).
[4] R. K. Asundi and M. R. Padhye, Ind. J. Phys. **23**, 339 (1949).
[5] K. W. F. Kohlrausch and H. Wittek, Monats. f. Chem. **74**, 1 (1941).
[6] K. S. Pitzer and D. W. Scott, J. Am. Chem. Soc. **65**, 803 (1943).
[7] J. Lecomte, J. de phys. et rad. **8**, 489 (1937).
[8] J. Savard, Ann. de Chim. **21**, 287 (1929).
[9] K. Masaki, Bull. Chem. Soc. Japan **11**, 346 (1936).
[10] Ginsburg, Robertson, and Matsen, J. Chem. Phys. **14**, 511 (1946).
[11] M. R. Padhye, Ind. J. Phys. **23**, 331 (1949).
[12] P. P. Dikun and B. Y. Sveshnikov, J. Exp. and Theor. Phys. (U.S.S.R.) **19**, 1000 (1949).
[13] L. Simons, Soc. Sci. Fennica, Commentations Phys. Math. **6**, Nr. 13 (1932).
[14] K. W. F. Kohlrausch and A. Pongratz, Sitz. Akad. Wiss. Wien **142**, 637 (1933); Monats. f. Chem. **63**, 427 (1933).
[15] P. Barchewitz and M. Parodi, Comptes Rendus **209**, 30 (1939); J. de phys. et rad. **10**, 143 (1939).
[16] H. E. Acly, Zeits. f. physik. Chem. **135**, 251 (1928).
[17] R. C. Hirt and J. P. Howe, J. Chem. Phys. **16**, 480 (1948).
[18] H. Schüler and A. Woeldike, Physik. Zeits. **42**, 390 (1941).
[19] H. Schüler and A. Woeldike, Physik. Zeits. **43**, 17 (1942).
[20] A. Woeldike, Zeits. f. Naturforsch. **1**, 566 (1946).
[21] H. Schüler, Zeits. f. Naturforsch. **2a**, 556 (1947).

the fluorescence we used Ni, Al, Fe, and Mn sparks, and the Hg arc, which have suitable exciting lines in or near some or all of the toluene absorption bands mentioned above. Strong fluorescence was observed to result from excitation by Al, Fe, and Hg, while Mn gave a moderately strong fluorescence and Ni only a very weak emission. Although the Hg arc spectrum has no lines coinciding with the toluene 0, 0 band, it does have the advantage of having only a few lines as compared with the spark spectra of Al or Fe. This fact made it possible to determine the exact nature of the excitation when the Hg spectrum was used as the source for the toluene fluorescence. Therefore, the Hg arc was used as the chief source of excitation for toluene. Figure 1 (A) shows the fluorescence spectrum that was obtained for toluene with a slit 35 microns wide upon excitation by an Al spark for 100 hours and using a Corning No. 9863 filter. Figure 1 (B) shows the fluorescence excited by a Hg arc under similar conditions. The similarity of the main features of the spectra is apparent. In both cases, the vapor pressure corresponded to approximately 10 mm of Hg.

The spectrum extends from about 37480 to about 34000 cm^{-1} (2667–2925A), and consists of some 100 bands which appear to degrade to the red. Table I lists the bands as measured in the toluene spectrum along with the intensities and probable assignments. The intensities were estimated visually according to the following scale: *s*—strong, *ms*—medium to strong, *m*—medium, *mw*—medium to weak, *w*—weak, *vw*—very weak; *d*—diffuse, *vd*—very diffuse; *b*—broad, *vb*—very broad. In the assignment column the number to the left of the comma gives the vibrational level of the lower electronic state, and the number to the right of the comma gives the vibrational level of the upper state involved in the transition. Numbers with negative signs to the right of the comma refer to *v*,*v* transitions. Less accurate measurements and assignments for which there may be some doubt are enclosed in parenthesis.

Bands marked by an asterisk correspond to emission bands observed by Asundi and Padhye. A cross on the left side of the wave numbers marks those bands which correspond to fluorescence bands given by Marsh. Owing the greater accuracy of the present measurements, the old values of the fluorescence bands deviate a little in position from the new ones. A few bands reported by Marsh on the short wave-length side of the 0, 0 transition were not found in this research.

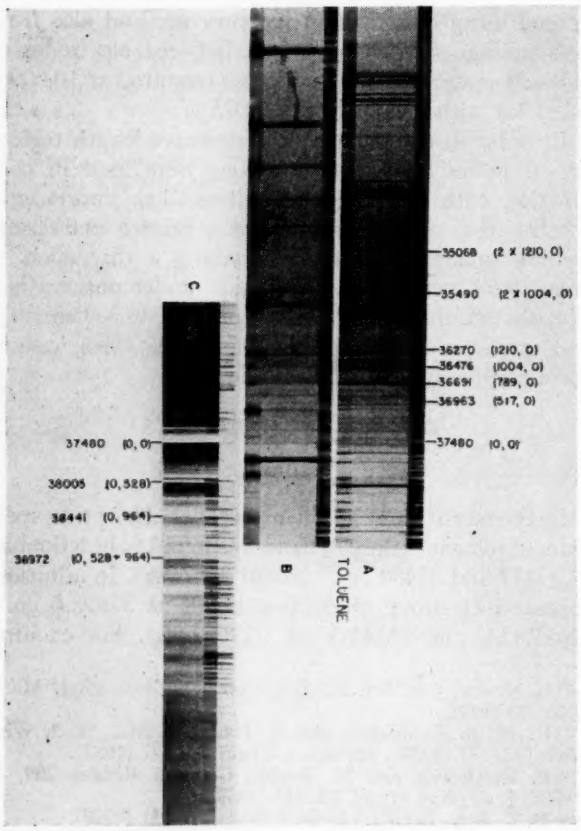

FIG. 1. Fluorescence spectrum of toluene vapor. (*A* excited by Al spark, Corning filter No. 9863, vapor pressure 10 mm; *B* excited by Hg arc under similar conditions) and absorption spectrum for comparison.

Benzonitrile

As mentioned above, the fluorescence of benzonitrile has not been studied before. Hirt and Howe[17] have recently measured the ultraviolet absorption spectrum of this substance and have found the 0, 0 band to be at 36516 cm^{-1} (2737.7A). There are other strong absorption bands at 37036, 37454, 37480, and 37696 cm^{-1} (2699.3, 2669.1, 2667.3, 2650.0A). For exciting the fluorescence in benzonitrile, sparks of Mn, Fe, and Cu were used, as well as the Hg arc. Excitation by Hg and Cu gave only very weak fluorescence, while excitation by Mn and Fe sparks gave very strong fluorescence. The spectrum obtained using the Fe spark consisted of some strong bands superposed on an almost continuous background. This continuum results probably from the excitation of many high levels in benzonitrile by the very rich iron spectrum.

The spectrum resulting from Mn excitation shows about 140 discrete bands extending from 36520 to about 33400 cm^{-1} (2735 to 2990A) which are listed in Table II in the same fashion as the toluene bands in Table I. The spectrum extends further to about 3500A, but the bands become broad and diffuse beyond 3000A and the spectrum takes on the appearance of a continuum. Figure 2 (A) shows the spectrum obtained on excitation by a Fe spark for 115 hours through a 60-micron slit, and using a Corning No. 9863 filter. The vapor pressure was about 20 mm.

DISCUSSION OF RESULTS

Toluene

The theory of the spectra of monosubstituted benzene derivatives has been reviewed elsewhere (see I). The

TABLE I. Fluorescence bands of toluene.

Wavelength A		Wave number cm^{-1}	Int.	Separation from 0, 0 37480 cm^{-1}	Assignment
2667.2		+37480*	*s*	0	0, 0
68.2		467	*ms*	13	0, −9
71.5	+	421*	*m,d*	59	517, 456; 0, −59
74.4		380*	*m,d*	100	623, 528
75.8	+	361*	*w*	119	2×517, 2×456; 0, −2×59
77.8		333	*mw*	147	
(78.3)		(326)*	*w*	(154)	
79.7	+	307*	*ms*	173	623, 456; 0, −173
80.6		294*	*m,d*	186	(3×517, 3×456); (0, −3×59)
81.4		283	*ms*	197	
83.8		250*	*mw*	230	517+623, 2×456; 0, −59−173
86.5	+	212	*mw,d,b*	268	789, 528
90.7		154	*mw,d,b*	326	789, 456
92.9	+	124*	*mw*	356	2×407, 456
95.1		093	*w*	387	845, 456
96.6		073	*ms*	407	407, 0
(98.7)	+	(044)	*vw*	(436)	(2×218, 0)
2701.9		000	*w*	480	1004, 528; 407, −59; 407+517, 456
02.6		36990	*w*	490	
04.6	+	963*	*s*	517	517, 0
06.0	+	944	*s*	536	517, −9
09.1		902	*mw,d*	578	1032, 456; 517, −59; 2×517, 456
(09.8)		(892)*	*w*	(588)	
12.4	+	857*	*s*	623	623, 0
17.2	+	792*	*mw,vd*	688	(688, 0); 623, −59; 623+517, 456; 517, −173
19.6		759	*mw*	721	1181, 456
21.5		734	*w*	746	1210, 456; 623, −2×59
(23.1)		(712)	*vw*	(768)	(2×1077, 932+456); (2×845, 932)
24.1		699	*m*	781	
24.6	+	691*	*ms*	789	789, 0
25.7		677	*s*	803	789, −9; 2×623, 456; 623, −173
26.7		664*	*m*	816	2×407, 0
28.8		635	*w*	845	845, 0
29.5	+	626*	*mw*	854	789, −59; 789+517, 456
30.7		610	*mw,vd*	870	2×407+517, 456
32.7	+	583	*mw*	897	897, 0
35.5		546	*w*	934	(2×467, 0)
37.0	+	526*	*mw,vd,b*	954	789, −173; 789+623, 456
39.1		498*	*w,vd*	982	982, 0
40.7	+	476	*ms*	1004	1004, 0
41.4		467*	*ms*	1013	1004, −9
42.8		448	*mw*	1032	1032, 0; 2×517, 0
45.1	+	418*	*w,vd,b*	1062	1004, −59; 1004+517, 456
(46.2)		(403)*	*vw*	(1077)	(1077, 0; 2×1004, 932)
48.5		372	*w,vd*	1108	(2×1032, 964)
(49.7)		(357)	*vw*	(1123)	2×789, 456
51.1		338	*w*	1142	517+623, 0
54.1		299*	*m*	1181	1181, 0; (1004, −173); (1004+623, 456)
56.3	+	270*	*m*	1210	1210, 0
57.5		254	*w*	1226	3×407, 0
58.5		241	*mw*	1239	2×623, 0; 1181, −59; 1181+517, 456
(60.7)		(212)*	*vw*	(1268)	1210, −59; 1210+517, 456
62.1		194	*w*	1286	(1286, 0)
(63.1)		(181)	*vw*	(1299)	(1299, 0)
(64.6)		(161)	*vw*	(1319)	(1319, 0); (2×1032, 751)
66.1		141	*w*	1339	1181, −173; 1181+623, 456; 517+2×407, 0
(68.4)		(111)	*vw*	(1369)	517+845, 0
69.3	+	100	*w*	1380	(1380, 0); (2×688, 0)
71.7	+	068	*w*	1412	407+1004, 0; 623+789, 0
75.5		019	*w*	1461	(2×730, 0)
(78.3)		(35983)	*vw*	(1497)	1497, 0; 517+982, 0
80.1		959	*m*	1521	517+1004, 0
81.2	+	945	*mw*	1535	(2×1032, 528)
84.4	+	904	*mw*	1576	2×789, 0; (2×1032, 456)
88.5	+	851*	*m*	1629	(1629, 0); 623+1004, 0
(89.7)		(836)	*vw*	(1644)	(407+517+730, 0); 407+517+1181, 456

TABLE I.—(*Continued*)

Wavelength A		Wave number cm^{-1}	Int.	Separation from 0, 0 37480 cm^{-1}	Assignment
2791.5		35812	*w*	1668	2×1210, 751
(92.4)		(801)	*vw*	(1679)	(789+897, 0)
93.2		791	*w*	1689	2×845, 0
94.4		775	*mw*	1705	517+1181, 0; (623+1077, 0)
96.6		747	*mw*	1733	517+1210, 0
97.7		733*	*w*	1747	845+897, 0
98.7		720	*mw*	1760	517+2×623, 0
99.8		706	*m*	1774	789+982, 0; 407+517+845, 0
2801.4		686*	*m*	1794	789+1004, 0; 2×897, 0
06.1		626	*vw*	1854	845+1004, 0; (407+517+2×467, 0)
07.5		608	*w*	1872	3×623, 0; (789+1077, 0)
08.3	+	598	*w*	1882	845+1032, 0; 897+982, 0
09.8		579	*w*	1901	897+1004, 0; 2×1181, 456
14.9		515	*w*	1965	789+1181, 0; 2×982, 0; 2×1210, 456
16.9	+	490	*mw*	1990	(2×1004, 0); 789+1210, 0; 2×789+407, 0
(23.7)		(404)	*vw,vd*	(2076)	2×1032, 0; (1004+1077, 0); (517+623+2×467, 0)
(25.5)		(382)	*vw*	(2098)	517+2×789, 0; 407+789+897, 0
30.8		315	*vw*	2165	982+1181, 0; (2×1077, 0)
32.6	+	293*	*mw*	2187	1181+1004, 0
(34.1)		(274)	*vw*	(2206)	407+789+1004, 0; 623+2×789, 0
35.3		259	*mw*	2221	1004+1210, 0; 407+789+1032, 0; (517+623+1077, 0)
36.9		239	*w*	2241	1032+1210, 0; 2×623+1004, 0
(39.4)		(208)	*w*	(2272)	(407+789+1077, 0)
40.5		195	*mw*	2285	517+789+982, 0; (1077+1210, 0)
48.3		098	*vw*	2382	1181+1210, 0; (2×1181, 0); 407+789+1181, 0
50.8	+	068*	*vw*	2412	2×1210, 0; 407+2×1004, 0; 623+789+1004, 0
53.5		034	*vw*	2446	407+1004+1032, 0; 623+789+1032, 0
(54.6)		(021)	*vw*	(2459)	2×623+1210, 0
55.1		015	*vw*	2465	407+845+1210, 0; (2×730+1004, 0)
59.4		34962	*vw*	2518	517+789+1210, 0; 517+2×1004, 0
61.3		939	*w*	2541	(3×845, 0); 517+845+1181, 0
63.7		910	*w*	2570	517+845+1210, 0
(65.8)	+	(884)	*vw*	(2596)	407+1004+1181; 623+789+1181, 0
69.5		839*	*mw*	2641	623+2×1004, 0; 407+1032+1210, 0
(73.5)		(791)	*vw*	(2689)	2×845+1004, 0; (407+1077+1210, 0)
81.6		693*	*w,d*	2787	2×789+1210, 0; 789+2×1004, 0
86.5	+	634	*w*	2846	789+2×1032, 0; 623+1004+1210, 0
(89.4)		(599)	*vw*	(2881)	517+2×1181, 0; 845+1004+1032, 0
(95.7)		(524)	*vw*	(2956)	(3×982); 789+982+1181, 0
98.2		494	*vw*	2986	982+2×1004, 0; 789+982+1210, 0
2901.7	+	452	*vw*	3028	3×1004, 0; 789+1032+1210, 0
02.4		444	*vw*	3036	(3036, 0); 1032+2×1004, 0; 623+2×1210, 0
(09.8)		(357)	*w,d*	(3123)	(1004+1032+1077, 0); (845+1077+1210, 0)
14.0		307	*w,vd,b*	3173	(3173, 0); 789+1181+1210, 0
21.9		214*	*vw,d*	3266	(2×1629); 845+1210, 0; (1004+1077+1181, 0)

toluene molecule is treated here as belonging to the symmetry class C_{2v}. Though this is not rigorously true, it serves to explain quite well the spectra observed in the ultraviolet absorption and also in emission. The electronic transition in toluene is considered to be $A_1 \leftrightarrow B_1$, which is allowed, as are transitions involving vibrational states of symmetry α_1, α_2, and β_1. Transitions involving vibrational states of symmetry β_2 are generally forbidden except for $2v,0$ and v,v transitions.

The strong fluorescence band at 37480 cm^{-1} (see Table I) was taken to correspond to the 0,0 band in toluene. The bands in the fluorescence spectrum are found to be in excellent agreement with the values measured in ultraviolet absorption and emission. The frequency differences of the fluorescence bands from the 0,0 band are listed in the fourth column of Table I. The vibrations which are most strongly excited in the ground state have the frequencies: 407, 517, 623, 789, 1004, 1032, 1181, and 1210 cm^{-1}. The fundamental ground-state vibration frequencies which have been observed in fluorescence are collected in Table III where symmetry assignments are given and where they are compared with the values obtained through other methods. Each of the strong totally symmetric vibrations is found to be excited in the ground state up to at least two quanta and also in many combinations.

The 407 cm^{-1} vibration has been assigned[5,6] the symmetry α_2 and is analogous to the 411 cm^{-1} vibration found in fluorobenzene (see I). According to Pitzer and

TABLE II. Fluorescence bands of benzonitrile.

Wavelength A	Wave number cm^{-1}	Int.	Separation from 0, 0 36519 cm^{-1}	Assignment
2737.5	36519	*w*	0	0, 0
38.6	504	*w*	15	0, −15
40.5	479	*w*	40	0, −40
(41.3)	(468)	*w*	(51)	
41.7	463	*w*	56	
42.9	447	*w*	72	(0, −2×40)
44.3	428	*mw*	91	
45.1	418	*mw*	101	
46.4	401	*w*	118	(0, −3×40)
(47.8)	(382)	*w*	(137)	(0, −137); (270, 130)
49.0	366	*mw*	153	(0, −153); (314, 160)
50.5	346	*w*	173	173, 0
(51.7)	(330)	*w*	(189)	173, −15
(53.8)	(303)	*mw*	(216)	173, −40
55.3	283	*mw*	236	
57.9	249	*mw*	270	270, 0
59.0	234	*w*	285	270, −15
61.2	205	*w,d*	314	314, 0; 270, −40
62.9	183	*mw*	336	(2×173, 0)
64.3	165	*mw*	354	314, −40; 270, −2×40
65.3	152	*mw*	367	
(66.4)	(137)	*m*	(382)	382, 0
67.2	127	*m*	392	
(68.1)	(115)	*m*	(404)	382, −15; (270, −137)
(69.0)	(103)	*m*	(416)	(382, −2×15)
69.9	092	*m*	427	382, −40; (270, −153)
71.3	074	*mw*	445	173+270, 0
(72.0)	(064)	*ms*	(452)	
72.6	057	*ms*	462	462, 0
(73.6)	(044)	*m*	(475)	462, −15
74.3	035	*m*	484	173+314, 0
75.4	020	*ms*	499	462, −40
76.3	009	*ms*	510	
77.1	35998	*m*	521	(382, −137); (3×173, 0)
78.2	984	*mw*	535	(382, −153)
(78.7)	(977)	*ms*	(542)	(2×270, 0)
79.6	966	*m*	553	548, 0
80.6	953	*mw*	566	548, −15
(81.3)	(944)	*w*	(575)	
81.7	939	*mw*	580	548, −2×15; 270+314, 0
82.9	923	*w*	596	548, −40; (462, −137)
84.0	909	*mw*	610	(462, −153)
84.6	901	*m*	618	618, 0
86.0	883	*m*	636	618, −15; 173+462, 0
86.5	877	*m*	642	(618, −2×15)
87.5	864	*mw*	655	618, −40; 270+382, 0
89.5	838	*m,d*	681	681, 0
91.8	809	*w,d*	710	(173+548, 0)
96.5	748	*m*	771	771, 0; (2×382, 0)
(97.1)	(741)	*m*	(778)	314+462, 0
97.9	731	*ms*	788	771, −15
(98.4)	(724)	*m*	(795)	173+618, 0
99.7	708	*mw*	811	771, −40; 3×270, 0
(2800.1)	(703)	*ms*	(816)	270+548, 0; (681, −137)
02.3	674	*mw,d*	845	845, 0; 382+462, 0
04.9	641	*m,d*	878	(845, −2×15)
(06.4)	(622)	*m*	(897)	
06.8	617	*mw*	902	
(07.3)	(610)	*w*	(909)	771, −137
(07.9)	(603)	*m*	(916)	
09.6	582	*w*	937	382+548, 0
(10.2)	(574)	*mw*	(945)	173+771, 0; 270+681, 0
14.8	516	*s*	1003	1003, 0
15.7	505	*s*	1014	1003, −15; 173+845, 0
16.6	493	*ms*	1026	1026, 0
17.9	477	*ms*	1042	1026, −15; 1003, −40; 270+771, 0
18.6	468	*ms*	1051	(1026, −2×15)
20.1	449	*mw*	1070	1026, −40; 382+681, 0
20.9	439	*mw*	1080	462+618, 0; 1003, −2×40
(21.6)	(430)	*m*	(1089)	314+771, 0
22.4	420	*m*	1099	2×548, 0
(22.9)	(414)	*mw*	(1105)	1026, −2×40; 173+382+548, 0
24.4	395	*m*	1124	
26.0	375	*m*	1141	(3×382, 0); 462+681, 0; (1003, −137)
2826.9	35364	*mw,d*	1155	382+771, 0; (1003, −153)
(27.6)	(355)	*w*	(1164)	548+618, 0; (1026, −137)
28.5	344	*mw*	1175	1175, 0; 173+1003, 0
30.0	325	*s*	1194	1194, 0
31.0	313	*ms*	1205	1194, −15; 270+382+548, 0
32.0	300	*m*	1219	1175, −40
33.2	285	*mw*	1234	2×618, 0; 1194, −40; 462+771, 0
(35.7)	(254)	*mw,d*	(1265)	
37.4	233	*mw,d*	1286	
(38.3)	(222)	*w*	(1297)	270+1026, 0; 618+681, 0
39.4	208	*mw*	1311	1311, 0; (2×382+548, 0); 548+771, 0
40.8	191	*m,d*	1328	1311, −15; (1194, −137)
42.5	170	*mw,vd*	1349	1311, −40; 173+1175, 0; (1349, 0)
44.3	148	*mw*	1371	173+1194, 0; (618+751, 0)
45.5	133	*mw*	1386	3×462, 0; 382+1003, 0; 548+845, 0
(48.6)	(095)	*w*	(1424)	382+270+771, 0
49.4	084	*w*	1435	270+548+618, 0; (681+751, 0)
51.3	061	*mw,d*	1458	618+845, 0; 270+1194, 0; 681+771, 0
52.3	049	*mw,vd*	1470	462+1003, 0; 548+2×462, 0
(53.2)	(038)	*mw*	(1481)	382+2×548, 0; 173+1311, 0; 314+548+618, 0
54.6	021	*m*	1498	1498, 0; 270+382+845, 0
(55.1)	(015)	*mw*	(1504)	(2×751, 0)
56.4	34999	*mw*	1520	681+845, 0; 1498, −15
(58.3)	(976)	*w,d*	(1543)	2×771, 0; 618+2×462, 0; 1498, −40
(60.7)	(946)	*mw*	(1573)	548+1026, 0; 382+1194, 0
63.2	916	*mw,d*	1603	681+2×462, 0; (1603, 0)
(64.0)	(906)	*mw,vd*	(1613)	771+845, 0; 618+1003, 0
66.4	877	*mw,d*	1642	3×548, 0; 618+1026, 0
68.7	849	*w,d*	1670	173+1498, 0
69.6	838	*m,d,b*	1681	681+1003, 0; 382+618+681, 0
(70.4)	(828)	*w*	(1691)	2×845, 0; 382+462+845, 0
72.2	806	*w,d*	1713	2×548+618, 0
74.2	782	*w*	1737	548+1194, 0
76.1	759	*w*	1760	2×382+1003, 0
(77.2)	(746)	*vw*	(1773)	771+1003, 0
81.0	700	*mw*	1819	618+1194, 0; 270+548+1003, 0
83.7	668	*w*	1851	3×618, 0; 845+1003, 0
84.9	653	*mw*	1866	2×548+771, 0; 845+1026, 0
91.6	573	*mw,d*	1946	173+771+1003, 0; 771+1175, 0
(92.9)	(557)	*m*	(1962)	771+1194, 0; 462+1498, 0
(95.4)	(527)	*w*	(1992)	681+1311, 0
96.7	512	*m*	2007	2×1003, 0
98.1	495	*m*	2024	1003+1026, 0
99.5	479	*mw*	2040	845+1194, 0; 548+1498, 0; (2×1026, 0)
2902.7	441	*vw*	2078	2×618+845, 0; 771+1311, 0
10.5	348	*vw*	2171	1003+1175, 0; 548+618+1003, 0
12.4	326	*mw*	2193	1003+1194, 0; 548+618+1026, 0; (4×548, 0)
14.5	301	*w*	2218	1026+1194, 0
(15.4)	(291)	*vw,d*	(2228)	382+845+1003, 0; (2228, 0)
17.3	268	*vw,d*	2251	382+845+1026, 0
(18.0)	(260)	*vw*	(2259)	2×618+1026, 0
(20.5)	(231)	*w*	(2288)	
24.6	183	*w*	2336	548+771+1026, 0; 1026+1311, 0
(29.4)	(127)	*w*	(2392)	2×1194, 0; 382+2×1003, 0
(35.6)	(055)	*w,vd*	(2464)	771+2×845, 0; 618+845+1003, 0; (4×618, 0)
41.3	33989	*vw*	2530	3×845, 0
42.8	971	*vw*	2548	2×771+1003, 0; 548+2×1003, 0;
46.0	934	*vw*	2585	548+845+1194, 0; 382+1003+1194, 0
55.0	831	*vw*	2688	2×845+1003, 0; 1194+1498, 0
(58.6)	(790)	*vw*	(2729)	
63.0	740	*vw*	2779	771+2×1003, 0
63.5	734	*vw*	2785	771+845+1175, 0
(70.0)	(660)	*vw*	(2859)	845+2×1003, 0
(74.9)	(605)	*vw*	(2914)	
76.4	588	*vw*	2931	(618+1003+1311, 0)
(80.5)	(542)	*vw*	(2977)	771+1026+1175, 0
(82.6)	(518)	*vw*	(3001)	2×1498, 0; 771+1026+1194, 0
(83.5)	(508)	*vw*	(3011)	3×1003, 0
(84.4)	(498)	*vw*	(3021)	(2×1003+1026, 0)
86.6	473	*vw*	3046	845+1003+1194, 0

Scott, this frequency is to be associated with an out-of-plane carbon bending vibration. The band has been reported neither in absorption or in emission.

The 517 cm^{-1} and 623 cm^{-1} frequencies have been discussed in detail a number of times.[4–6, 10, 11] They are analogous to the 517 cm^{-1} and 612 cm^{-1} frequencies in fluorobenzene absorption[22] (see I) and result from the splitting of the 606 cm^{-1} ϵ_g^+ benzene carbon vibration when the substitution of the CH_3 group reduces the symmetry of the molecule from D_{6h} to C_{2v}.

[22] S. H. Wollman, J. Chem. Phys. 14 123 (1946).

In the 1000 cm^{-1} region, three totally symmetric vibrations appear with frequencies 1004, 1032, and 1181 cm^{-1}. The corresponding frequencies found in the UV absorption spectrum[10, 11] are 1003, 1012, and 1176 cm^{-1}. Of these, the 1004 is without doubt a carbon ring vibration. The 1030 and the 1181 frequencies have been assigned[5–7, 23] to hydrogen planar bending vibrations which arise from the benzene vibrations ϵ_g^- and ϵ_g^+ upon reduction of symmetry D_{6h} to C_{2v}. The latter assignment (i.e., connected with ϵ_g^+) seems reasonable because a totally symmetric hydrogen vibration is ex-

pected in this region. From the types of combinations that occur in fluorescence in connection with the 1181 cm^{-1} band, it may also be concluded that a symmetric vibration is likely. Alternative explanations for the 1181 band which would give weak transitions are added in brackets in Table I.

The 1030 cm^{-1} frequency has also been assigned[5, 6, 23] to a symmetric hydrogen vibration. However, if the frequency 964 cm^{-1}, observed to occur strongly in absorption[10, 11] in the upper electronic state, is associated with this vibration, then it is more plausible to interpret it as a carbon vibration because these vibrations are, in general, more affected by the electronic excitation than hydrogen vibrations. This argument, however, would not apply to the ground state. Ginsburg, Robertson, and Matsen and Padhye list a totally symmetric band at 1012 cm^{-1} which they correlate with the 1030 cm^{-1} vibration found in Raman and infra-red spectra. There was observed in the fluorescence spectrum a fairly intense band at 36467 cm^{-1}, separated from the 0,0 band by 1013 cm^{-1}, and a medium weak band at 36448 cm^{-1}, separated from the 0,0 band by 1032 cm^{-1}. If the former band were a totally symmetric fundamental vibration, then one should expect to find the 1013 frequency repeated in various combinations. But, such is not the case. The 1032 cm^{-1} vibration does appear, albeit weakly, twice excited and in a number of combination bands, thus making its assignment as a totally symmetric vibration more reasonable than is the case for the 1013 cm^{-1} vibration. The 1013 band is probably the 1004 vibration on which is superposed a ρ,ρ transition with a very small frequency difference. A satellite band 11 cm^{-1} from the 0,0 band is observed in the absorption spectrum of toluene. Likewise the band in the fluorescence spectrum at 37467 cm^{-1} corresponds to the transition 0,−9. In chlorobenzene,[24] and phenol[25] such satellites with the same order of magnitude of separation from the 0,0 band have been observed, and have been explained[24] as arising from a 1,1 transition, probably of a low frequency vibration.

The band at 36691 cm^{-1} separated from the 0,0 band by 789 cm^{-1} corresponds to the 785 cm^{-1} vibration in the UV absorption. In analogy with the 808 cm^{-1} vibration in fluorobenzene (see I), this vibration of frequency 789 cm^{-1} is correlated with the totally symmetric $C-CH_3$ bond vibration.

As in fluorobenzene, there is observed in the toluene spectrum a fairly intense band in the 1200 cm^{-1} region, at 36270 cm^{-1} separated from the 0,0 band by 1210 cm^{-1}. The same vibration is observed in the UV absorption spectrum. Raman depolarization measurements indicate that this vibration is totally symmetric, and the fluorescence measurements tend to confirm this assignment. As to the nature of this vibration, it is not possible to choose between a carbon vibration suggested by Kohlrausch and Wittek and a hydrogen vibration suggested by Pitzer and Scott.

Pitzer and Scott list a Raman line of frequency 467 cm^{-1} and assign it to an out-of-plane carbon vibration of symmetry β_2. This vibration does not appear once excited in fluorescence, in accordance with the symmetry requirements. But there is observed a band in fluorescence at 36546 cm^{-1}, 934 cm^{-1} from the 0,0 band, which can be interpreted as resulting from the transition $2\times467,0$. This twice excited vibration appears also as a possible explanation of the 35404 cm^{-1} band. However, for lack of further substantiating evidence, the assignment of the 467 vibration is listed as uncertain.

The band of frequency 845 cm^{-1} is related to the Raman 840 cm^{-1} vibration. This band appears in fluorescence excited several times and in a number of combination bands. It seems to be closely related, in its origin, with the 824 cm^{-1} band in fluorobenzene (see I). However, while the latter appeared strongly in the upper electronic state in absorption, the 843 cm^{-1} toluene vibration does not. As in the case of fluorobenzene, Kohlrausch and Wittek assign the symmetries α_2 and β_2 to this vibration. However, as outlined in I for the case of fluorobenzene, this assignment is difficult to reconcile with the frequent appearances of this fre-

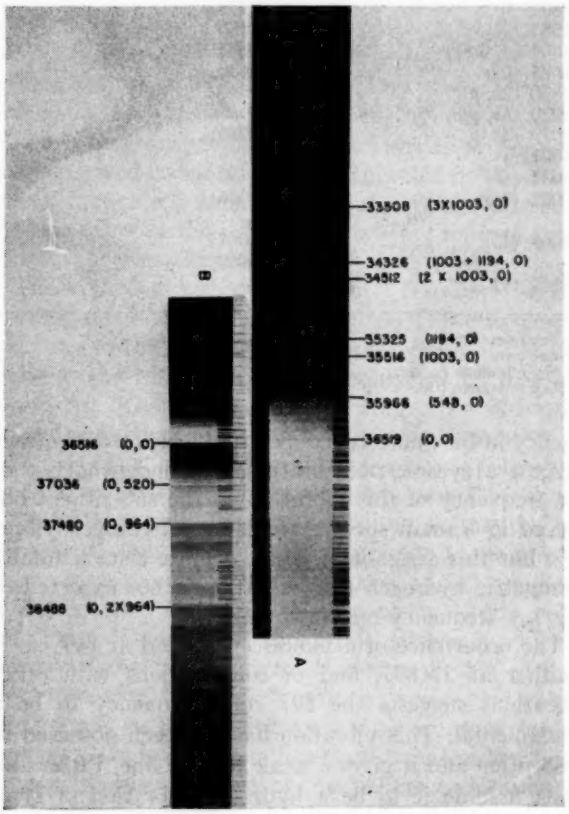

FIG. 2. A. Fluorescence spectrum of benzonitrile vapor excited by Fe spark, Corning filter No. 9863, vapor pressure about 20 mm. B. Absorption spectrum for comparison.

[23] A. R. Choppin and C. H. Smith, J. Am. Chem. Soc. **70**, 2520 (1948).
[24] H. Sponer and S. H. Wollman, J. Chem. Phys. **9**, 816 (1941).
[25] Matsen, Ginsburg, and Robertson, J. Chem. Phys. **13**, 309 (1945).

TABLE III. Ground-state vibration frequencies in toluene.

Raman Kohlrausch and Wittek[a]	Pitzer and Scott[b]	Infra-red Lecomte[c]	UV absorption Ginsburg, Robertson and Matsen[d]	This research	Symmetry Reference 5	Symmetry Reference 6	Symmetry This research
216 (5*b*, 0.68)	216			(218)	β_2	β_2	β_2
294 (00?)				(294)			
344 ($\frac{1}{2}$, *dp*)	340				β_1	β_1	
405 (0)	405			407	α_2	α_2	
	467			(467)		β_2	β_2
521 (6, 0.60)	521	520	514	517	α_1	α_1	α_1
623 (4, *dp*)	622	625	620	623	β_1	β_1	β_1
		690		(688)	α_2 and β_2	β_2	α_2
730 (1)	730	730	714	(730)	β_2	β_2	β_2
786 (9, 0.12)	785	790	785	789	α_1	α_1	α_1
814 ($\frac{1}{2}$)							
843 (1, *dp*)	842	840	845	845	α_2 and β_2	α_2	α_1
897 (1, *b*)	890	890	897	897	β_2	β_2	(α_2)
977 ($\frac{1}{2}$)	(985)	960	988	982		α_2	
993 ($\frac{1}{2}$)							
1004 (12) } (0.08)	1002		1003	1004	α_1	α_1	α_1
1030 (8)	1030	1030	1012	1032	α_1	α_1	α_1
1085 (0)	1060	1060	1062	(1077)		β_1	
1155 (2) } (0.64)	1155				α_1	β_1	
1177 (1)	1175	1175	1176	1181	α_1	α_1	
1189 (00)	1190		1189			β_2	
1208 (5, *p*)	1210		1212	1210	α_1	α_1	α_1
1278 (0)	1282			(1286)		β_1	
1301 (00?)	1310			(1299)		β_1	
1321 (00)				(1319)	β_1		
1379 (4, 0.55)	1380			(1380)		α_1	
1433 ($\frac{1}{2}$)					β_1		
1445 ($\frac{1}{2}$, *dp*)	1455					β_2	
	1483					α_1	
1502 (0)	1495			1497	α_1	β_1	
1585 (2)	1586					β_1	
1604 (4, 0.81)	1603				β_1	α_1	
1623 (0?)	1630					β_1	
2870 (2*b*, *p*)							
2920 (5*b*, *p*)							
2979 (3)	(2950)			(2986)		α_1	
3001 ($\frac{1}{2}$)							
3034 (4*b*)				(3036)		α_1	
3051 (7*sb*) } (0.38)	(3046)						
3067 (4*b*)	(3062)					α_1	
	(3080)					α_1	
3169 ($\frac{1}{2}$)				(3173)			

[a] See reference 5.
[b] See reference 6.
[c] See reference 7.
[d] See reference 10.

quency in the fluorescence spectrum which would rather suggest a symmetric vibration. The independence of the frequency of this vibration on the substituent observed in Raman spectra points to a hydrogen vibration but this assignment is not definite since a totally symmetric hydrogen ring vibration is not expected in this low frequency region.

The occurrence of a fluorescence band at 897 cm^{-1}, another at 2×897, and of combinations with other vibrations suggests the 897 cm^{-1} frequency to be a fundamental. This vibration has not been observed in absorption and it gives a weak Raman line. Pitzer and Scott assume it to be a hydrogen vibration of symmetry β_2. The results in fluorescence seem to indicate that the 897 cm^{-1} vibration has the symmetry α_2 rather than β_2. For if it were β_2, the 1,0 transition of this vibration would not be observed; while if it were β_1 the observed combinations with α_2-vibrations would be forbidden.

The fluorescence band at 36792 cm^{-1}, 688 cm^{-1} from the 0,0 band, arises from the same vibrations as the 690 cm^{-1} band observed in the infra-red absorption spectrum.[7] The interpretation of this band is the same as that given for the band involving the 673 cm^{-1} vibration in fluorobenzene, (see I). It is assigned to a hydrogen vibration of symmetry α_2. The band at 36100 cm^{-1}, 1380 cm^{-1} from the 0,0 band, may be explained as 2×688,0, but it is also possible that this band represents the transition 1380,0 corresponding to the 1379 cm^{-1} fundamental.

There appear in the fluorescence spectrum of toluene, as in that of fluorobenzene, bands of low frequency

TABLE IV. Ground-state vibration frequencies in benzonitrile.

Raman effect		Infra-red absorption		UV absorption		Symmetry			
							Reference		
Kohlrausch[a]	Hirt and Howe[b]	Barchewitz and Parodi[c]	Lecomte[d]	Masaki[a]	Hirt and Howe[b]	This research	13	16	7	This research
170 (8b, 0.85)	170 (10)				170	173	β_2	β_2		
		206								
		264			269	270				
		323			314	314				
381 (2, 0.36)	378 (3)	384			380	382				(α_1)
460 (6)	460 (6)			459	462	462				
549 (5)	548 (5)		548	547	548	548		α_1		α_1
624 (5, 0.84)	623 (5)		616	616	626	618	β_1	β_1	β_1	β_1
			676		670	681			α_1 and β_2	α_2
			686							
751 (3) } (0.15)	752 (4)		754		741	(751)	β_2		β_2	β_2
765 (5) }	764 (6)				773	771	α_1			α_1
			838		841	845				(α_1)
			922							
998 (15, 0.04)	1001 (10)		1002	1009		1003	α_1		α_1	α_1
1023 (3)	1026 (3)					1026	α_1			α_1
1178 (8) } (0.24)	1178					1175				α_1
1190 (8) }	1192					1194	α_1			α_1
1310 (1)						1311				
1353 (0)						(1349)				
1447 (1)										
1493 (2)						1498				α_1
1597 (10, 0.88)	1598 (10)					1603				
2224 (10b, 0.23)	2229 (10)					(2228)				
3071 (8b, 0.30)	3071 (8)									
3146 (1)										
3196 (1)										

[a] See reference 13.
[b] See reference 16.
[c] See reference 14.
[d] See reference 7.
[e] See reference 9.

which can be best interpreted as difference frequencies of v,v transitions. In UV absorption, difference frequencies of 59 and 178 cm^{-1} were found. In the fluorescence spectrum difference frequencies of 9, 59, and 173 cm^{-1} were observed which appear superposed on the 0,0 band and also on the strong totally symmetric vibrations. No assignments are made for the 9 cm^{-1} or the 173 cm^{-1} frequencies. The 59 cm^{-1} difference frequency is observed twice excited in fluorescence and appears in several combination bands. Numerically, the 59 fits the explanation 517, 456, but absorption measurements favor an explanation connecting it with a vibration of lower frequency.[10]

Benzonitrile

The analysis of the fluorescence spectrum of benzonitrile proceeds in much the same manner as in the cases of fluorobenzene and toluene. Hirt and Howe[17] have performed a successful analysis of the UV absorption spectrum considering that the molecule has C_{2v} symmetry. Taking the fluorescence band at 36519 cm^{-1} as 0,0 band (reported as 36516 cm^{-1} in absorption), the computed separations of the measured fluorescence bands from the 0,0 band are listed in the fourth column of Table II. The vibrations which are most strongly excited in the ground state have the frequencies: 173, 382, 462, 548, 618, 771, 845, 1003, 1026, and 1194 cm^{-1}. The fundamental ground state frequencies which have been observed in fluorescence are collected in Table IV, where they are compared with the values obtained through other methods,[7,13–16] and where proposed symmetry assignments are included.

The vibration frequency 173 cm^{-1} (170 cm^{-1} in UV absorption) is explained by Hirt and Howe as corresponding to the bending of the nitrile group out of the plane of the ring. This motion would belong to a β_2-symmetry. The fluorescence spectrum does not contribute new information concerning this assignment.

The 382 cm^{-1} vibration which gives rise to a band of medium intensity, has a Raman depolarization factor of 0.36 which indicates that the vibration may be totally symmetric. This suggestion seems to be confirmed by the large number of combination bands which occur in fluorescence involving this frequency. Barchewitz and Parodi[15] have attributed this frequency to the motion of the nitrile group. However, if this assignment were true, it could not refer to a symmetric vibration because such a vibration would have a much larger frequency. It is, therefore, concluded that either their assignment is not correct or the 382 cm^{-1} vibration is not totally symmetric.

As in fluorobenzene and toluene, a pair of frequencies of 548 and 618 cm^{-1} is observed in benzonitrile which is considered to result from the splitting of the $606\epsilon_g^+$

carbon vibration in benzene. The β_1-symmetry of the 618 vibration has been confirmed by polarization measurements in the Raman effect; the polarization character of the 548 line is not known. The vibration would have symmetry α_1 if the above assignment were correct. However, this is not entirely certain, because in some monosubstituted benzenes with heavier substituents like chlorobenzene, the totally symmetric component of the pair drops down below 500 cm^{-1}.

The fluorescence spectrum shows a band of medium intensity with frequency 771 cm^{-1}, with multiples and combinations indicating that it is a totally symmetric vibration. In the Raman effect, a pair of lines of frequencies 751 and 765 cm^{-1} is observed. Raman depolarization measurements give a value of 0.15 for the combination, in agreement with the suggested total symmetry of the vibration. In fluorescence, no band at the lower frequency (751 cm^{-1}) is observed, although there is some evidence from combination bands that there may be present a β_2-fundamental with this frequency. It is assumed that the 771 cm^{-1} vibration corresponds to the 789 cm^{-1} vibration in toluene and the 808 cm^{-1} vibration in fluorobenzene and therefore represents the C—CN bond vibration.

The remaining strong totally symmetric vibrations are directly correlated with vibrations of about the same frequencies in toluene and fluorobenzene. The 845 cm^{-1} vibration is correlated with the 824 cm^{-1} vibration in fluorobenzene and the 845 cm^{-1} vibration in toluene. The 1003 vibration, giving the strongest band in the spectrum, represents the totally symmetric carbon ring vibration (1012 cm^{-1} in fluorobenzene, 1004 cm^{-1} in toluene). The 1026 vibration is probably another carbon vibration (1030 cm^{-1} in fluorobenzene, 1032 cm^{-1} in toluene). The 1194 cm^{-1} vibration is analogous with the 1220 cm^{-1} in fluorobenzene frequency and the 1210 cm^{-1} toluene frequency. The band at 35838 cm^{-1}, which is 681 cm^{-1} from the 0,0 band, has been correlated with the 676 cm^{-1} frequency observed in the infra-red by Lecomte. This is similar to the 673 cm^{-1} vibration in fluorobenzene and the 688 cm^{-1} vibration of toluene. The vibrational modes connected with these various frequencies have been discussed either in the section on fluorobenzene or in that on toluene.

There appear in the fluorescence spectrum of benzonitrile bands of low frequency which can best be interpreted as difference frequencies of v,v transitions. Hirt and Howe found in the UV absorption spectrum difference frequencies of 40 and 221 cm^{-1}. In the fluorescence spectrum possible difference frequencies of 15, 40, 137, and 153 cm^{-1} are observed. No assignments are proposed here for these frequencies, although for the 40 cm^{-1} frequency the transition 170, 130 has been suggested.[17]

In the fluorescence spectra of both toluene and benzonitrile, weak bands are observed which correspond to transitions from vibrational levels of the excited state to vibrational levels of the ground state. However, these transitions are considerably weakened by the loss of the oscillation energy in the excited states through gas kinetic impacts.

The author wishes to thank Professor H. Sponer for her constant encouragement and many helpful discussions in directing this research.

Letters to the Editor

THIS section will accept reports of new work, provided these are terse and contain few figures, and especially few half-tone cuts. The Editorial Board will not hold itself responsible for opinions expressed by the correspondents. Contributions to this section should not exceed 600 words in length and must reach the office of the Managing Editor not later than the 15th of the month preceding that of the issue in which the letter is to appear. No proof will be sent to the authors. The usual publication charge ($8.00 per page) will not be made and no reprints will be furnished free.

The Infra-Red Spectrum of Nitrosyl Chloride

JOHN H. WISE AND JACK T. ELMER
Department of Chemistry, Stanford University, Stanford, California
July 31, 1950

THE effect of nitrosyl chloride as a possible contaminant due to reaction between various nitrogen compounds and the rock salt windows on infra-red gas cells has led to a re-examination of the infra-red spectrum of nitrosyl chloride. Bailey and Cassie[1] have reported the spectrum, but serious doubt of their assignment of fundamental frequencies was raised by the results of Beeson and Yost.[2] The latter authors proposed a different assignment based on the electron diffraction data of Ketelaar and Palmer[3] and some calculations involving Lechner's formulas.[4]

In the present research, nitrosyl chloride was prepared in two ways: by passing N_2O_4 over a column of damp KCl, and by a direct combination of Cl_2 with NO. The first procedure produced an impure, condensable, mixture consisting of N_2O_4, ClNO, and $ClNO_2$. This observation confirms the results of Ogg and Wilson[5] on the oxidation of ClNO by O_2 since oxygen was not rigidly excluded during the preparation. In the second procedure, tank chlorine was purified by the method described by Beeson and Yost,[2] and the nitric oxide was generated by a similar procedure to that of Johnston and Giauque.[6] The gases were collected in graduated traps, and then evaporated into the evacuated system. The mixture of gases, containing an excess of NO, was frozen out with liquid air and allowed to stand for about 36 hours in a bath originally containing dry ice and acetone. After refreezing in liquid air, the excess NO was removed by pumping from a dry ice bath. Unfortunately, a trace of N_2O_4 was detected in the product. The spectra were taken on a Perkin-Elmer Model 12-C Spectrometer using a 10-cm glass cell with NaCl or KBr windows.

The observed spectrum of nitrosyl chloride differs somewhat from that reported by Bailey and Cassie,[1] particularly their band at 633 cm^{-1}. A comparison of the various assignments is given in Table I. The assignment offered as a result of this work is similar to Beeson and Yost's[2] proposal of the most reasonable choice based on Bailey and Cassie's[1] results. Definite indication of absorption in the 650 cm^{-1} region is found, but the position was not accurately determined. The calculated value of the entropy of ClNO using Beeson and Yost's[2] Eq. (16) and substituting 327, 594, and 1800 cm^{-1} for the fundamentals gives:

$$S°_{ClNO} = 4R\ln T + S_{327} + S_{594} + S_{1800} + 15.460 \text{ E.U.}$$
$$= 62.466 \text{ E.U. at } 298°\text{K.}$$

This compares favorably with the value 63.0±0.3 cal./deg. found from thermal data.

TABLE I. Vibrational frequencies of ClNO.

Bailey and Cassie			Beeson and Yost proposals				This research		
ν (cm⁻¹)	Inten.	Assign.	ν (cm⁻¹)	Assign.	ν (cm⁻¹)	Assign.	ν (cm⁻¹)	Inten.	Assign.
					317	ν_2			
			290	ν_2	462	ν_3			
633	6	ν_2	633	ν_3	633	$2\nu_2$	594	VS	ν_3
							670	W?	$2\nu_2$
923	10	ν_3	923	$\nu_2+\nu_3$	923	$2\nu_3$	921	S	$\nu_2+\nu_3$
1200	3	$2\nu_2$					1185	W	$2\nu_3$ or $\nu_1-\nu_3$
1832	7	ν_1	1832	ν_1	1832	ν_1	1800	VS	ν_1
2155	4	$2\nu_2+\nu_3$					2130	S	$\nu_1+\nu_2$
							2390	M	$\nu_1+\nu_3$
							3562	S	$2\nu_1$
							>4000	M	?

[1] Bailey and Cassie, Proc. Roy. Soc. (London) **A145**, 336 (1934).
[2] Beeson and Yost, J. Chem. Phys. **7**, 44 (1939).
[3] Ketelaar and Palmer, J. Am. Chem. Soc. **59**, 2629 (1937).
[4] Lechner, Monatshefte für Chem. **61**, 385 (1932).
[5] Ogg and Wilson, J. Chem. Phys. **18**, 900 (1950).
[6] Johnston and Giauque, J. Am. Chem. Soc. **51**, 3194 (1933).

"Glass Electrode Behavior in Acid Solutions"

MALCOLM DOLE
Department of Chemistry, Northwestern University, Evanston, Illinois
July 31, 1950

UNDER the above title, Sinclair and Martell[1] have replied to my criticism[2] of their earlier paper[3] in which these authors advocated a negative ion theory for the acid solution errors of the glass electrode. In this most recent note Sinclair and Martell object to my description of the attack of hydrogen fluoride on glass as having no bearing on the interpretation of the results of their work in which they used sulfuric and hydrochloric acids. In my letter, I quoted our former work with hydrogen fluoride as a spectacular example of the way in which chemical attack on the glass surface can destroy the reversible glass electrode e.m.f.'s. I did not, of course, state or imply that the action of hydrofluoric acid is chemically similar to that of sulfuric or hydrochloric acid. I shall now explain in detail what is believed to be the action of strong acids such as sulfuric and hydrochloric on glass surfaces. In this connection I would like to refer to the excellent new book of Kratz,[4] in which his extensive work[5] on the chemical properties of glass surfaces is summarized. When Corning 015 glass electrodes are immersed in water, alkali is leached out of the surface leaving a layer or "skin" of hydrated silicic acid gel as residue. In contact with strong acids in which the vapor pressure of water has been significantly lowered, the surface film of silicic acid is dehydrated, the asymmetry potential is increased, the rate at which the glass gives up alkali to pure water is increased, the electrical resistance of the glass membrane is increased, and the hydrogen electrode function of the glass surface impaired. This is what I meant in my note by chemical attack, and its effects on the reversibility of glass electrode e.m.f.'s. I hope that this explanation of the mechanism of chemical attack clarifies my criticism of the negative ion theory of Sinclair and Martell.

[1] E. E. Sinclair and A. E. Martell, J. Chem. Phys. **18**, 992 (1950).
[2] M. Dole, J. Chem. Phys. **18**, 573 (1950).
[3] E. E. Sinclair and A. E. Martell, J. Chem. Phys. **18**, 224 (1950).
[4] L. Kratz, "Die Glaselektrode und ihre Anwendungen" *Wissenschaftliche Forschungsberichte*, Vol. 59 Frankfurt, 1950.
[5] L. Kratz, *Glastechn. Ber.* **20**, 15, 305 (1942).

Normal Modes of Ethane

T. S. G. KRISHNAMURTY AND S. SATYANARAYANARAO
Andhra University, Waltair, India
August 9, 1950

THE theory of groups has been successfully used to obtain the normal modes and frequencies of molecules, and the selection rules for spectral lines in the Raman effect and infra-red absorption. In these applications, only symmetry operations of the type rotations, reflections and rotation-reflections are usually

TABLE I.

	E	$2C_3$	$3C_2$	$3\sigma_h$	$4T$	$9\sigma_\vartheta$	$2TC_3$	$6S_3$	$6TC_2$	n_i	n_i'	Raman	Infra-red
A_1	1	1	1	1	1	1	1	1	1	3	3	P	P
A_2	1	1	1	−1	1	−1	1	−1	1	1	1	f	f
A_3	1	1	−1	1	1	−1	1	1	−1	1	0	f	f
A_4	1	1	−1	−1	1	1	1	−1	−1	3	2	f	P
E_1	2	2	2	0	−1	0	−1	0	−1	0	0	f	f
E_2	2	2	−2	0	−1	0	−1	0	1	0	0	f	f
E_3	2	−1	0	−2	−1	0	2	1	0	0	0	f	f
E_4	2	−1	0	2	−1	0	2	−1	0	0	0	f	f
G	4	−2	0	0	1	0	−2	0	0	4	3	P	P
	24	0	0	0	48	36	0	0	0				
	18	0	6	0	36	36	0	0	12				
	12	0	12	12	24	36	0	24	24				
	6	0	0	0	12	18	0	0	0				

taken into account. However, in some molecules, it may be possible to consider other elements of symmetry, as for example, a twist through 120° of one of the CH_3 groups against the other in the molecule C_2H_6. Using the point group D_{3h}' Howard† obtained the normal modes, etc., of this molecule. In this paper, assuming that the potential energy has the symmetry of the molecule including the twist also, the symmetry characters of the modes and the selection rules for their appearance in the Raman effect and the infra-red absorption are given. The results are tabulated in Table I. Details regarding the normal frequencies will be published separately.

† J. B. Howard, J. Chem. Phys. **5**, 442 (1937).

The Vibrational Energy of H_2S*

HARRY C. ALLEN, JR. AND PAUL C. CROSS
Department of Chemistry and Chemical Engineering, University of Washington, Seattle, Washington
AND
GILBERT W. KING
Arthur D. Little, Inc., Cambridge, Massachusetts
August 1, 1950

THE approximate location of four new band centers in the infra-red spectrum of hydrogen sulfide has enabled the evaluation of the complete quadratic expression for the unperturbed vibrational energies as

$$(E-E_0)\ \text{cm}^{-1}=2651n_\sigma+2635n_\pi+1189n_\delta-26n_\sigma^2-24n_\pi^2-6n_\delta^2-90n_\sigma n_\pi-19n_\sigma n_\delta-20n_\pi n_\delta. \quad (1)$$

Equation (1) yields the unperturbed levels shown in column two of Table I. From the observed perpendicular type bands[1,2] at 9911 cm^{-1} and 10194 cm^{-1}, the Darling-Dennison[3] parameter γ may be evaluated as 47 cm^{-1}. The calculated energy values for the two pairs of interacting levels are listed in column 3 of the table.

The constants in (1) and the Darling-Dennison interaction parameter were evaluated from the unstarred levels in Table I.

TABLE I.

n_σ	n_π	n_δ	Unperturbed	DD resonance
0	0	1	1183[7]	
0	0	2	2354[7]	
0	1	0	2611[4]	
1	0	0	2625[5]	
1	0	1	3789[7]	
1	1	0	5146[7]	
0	2	0	{5174}	*5138[7]
2	0	0	{5198}	*5234[8]
1	1	1	6290[6]	
2	2	0	*10012[8]	
1	3	0	{10044}	9911[1]
3	1	0	{10060}	10194[2]
0	4	0	*10156[8]	
4	0	0	10188[2]	

The absorption in the region[9] of 5146 cm^{-1} shows an overlapping spectrum centered at approximately 5143 cm^{-1} as compared to the calculated value 5138 cm^{-1} for the perturbed (020) band. The appearance of this parallel type band is presumably due to the borrowing of intensity through rotational interaction from the neighboring (110) perpendicular type band just as has been previously indicated in the appearance of the (400) band[2] at 10188 cm^{-1}.

The analysis of the 8μ-region reveals that recent investigators have not detected the P branch.[10–12] The early investigation of Mischke,[13] however, shows a weak P branch extending from 1180 cm^{-1} to nearly 1000 cm^{-1}.

As would reasonably be expected the results described by (1) are analogous to a similar treatment of the water vapor system.[2] The most conspicuous feature of this analysis is the low frequency of the bending fundamental, from 50 to 100 cm^{-1} less than it has recently been considered to be.[14]

* The work herein reported was supported in part by the ONR under Contract N8onr 52010.
[1] P. C. Cross, Phys. Rev. **47**, 7 (1935).
[2] Grady, Cross, and King, Phys. Rev. **75**, 1450 (1949).
[3] B. T. Darling and D. M. Dennison, Phys. Rev. **57**, 128 (1940).
[4] G. M. Murphy and J. E. Vance, J. Chem. Phys. **6**, 426 (1938).
[5] R. M. Hainer and G. W. King, J. Chem. Phys. **15**, 89 (1947).
[6] Allen, Cross, and Wilson, J. Chem. Phys. **18**, 691 (1950).
[7] To be reported shortly.
[8] Not yet observed.
[9] Unpublished data of M. K. Wilson.
[10] A. D. Sprague and H. H. Nielsen, J. Chem. Phys. **5**, 85 (1937).
[11] R. H. Noble, Thesis, Ohio State University (1946).
[12] E. A. Wilson, Thesis, Brown University (1947).
[13] W. Mischke, Zeits. f. Physik **67**, 106 (1931).
[14] G. Herzberg, *Infrared and Raman Spectra of Polyatomic Molecules* (D. Van Nostrand Company, Inc., New York, 1945), p. 283.

The Quantum-Mechanical Equation of State

ROBERT W. ZWANZIG
Gates and Crellin Laboratories of Chemistry, California Institute of Technology, Pasadena, California*
July 18, 1950

IN the last few years there has been some disagreement about the equivalence of the thermodynamic and kinetic pressure of a quantum liquid, with special emphasis on liquid helium II. The kinetic pressure is obtained from the quantum-mechanical virial theorem. Equations of state which do not appear to be identical have been derived from statistical thermodynamics by H. S. Green[1] and J. de Boer.[2] In this note, a simple derivation will be given, which may expose more clearly the assumptions required.

By differentiating the partition function with respect to volume, we get

$$-p=\frac{\partial A}{\partial v}=\sum_j e^{\beta(A-E_j)}\frac{\partial E_j}{\partial v} \quad (1)$$

where all symbols have their usual significance. The dependence of the energy levels of the system on its volume is needed. To get this, we introduce a scale factor, depending on the volume, into the Schrödinger equation for the system, and determine the dependence of the energy levels on this scale factor. This device is related to the one used by H. S. Green to get the classical equation of state, and by de Boer for the quantum-mechanical case. The Hamiltonian operator for the system is

$$H=-\frac{\hbar^2}{2m}\sum_{k=1}^{N}\nabla_{\mathbf{r}k}^2+V(\mathbf{r}_1,\cdots\mathbf{r}_N). \quad (2)$$

The potential is assumed to become infinite at the walls. This wall potential is taken into account by requiring eigenfunctions to vanish at the walls. We define a new coordinate system,

$$\mathbf{r}_k=v^{\frac{1}{3}}\mathbf{R}_k \quad (3)$$

where v is the volume of the system. A variation in v corresponds to an expansion or contraction of the system, without any change in its relative shape or configuration. The equation of state that will result will be valid only for such changes in volume. However, when the dimensions of the system are large compared with the

mean de Broglie wave-length of a particle, one may expect that its thermodynamic properties will not depend on its shape. Keeping $\mathbf{R}_k$ fixed, and varying v, the Hamiltonian becomes an explicit function of the volume:

$$H=-\frac{\hbar^2}{2m}v^{-\frac{1}{3}}\sum_{k=1}^{N}\nabla_{Rk}^2+V(v^{\frac{1}{3}}\mathbf{R}_1,\cdots v^{\frac{1}{3}}\mathbf{R}_N). \tag{4}$$

By differentiating the Schrödinger equation with respect to v, at constant $\mathbf{R}$,

$$\frac{\partial H\psi_j}{\partial v}=H\frac{\partial\psi_j}{\partial v}+\frac{\partial H}{\partial v}\cdot\psi_j=\frac{\partial E_j\psi_j}{\partial v}=E_j\frac{\partial\psi_j}{\partial v}+\frac{\partial E_j}{\partial v}\psi_j. \tag{5}$$

Multiply through by ψ_j^* and integrate over configuration space.

$$\frac{\partial E_j}{\partial v}=\int\psi_j^*\frac{\partial H}{\partial v}\psi_j d\tau+\int\psi_j^*(H-E_j)\frac{\partial\psi_j}{\partial v}d\tau. \tag{6}$$

Because of its Hermitian character, the latter term vanishes, and

$$\frac{\partial E_j}{\partial v}=\int\psi_j^*\frac{\partial H}{\partial v}\psi_j d\tau \tag{7}$$

—a not unexpected result. Put this into Eq. (1), and make use of the following property of the statistical operator,

$$\exp(\beta(A-H))\psi_j=\exp(\beta(A-E_j))\psi_j \tag{8}$$

to get

$$-p=\sum_j\exp(\beta(A-E_j))\frac{\partial E_j}{\partial v}=\sum_j\int\psi_j^*\frac{\partial H}{\partial v}\exp(\beta(A-H))\psi_j d\tau. \tag{9}$$

An important feature of this is that there is no difficulty here with the commutivity of the operators. This has been a source of confusion in the treatments of Green and de Boer. By carrying out the differentiation of the Hamiltonian, as de Boer has shown, the result is

$$pv=\tfrac{2}{3}\sum_{k=1}^{N}\left\langle\frac{P_k^2}{2m}\right\rangle-\tfrac{1}{3}\sum_{k=1}^{N}\langle\mathbf{r}_k\cdot\nabla_{r_k}V\rangle \tag{10}$$

where averages are taken over the canonical ensemble. (P_k is now the momentum operator.)

The final equation obtained by de Boer differs from this in that he uses an expansion of the energy eigenfunctions in free particle wave functions. This is justified, since the energy eigenfunctions correspond to a bound state, are quadratically integrable, and may be expressed as Fourier transforms.

This equation of state is identical with that obtained from the virial theorem, so that the kinetic and thermodynamic pressures are the same for a quantum fluid.

*Contribution No. 1441.

[1] H. S. Green, in Born and Green, *A General Kinetic Theory of Liquids* (Cambridge University Press, 1949) p. 23; Physica 15, 882 (1949).

[2] J. de Boer, Reports on Progress in Physics XII, pp. 325–335; Physica 15, 843 (1949).

Dissolution of Phenanthrene in Compressed Gases

S. Robin and B. Vodar
Laboratoire des Hautes Pressions, Bellevue
and
Laboratoire de Physique-Enseignement, Sorbonne, Paris, France

July 31, 1950

THE apparatus employed for the compression of argon and nitrogen has already been described.[1]

Our concentration measurement rests on Beer's law, of which the validity at the very low concentration of our solutions is unquestionable. But the optical density of a given band does not give directly the variation of the concentration with pressure, as one must take into account some specific effects of pressure and temperature on the intensity and position of the band. Those effects are given by the investigation of unsaturated solutions, where the concentration in g/cm³ is constant;[2] temperature and pressure are varied in such a way that the gas can never get out of the bomb for the duration of the experiment.

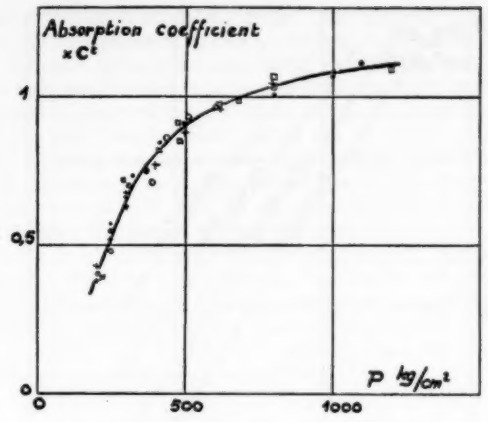

FIG. 1. Absorption coefficient times c^2 *versus* pressure.

Figure 1 shows that the specific effect of pressure is relatively important. On the other hand, between 0°C and 50°C, no measurable specific effect of temperature could be found.

The method used does not give the solubility in absolute value; this value is supplied approximately by the measure of the mass of phenanthrene used to make unsaturated solutions, and also by comparison with the spectrum of a solution in cyclohexane of known concentration; thus we evaluated to 10^{-6} g/cm³ the mass of phenanthrene contained in 1 cm³ of saturated solution in compressed nitrogen at 600 kg/cm² and 17°C.

Figure 2 represents the decimal logarithm of the mass m of phenanthrene dissolved in 1 cm³ of compressed gas as a function of the density of the gas. It can be seen that:

$$m=C\rho^n e^{\alpha\rho} \tag{1}$$

at constant temperature.[3] The measurements are not accurate enough for the exact determination of n; but they show nevertheless that n is certainly small. The curves in Fig. 3 show that:

$$m=Ae^{-B/T} \tag{2}$$

at constant density[4] where B is a constant which depends on the

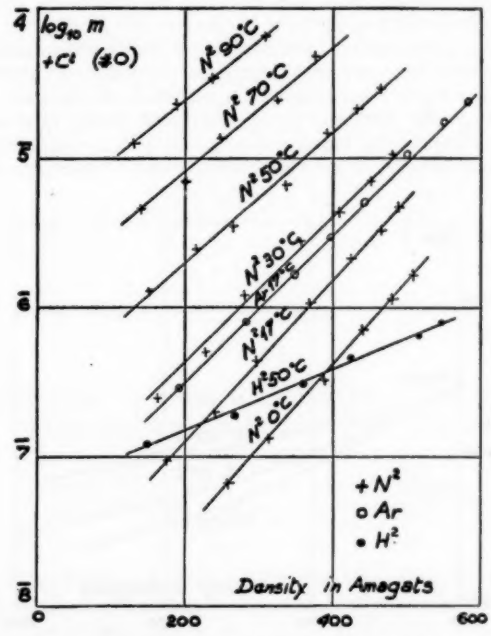

FIG. 2. $\log_{10} m - c^2$ *versus* density for N_2, A and H_2.

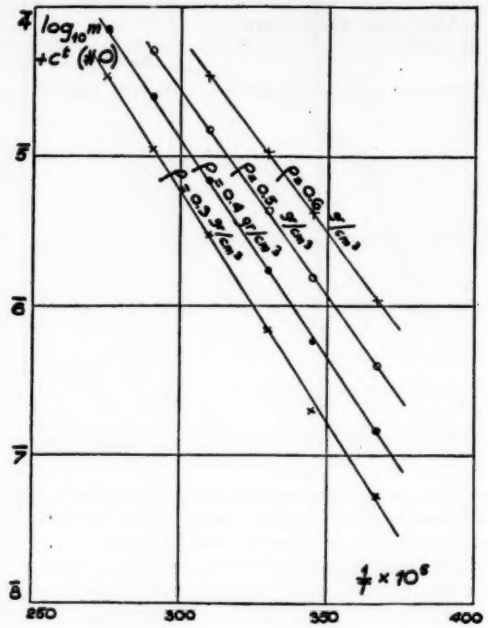

FIG. 3. $\text{Log}_{10}\, m - c^t$ *versus* $1/T$.

density of nitrogen and A another constant in first approximation, which could be nevertheless a slowly varying function of temperature.

The results of the previous works, concerning chiefly the systems[5,6] $C_6H_6-N_2$ and I_2-CO_2, from which we calculated m and ρ approximately fit in the relation mentioned above; the fact that m depends on the nature of the gas proves that the observed phenomenon could not be merely due to a variation of vapor pressure according to the Poynting's relation. Of course the quantity B in formula (2) is proportional to an activation energy; our results show a decrease of this energy as a function of the molecular density of the solvent, i.e., of the mean distance of approach between its molecules and the surface of the solid.

Figure 4 shows the displacement of an absorption band of phenanthrene for $\lambda = 2850$A for H_2, N_2 and Ar.[7] It is known that, according to the impact theory valid mainly at low densities,[8] the displacement must be a linear function of the density of the foreign gas; according to the statistical theories which are supposed to be valid at higher densities,[8] the displacement should vary as the square of the density. Experimentally, mostly linear displacements are known to have, within a few isolated cases, a tendency towards

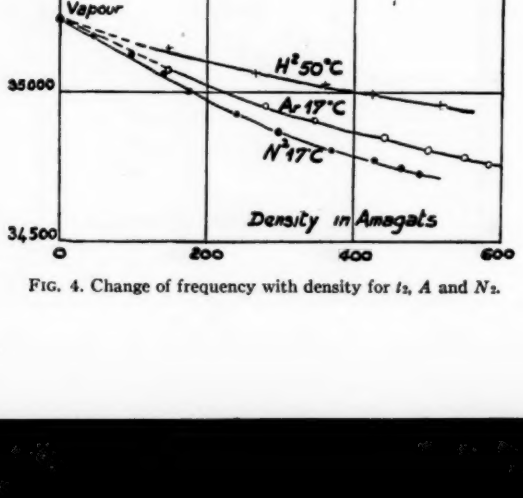

FIG. 4. Change of frequency with density for I_2, A and N_2.

a more rapid increase.[9] Though our results extend to far higher pressures no such square law was found; on the contrary, the displacement becomes slower at high densities. Of course it is difficult to derive a definite conclusion from this fact as phenanthrene is not well suited for such a comparison. On the other hand, in the above theories, the displacement does not depend on temperature; this agrees with our results.

[1] B. Vodar and S. Robin, J. Chem. Phys. **16**, 996 (1948).
[2] The solutions are made by introducing into the bomb an amount of phenanthrene of the order of 10^{-6} g obtained by evaporation titrated solutions in petroleum ether.
[3] S. Robin and B. Vodar, Comptes Rendus **230**, 1840 (1950).
[4] S. Robin, Comptes Rendus (to be published).
[5] I. Krichevsky and D. Gamburg, Acta Phys. (URSS) **16**, 362 (1942).
[6] H. Braune and F. Strassman, Zeits. f. physik. Chemie **A143**, 225 (1929).
[7] S. Robin, Comptes Rendus **230**, 1757 (1950).
[8] H. Margenau and W. Watson, Rev. Mod. Phys. **8**, 22 (1936).
[9] G. F. Hull, Jr., Phys. Rev. **50**, 1148 (1936).

An Electron Diffraction Study of Structures of Tetramethylorthosilicate, Hexamethyldisiloxane, and Hexachlorodisiloxane

KAZUO YAMASAKI, AKIRA KOTERA, MASATOKI YOKOI, AND YOSHIMITSU UEDA
Chemical Laboratory, Nagoya University, Nagoya, Japan
July 31, 1950

MOLECULAR structures of tetramethylorthosilicate, hexamethyldisiloxane, and hexachlorodisiloxane were determined by electron diffraction studies on their vapors. Tetramethylorthosilicate was prepared by the reaction of $SiCl_4$ with methanol. Hexachlorodisiloxane was prepared by passing a mixture of oxygen and chlorine over heated silicon. Hexamethyldisiloxane was given to us by Mr. I. Hizawa of Nissin Chemical Industries, Ltd., to whom we express our sincere thanks.

The camera was a non-sector type with the sample-plate distance of 11 cm. The photographs were taken at about 20°C with the accelerating voltage of 40–50 kv and photographs covering s values of 3–28 were obtained.

The interatomic distances and valence angles determined are as follows:

$Si(OCH_3)_4$:
Si−O = 1.64±0.03A, C−O = 1.42±0.04A,
∠SiOC: 113±2°.
$(CH_3)_3SiOSi(CH_3)_3$:
Si−O = 1.63±0.03A, Si−C = 1.88±0.03A,
∠SiOSi = 130±10°, <CSiC = 111±4°.
$Cl_3SiOSiCl_3$:
Si−O = 1.64±0.05A, Si−Cl = 2.02±0.03A,
∠SiOSi = undetermined, <ClSiCl = 109.5±2°.

In $Si(OCH_3)_4$ each methyl group has a staggered configuration to the non-bonded oxygen atoms. The visual intensity curve is well reproduced by assuming the temperature factor $a_i^2 = 0.004$. The theoretical intensity curves for the *cis*-configuration or the free rotation of methyl groups were not in accord with the visual curve.

In $(CH_3)_3SiOSi(CH_3)_3$ no information about the relative positions of $(CH_3)_3Si$ groups was obtained, but the theoretical intensity curve assuming the temperature factor of 0.004 is in accord with the visual curve.

In $Cl_3SiOSiCl_3$ the valence angle SiOSi was not determined. If this angle is assumed to be 130°, the visual curve is in good accord with the theoretical curve calculated for free rotation of Cl_3Si groups, while its match is poor with the theoretical curve assuming the temperature factor of 0.004.

The observed Si−O distances are about 1.64A and are in accord with the values reported for spirosiloxane,[1] 1.64±0.03A and hexamethylcyclotrisiloxane,[2] 1.66±0.04A. The SiOSi valence angle computed by Sauer and Mead[3] from data on dipole moments of

linear and cyclic dimethylpolysiloxanes is 160±15° and is larger than the value observed by Aggarwal and Bauer[2] for hexamethylcyclotrisiloxane, 125±5° and our results.

[1] W. L. Roth and D. Harker, Acta Krist. **1**, 34 (1948).
[2] E. H. Aggarwal and S. H. Bauer, J. Chem. Phys. **18**, 42 (1950).
[3] R. O. Sauer and D. J. Mead, J. Am. Chem. Soc. **68**, 1794 (1946).

The Raman Spectrum of Tetrafluoroethylene in the Condensed Phase, with Further Assignment of the Fundamental Frequencies

ANDRÉ MONFILS AND JULES DUCHESNE
Department of Chemical Physics, University of Liége, Belgium
July 31, 1950

MOLECULES having V_h symmetry have been under discussion for a long time. In particular, numerous studies have been devoted to C_2H_4[1] and C_2Cl_4,[2] with the aim of deducing a general potential function from the fundamental vibrations. A number of important problems have arisen from these analyses and a comparative study made by one of us[3] has drawn attention to the behavior of certain cross terms which may change sign on passing C_2H_4 to C_2Cl_4. It is, therefore, considered of great interest, from the point of view of comparison, to extend the previous work to include a study of C_2F_4, which is believed to be a member of the same group. Furthermore, it is to be expected that the very peculiar properties of this compound will be reflected in the potential function.

As the infra-red spectrum of gaseous C_2F_4 had already been obtained with fair resolution by Torkington and Thompson,[4] the Raman effect remained to be studied in order to complete the spectroscopic data for this molecule. The apparatus used in this investigation was the same as that described previously by de Hemptinne, Jungers and Delfosse.[5] The Huet spectrograph was a three-glass prism instrument giving a dispersion of about 7A mm in the region involved. The exciting frequencies employed were the 4050A and the 4358A lines of a mercury d.c. current discharge lamp. The following frequencies (cm^{-1}), corresponding to the condensed substance at about −100°C, were found:

397(m)	508(vs)	551(m)	779(s)	830(w)
930(vvw)	1018(vw)	1100(vw)	1350(vvw)	1872(m)

These data are accurate to ±1 cm^{-1} for the strong lines and to ±3 cm^{-1} for the weak ones. A comparison with the infra-red bands shows that there are no coincidences. This fact, which depends upon the selection rules for the V_h point group, favors V_h symmetry in the liquid as well as in the gas. A similar question is still under discussion for C_2H_4[6] where a breakdown of selection rules in the liquid state has been reported.

While this note was in preparation, we have had access to a paper by Nielsen, Claassen, and Smith[7] concerning the Raman effect for the gas. A comparative study of the results is therefore of interest. According to these authors the frequencies corresponding to the gaseous form are:

394(w)	503(m)	517(m)	769.4(vw)	777.9(S)	809.7(vvw)
818.9(m)	828.7(vw)		1018.5(w)	1340(vw)	1872(m)

The vapor-liquid frequency shifts, if any, are too small to be determined.

There are, however, a number of changes on passing from the gas to the liquid: the disappearance of the two maxima at 503 and 517 cm^{-1}, with replacement by a single maximum at 508; the appearance of the lines at 551, 930 and 1100; and the disappearance of the line at 818.9. It is difficult to distinguish exactly the changes induced by condensation from those depending upon instrumental conditions. This question is of great importance in connection with the influence of intermolecular forces on the intensities. One of the main points to be stressed concerns the line at 551 cm^{-1}; the present authors have assigned this line to the low frequency vibration of the B_{1g} group. This discovery checks the validity of the inferences drawn by Nielsen, Claassen, and Smith from the infra-red combination bands. On the other hand, the line at 1100 may be used as an alternative assignment for the high frequency vibration of the same group which was located at 1340. No final choice between these values can as yet be made with certainty, though the shape of the line at 1100 is in favor of a B_{1g} line. Furthermore, though our observations confirm the presence of a line at about 1340, it is not yet excluded that it could result from intensity fluctuation in the continuum.

We are in complete agreement with Nielsen, Claassen, and Smith with regard to their assignment of the infra-red bands. Indeed, the only set of infra-red frequencies which is consistent with a satisfactory potential function favors this assignment.

As a consequence of the above considerations the plane frequencies may now be assigned as follows:

Ag	397	779	1872
B_{1g}	1100	551	
B_{3u}	1186	558	
B_{2u}	1337	250	

The frequency at 250 cm^{-1}, which has not been observed directly, has been deduced by us from a potential function representing the other observed frequencies. This result is also in agreement with the suggestion of Nielsen, Claassen, and Smith as regards B_{2u}.

The C=C frequency vibration at 1872 cm^{-1} is strikingly higher than the corresponding vibration in C_2H_4 (1623) and C_2Cl_4 (1571). This fact is in agreement with preliminary calculations of the C=C bond force constant for C_2F_4; a value as high as 12×10^5 dynes/cm, as compared with 9.0×10^5 dynes/cm for C_2H_4, is obtained. A detailed study of the potential function will be made later on. However, it is already possible to ascertain that the peculiar stability of this compound can be explained in terms of the potential function.

The experimental part of this work has been carried out in the laboratory of Prof. M. de Hemptinne at the University of Louvain. We wish to express our deep gratitude to Prof. de Hemptinne for his great hospitality and for his invaluable help and advice during the course of the laboratory work. We are also very much indebted to Dr. R. N. Haszeldine of Cambridge University for kindly supplying us with a sample of the compound. We are grateful to the Fonds National de la Recherche Scientifique for the financial support given this research.

[1] C. Manneback and A. Verleysen, Ann. Soc. Sci. Brux. **56**, 349 (1936); Yong-Li-Tchang, Ann. Soc. Sci. Brux. **58**, 87 (1938); M. de Hemptinne and C. Manneback, Proc. Ind. Acad. Sci. **9**, 286 (1939); J. Duchesne, Puysica, La Haye **10**, 817 (1943).
[2] J. Duchesne, Physica, La Haye **9**, 249 (1942); H. Bernstein, J. Chem. Phys. **18**, 478 (1950); P. Torkington, J. Chem. Phys. **18**, 773 (1950).
[3] J. Duchesne, V. Henri Mem. Vol. (Desoer, Liége, 1948), p. 47.
[4] P. Torkington and H. W. Thompson, Trans. Faraday Soc. **41**, 236 (1945).
[5] M. de Hemptinne, J. Jungers, and J. M. Delfosse, J. Chem. Phys. **6**, 319 (1938).
[6] D. H. Rank, E. R. Shull and D. W. E. Axford, J. Chem. Phys. **18**, 116 (1950); R. L. Arnett and B. L. Crawford, J. Chem. Phys. **18**, 118 (1950); P. Torkington, J. Chem. Phys. **18**, 758 (1950).
[7] J. R. Nielsen, H. H. Claassen and D. C. Smith, J. Chem. Phys. **18**, 817 (1950).

Relationship between Conductivity of the System Ethanol+Water+Sulfuric Acid and the Solvent Composition

INDRA SANGHI, D. S. DATAR, AND S. H. ZAHEER
Central Laboratories for Scientific and Industrial Research, Hyderabad-Deccan, India
August 7, 1950

ALTHOUGH considerable work has been done on measurements of conductance of various electrolytes in mixed solvents,[1] no attempt has so far been made to define the relation existing between the conductivity and the solvent composition.

TABLE I.

G moles per liter Water	G moles per liter Alcohol	Equivalent conductivity in reciprocal ohms Observed	Water effect calculated	Alcohol effect by difference
4.25	15.95	30.73	19.92	10.81
6.96	15.16	39.00	30.98	8.02
9.67	14.42	48.28	41.92	6.36
12.38	13.67	56.97	52.85	4.12
23.19	10.43	100.4	95.01	5.39

The present note deals with the relationship between conductivity of sulfuric acid in alcohol water mixture and molar proportion of the two solvents in the mixture. The results of an experiment, in which conductivities of sulfuric acid+ethyl alcohol+water system were determined, keeping the amount of sulfuric acid constant and varying the proportion of ethyl alcohol and water, are given in Table I:—Cell constant=1.49; temperature=22.5°C; sulfuric acid=0.3056 N.

In a mixture of alcohol and water, sulfuric acid dissociates more or less completely and H^+ and SO_4^{--} ions get attached to water and alcohol molecules, the ions attached to water showing very high conductance compared to the ions attached to alcohol. In effect this amounts to the division of sulfuric acid in water and alcohol, the acid in water mainly contributing toward the conductance. The number of solvent molecules in association with ions should depend on the molar composition of the solvent mixture and the simplest possible way in which the acid may distribute itself between the two solvents will be in the ratio of the molar proportion of the two solvents in the mixture. On this basis the equivalent conductivity of sulfuric acid in ethyl alcohol and water will be equal to $(M_w/56.56)\Lambda_w+(M_A/17.54)\Lambda_A$ where M_w and M_A are number of gram moles of water and alcohol respectively in 1 liter of the solution and Λ_w and Λ_A are the equivalent conductivities of $M_w/(M_w+M_A)N$ sulfuric acid in water and $M_A/(M_w+M_A)N$ sulfuric acid in alcohol, N being the total normality of sulfuric acid.

For the calculation of the water effect, the equivalent conductivities at 22.5°C at different concentrations of sulfuric acid in water were obtained by extrapolation of the values at 18° and 25° given by A. A. Noyes and co-workers[2] and other investigators.[3] As similar values for conductance of sulfuric acid in ethyl alcohol are not known, the alcohol factors were obtained by difference. Equating the alcohol factors with the second term in the equation, it is possible to obtain the equivalent conductivities of sulfuric acid in alcohol for concentrations varying from 0.1 to 0.25N. The values lie near one another and the average may be taken to represent the equivalent conductivity at 22.5°C of 0.2N sulfuric acid in ethyl alcohol. This value works out to be 8.6 mhos which compares well with the value of 9.6 mhos given by Goldschmidt[4] for the equivalent conductivity at 25°C of 0.2N hydrochloric acid in ethyl alcohol.

Further work is in progress.

[1] Compare references cited by S. Glasstone, *The Electro-Chemistry of Solutions*, (1945), Third Edition, pp. 85–89 and also Robert Kremann and Walter Brassert, Monatsh. **31**, 195–200 (1910).
[2] A. A. Noyes and co-workers, J. Am. Chem. Soc. **30**, 335–353 (1908).
[3] International Critical Tables **VI**, 242 (1929).
[4] H. Goldschmidt, Zeits. f. physik. Chemie **89**, 129 (1915).

Near Ultraviolet Absorption Spectrum of Liquid Benzene from 2795 to 3560A

ANNA C. PITTS*
Chemistry Department, Duke University, Durham, North Carolina
August 10, 1950

SKLAR[1] reported finding weak absorption bands for benzene in the 3400A region, and the absorption spectrum of liquid benzene in this region was later reported by Lewis and Kasha.[2]

TABLE I.

$\bar{V}$, cm^{-1}(air)	$\Delta\bar{V}$, cm^{-1}	Liquid benzene logϵ	Isooctane solution logϵ
32150±20		−2.850	−2.812
	950±40		
31200±20		−2.940	−2.838
	850±40		
30350±20		−3.043	−2.904
	940±40		
29410±20		−3.293	−3.075
	890±40		
28520±20		−3.832	—

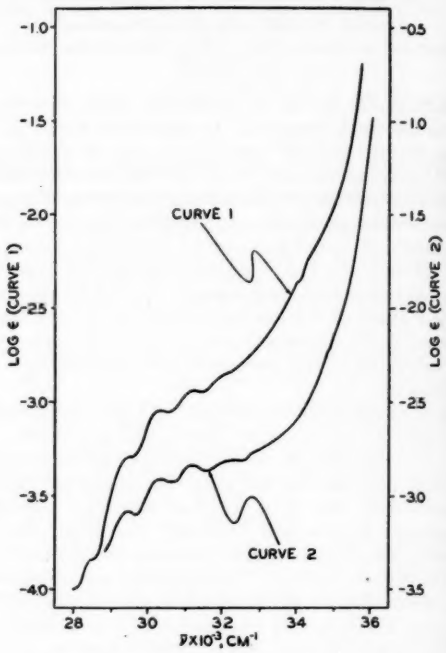

FIG. 1. Curve 1, pure liquid benzene (~32°C); curve 2, benzene in isooctane.

Through a study of phosphorescence emission Shull[3] has recently given a vibrational analysis of this band.

Some work by the author at Mount Holyoke College and by Mr. E. J. Hackney in this laboratory on benzene and some of its derivatives gave indications of some low intensity structure in this region and thus suggested a careful reinvestigation of the 3400A absorption region in benzene. In view of this, the following work was carried out.

A sample of very carefully purified benzene and concentrated solutions (approximately 3.0 M and 1.5 M) of benzene in various solvents with an optical path of 10.006 cm were measured with a calibrated Beckman Quartz Photoelectric spectrophotometer Model DU, using a slit width of 0.34 to 0.28 mm. Pure isooctane was used as the comparison standard in the measurements of liquid benzene and isooctane solution. The absorption spectra of liquid benzene (curve 1) and of isooctane solution (curve 2), Fig. 1, represent the average logϵ-values of four complete measurements of each phase from 2795 to 3560A. Table I gives the location of the bands, the separations, and the average logϵ-values. The band at 28520±20 cm^{-1} was not reported by Lewis and Kasha.[2] The concentrated solutions of benzene in the solvents 95 percent ethyl alcohol and chloroform showed similar structure in this region. It may be noted that the intensity of these bands is essentially 10^{-5} smaller than the 2600A series.

In liquid benzene there is an indication of a shoulder in the region of 34000 cm^{-1}, which may be related to the low intensity bands discussed by Shull,[3] and Roothaan and Mulliken.[4]

* The author acknowledges the suggestions and the study of the data made by Dr. Marcus E. Hobbs of this laboratory and Dr. Emma P. Carr, Professor Emeritus, Chemistry Department, Mount Holyoke College, South Hadley, Massachusetts.

[1] A. L. Sklar, J. Chem. Phys. 5, 669 (1937).
[2] G. N. Lewis and M. Kasha, J. Am. Chem. Soc. 67, 994 (1945).
[3] H. Shull, J. Chem. Phys. 17, 295 (1949).
[4] C. C. J. Roothaan and R. S. Mulliken, J. Chem. Phys. 16, 118 (1948).

Dielectric Relaxation in Glycerine

D. W. Davidson and R. H. Cole
Metcalf Chemical Laboratories, Brown University, Providence, Rhode Island
August 28, 1950

DATA of Morgan[1] and Mizushima[2] for dielectric polarization in glycerine are fitted only qualitatively by dispersion equations of the Debye type, but are not sufficiently extensive for a better function to be uniquely determined. We have made such measurements at temperatures from 0°C to −75°C, by a bridge method over the range 50 cycles/sec. to 5 Mc/sec. and by a transient method at longer times. A typical plot of the complex dielectric constant $\epsilon^*=\epsilon'-i\epsilon''$ at −50°C is shown in Fig. 1. At high frequencies the locus is similar to the arc function found to describe many relaxation processes,[3] but at low frequencies it approaches a semicircle as predicted by simple dispersion theory.

The data can be fitted, except for the small high frequency "bump," by the expression

$$\epsilon^*-\epsilon_\infty=(\epsilon_0-\epsilon_\infty)/(1+i\omega\tau_0)^{1-\alpha}, \quad (1)$$

where ϵ_0 and ϵ_∞ are the limiting low and high frequency values, ω is radian frequency, and τ_0 a characteristic relaxation time. The curve in Fig. 1 is computed from Eq. (1) with $\alpha=0.397$, $\epsilon_0=64.11$, $\epsilon_\infty=4.18$, and the value of τ_0 to fit the data is found to be 1.26×10^{-4} sec. The necessary values of α vary only slightly with temperature, while ϵ_0 increases gradually and τ_0 exponentially with reciprocal temperature. The slight high frequency increment in ϵ^* appears at all temperatures in a frequency range of the order 500 times that for the time τ_0.

The distribution function $F(\tau/\tau_0)$ for relaxation times τ in the interval $d\ln(\tau/\tau_0)$ is of interest, and is defined by the relation

$$\epsilon^*-\epsilon_\infty=(\epsilon_0-\epsilon_\infty)\int_{-\infty}^{\infty}\frac{F(\tau/\tau_0)d\ln(\tau/\tau_0)}{1+i\omega\tau}.$$

Inversion of this equation by use of Fourier transforms gives for the ϵ^* of Eq. (1) the result

$$F(\tau/\tau_0)=(\sin\alpha\pi/\pi)[\tau/(\tau_0-\tau)]^{1-\alpha}, \quad \tau<\tau_0,$$
$$=0, \quad \tau>\tau_0. \quad (2)$$

From this expression one finds that a broad distribution including significant contributions for τ as small as $\tau_0/100$ is necessary with $\alpha=0.4$.

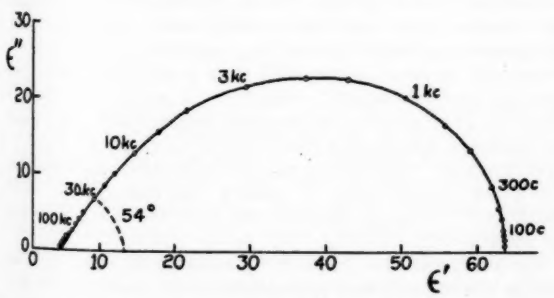

Fig. 1. Complex dielectric constant locus of glycerine at −50°C. Numbers beside points are frequencies of measurement.

Yager[4] has suggested that the earlier data could be explained by overlapping relaxation processes, possibly corresponding to orientations of molecules and of associated groups. This hypothesis becomes unattractive in the light of Eq. (2). In the first place, the largest value of τ, namely τ_0, is of the order of magnitude but smaller than the value predicted by the Debye relation[5] $\tau_0=3\eta V/kt$ for reasonable values of viscosity η and molecular volume V. Second, the spectrum of τ extends continuously in the direction of shorter rather than longer times.

The limitations of the Debye model of a molecular sphere reorienting in a viscous fluid are well known, and an argument involving its quantitative use to object to the concept of association in a simple sense necessarily loses some force as a result. The more important consideration is the fact that the necessary distribution of relaxation times behaves in a fashion quite contrary to what one would expect as a result of such association. We conclude that a more detailed analysis of the interaction of polar groups is necessary to account for the relaxation process satisfactorily. The observed complex locus of ϵ^* for glycerine is striking in being intermediate between the semicircle of simple theory and the arc locus found in many cases, and in this behavior being quantitatively described over most of the frequency range by such a simple expression.

This study is part of a program made possible by a Frederick Gardner Cottrell grant from the Research Corporation.

[1] S. O. Morgan, Trans. Electrochem. Soc. 65, 109 (1934).
[2] S. Mizushima, Bull. Chem. Soc. Japan 1, 47 (1926).
[3] K. S. Cole and R. H. Cole, J. Chem. Phys. 9, 341 (1941).
[4] W. A. Yager, Physics 7, 434 (1936).
[5] The correction factor for the Lorentz field in Debye's original treatment is omitted as being probably inappropriate and in any case increasing the discrepancy.

Rotational Isomerism in Perfluoro Paraffins

G. J. Szasz
U. S. Office of Naval Research, London, England
August 23, 1950

RECENT interest in the properties of fluorocarbons[1] has shown that these are generally similar to those of the corresponding hydrocarbons. One would thus expect that rotational isomerism, which has been exhaustively studied in the paraffin series[2–7] will make a significant contribution to the stereochemistry of the analogous completely fluorinated substances.

We have investigated the infra-red absorption spectra of perfluoro *n*-pentane, *n*-hexane, and *n*-heptane in the region 9 to 13μ. The spectra were obtained in the vapor, liquid, and crystalline solid phases. In addition quantitative intensity measurements were made on appropriately chosen pairs of lines belonging to different isomers as a function of temperature in the liquid phase. The detailed results and experimental techniques will be presented later.

As for the paraffin hydrocarbons a striking simplification occurs abruptly at the freezing point. This permits the separation of the bands belonging to the most stable isomer from the rest of the spectrum. The results of the quantitative intensity measurements are summarized in Table I. The results are very similar to those obtained for the corresponding hydrocarbons.[5] In the absence of additional information we assume that the extended, zig-zag form again represents the most stable configuration and is the only one present in the solid.

Recent evidence[8–10] suggests that there exist strong repulsive forces between fluorines on adjacent carbon atoms and thus one would perhaps expect higher values for the energy differences between the rotational isomers than those observed by us. While the "straight" forms of these molecules are non-polar, the "bent" forms will possess permanent electric dipoles. Consideration of the electrostatic forces shows[11] that this would tend to stabilize the "bent" forms in the liquid phase as compared with the vapor.

TABLE I. The energy difference between rotational isomers in liquid perfluoro *n*-paraffins.

Compound	Line pair(s), cm^{-1}	Temperature range, °K	Energy difference cal. $mole^{-1}$, $-\Delta H$
$n-C_6F_{12}$	834–881	150–220	460±100
	990–1022	150–220	350±150
$n-C_6F_{14}$	795–818	195–280	600±150
	818–833	195–280	580±150
$n-C_7F_{16}$	1030–1058	220–330	600±100

However, the similarity of the vapor and liquid spectra at comparable temperatures shows that the different rotational isomers are present in nearly the same relative concentration in the two phases. We believe therefore that the energy differences in the vapor phase will not be significantly higher than those obtained in this investigation.

We thank Professor F. J. W. Roughton, F.R.S., for permission to work in the Department of Colloid Science, Cambridge, and Dr. N. Sheppard and Mr. J. K. Brown for help with the spectroscopic equipment and measurements. We are greatly indebted to Dr. W. H. Pearlson of the Minnesota Mining and Manufacturing Company for the fluorocarbon samples and to the Office of Naval Research for permission to carry out this investigation.

[1] Report on Conference on Fluorides and Fluorocarbons, ONR, Washington, D. C. (1949).
[2] K. W. F. Kohlrausch and F. Köppl, Zeits. f. physik. Chemie **B26**, 209 (1934).
[3] Szasz, Sheppard, and Rank, J. Chem. Phys. **16**, 704 (1948).
[4] Rank, Sheppard, and Szasz, J. Chem. Phys. **17**, 83 (1949).
[5] N. Sheppard and G. J. Szasz, J. Chem. Phys. **17**, 86 (1949).
[6] D. W. E. Axford and D. H. Rank, J. Chem. Phys. **17**, 430 (1949).
[7] D. W. E. Axford and D. H. Rank, J. Chem. Phys. **18**, 51 (1950).
[8] H. P. Lemaire and R. L. Livingston, J. Chem. Phys. **18**, 569 (1950).
[9] F. A. M. Buck and R. L. Livingston, J. Chem. Phys. **18**, 570 (1950).
[10] W. F. Edgell and D. G. Weiblen, J. Chem. Phys. **18**, 571 (1950).
[11] Morino, Mizushima, Kuratani, and Katayama, J. Chem. Phys. **18**, 754 (1950).

The Variation of Rate of Desorption with Extent of Surface Coverage

JOSEPH WEBER AND KEITH J. LAIDLER
U. S. Naval Ordnance Laboratory, White Oak, Maryland and The Catholic University of America, Washington, D. C.
August 14, 1950

RECENTLY Rideal and Trapnell[1] reported results on adsorption heats which lead to the conclusion that whereas dilute films of hydrogen on tungsten evaporate very slowly, more concentrated films evaporate much more rapidly. This effect is due to the repulsive forces acting between adsorbed molecules, and has an important bearing on the mechanism of the para-orthohydrogen conversion and many other reactions. In connection with a study of the catalyzed ammonia-deuterium exchange reaction, using the technique of microwave spectroscopy to determine NH_3 concentrations, we have recently demonstrated directly that rates of desorption are markedly increased as the surface becomes more fully covered.

The work has been done with a singly promoted iron catalyst (No. 631) kindly supplied by Dr. P. H. Emmett. We have found that the rate of evaporation of deuterated ammonia from the surface is increased markedly as the pressure of NH_3 in the gas phase is increased. For example, with 40 g of catalyst at 122°C and a pressure of 1μ the rate of desorption of deuterated ammonia is 5×10^{-9} mole $sec.^{-1}$. With a NH_3 pressure of 20 cm on the other hand, the rate of desorption is 1.4×10^{-6} mole $sec.^{-1}$; in a 2-liter vessel deuterated ammonia corresponding to a pressure of 1 cm is in fact desorbed in less than 10 min. In view of the effect it is not sufficient, before starting a new experiment, merely to pump out the reaction vessel: the catalyst must be washed several times with the gas mixture to be employed in the experiment.

The effect was first noticed by us on the walls of the 1-cm copper wave guide used. Since the adsorption on an untreated wave guide was sufficient to interfere with the analysis, it was coated with a layer of Glyptal which was then baked; the coating thickness was 0.0003 in. If NH_3 is introduced into such a wave guide and the system then pumped down to 10^{-4} mm, the desorption can be followed both by observation of the increase of pressure and of the pressure broadening of the 3–3 line of the ammonia inversion spectrum. Under these conditions the initial pressure rise is about 5μ per minute. On adding a mixture of NH_3 and deuterated ammonias the rate of desorption of NH_3 can be followed by measuring the total pressure and the peak absorption of the 3–3 line, this peak being approximately proportional to the mole fraction of NH_3. In this way we have found, for example, that a pressure of 0.4 mm increases the rate of desorption of NH_3 by a factor of at least 100. The desorption of deuterated ammonia is found to be similarly increased. In order to analyze mixtures of the ammonias we have therefore found it necessary to wash several times with the mixture to be analyzed.

These results, like those of Rideal and Trapnell, cannot be explained on the basis of variability of the catalyst surface, but only in terms of repulsive forces. Since the rates of catalyzed reactions are sometimes controlled by desorption rates it follows that surfaces may be rendered more active catalytically by the adsorption of reactant or other molecules.

Further details of this work will be included in a later paper on the kinetics of the ammonia-deuterium exchange.

[1] E. K. Rideal and B. M. W. Trapnell, Faraday Soc. Discussion on Heterogeneous Catalysis, Liverpool (April, 1950).

The Magnetic Susceptibility of Europium and Samarium Amalgam

DAVID L. DOUGLAS AND DON M. YOST
*Gates and Crellin Laboratories of Chemistry, California Institute of Technology, Pasadena, California**
August 16, 1950

THE difficulties encountered in preparing the rare-earth metals have seriously hampered the investigation of the physical and chemical properties of these substances.[1] By far the most extensive piece of work is that of Klemm and Bommer.[2] These investigators prepared the metals by reducing the anhydrous trichlorides with the stoichiometric amount of potassium. We are reporting the results of some preliminary studies of the magnetochemical properties of the rare-earth amalgams. While the literature contains many references to the magnetochemical properties of amalgams,[3] particularly those of the alkali metals, it appears that this approach to the study of the rare-earth metals has been overlooked. Samarium and europium were chosen as the first objects of study because of the considerable theoretical importance attaching to their position near the middle of the lanthanide series.

The origin and purity of the europium used in this research has been discussed in a previous publication.[4] The samarium was obtained from Research Chemicals, Inc.,[5] and was reported by them to be better than 99 percent Sm_2O_3. Purification of the mercury was effected by the usual acid washing and a single distillation. The magnetic susceptibilities of the samarium and mercury were determined in order to establish their purity as regards paramagnetic or ferromagnetic substances. A solution of $SmCl_3$ in dilute HCl was used for the samarium measurement; and the result obtained was $\chi_{8m}=6.75\pm0.07\times10^{-6}$ c.g.s./g at 27.5°C, in good agreement with Sugden and Tailby's recent determination.[6] The specific susceptibility of mercury was found to be $-0.166\pm0.001\times10^{-6}$ c.g.s./g, agreeing well with the best values from the literature.[7,8]

The amalgams were prepared by reducing the rare-earth acetates in solution with sodium amalgam.[9] After washing with water to remove any unreacted sodium the amalgams were introduced into the sample tubes under dry nitrogen. The susceptibilities were

TABLE I. Magnetic susceptibility of europium amalgam.

Exp't. No.	(1) Force (mg)	(2) Field (oersteds)	(3) Temp. (°C)	(4) Wt. % Eu	(5) $\kappa_{obs}\times10^6$ (c.g.s./ml)	(6) $\chi_{obs}\times10^6$ (c.g.s./g)	(7) $\chi_M\times10^6$ (c.g.s./mole)	(8) μ_{eff}
1	3.9 — 3.4	9104 — 8580	25.0±0.1	0.104	0.47 — 0.48	0.035	29,200 ±1100	8.4±0.2
2	3.3 0.9	9140 8680	25.0±0.1	0.104	0.40 — 0.40	0.030	28600 ±1100	8.3±0.2
3	−19.4	9140	25±1	6.15×10^{-3}	−2.07	−0.154	30400 ±7500	8.5±1.0
4	50.0 — 43.9	9140 — 8680	25.8±0.2	0.307	5.18 — 5.25	0.386	27300 ±200	8.09±9.03
5	48.4 — 42.6	9140 — 8680	25.1±0.2	0.307	5.19 — 5.20	0.385	27200 ±200	8.08±0.03

TABLE II. Magnetic susceptibility of samarium amalgam.

Exp't. No.	(1) Force (mg)	(2) Field (oersteds)	(3) Temp. (°C)	(4) Wt. % Sm	(5) $\kappa_{obs}\times10^6$ (c.g.s./ml)	(6) $\chi_{obs}\times10^6$ (c.g.s./g)	(7) $\chi_M\times10^6$ (c.g.s./ml)	(8) μ_{eff}
1	−15.9	9140	25.0±0.1	0.323	−1.55	−0.115	2360±140	2.38±0.07
2	−14.3	9140	25.0±0.1	0.375	−1.51	−0.112	2160±120	2.28±0.06
3	−14.2 — −12.4	9140 8580	24±0.5	0.426	−1.38 — −1.39	−0.102	2250±90	2.32±0.05
4	−11.3 — −10.1	9140 — 8580	25±0.5	0.528	−1.19 — −1.19	-0.088_2	2220±90	2.31±0.05

measured by the Gouy method, the balance used having been described in a previous publication.[10] Analyses were carried out by extracting the rare-earth with warm 6*N* HCl, precipitating it as the oxalate and igniting to the oxide at 850°C. Precautions were taken during the weighings to prevent appreciable reaction of the oxide with the water and carbon dioxide in the air.

The results of the measurements with europium and samarium amalgams are given in Table I and Table II, respectively. Columns 1 to 5 list the observed quantities as indicated. In calculating the specific susceptibilities (column 6) the density of mercury at the indicated temperature was used. The validity of Wiedemann's additivity law was assumed in calculating the molar susceptibility of the rare-earth component.[11] Effective Bohr magneton numbers (μ_{eff}) are tabulated in column 8 only as a convenient method of comparing observed and theoretical susceptibilities.[12] A diamagnetic correction of -30×10^{-6} c.g.s./mole was applied to the samarium values. The errors indicated are the maximum errors, not probable errors.

Klemm and Bommer found an effective moment of 8.3 for metallic europium.[2] Our result, probably somewhat more accurate, is in good agreement with this. Spectroscopic evidence assigns a configuration (outer shells only) and term symbol to europium of $4f^75s^25p^66s^2\ {}^8S$, for which is calculated an effective moment[13] of 7.94. Thus the magnetic and spectroscopic results are in excellent agreement.

For the case of samarium no such agreement is to be found. At 20°C Klemm and Bommer determined the effective moment of the metal to be 2.07. Our value for the amalgam, namely, 2.28 to 2.38, is definitely greater than that found by Klemm and Bommer for the presumably pure metal. Selwood[14] has measured the susceptibilities of samarium (II) and samarium (III) compounds and reports the following effective moments: Sm(II) = 3.62; Sm(III) = 1.55. These values for the compounds have been put on a firm theoretical basis by Van Vleck and Frank.[15,16] Any satisfactory explanation of the anomalous moments found for metallic samarium and for its amalgam must await further experimental and theoretical work.

We wish to express our appreciation for a loan of some europium by Mrs. Ethel Terry McCoy. We are also grateful to the Research Corporation for a grant which aided, in part, the work reported here. The senior author (D.L.D.) is indebted to the United States Rubber Company for financial assistance in the form of a fellowship for the year 1949–50.

* Contribution No. 1449.

[1] Yost, Russell, and Garner, *The Rare-Earth Elements and their Compounds* (John Wiley and Sons, Inc., New York, 1947), p. 51.
[2] W. Klemm and H. Bommer, Zeits. f. anorg. u. allgem. Chemie **231**, 138 (1937).
[3] P. W. Selwood, *Magnetochemistry* (Interscience Publishers, Inc., New York, 1943), p. 188.
[4] D. L. Douglas and D. M. Yost, J. Chem. Phys. **17**, 1345 (1949).
[5] 831 North Lake Street, Burbank, California.
[6] S. Sugden and S. R. Tailby, J. Chem. Soc. **1949**, 136 (1949).
[7] L. F. Bates and C. J. W. Baker, Proc. Roy. Soc. London **50**, 409 (1938).
[8] S. R. Rao and S. Aravamuthachari, Proc. Ind. Acad. Sci. **9A**, 181 (1939).
[9] J. K. Marsh, J. Chem. Soc. **1942**, 398 (1942).
[10] A. Whittaker and D. M. Yost, J. Chem. Phys. **17**, 188 (1949).
[11] Reference 3, p. 2.
[12] J. H. Van Vleck, *The Theory of Electric and Magnetic Susceptibilities* (Oxford University Press, Cambridge, 1932), p. 242.
[13] Russell, Albertson, and Davis, Phys. Rev. **60**, 641 (1941).
[14] P. N. Selwood, J. Am. Chem. Soc. **56**, 2392 (1934).
[15] J. H. Van Vleck and A. Frank, Phys. Rev. **34**, 1494, 1625 (1929).
[16] A. Frank, Phys. Rev. **48**, 765 (1935).

Carrier-Free Radioisotopes from Cyclotron Targets XI. Preparation and Isolation of Os^{185} and $Re^{183,184}$ from Tungsten*

JEANNE D. GILE, WARREN M. GARRISON, AND JOSEPH G. HAMILTON
Crocker Laboratory, Radiation Laboratory, and Divisions of Medical Physics, Experimental Medicine, and Radiology; University of California, Berkeley and San Francisco, California

May 26, 1950

LONG-LIVED radioisotopes[1] of rhenium and osmium have been isolated in the carrier-free state from a tungsten exit strip which was removed from the 60-in. cyclotron at Crocker

Laboratory after a period of four months of almost continuous operation with protons (10 Mev), deuterons (20 Mev), and alpha-particles (40 Mev). The possible transmutation reactions include: W(d, xn)Re, W(p, xn)Re, W(α, pxn)Re, and W(α, xn)Os. In the procedure reported here, the long-lived isotopes of rhenium, $Re^{183,184}$, and osmium, Os^{185}, produced by the nuclear reactions $W^{182}(d, n)Re^{183}$, $W^{183}(d, 2n)Re^{183}$, $W^{183}(d, n)Re^{184}$, $W^{184}(d, 2n)Re^{184}$, $W^{182}(\alpha, pn)Re^{184}$, $W^{182}(\alpha, n)Os^{185}$, and $W^{183}(\alpha, 2n)Os^{185}$ were separated from the target element and from other possible long-lived transmutation products by a combination of volatility and solvent extraction methods.

The tungsten strip (approx. 2 g) was fused with 10 g of KOH and 0.5 g of KNO_3 at 500°C for 30 minutes to form the water-soluble tungstate, perrhenate, and osmate. The fused mass was dissolved in a minimum volume of cold water and centrifuged to remove insoluble matter. The solution was acidified with 16N HNO_3 precipitating tungstic acid which was removed by centrigugation. The supernatant containing the carrier-free radio-rhenium and radio-osmium was diluted to 5N and transferred to an all-glass distilling flask. The carrier-free radio-osmium, presumably as the volatile OsO_4, was distilled into an ice-cooled trap containing 5 N HNO_3. The rhenium activity remained in the residual solution. The HNO_3 distillate (25 ml) was extracted with two 25-ml aliquots of CCl_4 which removed over 95 percent of the radio-osmium from the aqueous phase. After washing with water to remove HNO_3, the radio-osmium was quantitatively re-extracted from the CCl_4 phase with 2 ml of 0.1N NaOH which on neutralization gave an isotonic saline solution for biological investigation. The carrier-free radio-rhenium was isolated from the residual HNO_3 solution using the distillation procedure previously[2] described in the preparation of carrier-free rhenium from tantalum. The Os^{185} was identified by the 97-day half-life and by the 0.75-Mev gamma-ray previously reported.[3,4] The $Re^{183,184}$ showed the 0.2- and 0.7-Mev beta-particle and the 1.0-Mev gamma-ray reported[5] for 50-day Re^{184}. Half-life measurements showed an approximately 57-day period which began to lengthen after three weeks due to the approximately 240-day Re^{183} isotope. The activities were further identified by chemical separation using W, Re, and Os carriers.

We wish to thank Professor G. T. Seaborg for helpful suggestions, Mr. T. Putnam and Mr. B. Rossi and the crew of the 60-in. cyclotron for bombardments and Mrs. Alberta Mozley for assistance in counting.

* This document is based on work performed under Contract No. W-7405-eng-48-A for the AEC.

[1] G. T. Seaborg and I. Perlman, Rev. Mod. Phys. **20**, 585 (1948).
[2] Gile, Garrison and Hamilton, J. Chem. Phys. **18**, 995 (1950).
[3] L. I. Katzin and M. Pobereskin, Phys. Rev. **74**, 264 (1948).
[4] L. J. Goodman and M. L. Pool, Phys. Rev. **71**, 288 (1947).
[5] G. Wilkinson and H. G. Hicks, Phys. Rev. **77**, 314 (1950).

On the Lattice Frequencies of 1,2-Dihalogenoethanes

ISAO ICHISHIMA AND SAN-ICHIRO MIZUSHIMA
Chemical Laboratory, Faculty of Science, Tokyo University, Bunkyoku, Tokyo, Japan
August 16, 1950

THE disappearance of many Raman lines of 1,2-dichloroethane and 1,2-dibromoethane (XH_2C-CH_2X) upon solidification was observed by Mizushima and Morino who explained this phenomenon, considering that these substances are in one molecular form (*trans*-) in the crystalline state and in two molecular forms (*trans*- and gauche) in the liquid state.[1] They also found low frequency Raman lines characteristic to the crystalline state which were considered to correspond to lattice vibrations. The assignment of these lattice frequencies can be made by the selection rule for molecular crystals recently developed by Ichishima[2] which is similar to that proposed by Halford.[3]

The lattice frequencies of a molecular crystal so far observed in the Raman effect are related closely to the structure of a single molecule. This enables us to adopt an approximate method in which we treat the motions of a molecule moving in a potential field formed by surrounding molecules in their equilibrium positions. According to our view the anharmonicity of the intermolecular forces which would give rise to the observed considerable temperature dependence[2] of lattice frequencies and the large value of thermal expansion coefficient of molecular crystals may be partly responsible for the characteristic vibrational modes of molecular crystals.

The molecules of 1,2-dihalogenoethanes in the crystalline state being in the *trans*- form with the symmetry C_{2h}, the symmetry of the said potential field would correspond to one of the subgroups of C_{2h}: i.e., C_i, C_2, C_s, and C_{2h}. The existence of the center of symmetry (C_i) which is very probable in this case allows only the rotatory vibrations in the Raman effect and forbids the translatory vibrations. Of the three Raman active rotatory vibrations one about the molecular axis or the axis joining two halogen atoms would escape detection owing to the small change of polarizability. Therefore, the frequencies 53 and 74 cm^{-1} of 1,2-dichloroethane and 41 and 53 cm^{-1} of 1,2-dibromoethane observed below the transition point should be assigned to the rotatory vibrations about the two axes, both perpendicular to the molecular axis. Since the moments of inertia about these two axes are practically equal to each other, the appearance of two different frequencies for each of these two substances would be due to the difference of the restoring forces for these two motions. This would be seen from the result of the crystal structure analysis made for 1,2-diiodoethane[4] which would not be much different from that for 1,2-dichloroethane or for 1,2-dibromoethane. The fact that only one lattice frequency (66 cm^{-1} for 1,2-dichloroethane and 49 cm^{-1} for 1,2-dibromoethane) was observed for each of these 1,2-dihalogenoethanes above the transition point can be reconciled with this view, since the free rotation about the molecular axis sets in above the transition point[5] and the restoring forces tend to become equal to each other.

[1] S. Mizushima and Y. Morino, Proc. Ind. Acad. Sci. **8**, 315 (1938). Raman Jubilee Volume. See also Mizushima, Morino, Watanabe, Shimanouchi, and Yamaguchi, J. Chem. Phys. **17**, 591 (1949).
[2] I. Ichishima, Rep. Rad. Chem. Res. Inst. (Tokyo University) **4**, 9 (1949).
[3] R. S. Halford, J. Chem. Phys. **14**, 8 (1946).
[4] H. P. Klug, J. Chem. Phys. **3**, 747 (1935).
[5] H. S. Gutowsky and G. E. Pake, J. Chem. Phys. **18**, 162 (1950).

Directed Valence in IF_5 and IF_7

ROBERT L. SCOTT
Department of Chemistry, University of California, Los Angeles, California
August 16, 1950

RECENTLY Lord and co-workers[1] have studied the infra-red and Raman spectra of iodine pentafluoride and iodine heptafluoride and have concluded that the IF_5 molecule is a tetragonal pyramid (C_{4v} symmetry) while the IF_7 molecule is a pentagonal bipyramid (D_{5h} symmetry). By applying group theory to the problem of directed valence, Kimball[2] showed that the former structure is consistent with sp^2d^2, sd^4, p^3d^2, or pd^4 hybridization, but he did not consider the pentagonal bipyramid for the coordination number seven.[3] Duffey[4] has recently shown that a plausible orthogonal set of pentagonal bipyramidal orbitals can be constructed with the over-all composition sp^3d^3.

Since atomic iodine has the electronic structure $(1s)^2(2s)^2(2p)^6(3s)^2(3p)^6(3d)^{10}(4s)^2(4p)^6(4d)^{10}(5s)^2(5p)^5$, it is evident that in compounds where iodine has a multiple valency it is necessary to use either the 5d or 4f orbitals or both. Since it does not appear obvious that the 5d orbitals must necessarily be chosen in preference to the 4f, it seems desirable to extend Kimball's group theoretical treatment to include f electrons for the symmetries C_{4v} and D_{5h}.

Tables I and II give the possible compositions for bonds corresponding to these symmetries. The representations leading to

TABLE I. Five tetragonal pyramidal bonds.

C_{4v}	A_1	A_2	B_1	B_2	E
s	1	0	0	0	0
p	1	0	0	0	1
d	1	0	1	1	1
f	1	0	1	1	2
σ	2	0	0	1	1
π	1	1	1	1	3

TABLE II. Seven pentagonal bypyramidal bonds.[a]

D_{5h}	A_1'	A_1''	A_2'	A_2''	E_1'	E_1''	E_2'	E_2''
s	1	0	0	0	0	0	0	0
p	0	0	0	1	1	0	0	0
d	1	0	0	0	0	1	1	0
f	0	0	0	1	1	0	1	1
σ	2	0	0	1	1	0	1	0
π	0	0	1	1	2	2	1	1

[a] The representation A_2'' in this table is labeled A_1'' in Kimball's Table XIII.

π-bonds are included in the tables, although the high electronegativity of fluorine would seem to preclude any significant contribution of bonds of the type $I^-=F^+$.

For IF_5 there are 21 distinct configurations consistent with C_{4v} symmetry, as well as an infinite number of linear combinations. There are seven valence electrons outside the closed shells of iodine; so we must also account for two non-bonding electrons. Since the energy of electrons in the $5s$ and $5p$ orbitals is appreciably lower than that for $5d$ or $4f$, it seems reasonable to exclude all those configurations which fail to make maximum use of these orbitals, either for bonding or for the non-bonding pair. When this is done, only six remain: sp^3d, fsp^3, sp^2d^2, fsp^2d, and fp^3d.

A particularly inviting explanation for the IF_5 structure is obtained by forming six approximately octahedral orbitals, one of which is occupied by the non-bonding pair, thus minimizing the overlap. For full octahedral symmetry (O_h), the only allowed combinations are sp^3d and f^2sd^2 and the latter does not use the $5p$ orbitals. In addition to these two, f^2spd^2 and fsp^2d^2 satisfy the symmetry (D_{4h}) of a tetragonal bipyramid, but neither uses all the p orbitals. Many combinations give non-planar tetragonal bonds (C_{4v} symmetry) but only three satisfy our additional requirements: sp^3d^2, sp^3df, and sp^2f^2.

For IF_7, which uses all the valence electrons for bonding, the possibilities are more limited. Of the eight configurations allowed, only two, dp^3d^3 and f^2sp^2d, utilize fully the $5s$ and $5p$ orbitals. Both of these are also consistent with the ZrF_7^{-3} and TaF_7^{-2} structures, the only other experimentally observed spatial arrangements with coordination number seven.

It is evident that further study and experiments are required before one can attempt to assess the contributions (if any) of f electrons to these structures.

The author wishes to express his indebtedness to Professor W. G. McMillan, Jr. for many helpful discussions.

[1] Lord, Lynch, Schumb, and Slowinski, J. Am. Chem. Soc. **72**, 522 (1950).
[2] G. E. Kimball, J. Chem. Phys. **8**, 188 (1940).
[3] Kimball discussed pentagonal plane orbitals (p^2d^3) for coordination number five, but excluded them as unstable because of steric interference.
[4] G. H. Duffey, J. Chem. Phys. **18**, 943 (1950).

On Heat Conductivity in Liquids*

A. W. LAWSON
Institute for the Study of Metals, University of Chicago, Chicago 37, Illinois
August 18, 1950

THIS note is not concerned with the more formal and rigorous statistical theories of transport phenomena in liquids such as those of Kirkwood[1] and Born and Green.[2] Rather, its purpose is to call attention to a simple quasi-empirical relation which permits estimates of the temperature and pressure variations of heat conductivities.

TABLE I. The relative variation of heat conductivity in C_2H_5OH as a function of temperature and pressure.

	Eq. (1)	Eq. (2)	Eq. (3)	Eq. (4)	Experiment
$\frac{K_{30°C}}{K_{75°C}}$	0.93	1.17	1.08	1.02	1.03
$\frac{K_{9000\ kg/cm^2}}{K_{2000\ kg/cm^2}}$	1.00	1.82	2.60	1.49	1.45

TABLE II. Pressure variation of heat conductivity in C_2H_5OH.

Pressure in $kg/cm^2\times10^{-3}$	$\frac{K_{(P)}}{K_{(0)}}$ from Eq. (4)	$\frac{K_{(P)}}{K_{(0)}}$ from experiment
0	1.00	1.00
1	1.16	1.20
2	1.32	1.34
4	1.52	1.55
6	1.76	1.72
9	1.92	1.92
12	2.45	2.09

Three formulas have been used in the past for the heat conductivity of a liquid; one of these is

$$K\sim C\lambda(mkT)^{\frac{1}{2}}\delta^{-2}, \tag{1}$$

where C is the specific heat per unit mass, λ the mean free path, k Boltzmann's constant, m the molecular weight, and T the absolute temperature. This equation is that used in elementary kinetic theory of gases, in which λ for liquids is usually assumed approximately equal to the interatomic distance δ.

Bridgman[3] has suggested the use of

$$K\sim C\delta^{-2}v_s m, \tag{2}$$

where v_s is the velocity of sound. This dimensional equation gave surprisingly good values for the heat conductivity of liquids but failed to predict the pressure variation satisfactorily.

Kittel[4] and Kincaid and Eyring[5] have applied the equation

$$K\sim Cv_T\delta^{-1}S^{-1}m, \tag{3}$$

where S is the free path in the available volume, which the molecule is assumed to traverse in a gas-like manner in order to execute a collision with a neighbor. This formula also fails to give satisfactory agreement for temperature and pressure variations.

We would like to call attention to the fact that a combination of Eq. (2) and Eq. (3) leads to a more satisfactory model. Thus we propose to write

$$K\sim C\delta^{-1}[(S/v_T)+(\delta/v_s)]^{-1}m. \tag{4}$$

This equation may be interpreted as endowing the available volume with a gas-like resistivity in series with which is the resistivity of the imperfectly rigid but elastic molecule. In other words, a time $t=\delta/v_s$ is required during the actual collision for the momentum of one molecule to be transferred to its neighbor. This t is the order of magnitude of the reciprocal of a low frequency molecular vibration.

We must not expect accurate predictions of the absolute value of heat conductivity, owing to the crude nature of Eqs. (1)–(4) and our inability to estimate the role of vibrational, rotational, and translational degrees of freedom, respectively. We may, however, inquire concerning the temperature and pressure variation of the heat conductivity. A comparison of the various models with experiment is shown in Table I, where to v_s we have arbitrarily assigned the value 2.85×10^5 cm/sec., a not implausible value. Such a value implies that the collision time is comparable to the time required to cross the mean free path at ordinary pressures and is the dominant effect at high pressures. For the available volume V_a of C_2H_5OH at 30°C we have used 17 cm³. The value of

S is computed after the manner of Tonks,[6] namely, $S/\delta=(1-\theta^{\frac{1}{2}})/\theta^{\frac{1}{2}}$ where $\theta=1-V_a/V$. It will be observed that the best agreement is for Eq. (4).

Table II shows the variation of K at 30°C in C_2H_5OH as a function of pressure over a wider range of pressure. The agreement is worst at the higher pressures where results are quite sensitive to the choice of V_a. It should be remarked that in all computations made above, we have neglected the variation of specific heat with temperature and pressure. The choice of C_2H_5OH is purely arbitrary but the agreement would be about as good for other alcohols and hydrocarbons which have been measured.

In conclusion, it should be remarked that a simple extension of this model is possible by assuming an interatomic potential of the type previously used by Kincaid and Eyring.[7] However, the uncertainty concerning the effects of rotation does not seem to justify a more refined treatment.

* This work was supported in part by the ONR under Contract 6-ori-20-XX.

[1] J. G. Kirkwood, J. Chem. Phys. **14**, 180 (1946).
[2] M. Born and H. S. Green, Proc. Roy. Soc. **A188**, 10 (1946) and **A190**, 455 (1947).
[3] P. W. Bridgman, *Physics of High Pressures* (G. Bell and Sons, Ltd., London, 1931).
[4] C. Kittel, J. Chem. Phys. **14**, 614 (1946).
[5] J. F. Kincaid and H. Eyring, J. Chem. Phys. **6**, 621 (1938).
[6] L. Tonks, Phys. Rev. **50**, 955 (1936).
[7] J. F. Kincaid and H. Eyring **5**, 587 (1937).

The Structure and Dipole Moment of Hydrazoic Acid*

EILIF AMBLE†
Department of Physics
AND
B. P. DAILEY
Department of Chemistry, Columbia University, New York, New York
August 21, 1950

THE structure of the simple molecule hydrazoic acid, HN_3, has been determined previously from infra-red[1] and electron diffraction data.[2] However, these structures can be improved in accuracy and reliability with the use of data obtained from a study of the microwave spectrum. In addition, the dipole moment can be obtained.

In this study, hydrazoic acid was prepared by treating samples of a few milligrams of sodium azide with phosphoric acid. The hydrazoic acid vapors were dried with $CaCl_2$. DN_3 was prepared by the same procedure using $D_3PO_4(D_2O+P_2O_5)$. To prepare the molecules containing N^{15}, N_2O made by heating $N^{15}H_4N^{14}O_3$ was passed over sodium amide at 200°C to form sodium azide. It is interesting to note that all of the three possible isotopic molecules (listed in Table II) were prepared simultaneously by this procedure.

The microwave spectra of the hydrazoic acids were observed using a Stark modulation spectrometer. From the measured frequencies of the $0_{0,0}-1_{0,1}$ rotational transitions the values of the sum of the rotational constants B_0+C_0 were obtained. In the case of HN_3^{14} a very accurately measured value of $A_0-(B_0+C_0)_2$ was available from infra-red data.[1] For this molecule A_0 has been calculated with great accuracy.

Hydrazoic acid is a very slightly asymmetric rotor ($\kappa=0.99921$). However, because of its asymmetry, it is difficult to relate directly the rotational constants to the structural parameters. With the aid of Eyster's parameters as a first approximation, I_z has been calculated from the new A_0 and the distance of H above the N_3 axis obtained directly. The remaining three structural parameters were evaluated from the changes in (B_0+C_0) produced by the isotopic substitutions. The equations relating the rotational constants of the mono-isotopically substituted molecules to the four structural parameters were solved numerically by a method of successive approximations. The structure is completely determined from the experimental data.

The effective values of the structural parameters in the ground vibrational state, obtained in this manner, are given in Table I

TABLE I. Structural parameters for HN_3.

	HN_3 parameters derived from infra-red spectrum (a)	Electron diffraction values (b)	HN_3 parameters derived from microwave and infra-red spectra
N_2-N_3 distance	1.128	1.136±0.01A°	1.134±0.003A°
N_1-N_2 distance	1.241	1.247±0.01	1.240±0.003
H−N distance	1.012		1.021±0.01
HN_1-N_2	110°52′		112°39′±30′

TABLE II. Rotational constants for HN_3.

	Frequencies of $0_{0,0}\rightarrow 1_{1,0}$ rotational transition (B_0+C_0)	$A_0-\frac{B_0+C_0}{2}$	A_0
$H^1N^{14}N^{14}N^{14}$	23,815.7 Mc	621,757 Mc	609,849 Mc
$DN^{14}N^{14}N^{14}$	22,316.1		
$HN^{14}N^{14}N^{15}$	23,048.2		
$HN^{15}N^{14}N^{14}$	23,096.7		
$HN^{14}N^{15}N^{14}$	23,814		

[a] See reference 1.

along with the comparable values from the infra-red and electron diffraction studies. The agreement may be seen to be excellent, the main change being to increase the H−N distance and H−N−N angle. The experimental error was actually much less than that indicated in Table I. However, the effects of zero-point vibration produce errors of larger magnitude, especially in the case of the H−N distance.

The Stark effect of HN_3 is to a good approximation that of a symmetric rotor. In addition, at sufficiently large displacements, the complicating effects of the quadrupole coupling may be neglected. The component of the dipole moment along the approximate figure axis of HN_3 was determined to be 0.847±0.005 debye units. The observation that this moment is less than half that found in HNCS[3] is an interesting confirmation of the fact that the formal charges are on adjacent atoms in HN_3 while they are on opposite ends of the NCS group.

A more thorough study of the quadrupole coupling in this molecule will be made with a higher resolution instrument. The observed fine structure pattern, while similar to that of a single triply bonded N^{14} atom, contained contributions from both end N atoms.

The authors wish to thank Professor C. H. Townes for much valuable advice and assistance. One of the authors wishes to thank the Norwegian Royal Council for Scientific Research for the grant of a fellowship.

*Work supported jointly by the Signal Corps and the ONR.
† On leave from University of Oslo, Oslo, Norway.
[1] E. H. Eyster, J. Chem. Phys. **8**, 135 (1940).
[2] V. Schomaker and R. A. Spurr, J. Am. Chem. Soc. **64**, 1184 (1942).
[3] C. I. Beard and B. P. Dailey, Phys. Rev. **75**, 1318 (1949).